universität wien

MASTERARBEIT | MASTER'S THESIS

Titel | Title

Photoredox synthesis of a series of tetrabenzocyclooctatetraenes

verfasst von | submitted by

Jan Heckhausen BSc

angestrebter akademischer Grad | in partial fulfilment of the requirements for the degree of

Master of Science (MSc)

Wien | Vienna, 2024

Studienkennzahl lt. Studienblatt | Degree programme code as it appears on the student record sheet:	UA 066 862
Studienrichtung lt. Studienblatt | Degree programme as it appears on the student record sheet:	Masterstudium Chemie
Betreut von | Supervisor:	Univ.-Prof. Davide Bonifazi PhD

Kurzfassung

In einer Welt, in der erneuerbare Energien eine zunehmend bedeutende Rolle spielen, steigt die Nachfrage nach fortschrittlichen Anodenmaterialien für wiederaufladbare Lithium-Ionen-Batterien, um die herkömmlichen Graphitanoden zu ersetzen. Ein vielversprechender Kandidat für ein neuartiges Anodenmaterial wird im „cubic graphite“ vermutet – einer Struktur, die erstmals 1946 von Gibson *et al*. vorgeschlagen wurde, aber bis heute synthetisch unzugänglich bleibt. Diese Arbeit untersucht einen innovativen, photoredoxkatalyse-basierten Ansatz zur Synthese von „cubic graphite“, der sich auf die Zyklisierung von Quaterphenyl zu Tetraphenylenen konzentriert, welche als fundamentale Untereinheiten des „cubic graphite“ vermutet werden.

Zyklisierungsreaktionen von cyano- und chlorsubstituierten Quaterphenylen wurden unter milden Bedingungen und Verwendung des leistungsstarken organischen Photoredoxkatalysators *peri*-Xanthenoxanthen (PXX) durchgeführt, nach einem von der Bonifazi Forschungsgruppe entwickelten Verfahren. Der Einfluss der Position der CN-Gruppe wurde evaluiert.

Die notwendigen Ausgangsmaterialien wurden mittels einer mizellengestützten Suzuki-Miyaura-Kupplungsmethode synthetisiert. Anschließend wurden verschiedene PXX-katalysierte Quaterphenyl-Zyklisierungsreaktionen durchgeführt, wobei ein Einfluss der CN-Position auf die Bildung von Tetraphenylenen festgestellt wurde. Bemerkenswerterweise ergaben einige Reaktionen eine zweite Tetraphenylen-Isomerstruktur, die wahrscheinlich durch einen untypischen biradikalischen Umlagerungsmechanismus entstanden ist. Die radikalische Natur der Zyklisierungsreaktionen wurde untersucht. Darüber hinaus wurde die Synthese zusätzlicher Quaterphenyle mit elektronenziehenden und -spendenden Gruppen versucht.

Die Ergebnisse zeigen das große Potenzial der Photoredoxkatalyse bei der Förderung von Radikal-Radikal Bindungen, was möglicherweise den Weg für die Synthese größerer und komplexerer benzenbasierter Strukturen wie „cubic graphite“ ebnen könnte.

Abstract

In a world where renewable energy plays an increasing role, more advanced anode materials for rechargeable lithium-ion batteries to supplant conventional graphite anodes are in high demand. A promising candidate for a novel anode material is hypothesized to be cubic graphite - a structure first proposed by Gibson *et al*. in 1946, that remains synthetically elusive to this day. This thesis explores an innovative photoredox catalysis-based path towards the synthesis of cubic graphite, focusing on the cyclization of quaterphenyls into tetraphenylenes, which are theorized as fundamental subunits of cubic graphite.

Following a procedure developed by the Bonifazi research group, cyano- and chloro-substituted quaterphenyl cyclization reactions were conducted under mild conditions, employing the potent organic photoredox catalyst *peri*-Xanthenoxanthene (PXX). The influence of the position of the CN group on the final cyclization was assessed.

The necessary starting materials were synthesized *via* a micelle-assisted Suzuki-Miyaura coupling method. Subsequently, various PXX-photocatalysed quaterphenyl cyclization reactions were performed, revealing an influence of CN-position on tetraphenylene formation. Remarkably, some reactions yielded a second tetraphenylene isomer structure, likely arising from an atypical biradical rearrangement mechanism. The radical nature of the cyclization reactions was explored. Furthermore, the synthesis of additional quaterphenyls incorporating electron-withdrawing and electron-donating groups was attempted.

The findings show the great potential of photoredox catalysis in facilitating radical-radical bond formation, potentially paving the way for the synthesis of larger, more complex benzene-based structures, such as cubic graphite.

Acknowledgements

I want to thank Professor Davide Bonifazi for giving me the opportunity to work on this project in his research group. I have learned incredibly much about how to work well in a laboratory, and I cherish learning about the value of scientific standards – especially when presenting one's work to other scientists. I am also thankful for the flexibility and the acceptance towards me doing research in the group and working as both a student representative and a tutor in introductory student laboratory courses, as well as me getting sick with COVID-19 so many times.

Special thanks go towards Davide Zanetti, who supported me and my research in both the fruitful and fruitless moments. I am also thankful for taking the time to help me out even when it's stressful and time is short – especially regarding correcting this thesis. I will fondly remember our musical moments in the 1H14 laboratory.

I would also like to thank the rest of the Bonifazi research group for their help whenever I had questions. Here, I particularly want to thank Vivek Wakchaure for his helpful lab tips and Martina Crosta for all her help with my crystal structures.

I also want to thank Florian Traxler for being there when I came knocking with NMR questions and Professor Mathea Sophia Galanski for her help with a difficult 2D NMR analysis towards the end of my laboratory work, allowing me to finally understand the structures of my final products.

Further thanks go to my friends and colleagues from the student representation. You guys have helped me back up when I was struggling, and I appreciate what a community we have built together. Let's keep the party going!

I'd like to thank my parents for believing in me and for giving me the time and space to thrive. Your support made a difference. Great thanks also to all my other friends and relatives, who surely can't wait to see me more often, now that I am finishing my studies.

Thank you!

Table of contents

I Introduction

1.1 The science behind cubic graphite

1.1.1 Carbon allotropes

To better understand the potential properties of cubic graphite, the introduction will begin by examining the established carbon allotropes also constructed from benzene rings. Particular emphasis will be placed on their chemical properties, current applications and the most common synthetic methods used for their production. As depicted in **Figure 1**, the discussed carbon allotropes will be derived from graphene, as that is the simplest macromolecular structure formed by only benzene rings in a flat plane. Other carbon allotropes expand the complexity of benzene-based structures.

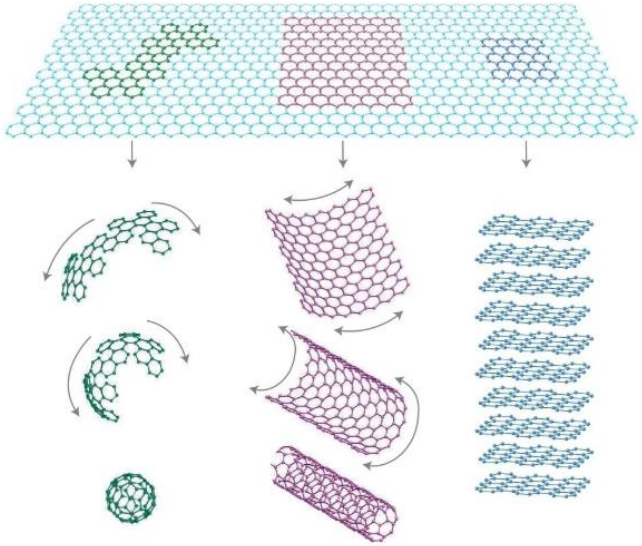

Figure 1: *Graphene, Fullerenes, carbon nanotubes and 3D graphite* [1]

1.1.1.1 Graphenes

Graphene is a single-layer sheet structure formed by sp^2 hybridized carbon atoms connected with covalent bonds in a honeycomb arrangement. A thin monolayer of just a single sheet is called graphene, while a 3D bulk structure of stacked graphene sheets that is being held together by weak Van der Waals interactions is called graphite.[1]

In graphene, each atom possesses one *s* orbital and two in-plane *p* orbitals, contributing to the sheet's mechanical stability. The remaining *p* orbital is oriented perpendicular to the plane and undergoes hybridization, resulting in the formation of π (valence) and π* (conduction) bands.[2]

Graphene is known for properties like its high intrinsic strength (Young's modulus of up to 1.0 TPA and 130 GPa) and flexibility, remarkable transparency, great electrical

conductivity (~ 10^6 S/cm) as well as thermal conductivity ($5 \cdot 10^3$ W/mK), its high charge mobility (~ $2 \cdot 10^5$ cm^2/Vs) and electron transport capability, as well as its thermal and chemical stability. [1-3] It also has an extremely high theoretical specific surface area (2630 m^2/g) and has been shown to be biocompatible and quite safe while used *in vitro* in cells and *in vivo* in animals.[4] While graphene itself lacks a band gap and exhibits inertness towards reaction, a large number of functionalization methods have been developed.[5]

These various useful properties of graphene make it a candidate for a diverse range of applications, such as in energy research, nanoelectronics, catalysis, drug delivery in nanomedicine, bioimaging, gene therapy, nanocomposites, and biomaterials.[1, 4a, 6] Nobel Prize winners K. Novoselov and A. Geim published their first preparation of graphene in 2004. They used Scotch tape to peel singular graphene layers.[7] In general, graphene syntheses can be divided into two categories: bottom-up approaches, in which smaller chemical units are grown into larger ones, and top-down approaches, in which higher-order entities are turned into lower-order entities.[1, 8] Examples of bottom-up approaches include epitaxial growth, where an isolated monolayer of graphene is grown on single-crystal silicon carbide (SiC) *via* vacuum graphitization or methods like growth on silicon carbide.[8b, 9] Another common bottom-up method also includes chemical vapour deposition, in which transition metal substrates like nickel are exposed at high temperatures to carbon-containing gases like methane or solution phase synthesis-based methods, for example *via* density differentiation.[10] Top-down approaches, on the other hand, include mechanical exfoliation from graphite, chemical exfoliation by oxidation or through solvent use as well as the method of arc discharge, in which pure graphite electrodes come in contact with buffer gases like H_2.[11]

1.1.1.2 Graphite

Graphite is a carbon allotrope consisting of closely packed sheets of sp^2 hybridized carbon atoms organized in a hexagonal pattern that are arranged in an ABAB sequence and are linked by weak van der Waals interaction coming from delocalized π-orbitals.[12]

It is a good electrical (~ 1 $ohm^{-1}cm^{-1}$) and thermal (~ 3000 $Wm^{-1}K^{-1}$) conductor within its layers due to electron delocalization while being a bad electrical (~ $1 \cdot 10^4$ $ohm^{-1}cm^{-1}$) and thermal (~ 6 $Wm^{-1}K^{-1}$) conductor in a perpendicular direction to its layers.[13] The carbon layers can easily slide off each other, giving graphite the application as a good

lubricant and pencil material.[14] It allows for the intercalation of reactants in between its layers, which leads to enhanced electrical conductivity.[15] When compressed without a binder it can lead to mechanical interlocking, giving rise to a flexible and resilient sheet with the name flexible graphite.[12, 16] Graphite can have a variety of further properties depending on whether it is of natural or synthetic origin and there are different varieties of graphite such as amorphous graphite, flake graphite and vein graphite.[17] Amorphous graphite forms multiple clusters instead of continuous layers and contains 5-, 7-, and 8-membered rings that lead to the buckling of layers, inducing aberrations from perfect planarity.[18] Flake graphite is a structure of flat, plate-like crystals ranging in size from 1 to 25 mm.[19] Vein graphite is homogeneous, has varying interlayer space has a highly ordered crystalline structure and is notable for mainly being naturally found in Sri Lanka.[20]

Graphite is commonly used in primary and secondary alkaline batteries as both an electrical conductor and lubricant.[17] However, modern use of electronics demands an enhanced performance of Li-ion batteries and graphite is seen as the main culprit stifling advances in performance.[16a] This carbon allotrope functions as an anodic “lithium sink” in Li-ion batteries as it provides a balance of high energy and power density as well as a very long cycle life in addition to low cost and abundance.[16a] Graphite can be found as a mineral in nature. However, it needs to be of high purity when mined for use in electronics. Synthetic graphite can be prepared by heating unstructured carbon to temperatures above 2500 °C. The exact conditions can be varied to achieve desired properties.[17]

1.1.1.3 Fullerenes

Fullerenes are a family of closed-cage molecules that are entirely formed by sp^2-hybridized carbon atoms. Every fullerene C_n is made from 12 pentagonal rings and m hexagonal states with $m = (C_n\text{-}20)/2$. The most investigated variants are C_{60} and C_{70}.[21] They come in various shapes like hollow spheres, ellipsoids or tubes and they are named after the Architect Buckminster Fuller who is known for fabricating cage-like geodesic domes.[22] A curious variant of fullerenes are nano-onions, which are multilayered carbon spheres that have bucky-ball cores between the layers.[22]

Initially, fullerenes were assumed to be extremely stable aromatic molecules due to having many resonance structures, as seemed to be supported by calculations. However, the tendency to avoid double bonds in the strained pentagonal rings adjacent to the benzenoid rings leads to poor electron delocalization and higher reactivity than

expected. As fullerenes are entirely constructed of sp^2-hybridized carbons that have electron-withdrawing -I inductive effects, they are strongly electron-attracting, leading to a large variety of possible reactions with nucleophiles.[21] Fullerene C_{60} has high electronegativity and can accept up to 6 further electrons in solution.[23]

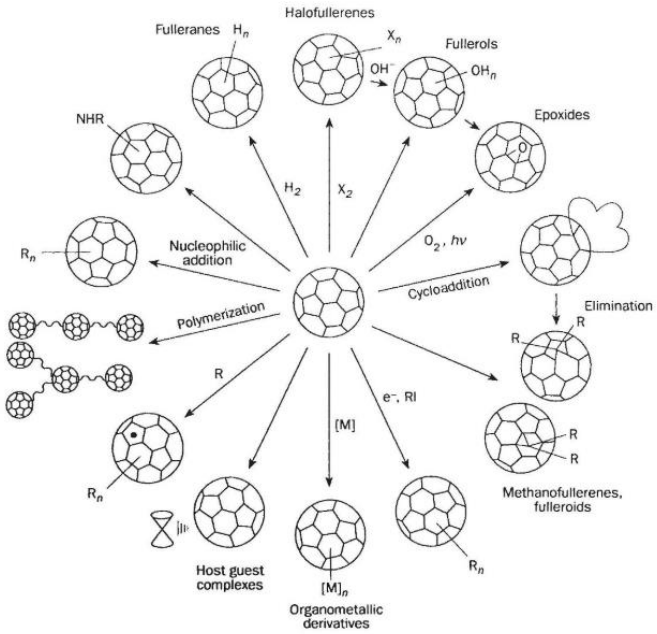

Figure 2: *Examples of reactions with fullerenes by Taylor and Dalton.[21]*

Fullerenes exhibit decomposition by light and oxygen and films of C_{60} degrade on storage because of the ability to chemisorb oxygen.[24] Decomposition of C_{60} can occur when heated in the presence of oxygen, C-O adducts are formed at 200 °C and 400-500 °C decomposition is observed.[25] Known reactions with fullerenes include their use as oxidizing agents,[26] nucleophilic additions with halogens and hydrogen,[27] Diels-Alder (2+4) cycloadditions,[28] epoxidation,[29] formation of carbon and metallic bridges,[30] nucleophilic and electrophilic substitution,[31] radical reaction,[32] metal complex reaction and polymerization.[30a] The following properties also apply to fullerenes: They have good close packing, and they have low density (1.65 g/cc).[21-22] Fullerene C_{60} is soluble in conventional solvents at room temperature but has low solubility in water and the tendency to agglomerate easily.[23a]

In vitro studies on the toxicity of Fullerene C_{60} show no cytotoxicity in humans and animal cells and studies in animal tissues indicate low acute *in vivo* toxicity (all injected mice survived one week; estimated lethal dose is 500 $mg \cdot kg^{-1}$ i.p.).[22, 33] It was also proven that fullerene can both be used as a photocatalytic enhancer for other semiconductors and as a photocatalyst itself due to having a narrow band gap energy (1.6-1.9 eV), which leads to intensive adsorption of UV light and moderate absorption

of visible light.[23a, 34] They have also been shown to be good photosensitizers with a good quantum efficiency ($\Phi \approx 1$), capable of generating photochemically reactive oxygen species.[35] However, for retaining its photoactivity, immobilization onto solid supports like for example silica is needed.[23a, 34, 36]

This carbon allotrope is used in organic photovoltaics,[37] as a lubricant,[38] and as a drug delivery machine.[39] Fullerene and its derivatives also have a multitude of diagnostic and therapeutic applications. Examples include acting as an anti-HIV agent,[40] being able to neutralize reactive oxygen species and therefore defending apoptosis as an antioxidant,[41] as well as being able to cross cell membranes as a hydrophobic drug- and gene-delivery substance.[42] As fullerenes are biologically stable and can be covalently linked to many drugs, their use in prolonged drug release systems is being investigated.[43] It is also used as an acceptor material and cathode modification layer of organic polymer solar cells[44] as well as the electron transport layer of perovskite cells.[23a, 45]

The traditional synthesis of fullerenes occurs by the arc-discharge vaporization of graphite rods by resistive heating in a He atmosphere,[46] by chemical vapour deposition methods[47] and by combustion processes.[48] The methods to obtain fullerenes on a commercial scale are based on the vaporization of graphite by pyrolysis, arc-discharge-plasma and radio-frequency plasma techniques.[49]

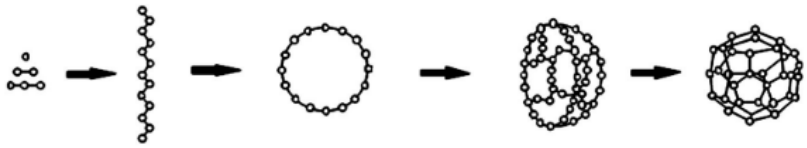

Figure 3: *Model 1 for formation of fullerenes.[49]*

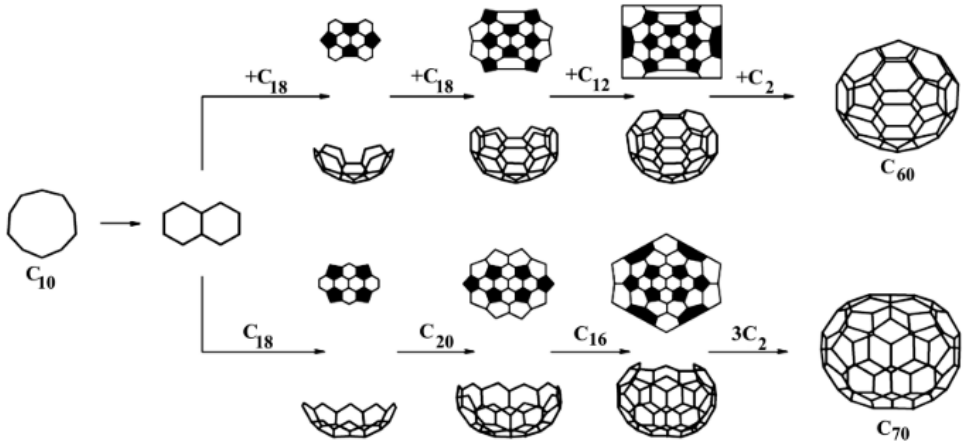

Figure 4: *Model 2 for formation of fullerenes.[49]*

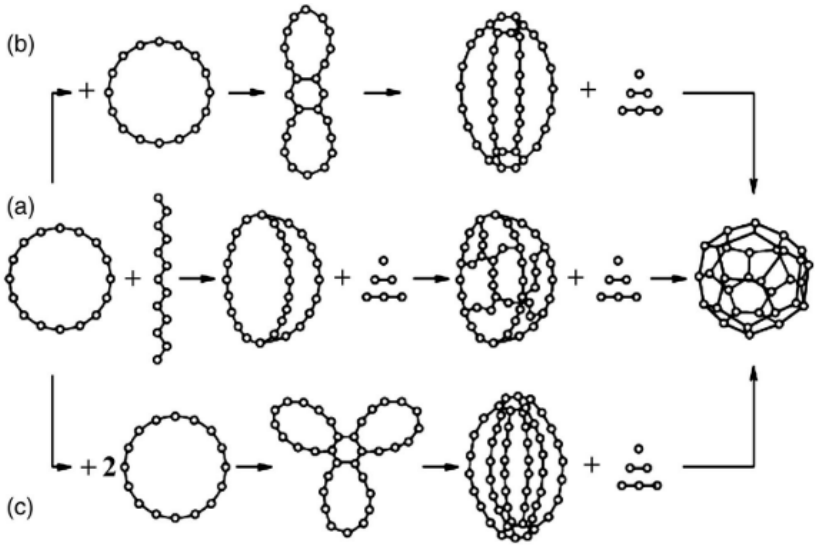

Figure 5: *Model 3 of formation of fullerenes.*[49]

A successful chemical synthesis of fullerene involved the pyrolysis of $C_{60}H_{27}Cl_3$ at 1100 °C. This process selectively led to the C_{60} fullerene, but it only had a yield lower than 1 %, since the reactive compound was decomposed by harsh conditions.[49]

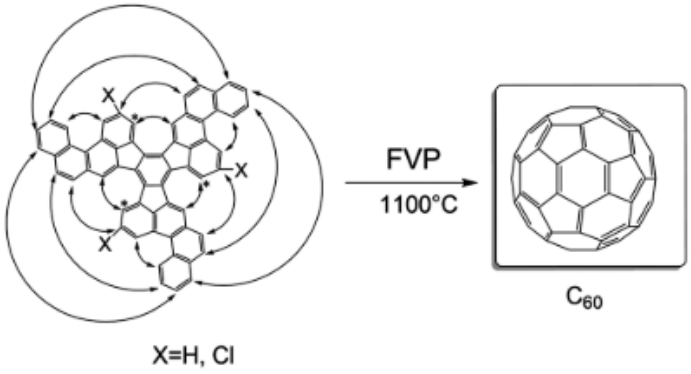

Figure 6: *Rational Chemical Synthesis of Fullerene* C_{60}.[49]

1.1.1.4 Carbon Nanotubes

Carbon nanotubes are a carbon allotrope consisting of sp^2 hybridized carbon atoms that was first characterized in 1991 by S. Iijima.[50] The structure of carbon nanotubes is derived from graphene and as such it can be understood as a sheet rolled into a hollow tube of the hexagonal lattice of graphene as visualized in **Figure 7** and **Figure 8**. Their basic structure consists of the honeycomb arrangement that is typical for graphene. They usually have a diameter of a few nanometres and a length of micrometres. There are many types of them such as long/short, single-walled/multi-walled, open/closed and of a spiral structure. They can further be sorted by their crystallographic configurations like armchair, zigzag and chiral based on the way the sheet of graphene is rolled up.[51]

Figure 7: *Open and closed carbon nanotubes*[51]

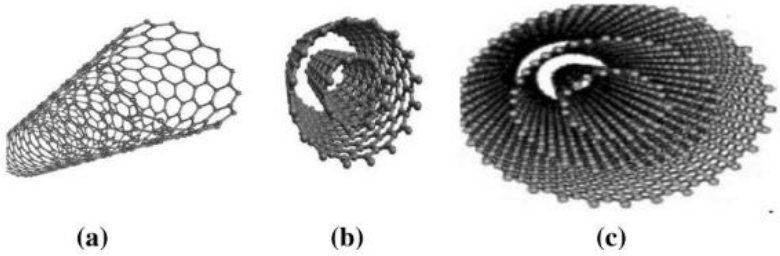

Figure 8: *Single-walled carbon nanotubes, double-walled carbon nanotubes and multi-walled carbon nanotubes*[51]

Carbon nanotubes are known for their extremely large surface area (up to 1315 m^2/g depending on the number of walls). They also have large thermal (> 200 $Wm^{-1}K^{-1}$ at r.t.) and electrical conductivity as well as high mechanical strength (estimated up to 22.2±2.2 GPa).[52] Carbon nanotubes are insoluble in water and other solvents as they tend to agglomerate, thus they can only be dispersed in some solvents using sonication but strategies are being developed to improve solubility.[53] Furthermore, they have been demonstrated to be toxic in mice lungs.[54] The issues around insolubility and toxicity can be mitigated by functionalization, like for example ammonium functionalized carbon nanotubes obtained *via* 1,3 dipolar cycloaddition reaction.[51, 55] The large surface-to-volume ratio makes carbon nanotubes useful as chemical- and biosensors.[56] Additionally, functionalized carbon nanotubes are used as a nano-vehicle for drug delivery in cancer treatment.[57] Applications such as scanning probe tips as well as in electron guns in field emission are also known.[58] Furthermore, it is utilized as a material in electrochemical devices such as supercapacitors,[59] and in electronic devices on flexible substrates like large-area flexible displays or printed electronics.[60] Further applications in photonic crystals, and solar cells with peak efficiency at an angle of 45 ° have also been reported[61] and its use in storage devices such as fuel cells[62] or Li-ion batteries is being investigated.[63] Known methods of synthesis of carbon nanotubes include laser ablation,[64] arc discharge[50, 65] and chemical vapour deposition.[51, 66]

During laser ablation, a laser is used to vaporize a graphite target which is holding a catalyst material in a quartz tube furnace at 1200 °C while an inert gas is blended into the chamber. This leads to the formation of a hot vapour plume, which quickly cools, leading to the condensation of small carbon atoms to larger clusters. The catalyst condenses more slowly and attaches to carbon clusters hindering them from closing into caged forms.[51, 67]

In the arc discharge technique, a gas is electrically broken down to plasma. Two graphite electrodes with a potential difference are mounted to an electrical current and heated to a temperature between 1000-2000 °C while surrounded by inert gas. The carbon nanotubes deposit on the graphite cathode while the anode is eroded.[51, 65]

In chemical vapour deposition a hydrocarbon vapour is passed through a tubular reactor containing a transition metal catalyst at a sufficiently high temperature (600-1200 °C) that decomposes the hydrocarbon, which then grows as carbon nanotubes on the catalyst when it is cooled to room temperature.[51, 68]

1.1.1.5 3D graphene

While there is no specific definition for 3D-graphene materials, a review by Sun *et al.* defines it as such: “It can be clearly defined that 3D graphene materials are nongraphite 3D structured graphene materials. The graphene walls in a 3D graphene material should consist of less than 10 graphene layers and maintain the general properties of graphene materials.”[69]

3D graphene materials are classified into multiple different types. They can be either macroscopic 3D graphene materials (> 100 µm) or microscopic 3D graphene materials (< 100 µm). They can also either be joint 3D graphene architectures that are mainly connected *via* van der Waal’s forces or integrated 3D graphene architectures which are continuously connected by chemical bonds. A further way of classifying 3D graphene is by dividing it into graphene-oxide-derived 3D graphene materials, hydrocarbon-synthesized 3D graphene materials and inorganic carbon-formed 3D graphene materials as portrayed in **Figure 9**.[69]

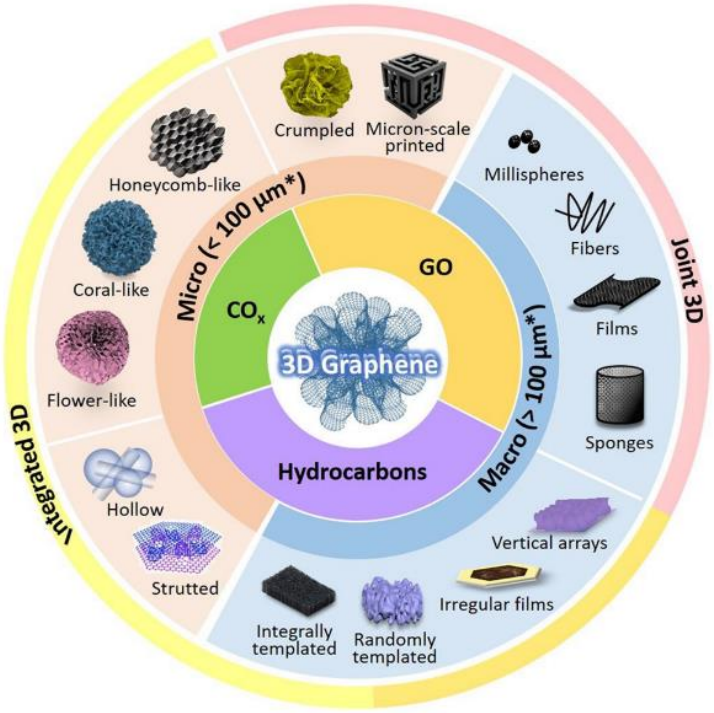

Figure 9**:** *Classification of the types of 3D graphene materials.*[69]

The properties of 3D graphenes differ based on their type. Strong variation is present in size and shape, as well as in the amount and size of pores, if present. The density of 3D graphene materials can also greatly vary, albeit with a trade-off between specific capacitance/capacity on the one side and conductivity and mechanical stiffness on the other.[69-70]

3D reduced graphene oxides generally have a smaller specific surface area (200-600 m^2/g and up to 884 m^2/g)[69, 71] and weaker strength (architecture with density ~100 mg/cm^3 → Young's modulus of ~1 MPa)[72] than graphene as a monolayer sheet. Their electrical conductivity values are highly dependent on the mass density of the materials with increasing mass density generally leading to higher conductivity (conductivities between ~100 000 to <1 S/m reported).[69, 73] Notably, the conductivity of low-density 3D reduced graphene oxide architectures was reported to be able to sensitively increase with compression.[74] In general, 3D reduced graphene oxides show low thermal conductivity (4.7-5.9 · 10^{-3} $Wm^{-1}K^{-1}$ bulk thermal conductivity at r.t.; 2.96 ± 0.02 $Wm^{-1}K^{-1}$ in-plane thermal conductivity at r.t.; 0.3 $Wm^{-1}K^{-1}$ cross-plane thermal conductivity at r.t.),[75] however, it can be increased by enhancing the reduction degree of the graphene oxide sheets.[76] 3D reduced graphene architectures have also demonstrated efficient function as absorbers of microwaves in the ranges of 26.5-40

and 75-110 GHz, with the absorption being tuneable mechanically with compression.[69, 77]

Hydrocarbon-formed 3D graphene synthesis usually results in surface areas of 500-1000 m^2/g,[78] but if the wall thickness can be controlled to 1-2 graphene layers thick a surface area close to 2000 m^2/g can be reached.[79] These graphenes also exhibit high hydrophobicity due to having a low amount of defects and functional groups, which makes their use in organic solvents advantageous.[80] Furthermore, they exhibit an increased isotropic electrical conductivity at the same mass density compared to 3D reduced graphene oxides, however, the density of most of them is low (2-150 mg/cm^3) and the overall conductivity ranges from 1000 to 160000 S/m.[69, 81] Their thermal conductivity is reported as generally low but could increase with a higher mass density (a structure with a low density of 10 mg/cm^3 has a thermal conductivity of 0.26 $Wm^{-1}K^{-1}$ while one with 30 mg/cm^3 has a thermal conductivity of 2.28 $Wm^{-1}K^{-1}$).[69, 82]

3D graphene materials built from carbon oxides can have a wide diversity of specific surface areas ranging from 100 to 2000 m^2/g, which can be controlled by the choice of reaction conditions.[83] Their accessible surface area is usually high due to the common presence of micro-, meso-, and macropores throughout the structures.[69] A distinct property of such CO/CO_2 derived 3D graphene materials is the presence of a small number of oxygen-bearing groups or oxygen dopants varying from ~1 % to ~12 %.[84] Their tightly interconnected porous frameworks lead to a low interface resistance (0.4-8 kΩ/sq corresponding to 200-300 S/m) thus making them capable of conducting electricity, although at a far smaller rate than exfoliated graphene.[69, 83a, 85] Owing to their intrinsic microscopic structure, they demonstrate a higher degree of mechanical strength when compared to macroscopic 3D graphene materials and the powdery form of 3D graphene materials built from carbon oxides opens up their use in macro 3D constructing strategies such as 3D printing.[69]

3D graphene architectures solve the problem of the tendency of graphene layers to restack, which is responsible for the loss of large surface areas.[70b] They are expected to find future utility in applications such as in solar cells,[86] electrochemical sensors,[87] batteries[88] and flexible electronics[89]. They are showing promising results for their use

in supercapacitors[90] and metal-ion-batteries.[91] Some reported examples of 3D graphene architectures have been reported to exhibit remarkable reversible capacity (540 mAh/g) in Li^+-ion batteries[92]. Additionally, a porous 3D graphene foam used in a flexible Al^{3+}-ion battery was demonstrated to have a low charge voltage (cutoff 2.3 V), high capacity (123 $mAhg^{-1}$ at a current of 5000 mAg^{-1}) and excellent cycling ability with little loss of capacity after 10 000 cycles.[93] Thus, 3D graphene structures hold great promise as anodes for use in various novel metal-ion batteries to overcome the limitations of the commonly used graphite anodes in Li^+-ion batteries. 3D graphene architectures are furthermore explored for novel uses in other types of batteries for example as cathodes in Li-S batteries or as air cathodes in Li-O_2 air batteries, wherein some successful applications have been reported that, however, still leave room for improvement and as such require further research to solve issues like instability.[69, 94] Furthermore, 3D graphene materials have received attention as counter electrodes in solar cells due to their promising conductivity as well as in their use as electrodes in flexible electronics stemming from the inherent flexibility of macroscopic 3D graphene architectures such as graphene foams,[95] sponges[96] and aerogels[97] that can still exhibit excellent electrochemical performance.[85] There is also an interest in 3D graphene structures in the role of gas- and electrochemical sensors with reports stating that a 3D graphene foam exhibited a remarkable sensitivity to dopamine.[69, 87] Their sensitivity to structural deformation also allows their use as strain sensors.[98] Further applications in photodetectors or plasmonic sensors have been reported as well.[69, 99]

One synthesis method for 3D graphene structures includes graphene oxide reduction, which involves the elimination of oxygen-containing groups on its plane.[100] For this purpose, various strategies are employed, such as chemical reduction using a series of reducing agents like for example $NaBH_4$,[101] photocatalytic reduction,[102] laser/flash irradiation,[103] hydrogen-plasma/arc discharge[11c] and many more. A second synthesis method involves the decomposition of hydrocarbons to obtain active carbon building blocks for the growth of graphene architectures, for example using metal particles as catalysts.[104] The active carbon building blocks would then grow creating 2D and 3D thin-layer graphene materials.[10b] A third synthesis method uses the decomposition of hydrocarbons into active carbon radicals followed by the rearrangement into an energetically favourable graphene structure, also known as graphenization.[105] For graphenization, metals that can dissolve in amorphous carbon, like Co and Ni, have

been shown to be able to rearrange the amorphous carbon into graphene layers, especially when annealing at temperatures of 600 °C.[106] K_2CO_3 can also be used for graphenization at high temperatures of 900 °C in a process involving the melting of K_2CO_3 and graphene sheet catalysis by *in situ* formed metallic K.[107] Catalyst-free forms of graphenization are also known, however, they require harsh conditions such as temperatures up to 3000 °C.[108] A further synthesis method for 3D honeycomb-like structures applies a reaction between Li_2O and CO, where the products of the reaction are elemental carbon and Li_2CO_3, which serves as an isolator and prevents the restacking of graphitic layers while determining the 3D structure.[83a]

1.1.1.6 The importance of Li-ion batteries

Energy storage devices are of great importance in the switch from fossil fuels to renewable energy sources. In this regard, secondary (rechargeable) batteries like Ni-Cd or Pb-acid batteries receive the most attention.[109] However, these batteries suffer from issues such as toxicity and memory effect, which is an effect that occurs when the battery is continuously charged and discharged to the same level, where the battery "remembers" the point at which recharging was started, leading to a sudden voltage drop when the same level is reached during discharging, giving the appearance of a discharged battery.[110] Lithium-ion batteries (LIBs) have established themselves as the high working voltage having battery of choice that doesn't suffer from memory effect. Their light weight and good performance have led to their widescale application in vehicles, aviation and communications.[109]

1.1.1.6.1 A short refresher on the function of Li-ion batteries

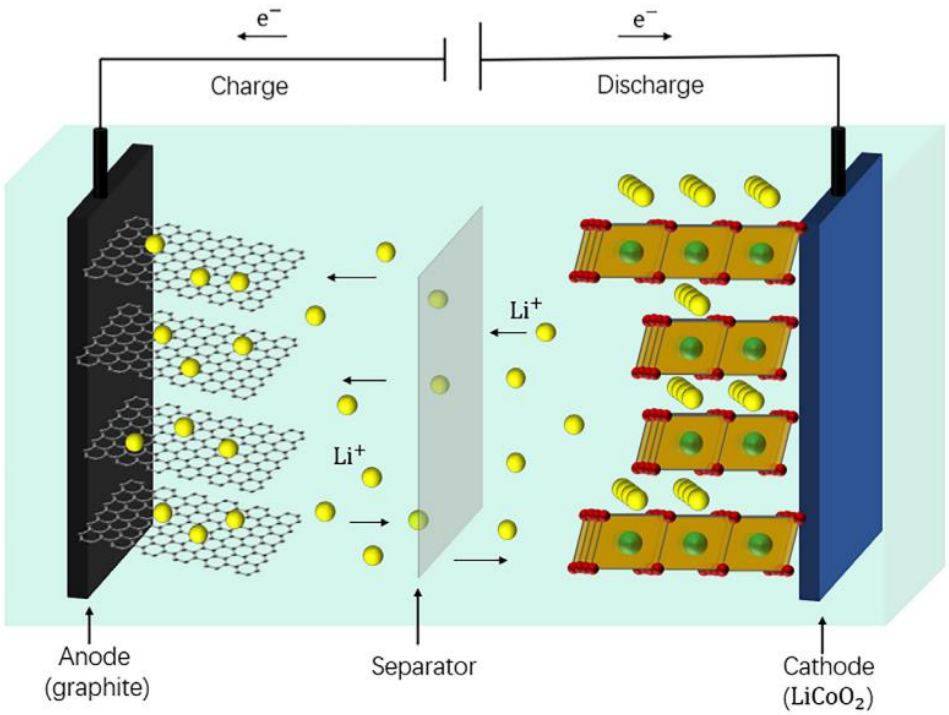

Fig. 2. Schematic illustration of LIBs.

Figure 10: *Schematic description of Li^+-ion Batteries (LIBs).*[109]

Lithium-ion batteries consist of a cathode, an anode, an electrolytic separator and a current collector as visualized in **Figure 10**. Classically, the cathode consists of $LiCoO_2$ and the anode consists of graphite. During the charging process, Li^+-ions are extracted from the cathode and embedded in the anode after travelling through the electrolyte and separator, while simultaneously electrons pass from the cathode to the anode through an external circuit to maintain the overall neutrality. During the battery discharge, this process occurs in reverse. Since the insertion/extraction of Li^+-ions coincides with the flow of electrons through a peripheral circuit, a mutual conversion between electrical and chemical energy is possible.[109]

1.1.1.6.2 Current strategies in the advancement of carbonaceous anode materials

Currently, layered $LiMO_2$ (M=Co, Ni, Mn) and $LiFeO_4$ are used as cathode materials in commercial LIBs and the anode material mainly consists of graphite. However, graphite cannot meet the demand for high-performance lithium batteries due to its comparatively low theoretical specific capacity (372 $mAhg^{-1}$), which is why alternative anode materials for LIBs are currently being pursued.[109, 111]

Important properties for anode materials include the potential energy of the anode being lower than the LUMO of the electrolyte, increase in storage sites of Li^+-ions, diffusion rate, high specific surface area, stability life, safety, shape and flexibility of the

battery, dynamic diffusion of ions over long distances, density, thickness and porosity.[109]

Carbonaceous materials can be categorized as graphitic and non-graphitic carbon. Graphitic carbon (also known as soft carbon) is known to be highly crystalline, while non-graphitic carbon (also known as hard carbon) shows an amorphous form. Both forms include sp^2- and sp^3-hybridized carbons in graphite structures consisting of graphene planes piled up over each other.[112]

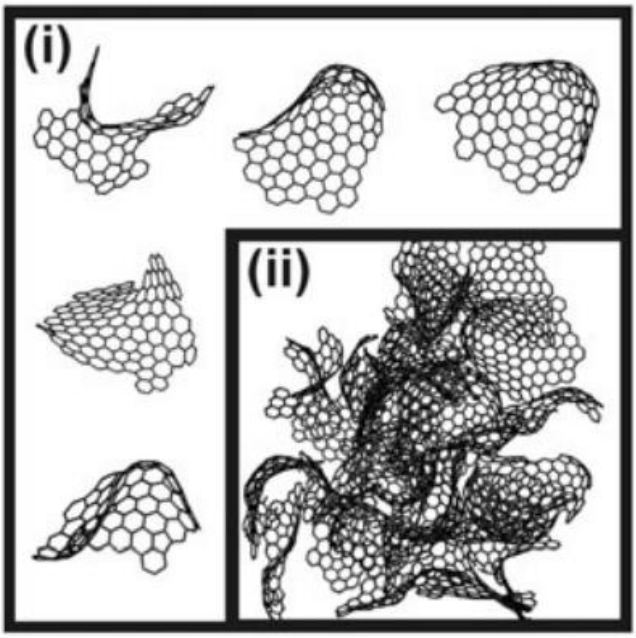

Figure 11: *Model of hard carbon.[113]*

A comparative study was conducted comparing the viability of graphite, soft carbon and hard carbon and showed that hard carbon is more favourable as an anode in LIBs due to its higher capacity retention (96.9 %) and rate capability (72.5 % energy retention).[114] Hard carbons are characterized by their large fraction of randomly distributed sheets that cannot be reshaped into graphite at a temperature of 3000 °C and are known for their porous, wire-like and microspherical morphologies, which stem from the rigid cross-linking of precursors during pyrolysis. These unique structural properties allow for a shortening of Li^+-ion transport distance and lead to an abundance of active sites for charge-transfer reactions. However, they are less competitive to graphite in commercial LIBs due to issues concerning “loss” during the first charge/discharge cycle, in which some lithium is trapped inside the carbon matrix. Therefore their reversible capacity is low (up to ~300 $mAhg^{-1}$)[115] as well as hard carbon’s low initial coulomb efficiency (62 %)[116].[117]

Further research strategies focus on the analysis of carbon nanotubes and graphene as anodes in LIBs.[109]

1.1.2 Cubic graphite

1.1.2.1 Structure of cubic graphite

The structure of cubic graphite was proposed by Gibson *et al*. in 1946 as a lattice of three-dimensional repetition of *o*-tetraphenylene residues.[118] Its name comes from the cubic symmetry and not its relationship between the solid-state structure and that of normal graphite.[119] It is also been referred to as polybenzene. [120]

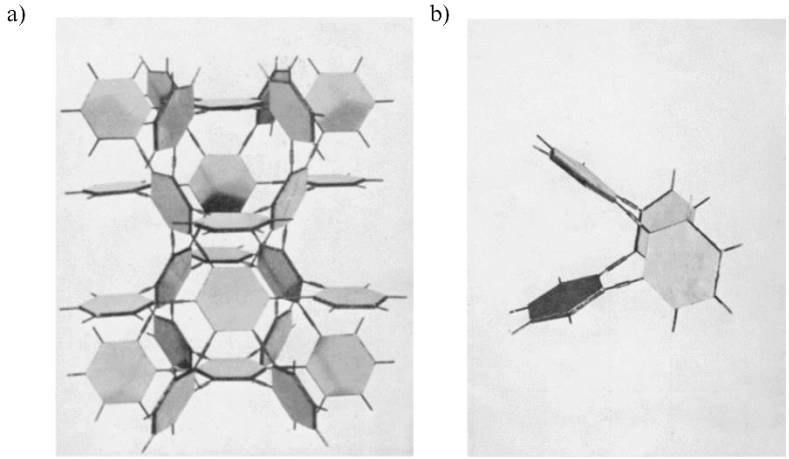

Figure 12: *a) Image of cubic graphite; b) Image of subunit of cubic graphite; as proposed by Gibson et al.[118]*

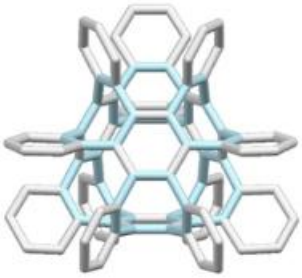

Figure 13: *Cubic Graphite as depicted by Müllen et al.[121]*

According to Shen *et al.*, Cubic graphite is a structure fully built from benzene rings where each benzene ring is attached to further six different benzene rings with a dihedral angle between the rings being 109.5°. They also divide the benzene into two groups that they illustrated with plain and bold rings as seen in **Figure 14**. Their structure has every bold benzene being bound to six plain benzenes and *vice versa*.[122] Furthermore, they describe an analogue of cubic graphite, named “phenylogous cubic graphite”, also depicted in **Figure 14**.[123] It is formed by hexaphenylbenzene subunits

that are bound together in a similar form to the benzene rings in cubic graphite and it is expected to be easier to synthesize due to its larger cavities and the larger structure of precursors.[122-123]

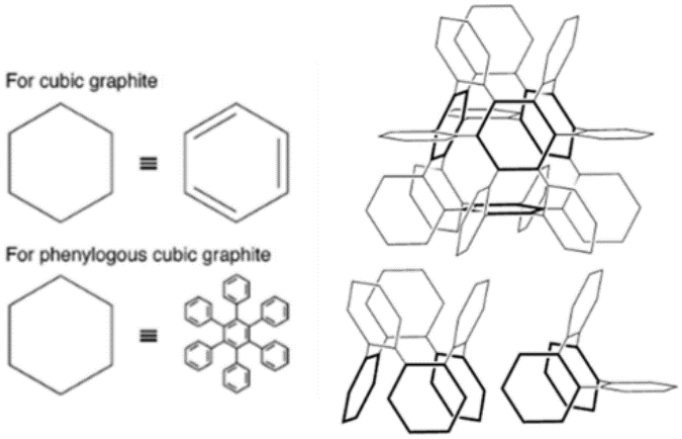

Figure 14: *Cubic graphite and phenylogous cubic graphite by Shen et al.[122]*

In the proposed structure by Baughman *et al.,* all the carbon atoms are equivalent to each other. They are positioned in *para* position relative to each other in a poly(*p*-phenylene) C-chain. Every phenyl ring in the structure is part of three equivalent poly(*p*-phenylene) C-chains.[124] The structure includes carbon cages, which are formed by 48 C-atoms. 24 of these are part of 4 phenyls that are coordinated tetrahedrally around the centre of the cage. The other 24 C-atoms belong to 12 phenyls. They each contribute one aromatic bond and two carbons to the cage.[124]

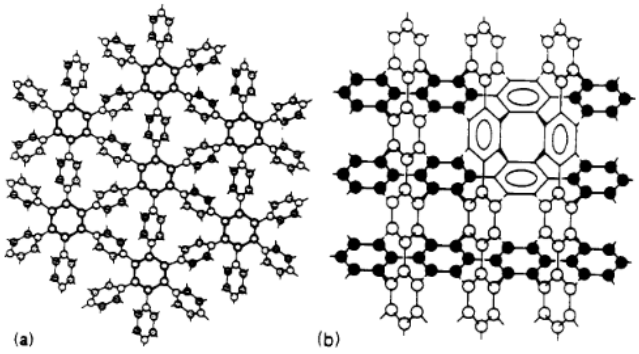

Figure 15: *Illustrations of sheets of cubic graphite a) as seen from the [111] direction and b) viewed through the [100] projection; as imaged by Baughman and Cui.[124]*

According to O'Keeffe *et al*., cubic graphite, or as they call it - 6.8^2D, or polybenzene, consists of six- and eight-membered rings occurring in the ratio 2:3 and has a primitive unit cell of 24 atoms and the space group $Pn\bar{3}m$. They describe it as consisting of benzene rings connected in a three-dimensional framework by single bonds. They claim that the initial paper by Gibson *et al*. described the wrong symmetry and thus

they propose their own. According to them, the unit cell consists of four hexagonal rings on the faces and a tetrahedron as shown in **Figure 16**.[120]

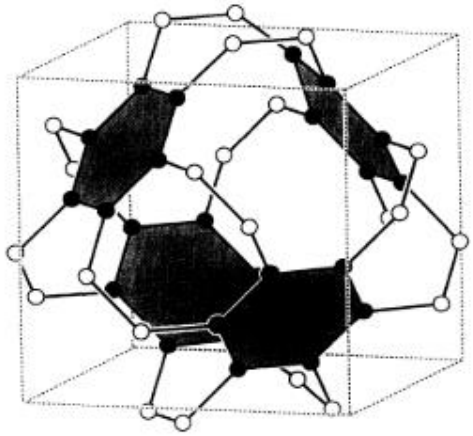

Figure 16: *Unit cell of the polybenzene (6.8^2 D) structure by O'Keeffe et al.*[120]

Ockwig *et al.* claim that following electronic structure calculations cubic graphite should be thought of like aromatic C_6 rings linked by single bonds.[125]

1.1.2.2 Analogues of cubic graphite

In some papers, the term “cubic graphite” refers to a different structure. For example, Pokropivny *et al.* use the name “cubic graphite” to describe a “cubic fullerite” structure consisting of fullerene C_{24} units bonded together in such a way as to form hexagonal C_6 faces and quadratic C_4 faces.[126] They cite papers describing the discovery of this kind of “cubic graphite” by Aust and Drickamer[127] as well as Bundy and Kasper[128]. They also claim that Fedoseev *et al.*[129] and Slodkevich[130] discovered the same structure in 1976 and 1980 respectively but their publications could not be found after searching various databases. This might be due to having been published in the USSR and lost with time. In the paper by Aust and Drickamer[127] the name “cubic graphite” is never used but they claim that “the new phase could be indexed as cubic with a unit cell edge of 5.54 Å” when discussing their newly discovered form of graphite. Bundy and Kasper[128] also don’t use the expression “cubic graphite” but they rather mention “cubic diamond”. Pokropivny *et al.*[126a] curiously also cite a paper by Smolyar *et al*.[131] from 2002 where they accuse Aust and Drickamer of having made a mistake by assigning cubic graphite to the phases interpreted (which they had apparently admitted in private discussion but never reported in the scientific literature), and Smolyar *et al*. further claim that they have actually revealed the correct cubic graphite.[131] The discussed forms of “cubic graphite” do not seem to match the previously discussed structures proposed by Gibson *et al*.[118] and O’Keefe *et al*.[120] and this example shows

that the term “cubic graphite” has been used to describe different forms of carbon structures throughout the years, perhaps because of cultural boundaries and misinterpretations.

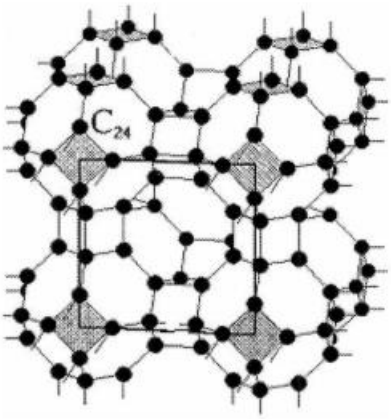

Figure 17: *Structure of cubic fullerite by Pokropivny et al. which they call “cubic graphite”*[126b]

Baughman *et al*. describe analogues of cubic graphite they call cubic α-graphyne and β-graphyne. Their description of α-graphyne reads as follows: “Expansion of the polyphenylene bonds between phenyl rings in cubic graphite by insertion of -C≡C- units provides the cubic carbon phase called cubic α-graphyne, which has six sets of nonparallel chains of the type found in the known hydrocarbon polymer $(-C{\equiv}C-C_6H_4-)_x$, poly(p-phenylene xylylidene)” Regarding cubic β-graphyne they state that “each carbon atom is in either one or two $(-C{=}C-C{\equiv}C-C{=}C-)_x$ chains within six sets of non-parallel, non-planar chains of this type”. It is supposed to provide “a three-dimensional array consisting of the same type of carbon ring as found in the known cyclic hydrocarbon $(=HC-C{\equiv}C-CH=)_3$.” with each of the rings being directly sp^2-sp^2 bonded to six equivalent rings building a covalently bonded three-dimensional structure. They describe that both cubic α-graphyne and cubic β-graphyne are named based on structural relationships to graphyne, a planar sheet carbon phase Baughman and Eckhardt proposed in 1987 and they claim that these relationships are “analogous to that between cubic graphite and two-dimensional graphite sheets”.[124, 132]

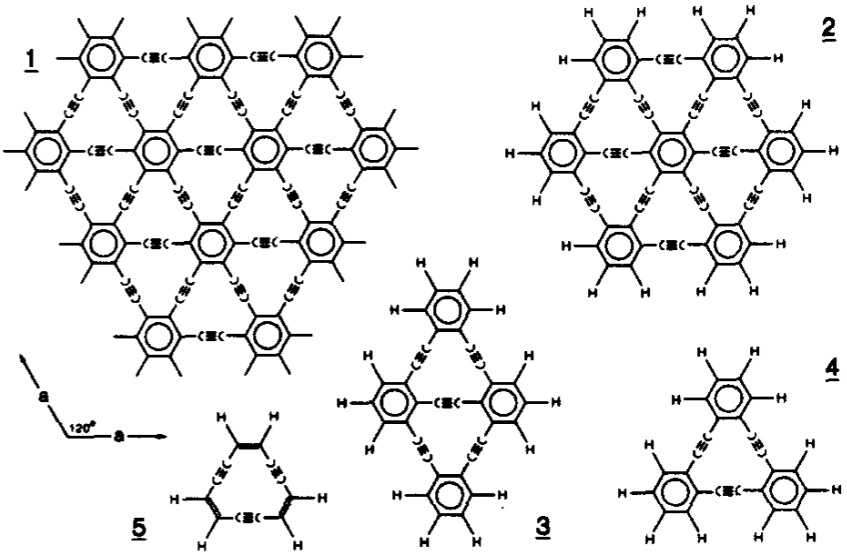

Figure 18: *Proposed structure of graphyne (1) and four model compounds (2, 3, 4 and 5) by Baughman et al.*[132]

1.1.2.3 Expected properties of cubic graphite

The material has never truly been synthesized, so all proposed properties rely solely on predictions rather than on empirical data. Calculations predict that cubic graphite shares features with benzene C_6H_6 since the bonds in the planar C_6 rings are predicted to be of almost identical lengths and the band gap calculated for it is 3.4 eV, which is similar to the highest occupied molecular orbital-lowest unoccupied molecular orbital separation in benzene, which is 3.7 eV. Inside the molecule hexaphenyl benzene $C_6(C_6H_5)_6$ a 42-atom-containing fragment of cubic graphite can be found, which suggests similar bond lengths. Hexaphenyl benzene was discovered to have bonds in the central benzene ring of 1.397 Å while cubic graphite was calculated to have 1.396 Å. The bond length between rings in hexaphenyl benzene was measured to be 1.499 Å while the calculations of cubic graphite predict 1.474 Å.[120]

The density of cubic graphite (2.136 gm/cm^3) was calculated to be close to the density of graphite (2.266 gm/cm^3). It has a high predicted maximum charge storage capacity (397 mA hr/cm^3) and the bandgap and redox potentials for cubic graphite have been calculated to be similar to those of poly(p-phenylene) being Eg = 3.0 V, Eox. = 0.9 V, and Ered. = -2.12 V (versus SCE).[124]

The structure was calculated to be way more energetically stable than the C_{60} fullerene by 0.23 eV/atom while having comparable energy to previously suggested structures with larger unit cells. Furthermore, it is predicted to have insulating properties.[120]

Cubic graphite is predicted to form reversible charge-transfer complexes without the need for phase nucleation and growth for doping and de-doping. The van der Waals

radius of the pathway constrictions (0.49 Å) is calculated to be large enough for the rapid transport of Li^+-ions and the van der Waals void radius (1.28 Å) is calculated to be big enough to incorporate ions like K^+. Such large ions are predicted to remain trapped and immobile thus not being able to react with the atmosphere. The cubic symmetry and three-dimensional electronic structure of cubic graphite lead to interest in the use of the donor-doped material for superconductivity.[124]

Cubic graphite contains large cavities that suggest possible applications for intercalation compounds like small alkali atoms in $LiCl_2$.[120]

Owing to the presence of sufficiently large diffusion channels for lithium cations it is predicted that cubic graphite might show potential as a material used in rechargeable Li-Ion batteries. Additionally, the absence of required phase nucleation during charging processes as well as high thermal and mechanical stability are predicted – all of which would make it a potential candidate for novel and better battery designs.[119] It is also predicted to have reversible donor dopability and radiation stability.[124]

The predictions propose extremely high cycle life, high cycle rate, and high-capacity redox devices. These could potentially be included in rechargeable batteries, battery-like supercapacitors and electrochromic displays. Further application possibilities are for example radiation-hard, high-temperature semiconductor devices as well as highly durable, highly reflective coatings.[124]

It is speculated that the presence of even-membered rings makes cubic graphite a candidate for new compound solids (such as BN) and its low energy and low-density open structure opens applications such as gas storage. The cubic graphite net could also be the basis for an MOF structure when designing the primary units with a metal-organic composition.[120, 125]

1.1.2.4 Hurdles and approaches in the synthesis of cubic graphite

A synthesis seems to be highly difficult and has hitherto never been accomplished. One approach proposed by Gibson et al. includes a reaction of C_6I_6 with metallic sodium that could not yet be performed successfully.[118]

Another approach proposed by Ockwig *et al*. would be to perceive the structure as consisting of one eight- and four six-membered rings that are to be chemically joint. They assume that with this approach four-membered and planar structures like graphite are unlikely to form and claim that this approach would indeed form the desired six and eight-membered rings in the correct 2:3 ratio. They anticipate that a C-C bond-forming reaction in organic chemistry can be utilized to achieve this goal but

themselves, coming from the field of materials chemistry, do not suggest a concrete synthetic method.[125]

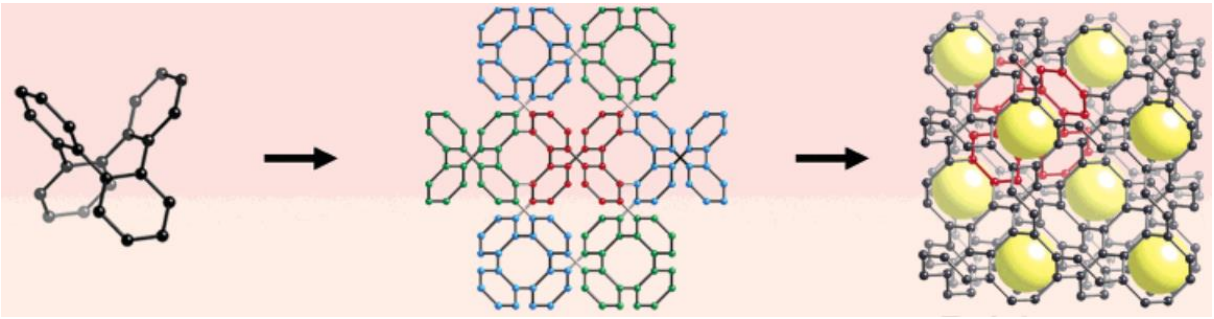

Figure 19: *Overview of synthesis strategy for cubic graphite as proposed by Ockwig et al.*[125]

1.2 Tetraphenylenes

Tetraphenylene (also called tetrabenzo[a,c,e,g]-cyclooctatetraene or tetrabenzo[8]annulene) is a non-planar saddle-shaped molecule consisting of four benzene rings at opposite sides of a central eight-membered ring in an alternating up and down arrangement above and below the average plane of the molecule. Since the central cyclooctatetraene ring lacks planarity, it does not exhibit aromaticity.[133] Its first synthesis was published by Rapson *et al.* in 1943, [134] the structure was determined by Karle *et al.* in 1944 [135] and the structure was confirmed by X-ray crystallography by Irngartinger *et al.* in 1985.[136]

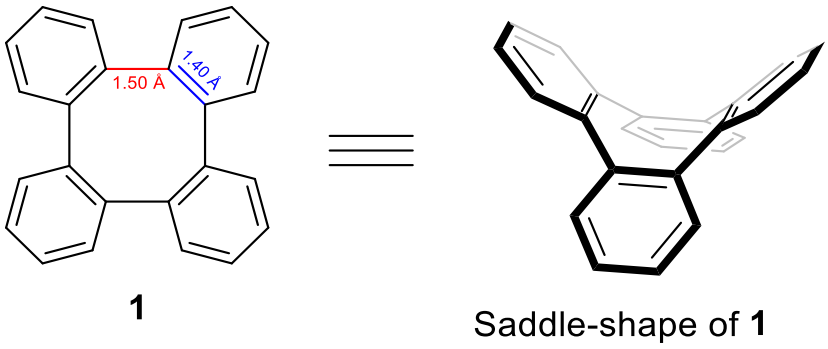

Figure 20: *The saddle-shaped structure of tetraphenylene* ***1****.*

1.2.1 Chemical properties of tetraphenylenes

Tetraphenylenes are known for their extremely high inversion barrier, being so high that the molecule will not flip at 550 °C in thermal experiments due to a high energy barrier of 80 kcal/mol, meaning that their saddle shape is thermally highly stable. They are also achiral belonging to the D_{2d} point group but nonetheless, the introduction of substituents to the benzene rings can contribute to the chirality of the molecule.[133b]

1.2.2 Possible uses of Tetraphenylenes

Due to the strong host-guest interactions between tetraphenylene and certain solvent molecules (like CH_2Cl_2, $CHCl_3$, benzene, and cyclohexane)[137], the structure has garnered interest for clathrate inclusion compounds. The distinct shape of tetraphenylenes enabled the creation of tetraphenylene-based tweezers that have shown good molecular recognition towards a paraquat derivative. Further hypothesized uses for tetraphenylene derivatives include as a building block in self-assembly for supramolecular nanomaterials. The stable and rigid structure makes tetraphenylene an excellent molecular framework for the design of novel chiral catalysts or ligands in asymmetric synthesis.[133b] Additionally the careful design and manipulation of the unique 3D structure of chiral tetraphenylenes and its derivatives enables, applications in supramolecular chemistry, liquid crystalline materials, organic light-emitting diodes and helical scaffolds. However, the practical use of chiral tetraphenylene derivates has been challenging due to the difficulty and rarity of synthesis methods for enantiopure products.[133c]

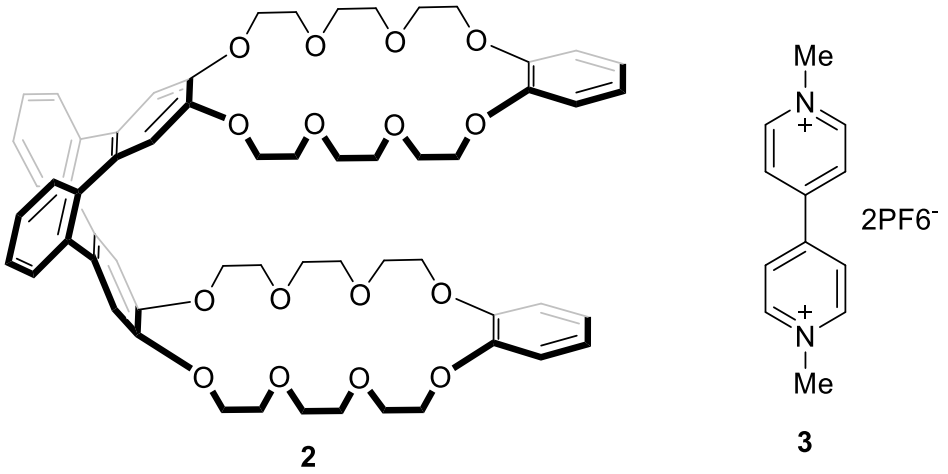

Figure 21: *Tetraphenylene-based molecular tweezers **2** and guest molecule **3**.*

1.2.3 Tetraphenylene synthesis

In 1943, Rapson *et al.* reported the first synthesis of tetraphenylene *via* a Grignard reaction with the assistance of a copper chloride using 2'-dibromophenyl as starting material yielding 16% of "almost pure tetraphenylene".[134]

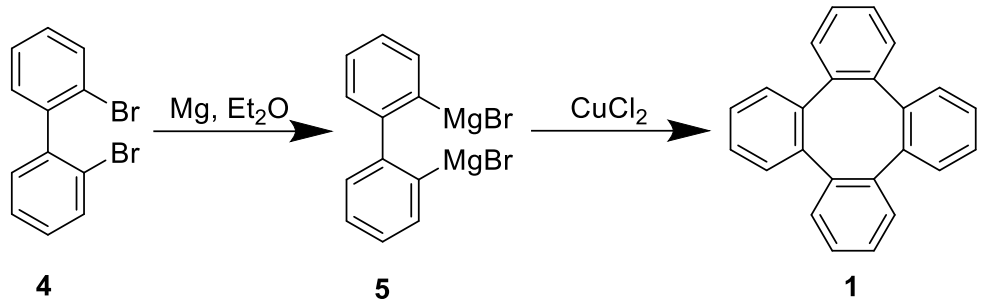

Scheme 1: *The first synthesis of tetraphenylene* ***1****.*

Since then, various other synthesis methods for tetraphenylenes and their derivatives have been discovered which will be explored in the following paragraphs.

1.2.3.1 Pyrolysis and/or metal-catalyzed dimerization of biphenylenes

In 1967, Lindow and Friedman published the hitherto highest-yielding synthesis of tetraphenylene involving the pyrolysis of biphenylene at 400 °C in an evacuated sealed tube with a yield of 96 %. It has been discovered that the reaction occurs through the dimerization of biphenylene radicals. [138] Further dimerizations are also possible under the catalysis of metals such as Ni, Pd, Pt and Rh with yields up to 92 %.[139] Unfortunately, pyrolysis is not a viable method for the synthesis of substituted tetraphenylene derivates and dimerization is limited by the availability of biphenylene.[133a]

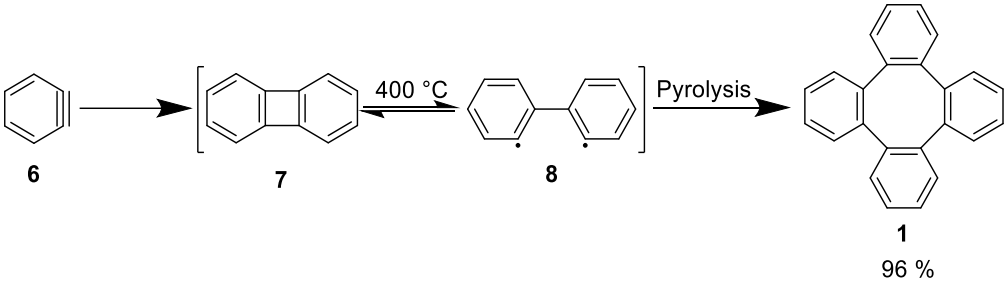

Scheme 2: *Pyrolysis synthesis of tetraphenylene* ***1****.*

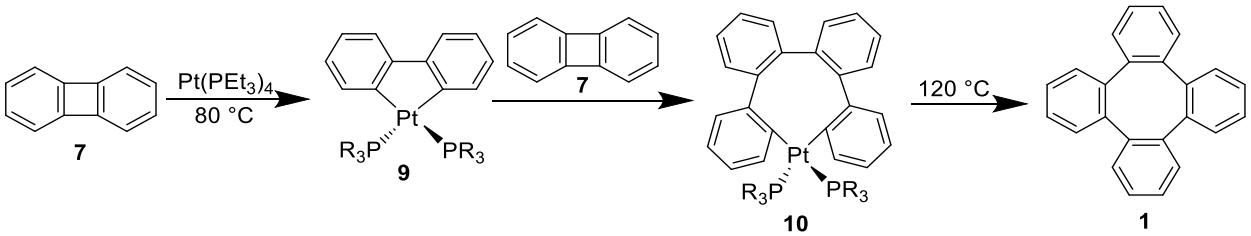

Scheme 3: *Pt-catalysed biphenylene dimerization synthesis of tetraphenylene* ***1****.*

1.2.3.2 Diels-Alder cycloaddition and subsequent deoxygenation

A versatile synthesis strategy for tetraphenylenes consists of a cycloaddition reaction between a planar diyne and a furane ring, which leads to the formation of an endoxide that can be deoxygenated with a reducing agent such as $LiAlH_4$ with $TiCl_4$.[140] This

cycloaddition-deoxygenation protocol allows for the controlled synthesis of substituted tetraphenylenes depending on the chosen substituted diyne and furane ring.[133a, 141]

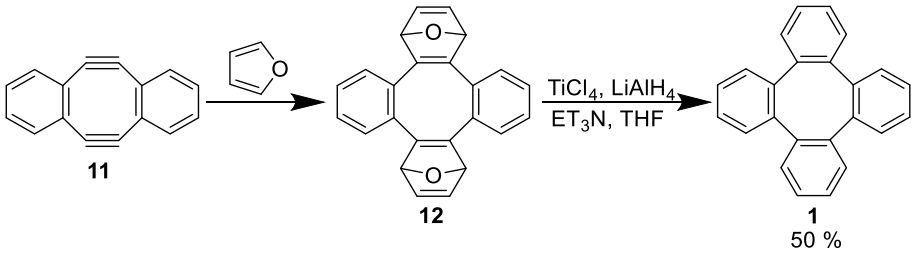

Scheme 4: *Synthesis of tetraphenylene **1** by cycloaddition-deoxygenation protocol.*

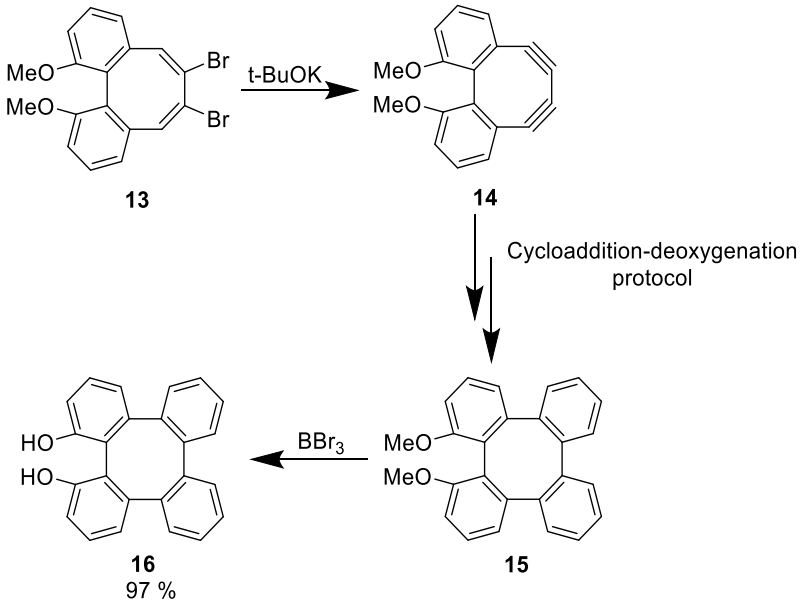

Scheme 5: *Synthesis of substituted tetraphenylene derivative **16** by cycloaddition-deoxygenation protocol.*

1.2.3.3 Oxidative coupling reaction of dilithiobiphenyl derivatives

Coupling reactions *via* organometallic reagents utilizing transition metal catalysts are of great use in the synthesis of tetraphenylenes and they are seen as their principal preparative method. The process involves the lithiation of a dihalogenated biphenyl structure **17** into a dilithiobiphenyl structure **18** followed by a coupling reagent like $CuCl_2$ or $CuBr_2$ for transmetallation and the later formation of tetraphenylenes **19** and biphenylenes **20**. The selectivity between those two products is highly dependent on the reaction factors.[142] This procedure is beneficial since the structural features of tetraphenylenes with various substituents can be manipulated in multiple ways. The method can also be applied for the synthesis of oligotetraphenylenes like a racemic double helical octaphenylene **24**.[143]

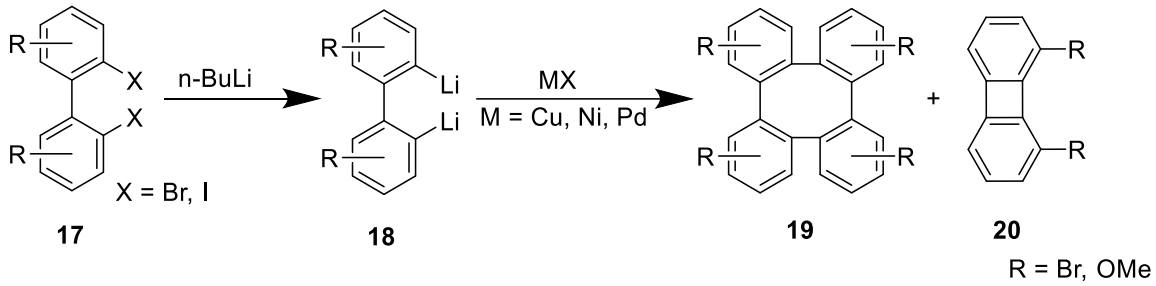

Scheme 6: *Synthesis of substituted tetraphenylene derivative **19** by metal-mediated oxidative coupling.*

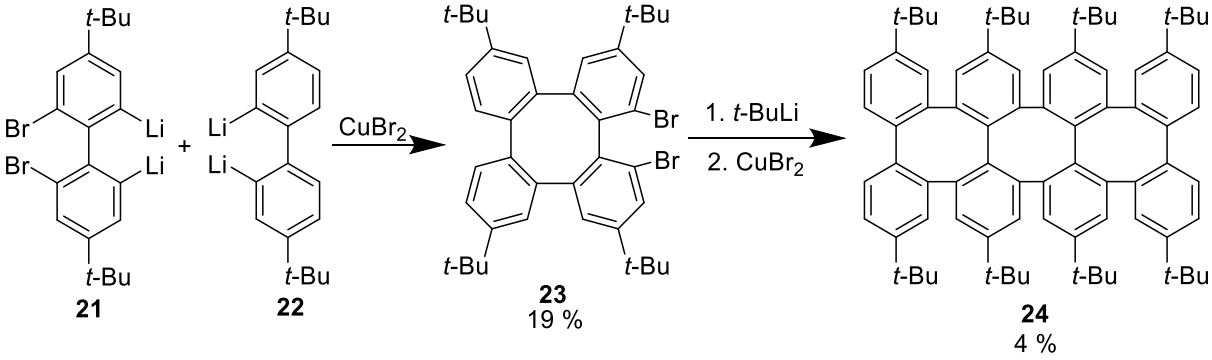

Scheme 7: *Synthesis of a racemic double helical octaphenylene **24** by oxidative coupling.*

1.2.3.4 Transition metal-catalysed double coupling reactions

The application of transition metals like Pd for catalysis of double coupling reactions like Suzuki or Ullman reactions or dimerizations for the synthesis of tetraphenylenes gives a straightforward approach toward the regio- and stereospecific synthesis of a variety of diversely symmetrically and unsymmetrically substituted tetraphenylenes. Some reactions as such have[144] been capable of giving good yields of up to 92 % while performed on a gram scale.[133a, 145]

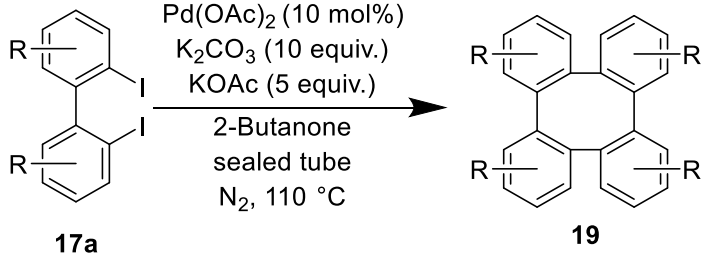

Scheme 8: *Double Ullmann coupling reaction of diiodobiphenyl **17a**.*

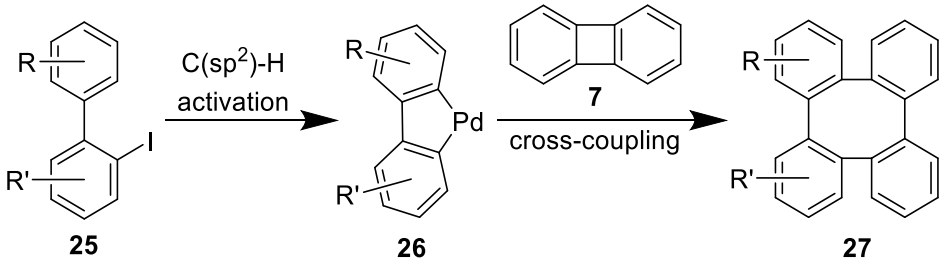

Scheme 9: *Palladium-catalyzed C(sp^2)– H-activation-enabled coupling reaction.*

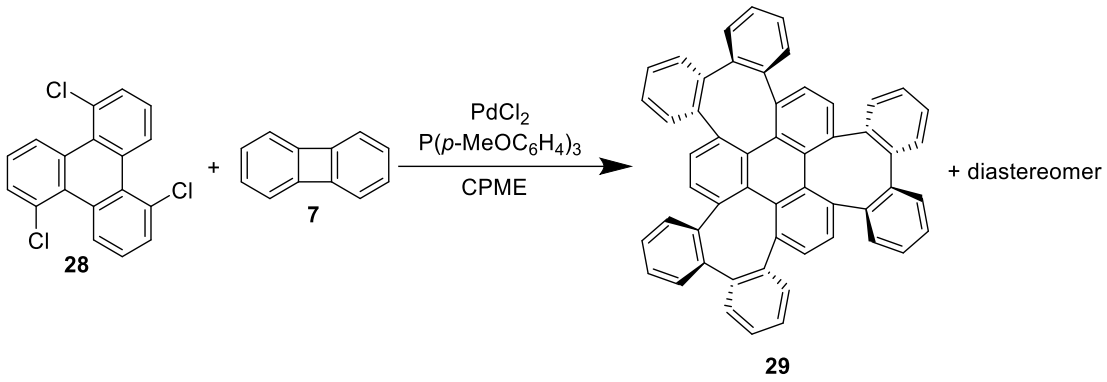

Scheme 10: *Annulative coupling of PAH that forms eight-membered rings* ***29****.*

1.2.3.5 Inter- and intramolecular cycloadditions of two ortho-phenylene-tethered triynes

The use of a [2+2+2] cycloaddition of tryines for the synthesis of chiral tetraphenylenes using catalysts like (R)-Cy-BINAP has resulted in yields of up to 93 % with excellent enantioselectivities of up to 99 %.[146]

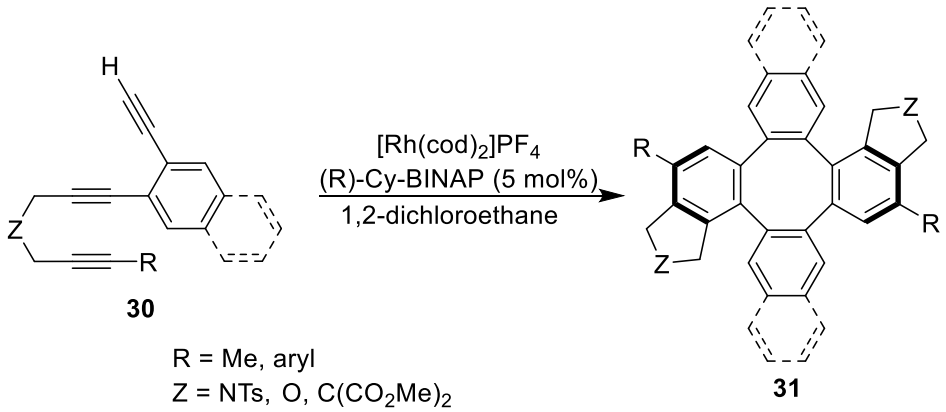

Scheme 11: *Cycloaddition of triynes* ***30*** *in synthesis of tetraphenylenes* ***31****.*

1.2.3.6 Scholl reaction

A further reported synthesis method for saddleshaped tetrabenzo[8]circulenes involves the use of cyclic octaphenylene precursors in a Scholl reaction using $Cu(OTf)_2$ and $AlCl_3$ in CS_2 with yields of up to 35 % for some derivatives when the reaction was preceded with $FeCl_3$ in CH_2Cl_2.[147]

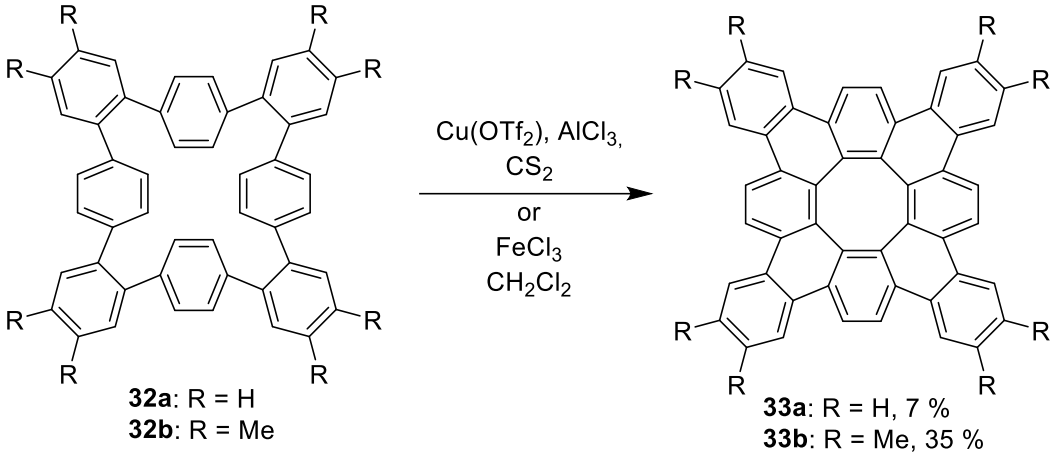

Scheme 12: *Scholl reaction for the synthesis of tetraphenylenes* ***33****.*

1.2.3.7 Tetrameric condensations

A synthesis method for tetraphenylenes as well as circulenes includes the application of tetrameric condensation, which can for example occur with quinons under harsh conditions with strong acids like $AlCl_3$.[148]

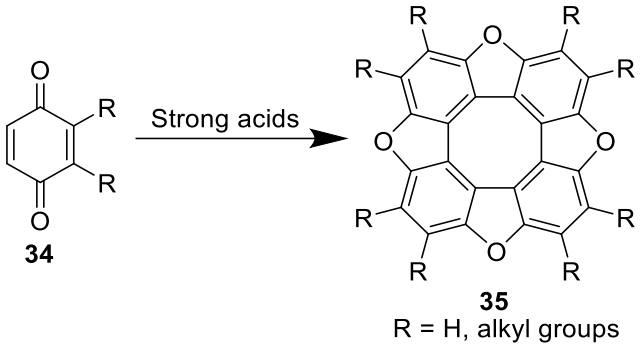

Scheme 13: *Tetrameric condensation for the synthesis of tetraoxa[8]circulenes* ***35****.*

1.2.3.8 Ring expansion

In 2022 a novel method was published that allows for the synthesis of saddle-shaped polycyclic arenes fused with cyclooctatetraene, otherwise known as dibenzo[3,4:7,8]cycloocta[1,2-l]phenanthrenes, by the application of $Cu(OTf)_2$ catalyst with 2,3-Dichlor-5,6-dicyano-1,4-benzochinon (DDQ) on *o*-biphenyl-tethered methylenecirculenes fused with a seven-membered ring. The cyclooctatetraene can be further modified into a tetraphenylene structure, for example by a Diels-Alder cycloaddition and deoxygenation. The mechanism of the ring expansion of the seven- to eight-membered ring occurs *via* selective single-electron oxidation of the benzylidene moiety, intramolecular spirocyclization, and 1,2-aryl migration sequence with radical and cation intermediates.[149]

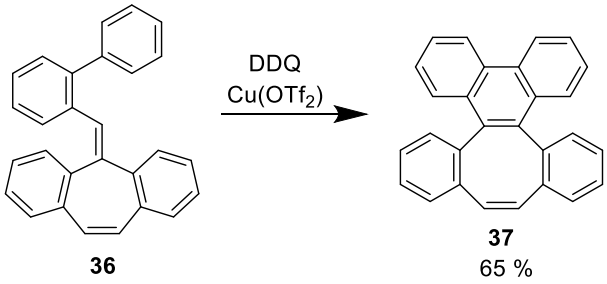

Scheme 14: *Ring expansion strategy for the synthesis of eight-membered rings* ***37****.*

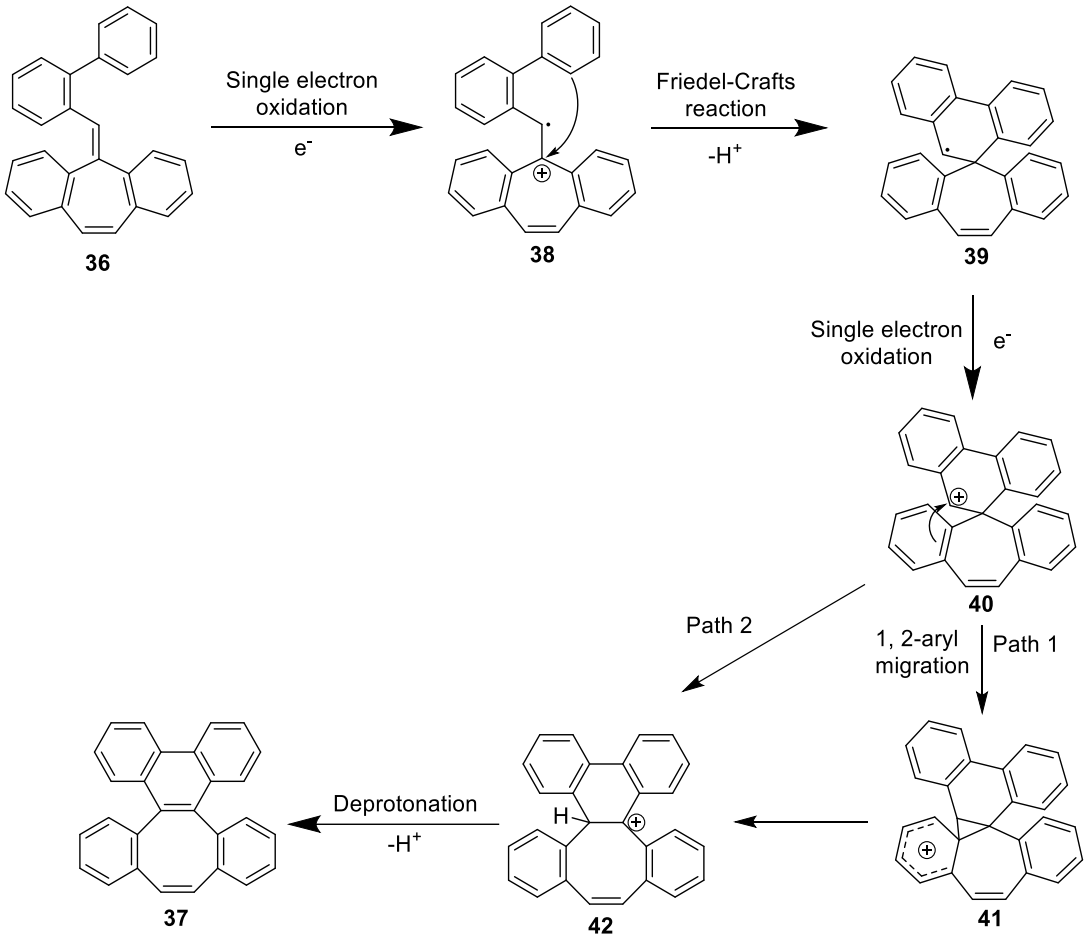

Scheme 15: *Proposed mechanism for oxidative ring expansion of* ***36****.*

1.3 The science of PXX and photocatalysis

The discovery, development and use of light-mediated catalysis have given rise to a whole new way to exploit reactions for the formation of nontraditional bond constructions and unique chemical reactivities that can activate substrates by selectively targeting them with a uniquely chosen photon-absorbing catalyst. Photoredox catalysis is being used in many applications such as the development of novel solar cell materials or water splitting.[150]

1.3.1 The concept of photocatalysis explained

Photoredox catalysis allows for many unique chemical reactivities under milder conditions while harnessing a more controlled form of radical chemistry. For a photophysical process to occur, light (*hv*) must be absorbed by a molecule, which then becomes an electronically excited molecule. Usually, this involves the excitation of an electron to a higher energy level from a ground state singlet (S_0) to a singlet excited state. Depending on the energy given to the electron, higher singlet excited states with higher vibrational energies can be reached, however, quickly relaxation to a lowest energy vibrationally equilibrated S_1 will occur. Next, either a radiative or a non-radiative pathway can be followed. If a radiative pathway is taken, a transition back to lower states like S_0 will occur concurrently with the emission of light. If a non-radiative pathway is followed, then energy will dissipate in a nonradiative transition in the form of heat. The return from S_1 to S_0 can occur through the radiative transition of fluorescence or the nonradiative transition of internal conversion (IC) or through a third pathway involving the spin-forbidden process of intersystem crossing (ISC) to the triplet state T_1. The transition from the triplet state T_1 back to the original singlet state S_0 is spin-forbidden, which usually makes T_1 states the most long-living process. S_1 and T_1 states are long-living enough (lifetime of nanoseconds to milliseconds), to go through energy and electron transfer processes in bimolecular reactions. The name for this process of excitation and electron transfer between an excited state molecule and a ground state molecule is called photoinduced electron transfer.[151]

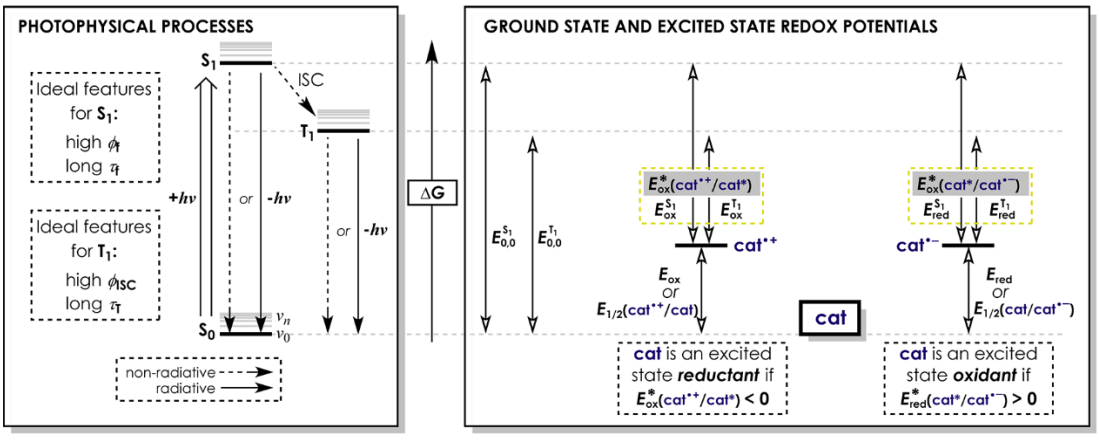

Figure 22: *Photophysical and Electrochemical Processes and Properties of Photoredox Catalysts.*[151]

Figure 23 shows the typical catalytical cycles for reactions using photoredox catalysts. Photoredox catalysts either work as excited state reductants, when the excited state cat* donates an electron or as excited state oxidants, when the excited state cat* instead accepts an electron. Excited state reductants take part in a catalytic cycle

called oxidative quenching where the electron of the cat* is transferred to a substrate or an oxidant, generating the oxidized catalyst $cat^{\bullet+}$, which in turn is reduced back to its initial base state by accepting an electron from a substrate or reductant. Excited state oxidants take part in the opposing catalytic cycle called reductive quenching where the electron of a substrate or reductant is transferred to the excited state cat*, reducing the catalyst to $cat^{\bullet-}$, which is then similarly reduced back to its initial base state by donating an electron to a substrate or oxidant. Electron excess or deficiencies need to be restored, either by application of a sacrificial agent or alternatively two complementary oxidant and reductant photoredox catalysts can be used *in tandem* to create a net redox-neutral process.[151]

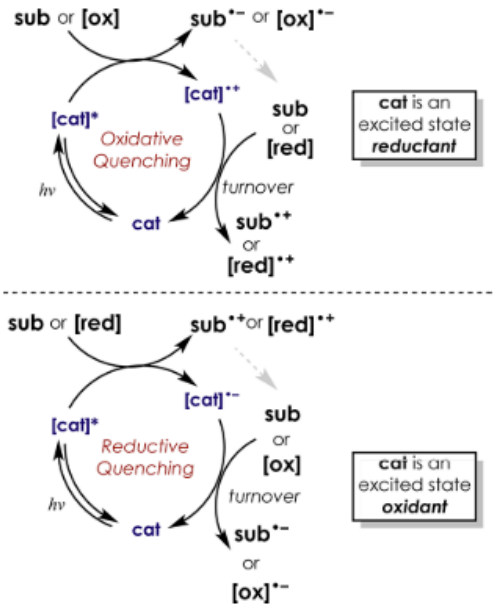

Figure 23: *Oxidative and Reductive Quenching Cycles of a Photoredox Catalyst.*[151]

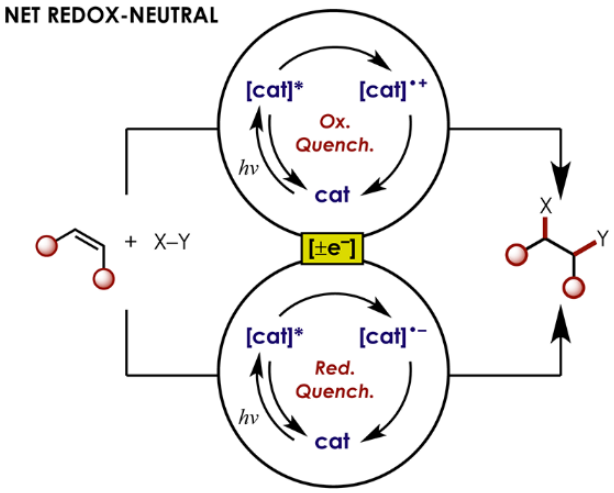

Figure 24: *Net Redox-Neutral photoredox process.*[151]

1.3.2 Common photocatalysts and common photocatalyzed reactions.

The first photoredox catalyst was Tris(bipyridine)ruthenium(II)chloride ($[Ru(bpy)_3]Cl_2$), which was used by Kellog *et al.* in 1978 during a photo-mediated reduction of sulfonium ions to the corresponding alkanes and thioethers where it was capable of accelerating the reaction.[152]

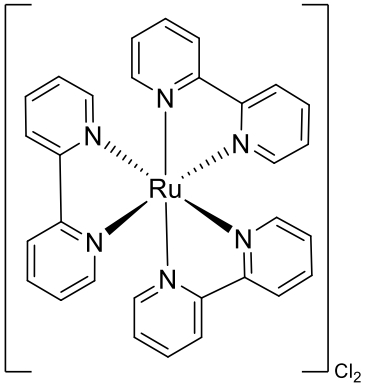

43

Figure 25: *Tris(bipyridine)ruthenium(II)chloride ($[Ru(bpy)_3]Cl_2$).*

Since then, many further photoredox catalysts have been discovered and developed, which have found diverse applications since they allow for reactions under milder conditions that work well with a wide array of diverse molecules while also allowing hitherto unavailable reactions.[153] The field of natural product synthesis has embraced photoredox catalysis since the use of low-energy light, like visible light, allows for a reduction of degradation in sensitive structurally complex molecules.[150, 154] In medicinal chemistry the unique ability of photoredox catalysts to generate reactive radical intermediates while employing mild conditions allows for late-stage functionalization of complex druglike molecules.[154a, 155] Furthermore, photocatalysis allows for various transformations to occur in a highly regio- and enantioselective manner and for highly regioselective homolytic bond cleavage.[156] Possible reactions include C-C[157] or C-X[158] bond formation, amine α-functionalization[159] or cycloadditions.[150, 160] A potential future for photoredox catalysis could be the development of chemoselective reactions triggered by specific excitation wavelengths.[161]

The mainly used photoredox catalysts are based on Ru(II) and Ir(III) complexes since they offer tunability of the photoredox properties through ligand modifications, chemical stability and long excited state lifetimes (µs). However, metal-free alternatives to these classical metal catalysts are being researched since some organic dyes are capable of reaching similar redox potentials while simultaneously being cheaper, having a

better environmental profile and allowing for a wider structural variation.[162] Just for comparison, metal-based catalysts like $[Ru(bpy)_3]^{2+}$ and $[Ir(ppy)_3]$ can cost 98.4 €/mmol and 1240 €/mmol respectively, while an organic dye like eosin Y can be purchased for just 0.95 €/mmol (prices from 2016).[162b]

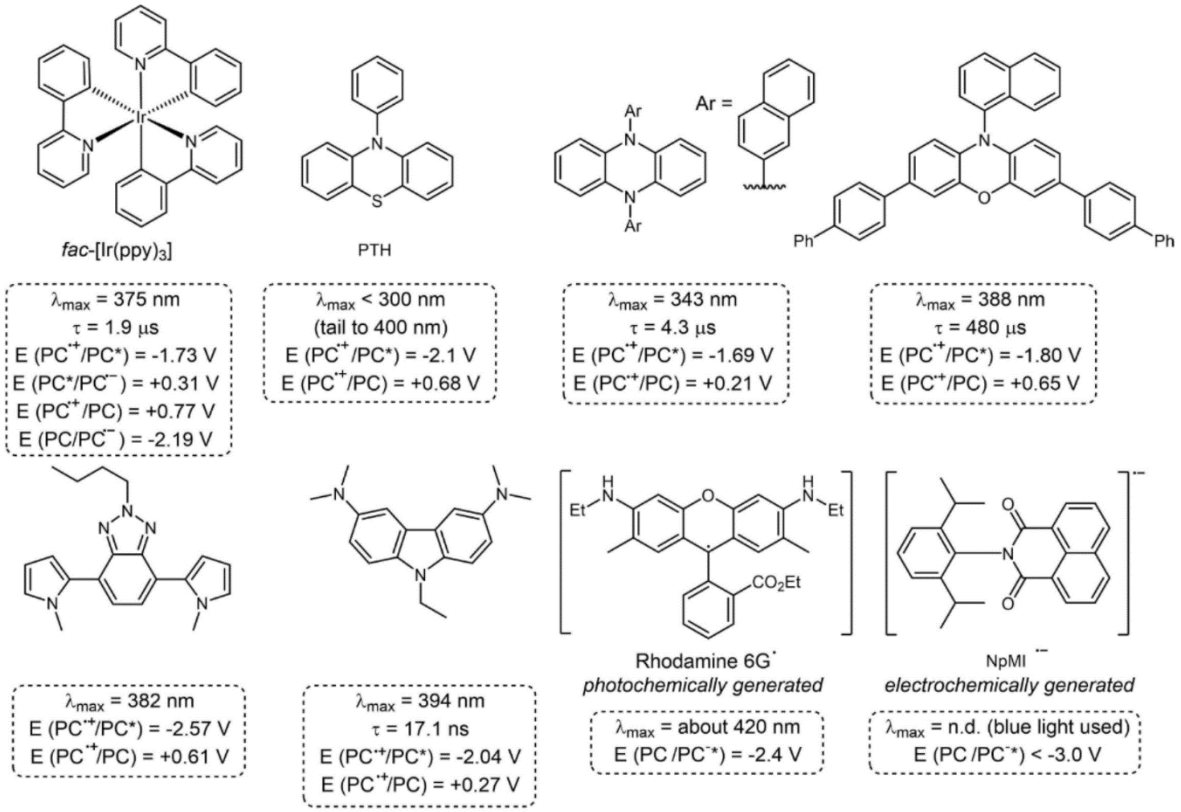

Figure 26: *Selection of highly reducing photocatalysts and photocatalytic systems from the literature, along with their reported photophysical properties. Reduction potentials reported vs SCE in CH_3CN.[162a]*

1.3.3 PXX – a versatile photoredox catalyst

Peri-xanthenoxanthene (PXX) is a brightly yellow highly reducing photoredox catalyst that is an *O*-doped analogue of anthanthrene. It is remarkably easy and cheap (2.69 €/mmol price from 2021) to synthesize and is known for its easy processability, chemical inertness and thermal stability which, in addition to their good carrier-transport and electron injection properties, gave them ample use in organic semiconductors and transistors in the form of a conducting polymer.[162a, 163]

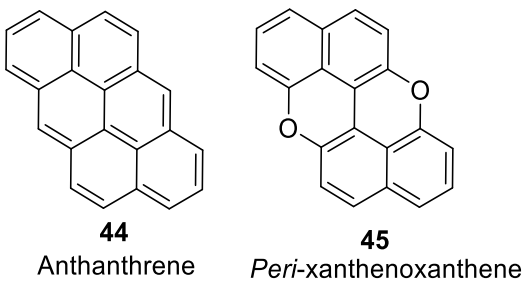

Figure 27: *Structures of Anthanthrene and Peri-xanthenoxanthene.*

PXX shows absorption of light in UV and Vis parts of the spectrum presenting a lower energy peak in the blue light range at 439 nm in CH_3CN and its S_1 state PXX* exhibits a reduction potential $E^{1/2}(PXX^{\bullet+}/PXX^*)$ of -2.00 V *vs* SCE, which allows it to efficiently reduce an extended number of organic reagents through single electron transfer (SET) reduction as the reduction potential is comparable to some classically used reducing photoredox catalysts. Since the PXX radical cation has a potential $E^{1/2}(PXX^{\bullet+}/PXX)$ of 0.77 V, a turnover of the photocatalytic oxidative quenching cycle with reagents like NET_3 can occur.[161a, 162a]

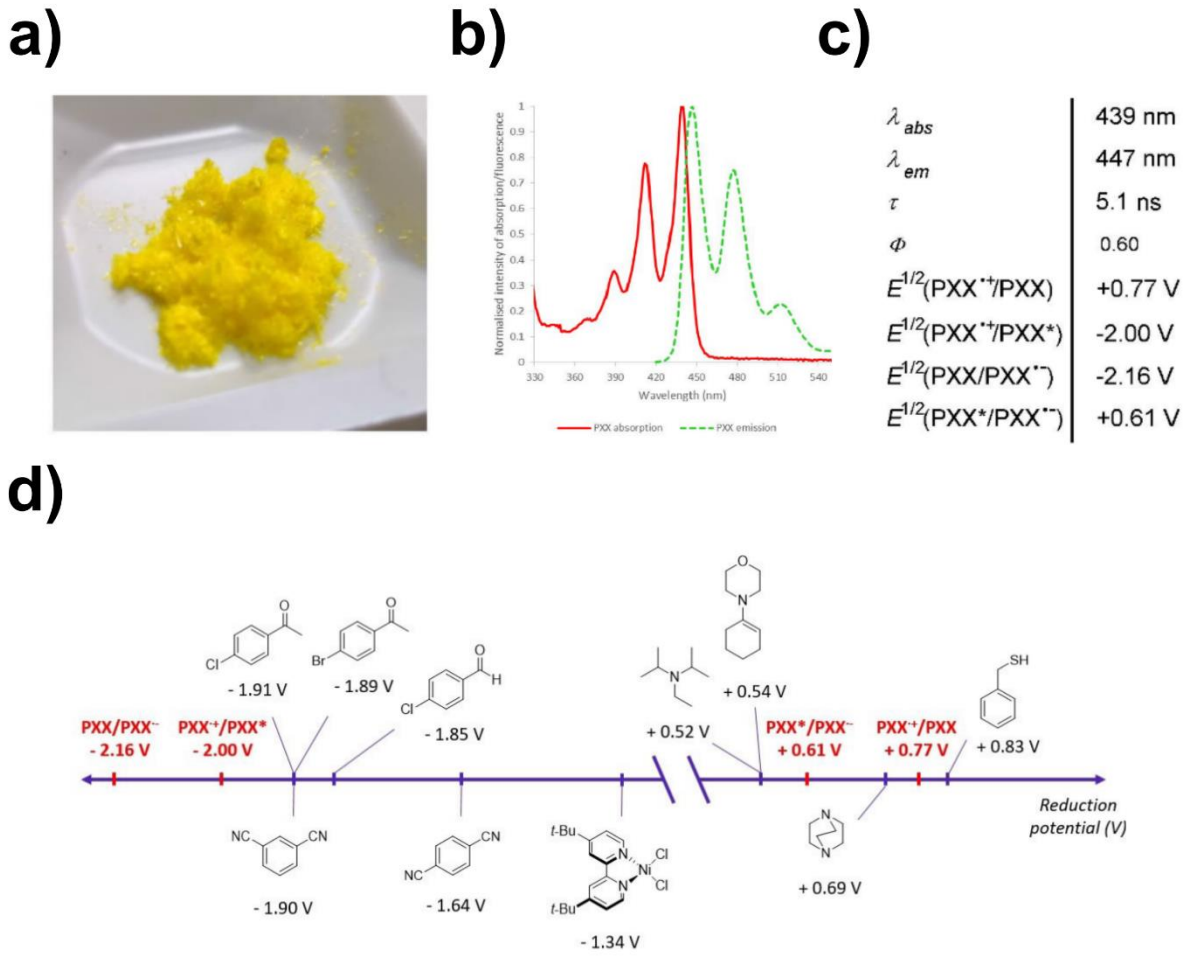

Figure 28: *a) Appearance of PXX; b) absorption and emission (λ_{exc} at 412 nm) spectra of a 10^{-4} M PXX solution in CH_3CN; c) Summary of photophysical and electrochemical properties of PXX in CH_3CN and vs SCE in CH_3CN; d) Reduction potentials of selected organic compounds compared to ground and excited state reduction potentials of PXX. Values given vs SCE in CH_3CN.[162a]*

PXX has proven itself to be a versatile photoredox catalyst for reductions of substrates like aryl, alkyl and perfluoroalkyl halides showing the capability of catalysing the formation of new C-C bonds as well as C-N and C-S bonds while also being capable of coupling with organocatalytic and metallocatalytic processes like for example by reacting in *β*-arylations of carbonyl compounds or as a photocatalyst partner in Ni-

catalysed C-heteroatom cross-coupling reactions. Thus it can compete with established but more expensive Ir(III) complexes.[162a]

1.4 Aryl radical formation and radical-radical cross-coupling

1.4.1 Aryl radicals

Aryl radicals are generally known to be rather unstable radicals due to having a radical stabilization energy of +10.3 kJ/mol[164] and a bond dissociation energy of 472.2 kJ/mol[165]. Nonetheless, they have been shown to be versatile intermediates in organic synthesis known for their C-C bond-forming reactions as well as their application in functional group interconversion.[166] They are also thermodynamically able to abstract a hydrogen atom from even an unactivated C(sp^3)-H bond,[167] being able to abstract hydrogens from both electron-poor and -rich C-H bonds due to their relative ambiphilicity.[168]

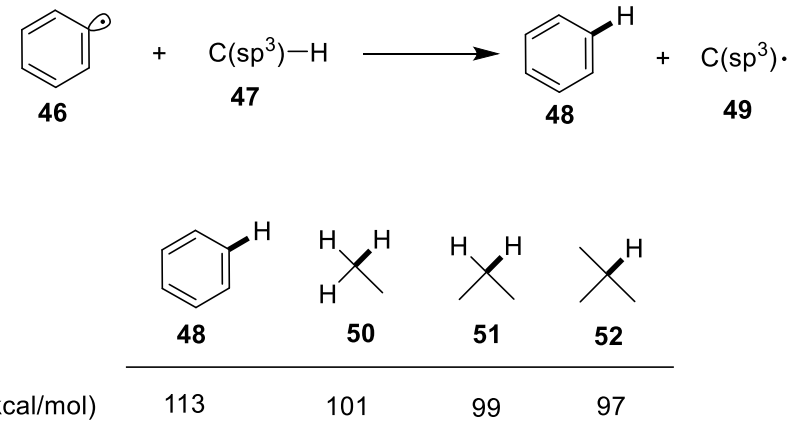

Figure 29: *C-H bond dissociation energy comparison.[168]*

The first aryl radical source were diazonium salts that were utilized by Meerwein *et al*. in their 1939 published Meerwein arylation.[169] Since then, further structures have emerged that are capable of generating aryl radicals such as aryl halides, aryl carboxylic acids, aryl triflates, aryl boronic acids, aryl sulfonium salts or diaryliodonium salts. Among them, diazonium salts and aryl halides are the major sources of aryl radicals with diazoniums being useful for their high reactivity and low reduction potential (-0.16 V *vs.* SCE)[170] while aryl halides allow for the more stable and more easily handleable alternative with the downside of having strong reduction potentials ($E_{red}(ArI/ArI^{\bullet-})$ = -2.0 V, $E_{red}(ArBr/ArBr^{\bullet-})$ = -2.4 V and $E_{red}(ArCl/ArCl^{\bullet-})$ = -2.8 V)[171].[168] The methods used to generate the aryl radicals from diazonium salts can include nucleophilic bases and very often include photoredox catalysis and/or electrochemistry as well as methods like ball milling. Aryl radicals from aryl halides are also generated

by methods like photoredox catalysis and/or electrochemistry in addition to transition metal catalysis. The other aryl halide sources are mainly generated by photoredox and/or metal catalysis. In the past years, the possibilities for the generation of aryl halides have been vastly increased due to the emergence of the field of photoredox catalysis, which is especially noteworthy for its smaller degree of toxic waste generation in comparison to metal catalysis.[168]

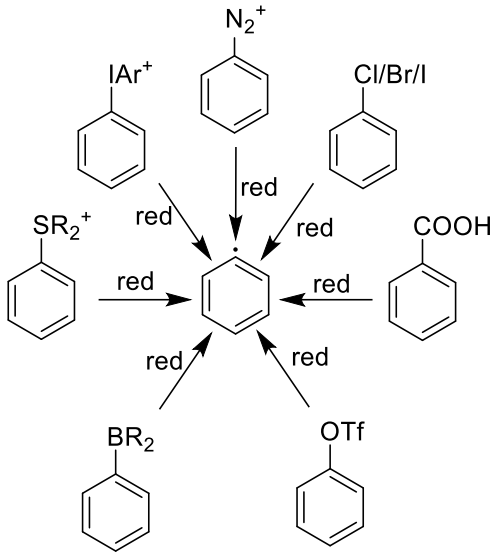

Figure 30: *Reductive generation of aryl radicals from different precursors.*

1.4.2 Photoredox catalyzed aryl-aryl bond formation

For this thesis, reactions involving photoredox catalysis leading to aryl-aryl bonds are of particular interest therefore 4 different of such reactions involving aryl radicals will be presented. The first example is a reaction published by König *et al*. in 2014 as shown in **Scheme 16** involving a chlorobenzonitrile **53** and *N*-methylpyrole **54** with triethylamine as a base and PDI as a photoredox catalyst enabling a C-H arylation of a heteroarene.[172] This represents one of the many heteroarylations using aryl radicals which are more commonly published than arylations without heteroatoms.[173]

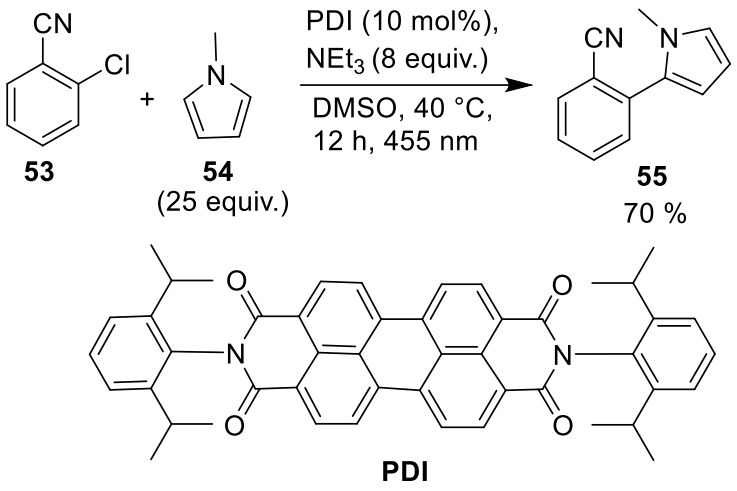

Scheme 16: *Heteroarylation of a chlorobenzonitrile **53** by König et al.*

The second example was published by Lin *et al*. in 2020 and involves an electrophotocatalytic process to generate aryl radicals from the aryl halide ethyl 4-chlorobenzoate **56** capable of forming an Ar-Ar bond with 1,4-difluorobenzene **57** under the catalysis of DCA with $TBAPF_6$ as a base using a porous carbon cathode and a zinc plate sacrificial anode as depicted in **Scheme 17**.[174]

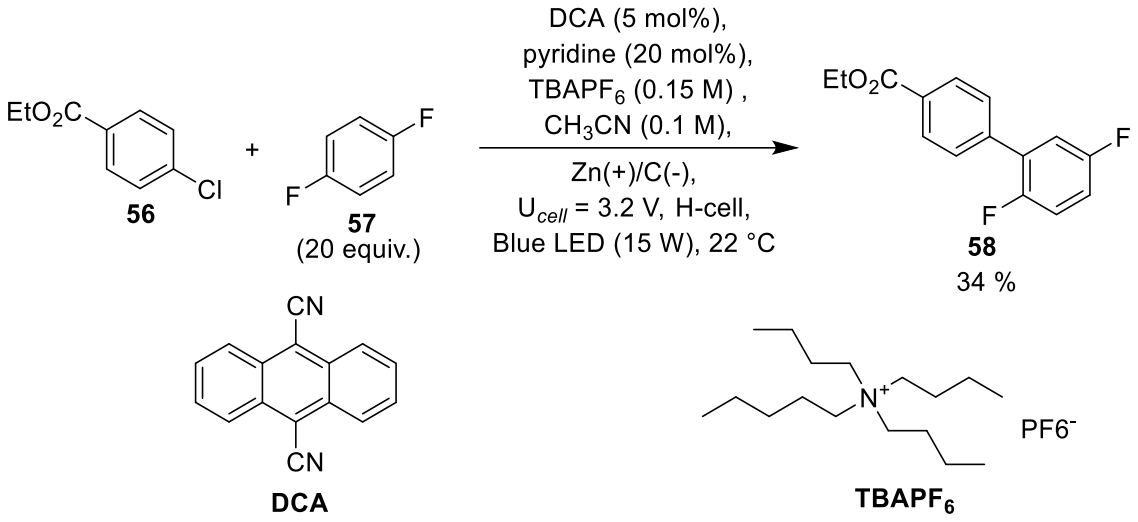

Scheme 17: *Arylation of ethyl 4-chlorobenzoate **56** by electrophotoredox catalysis by Lin et al. Cathodic chamber: aryl chloride (0.4 mmol, 1.0 equiv), DCA (5 mol%), Sn_2Me_6 (2.0 equiv), $TBAPF_6$ (0.15 M), CH_3CN (0.1 M); anodic chamber: $TBAPF_6$ (0.15 M), CH_3CN (0.1 M); cell voltage (U_{cell}) =3.2 V.*

In 2017, Glorius *et al*. published the third example; the first aryl radical formation *via* light-mediated decarboxylation of aryl carboxylic acids using photoredox catalysis. The presented reaction in **Scheme 18** involves the arylation of a 4-cyanobenzoic acid **59** with benzene **48** and with diethyl 2-bromo-2-methylmalonate **60** as a brominating agent, PC as a photoredox catalyst and Cs_2CO_3 as a base at 415 nm. The arylation mechanism they proposed (**Scheme 19**) involves the formation of an aroyloxy radical

63 that is brominated and decarboxylated leading to the formation of the aryl radical **66**, which then reacts with benzene **48** to form the biaryl product **68**.[175]

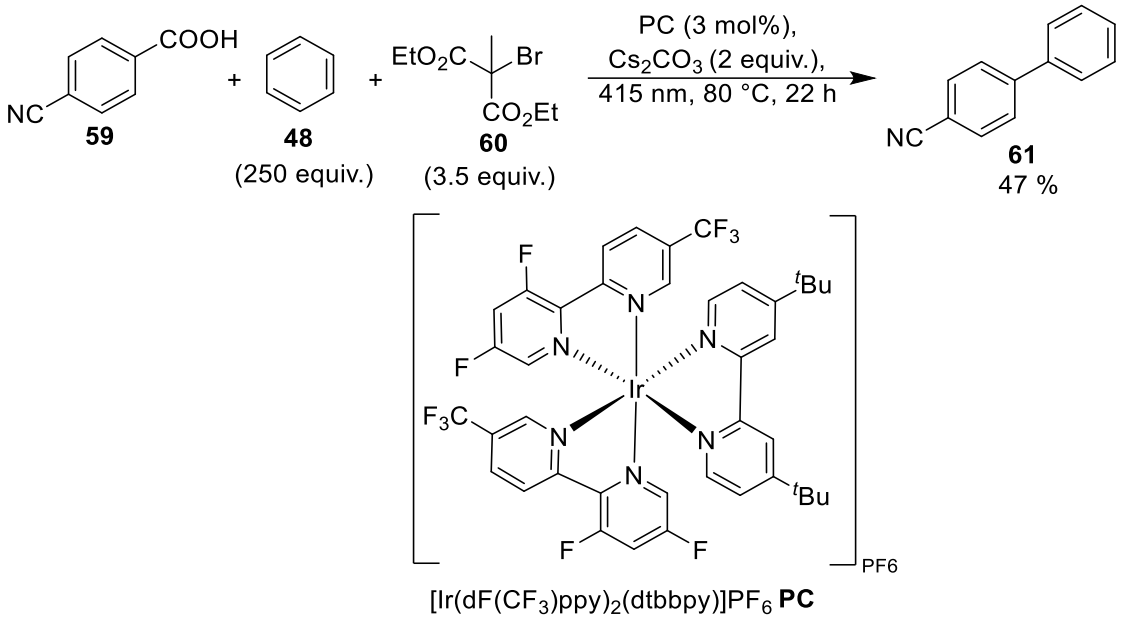

Scheme 18: *Arylation of a chlorobenzonitrile **59** by Glorius et al.*

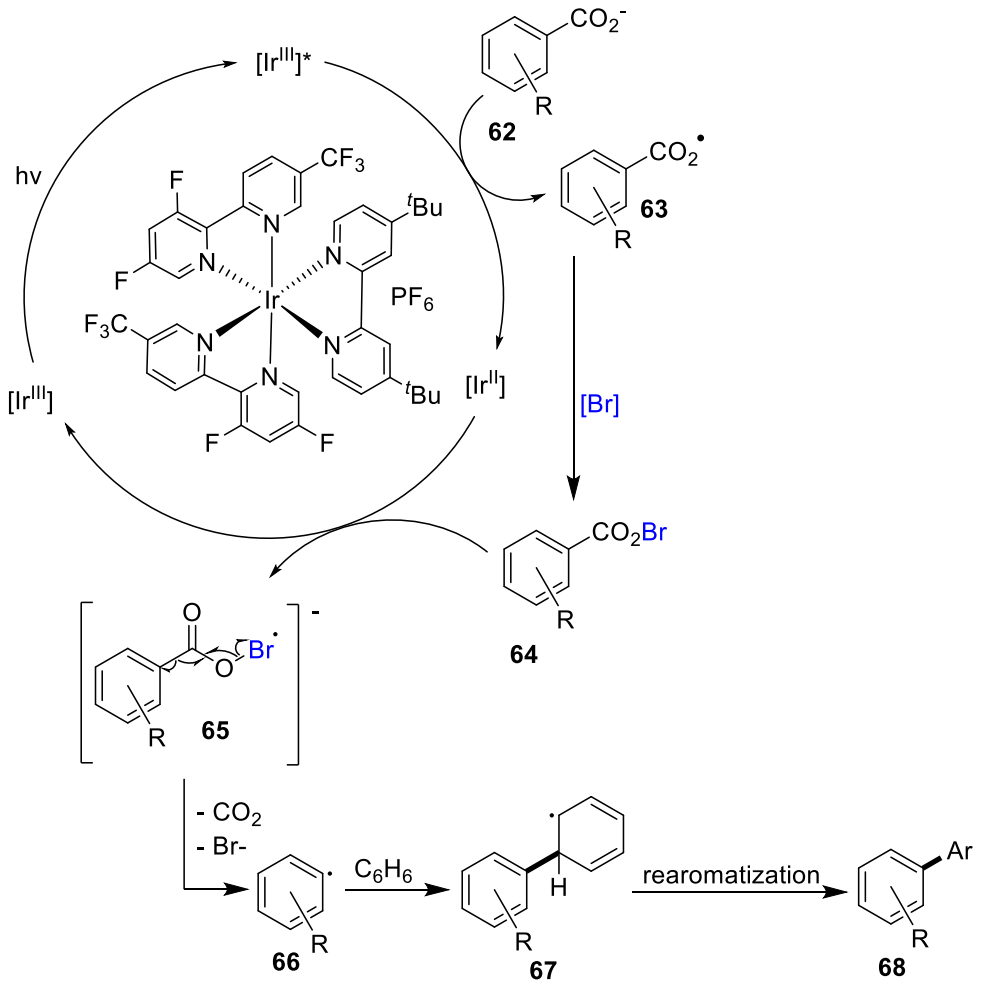

Scheme 19: *Mechanism of aryl radical arylation as proposed by Glorius et al. Counterions and ligand sphere of Ir are omitted for clarity.[175]*

The fourth example shows that PXX is also capable of photo-catalysing aryl-aryl bond formations as demonstrated by Bonifazi *et al*. in 2021 in an arylation reaction of 4'-bromoacetophenone **69** using PXX, DBU, and Benzene as seen in **Scheme 20**.[162a]

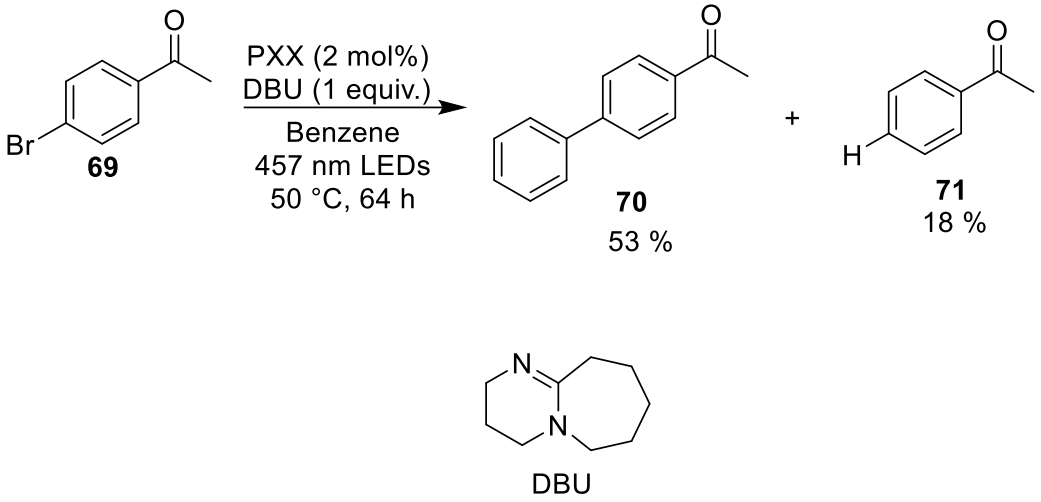

Scheme 20: *Arylation of 4'-bromoacetophenone* ***69*** *with PXX.*

These 4 examples show how Ar-Ar coupling is possible by smart application of photoredox and/or electrochemical methods. Although these reactions have mainly been successful on heteroarenes like pyrroles as seen in example 1, there have been successful couplings of aromatic rings using these methods as shown in examples 2 3 and 4.

1.4.3 Radical-radical coupling

Historically, the use of biradicals in organic synthesis has been rare since thermal reactions can only access them in a limited capacity. Photocatalyzed reactions can make the photo-fragmentation of single bonds possible due to the high energy of excited states. The formed radicals can then either react as a radical centre or by radical recombination.[176] The general issue with radical-radical reactions, however, is that the energy as it comes back during product formation is hard to control and that these reactions are usually highly exothermic and unselective.[177] For a long time, highly selective radical-radical cross-coupling was considered to be unfeasible due to its high reactivity.[178] But based on the findings of his contemporaries, Fischer formulated the "persistent radical effect" (PRE) also known as the "Ingold-Fischer effect", which states that for highly selective radical-radical couplings to occur, the following two criteria have to be met: 1) one radical must be more persistent than the other (which is more transient), and 2) both radical species must be generated at equal rates.[179] Here it must be emphasized that persistence is a kinetic effect that is not to

be mixed up with stability, which is a thermodynamic effect.[180] The EPR effect occurs due to the short-lived transient radicals being available in small concentration in solution because of fast termination almost right after being generated, while the concentration of persistent radicals will exceed their concentration. Then, when a transient radical collides with a persistent radical, an across-coupled product can be formed. Due to the high exothermic nature of most radical-radical reactions, differences in stability make less of a difference.[177]

There are various known methods to induce radical-radical cross couplings such as by using Lewis acids like $TiCl_4$ to stabilize radical intermediates,[181] or by applying Lewis bases like 4-phenylpyridine as catalysts.[182] Electrochemistry, for example with the aid of a cyanopyridine, has also been reported as a radical-radical cross-coupling method,[183] as well as transition-metal-mediated methods like with nickel(II)iodide.[184] The last strategy for radical-radical couplings involves the application of the already mentioned photoinduced methods,[178] of which a few examples will be presented in more detail:

A good example of a radical-radical reaction involving a persistent aryl radical is the direct photoredox catalysed *β*-arylation of ketones and aldehydes published by McMillan *et al*. in 2013 which uses an [Ir(ppy)$_3$] photoredox catalyst to couple cyclohexanone **72** and dicyanobenzene **73** as shown in **Scheme 21** according to the proposed mechanism in **Scheme 22**.[185]

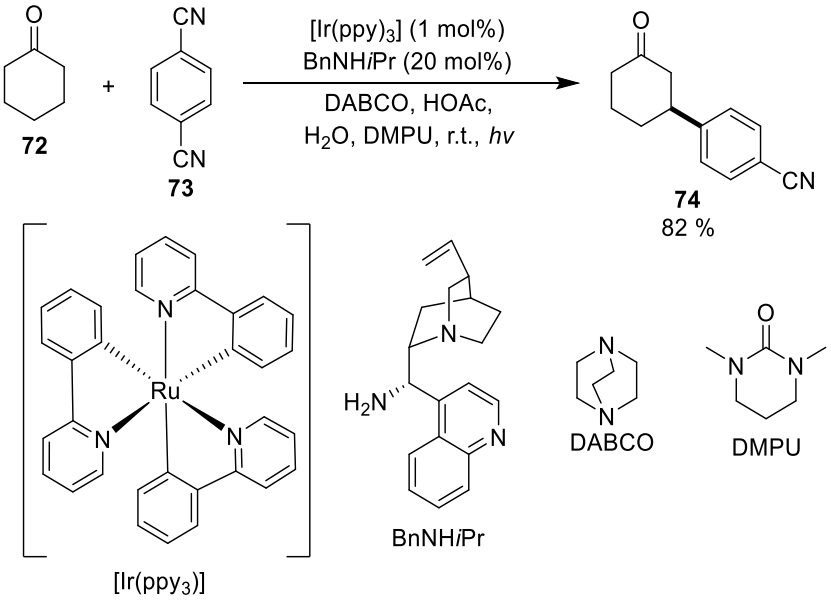

Scheme 21: *Direct photoredox catalysed β-arylation of ketone* ***72****.*

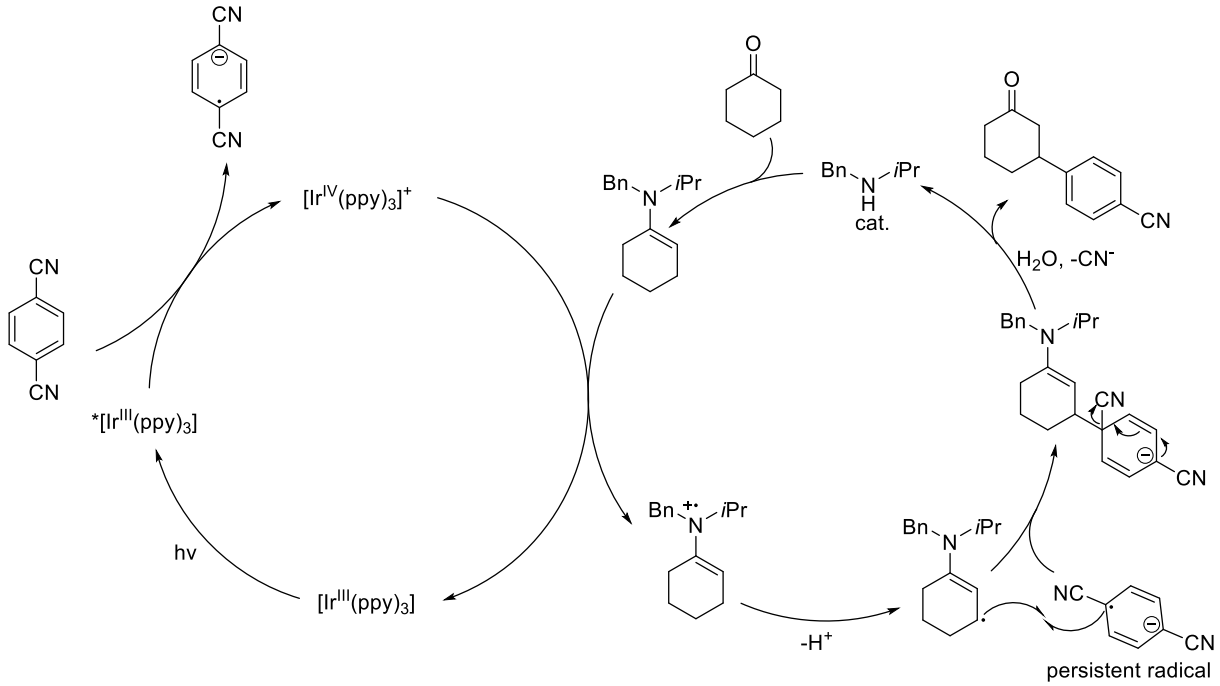

Scheme 22: *Mechanism of direct photoredox catalysed β-arylation of ketone* ***72****.*

A similar coupling reaction has also been published by Bonifazi *et al*. with PXX as the photoredox catalyst as shown in **Scheme 23**.[162a]

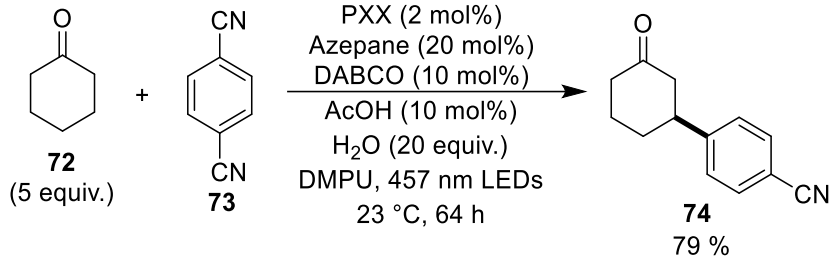

Scheme 23: *PXX-catalysed coupling reaction of cyclohexanone* ***72*** *with 1,4-dicyanobenzene* ***73****.*

An example of a further reaction involving cyclization with biradicals would be the Norrish Type II reaction as shown in **Scheme 24**.[186]

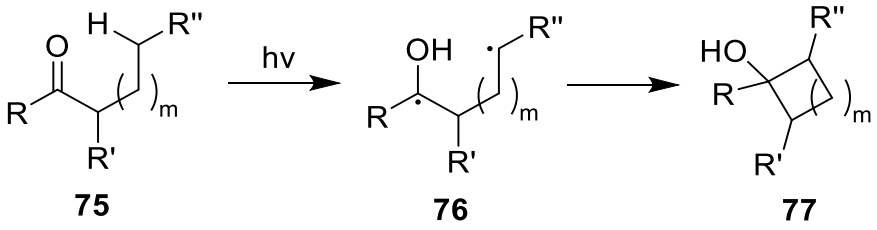

Scheme 24: *Norrish Type II reaction.*

There are many further known cyclization reactions involving biradicals ranging from rings as small as three-membered rings **81**[187] up to larger macrocycles **85**[188] as portrayed in **Scheme 25**.

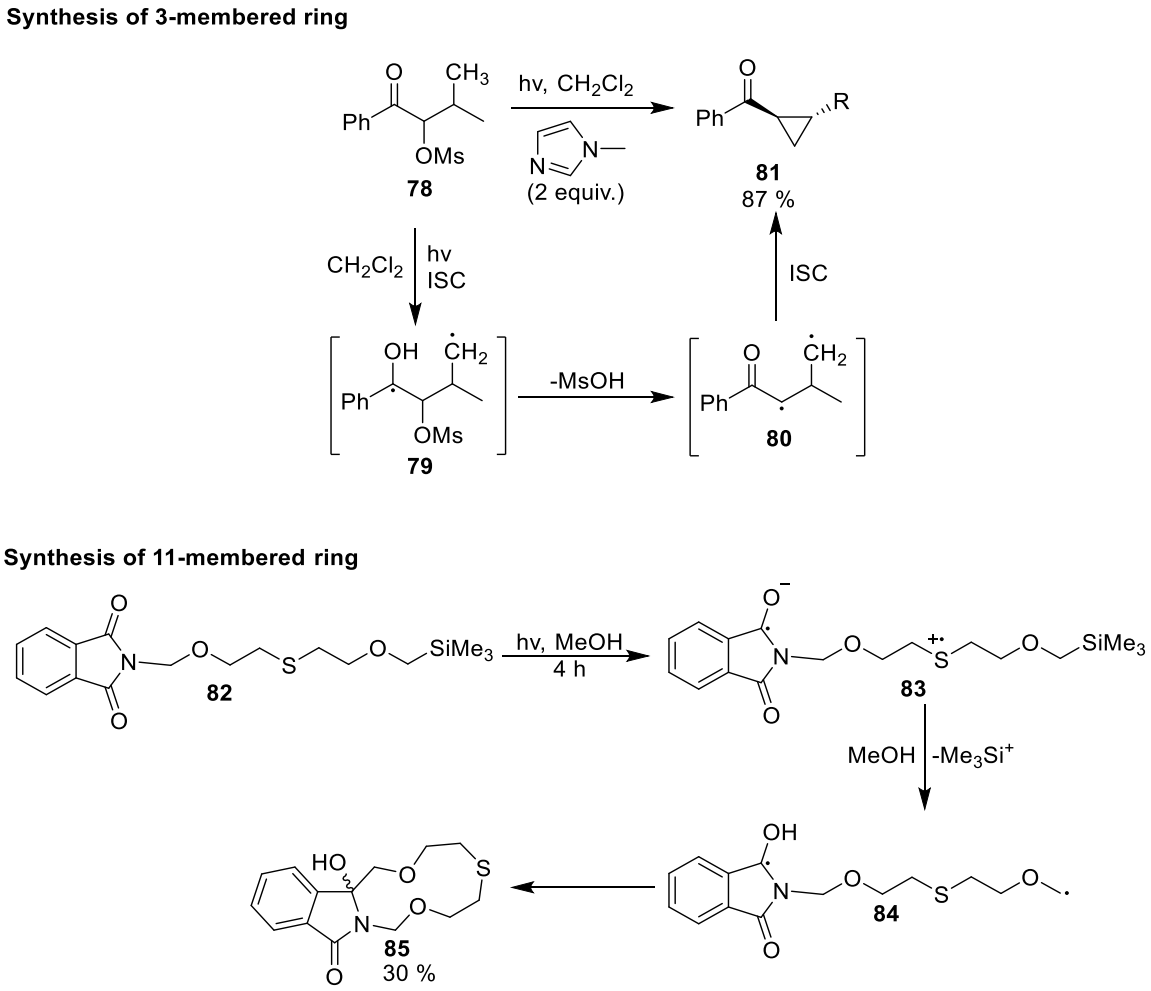

Scheme 25: *Synthesis of 3-membered and 11-membered rings* ***81*** *and* ***85*** *by a Norrish II Type reaction.*

Another known reaction type involving photochemically induced biradicals is the Photo-Fries rearrangement, which was for example used to perform a total synthesis of the antibiotic kendomycin as portrayed in **Scheme 26**.[189]

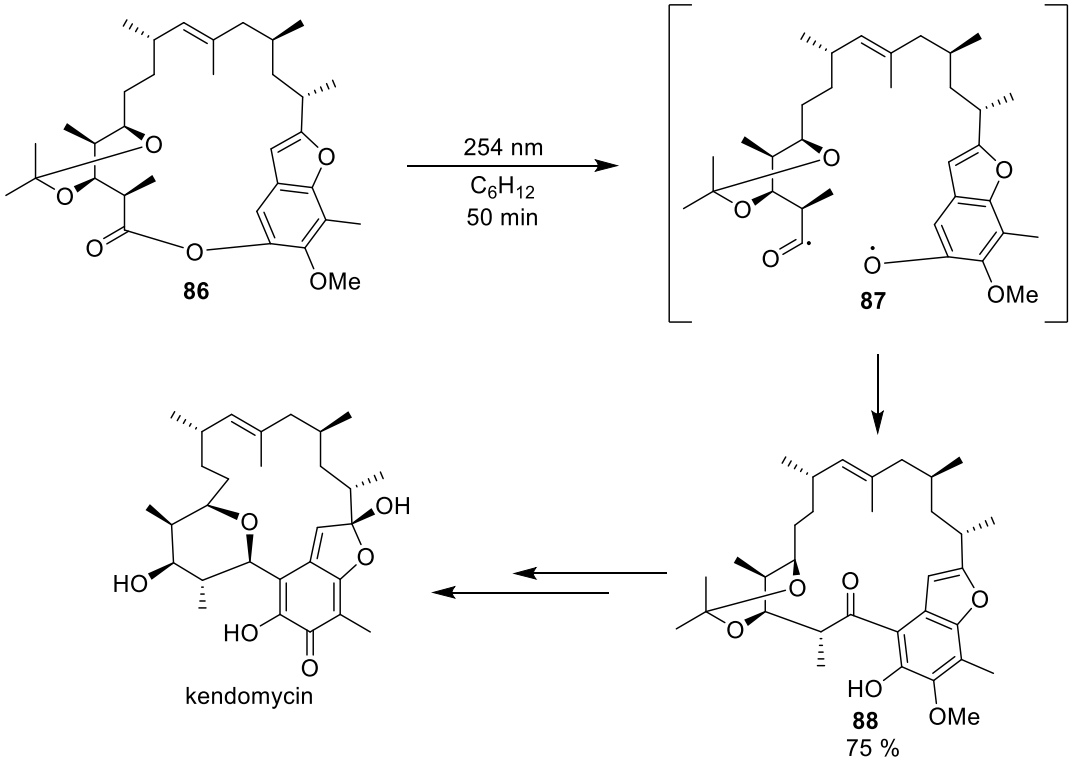

Scheme 26: *Synthesis of kendomycin involving Photo-Fries rearrangement.*

1.5 Radical reactions and Tetraphenylenes for the synthesis of cubic graphite

The closest that anyone came to synthesizing a structure on the path to cubic graphite have arguably been Müllen *et al*. in 2021 when they formed two tri[8]annulene isomers either by Pd-catalysis for isomer **90** or by Ru-catalysis for isomer **91** under temperature control as depicted in **Scheme 27**. [121]

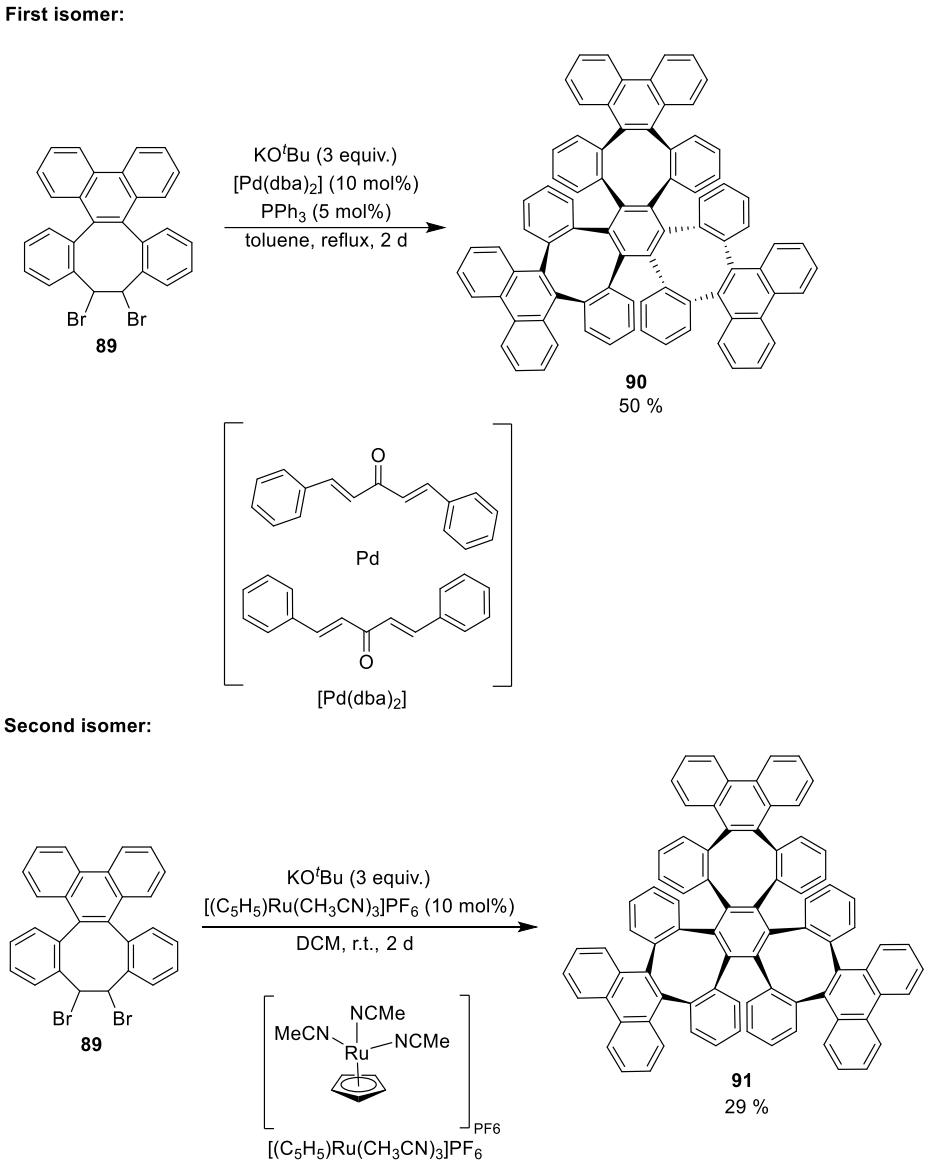

Scheme 27: *Synthesis of two tri[8]annulene isomers **90** and **91**.*

While the structures that were synthesized here are impressive and a step closer towards cubic graphite, the science of cubic graphite synthesis is nonetheless at its current limits. This might stem from the limitations of classical aryl-aryl coupling methods such as when utilizing transition metal catalysis. This might be explained by how the metal-substrate complexes formed during transition-metal catalysis might be too bulky for the catalysis of the formation of the crowded and compact structure of cubic graphite. Perhaps new, more modern and more controlled approaches are necessary to finally achieve the creation of cubic graphite.

1.5.1 How Tetraphenylenes and radical reactions could help in the synthesis of cubic graphite.

As tetraphenylenes, with their mix of eight- and six-membered rings, are known subunits of cubic graphite it is reasonable to research their reactivity as a possible building block for cubic graphite. While there are multiple known ways to synthesize tetraphenylenes, as described in **chapter 1.2.3**, many of them require metal catalysis to form. One of the known synthesis methods, however, does not need any metal catalyst: the pyrolysis of biphenylenes as discussed in **chapter 1.2.3.1**. This method is noteworthy since it occurs through a biradical intermediate that becomes a tetraphenylene at high temperatures of 400 °C. Yet, this reaction can only be used to create unsubstituted tetraphenylenes, since it is not feasible to control radical reactivity at such high temperatures due to the excess of energy involved.

It is also important to analyse cubic graphite synthesis in relation to its chemical cousins, the carbon allotropes. Among their synthesis methods are many, which involve giving the carbon building blocks a big amount of energy such as in arc-discharge-plasma (used for the synthesis of fullerenes, carbon nanotubes and 3D graphene), chemical vapour deposition (used for the synthesis of graphenes, fullerenes and carbon nanotubes), and pyrolysis (used for the synthesis of fullerenes). It is noteworthy how high the temperatures in these carbon allotrope creation methods can become, ranging from 600 °C to up to 4000 °C. At such high temperatures, it is difficult to control which specific bonds are to be formed and the structures that are formed will usually be attempting to reach their most thermodynamically stable structure rather than a compact and hindered one like that of cubic graphite.

Here is where the emerging and expanding field of photoredox catalysis could play a crucial role. By using precisely chosen photoredox catalysts, the π-systems of aromatic rings involved in the formation of carbon allotropes can be given specific and controlled amounts of energy. This could potentially enable the formation of specifically chosen Ar-Ar bonds with exact substitution patterns. Such bonds could be formed by precisely placed aryl radicals, which, as described in **chapter 1.4.2**, are known to be accessible *via* photoredox catalysis. While aryl radicals are not known to be particularly stable radicals, they have nevertheless been shown to be capable of forming aryl-aryl bonds by using smartly designed photocatalytic methods as discussed in **chapter 1.4.2**. Additionally, aromatic molecules such as dicyanobenzene have shown their capability to form persistent radicals that are capable of reacting in radical-radical coupling

reactions, which, as we know from Norris-Type-II reactions (see **chapter 1.4.3**), can form rings of differing sizes, such as the eight-membered-rings in tetraphenylenes.

Photoredox catalysis is still a developing and novel field of synthetic chemistry. Therefore, the chance to find a completely novel photocatalytic synthesis method that was hitherto synthetically impossible to perform with classical synthetic methods seems relatively optimistic. While it is unsure whether cubic graphite can ever be truly created, photoredox catalysis might be the missing puzzle piece on that journey since it might allow for aryl-aryl biradical coupling without the need for bulky metal-catalysts that might be hindering the formation of a tight structure like cubic graphite. Hopefully this thesis, with its focus on a novel metal-free photoredox catalysed method to synthesize tetraphenylenes, is a small step towards the elusive goal of someday creating cubic graphite and perhaps even towards the new battery that finally improves on the current flaws of Li-ion batteries.

II Aim of the project

The Bonifazi group has conducted a series of experiments investigating a radical annulation protocol for the synthesis of substituted polyaromatic hydrocarbons, utilizing the photoredox catalyst PXX. A significant focus of these studies was on the annulation of terphenyls bearing electron-withdrawing cyano (CN) groups under mild photoredox conditions, with PXX serving as the photocatalyst and DIPEA functioning as both the base and sacrificial agent, with DMSO as the solvent. The presence of the electron-withdrawing group was crucial as it adjusted the substrates' reduction potential to -1.88 V *vs* SCE, thereby aligning it with the reduction potential of PXX ($E^{1/2}(PXX^{\bullet+}/PXX^{*})$ of -2.00 V *vs* SCE). The experiments revealed the formation of a new bond between the originally halogenated ring and the ortho-positioned neighbouring aromatic ring resulting in the formation of a six-membered ring in the core of the structure. A proposed mechanism involves a single electron transfer from PXX to the substrate generating a radical anion intermediate that undergoes an intermolecular reaction after dissociation of the chloride.[190]

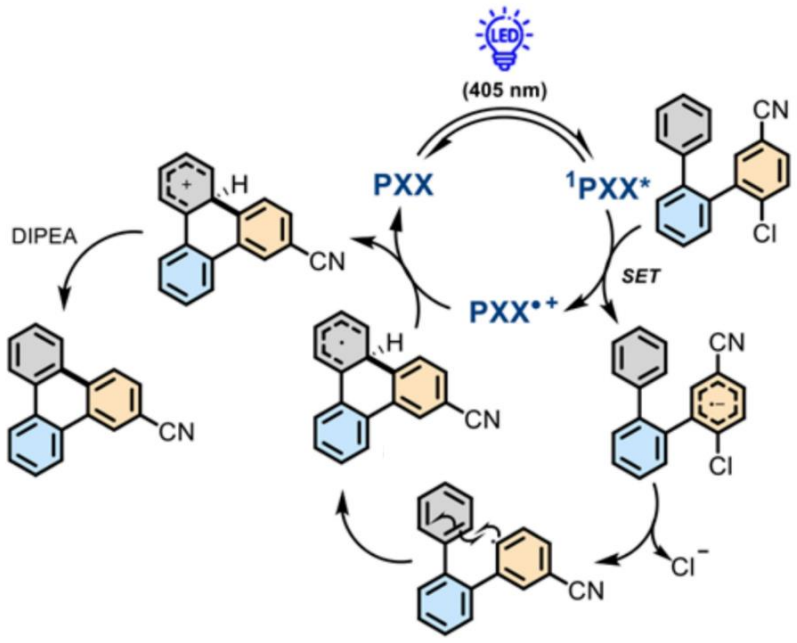

Scheme 28: *A proposed photooxidative mechanism for the annulation reaction of terphenyls through C−C bond formation triggered by light under the catalysis of PXX.*[190]

Among the tested substrates were also di-chlorinated and di-cyano-substituted quaterphenyls **94** which were tested with the expectation to replicate the mechanism of the terphenyl **92** annulation but this time with a double annulation creating dibenzotetracene **96**. However, surprisingly, the reaction resulted in a tetraphenylene structure **95** with a central eight-membered ring instead of the double annulation. This

turned out to be the first photoredox-catalyzed synthesis of tetraphenylenes according to hitherto published literature.

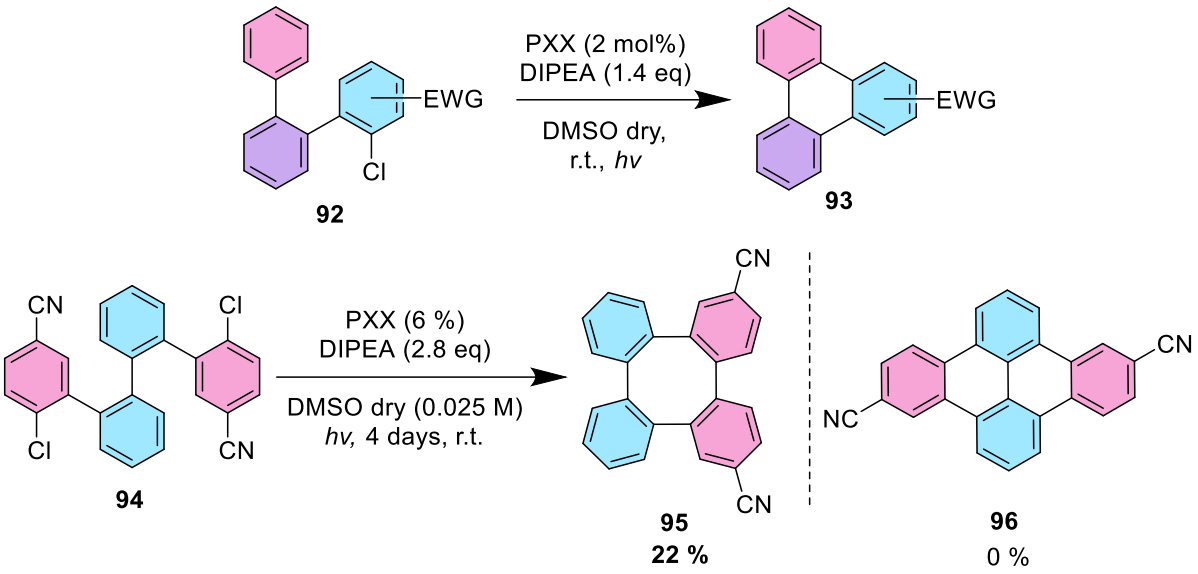

Scheme 29: *Top) Reaction scheme for annulations of terphenyls **92** into triphenyl **93** using a photoredox reaction catalysed by PXX; Bottom) Reaction scheme for a tested photoredox reaction of a quaterphenyl **94** catalysed by PXX.*

The objective of this project was to advance the understanding of the synthesis and reactivity of tetraphenylenes *via* PXX-photoredox-catalysed transformations, specifically focusing on di-chlorinated and di-cyano-substituted quaterphenyls as precursors. Additionally, the study aimed to elucidate the underlying mechanism, with a particular emphasis on the role of photoredox catalysis and radical intermediates in the formation of tetraphenylenes. This investigation also sought to identify potential new strategies for the synthesis of cubic graphite using photoredox catalysis, informed by the insights gained from the mechanistic studies.

III Results and Discussion

3.1 Target molecules and scope.

Initially, the goal was to replicate the synthesis of the formation of tetraphenylene-2,7-dicarbonitrile **95** from the di-meta cyano substituted 6,6'''-dichloro-[1,1':2',1'':2'',1'''-quaterphenyl]-3,3'''-dicarbonitrile **94** (cyano-group on position 3). Next, the reaction was to be investigated with starting materials with the rest of the missing cyano substitution patterns being on positions 5, 4 and 2 using starting materials **97**, **99** and **101** respectively expecting to arrive at the tetraphenylenes **98**, **100** and **102** as seen in **Scheme 30**.

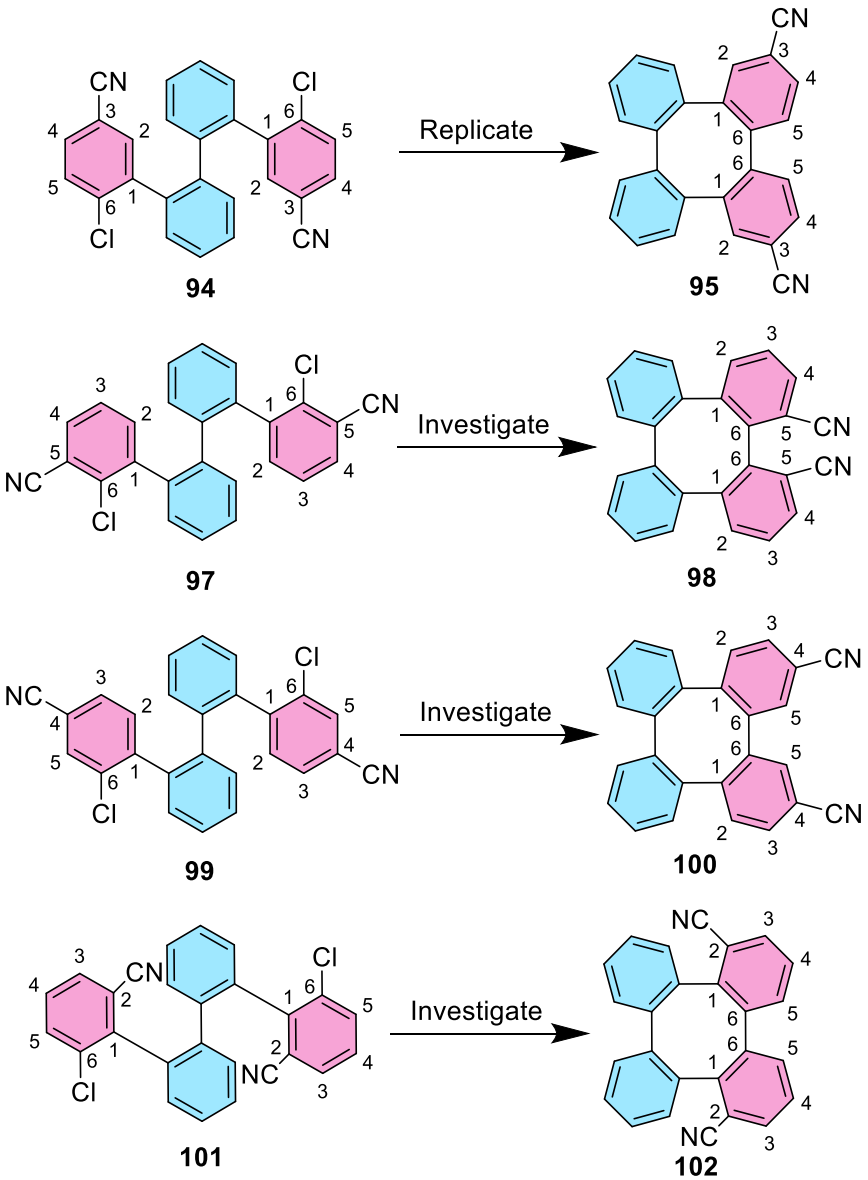

Scheme 30: *Initial main reactions to be investigated.*

3.2 Synthesis of starting materials

3.2.1 General strategy for synthesis of starting materials

For the synthesis of the desired quaterphenyls **94**, **97**, **99** and **101** which all share a chloride at position 6 and are each substituted with a cyano-group at either position 5, 4, 3 or 2, Suzuki-Miyaura reactions inspired by a procedure utilizing micelles in water by Mattiello *et al*. was employed.[191] The approach was to couple two chloro- and cyano-substituted rings onto a central scaffold consisting of two aromatic rings. There were two possible strategies: A) The central scaffold would be brominated in *ortho*-position of each of its two rings and the coupled substituted aromatic rings would bear a boronic ester or boronic acid on position 1 or; B) The central scaffold would bear a boronic ester or boronic acid in *ortho*-position of each of its two rings and the coupled substituted aromatic rings would be brominated on position 1.

As palladium catalysts either [1,1'-Bis(di-tert-butylphosphino)ferrocen]-dichlorpalladium(II) [Pd(dtbpf)Cl_2] or [1,1'-Bis(diphenylphosphino)ferrocen]-dichlorpalladium(II) [Pd(dppf)Cl_2] were used and triethylamine (NEt_3) as a base. The solvent mixture of H_2O/Toluene in a ratio of 9:1 was used with 2 %w/w of Kolliphor EL as surfactant as described in **Scheme 31**.

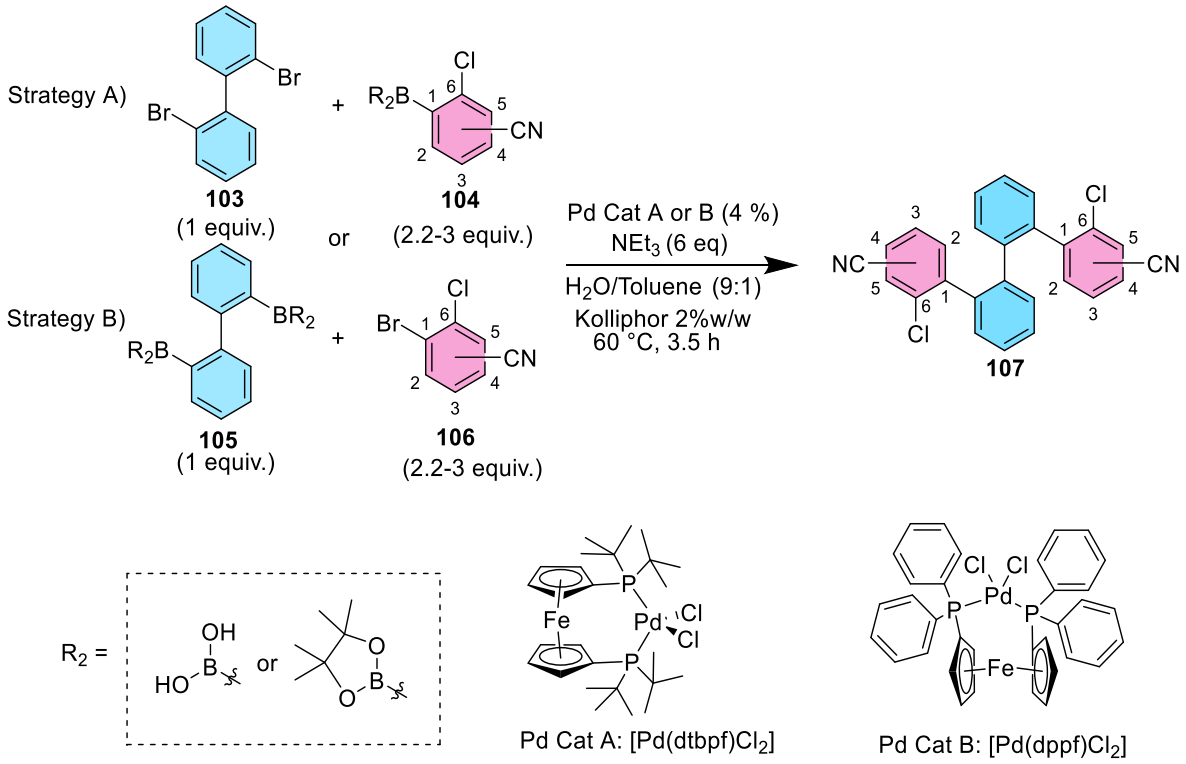

Scheme 31: *Strategy for the synthesis of substituted quaterphenyls* ***107****.*

3.2.2 Synthesis of starting material with CN on position 3

The first Suzuki-Miyaura coupling for position 3 cyano-substituted starting material **94** was performed with the strategy A procedure with a brominated scaffold **103** and a boronic-acid substituted ring **108** depicted in **Scheme 32** was repeated multiple times since the following photoredox catalysed reaction would necessitate more starting material than initially anticipated. In total, the reaction was performed five times; four times with [Pd(dtbpf)Cl_2] as catalyst with isolated yields increasing from 31 % up to **86 %** with every attempt and once with [Pd(dppf)Cl_2] as catalyst, which gave no product. The latter catalyst was chosen when the former catalyst had been unavailable while waiting for it to be purchased and delivered to the laboratory and the unsuccessful reaction meant that only [Pd(dtbf)Cl_2] would be used in further Suzuki-Miyaura coupling reactions.

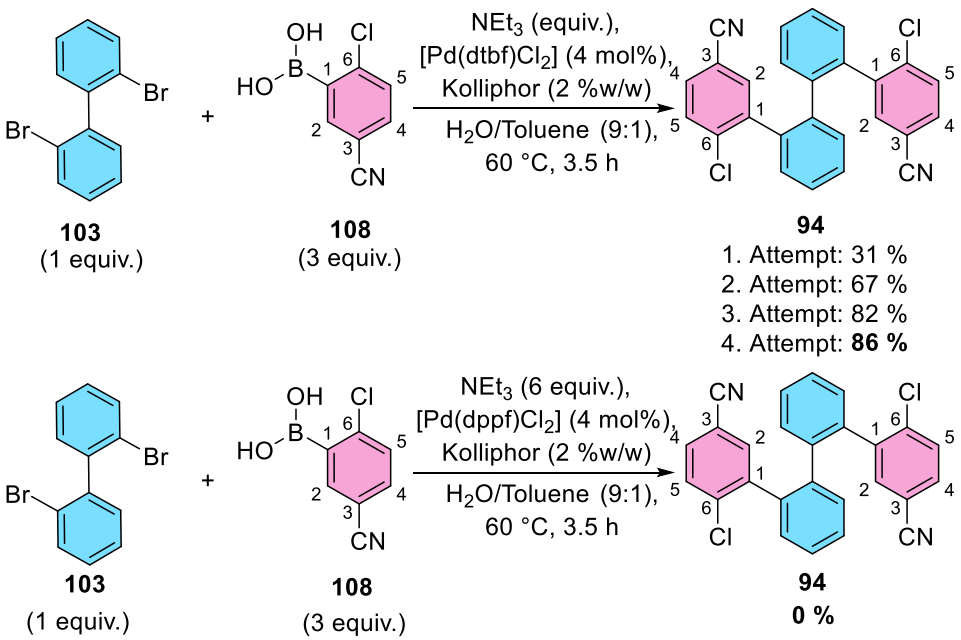

Scheme 32: *Synthesis of quaterphenyl with CN on position 3* ***94****.*

3.2.2.1 High-Temperature NMR for structural elucidation of 3 cyano-substituted starting material 94

After isolating the 3 cyano-substituted quaterphenyl **94**, the obtained ^{1}H-NMR spectrum in $CDCl_3$ contained only broad peaks that could not be assigned to concrete H-atoms of the target structure as seen in **Figure 31**.

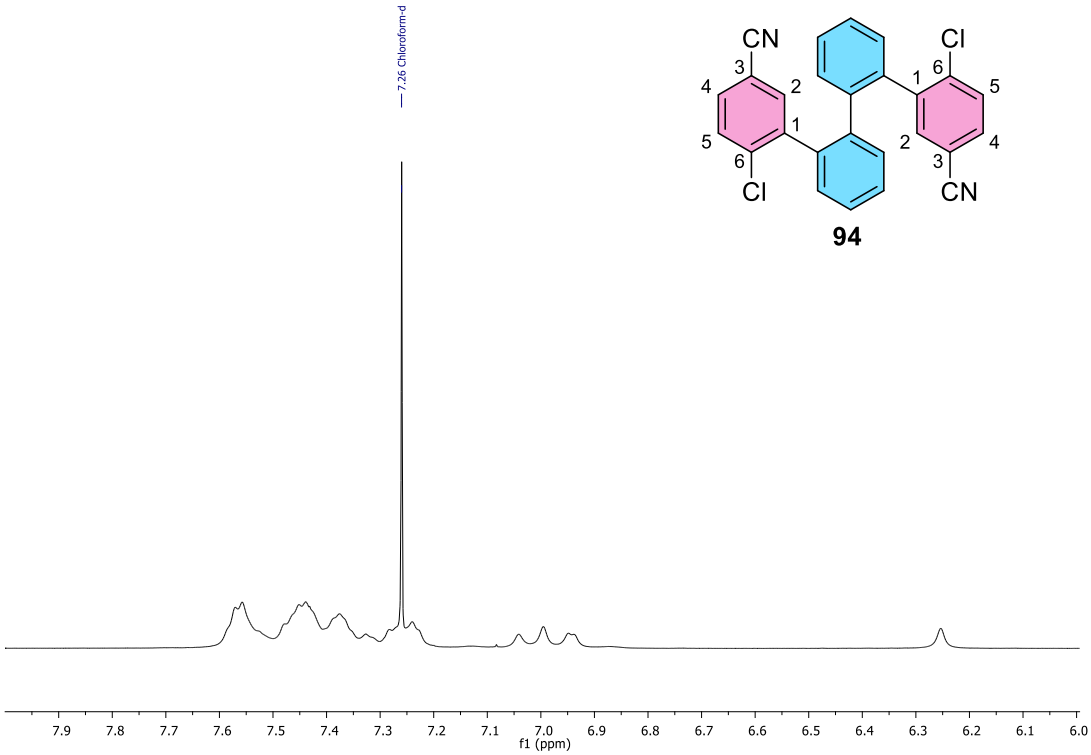

Figure 31: *^{1}H-NMR (600 MHz) spectrum of quaterphenyl **94** in $CDCl_3$ at room temperature zoomed into the aromatic part of the spectrum.*

To solve this issue, it was decided to perform high-temperature ^{1}H-NMR measurements to test whether the signals would separate and sharpen with an increase in temperature. DMSO-d_6 was chosen due to its high boiling point of 189 °C at atmospheric pressure[192] and its ability to solubilize the substrate **94**. Measurements were performed at 25 °C, 45 °C, 65 °C, 85 °C, 105 °C and 125 °C and the results are shown in **Figure 32**.

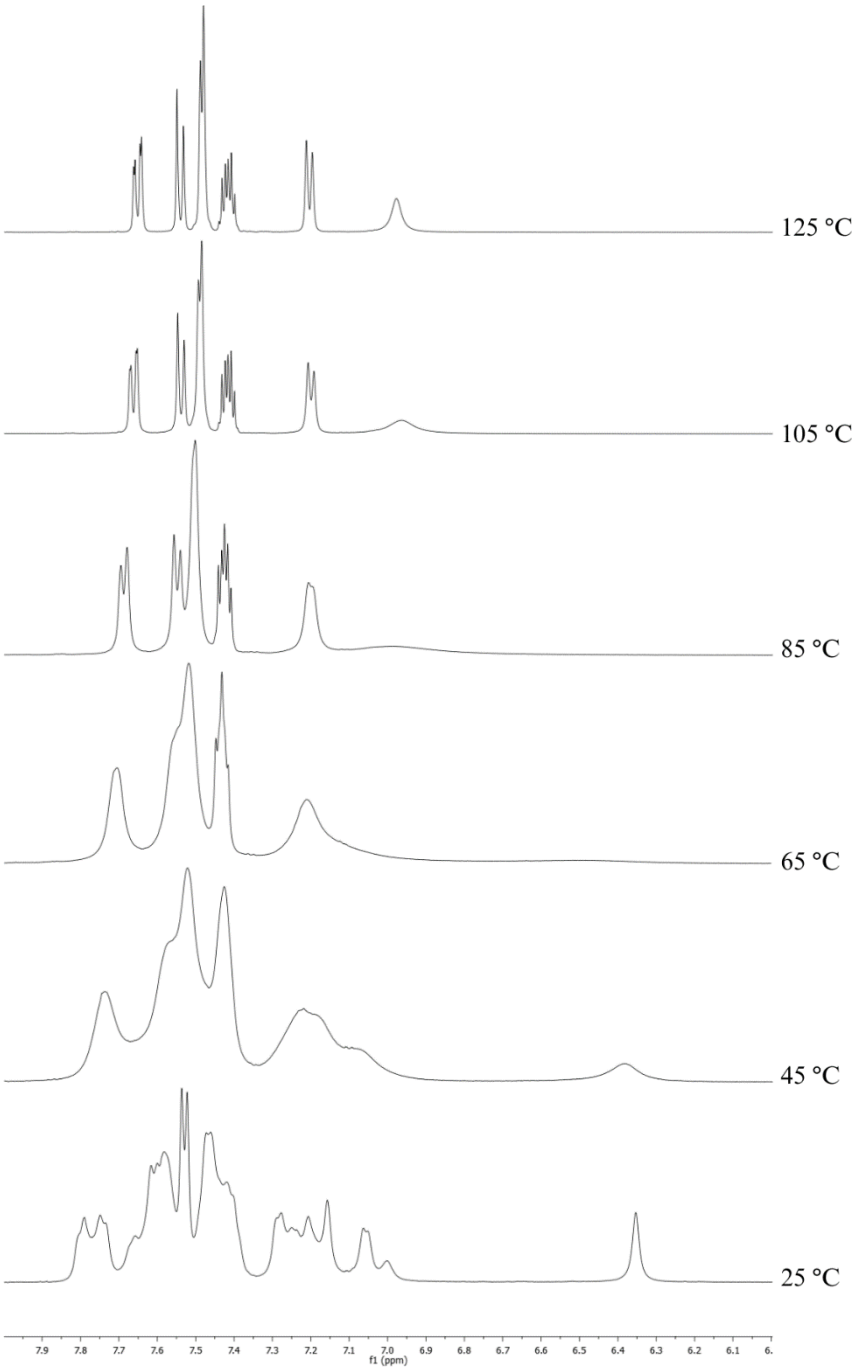

Figure 32: *^{1}H-NMR (400 MHz) spectra of quaterphenyl **94** in DMSO-d_6 zoomed into the aromatic part of the spectrum (6 – 8 ppm) at various temperatures.*

A clear separation of peaks could be observed in the measured spectra with the increase in temperature. Curiously the peak at 6.35 ppm vanished from 65 °C and up while a new peak emerged at 6.95 ppm from 85 °C. The broad peaks from 6.9 – 7.9 ppm separated into clearly distinguishable peaks with a clearly defined multiplicity. After interpretation of the ^{1}H-NMR spectrum at 125 °C a sum of integrals of 7 could easily be distinguished, matching the quaterphenyl **94** as shown in **Figure 33**. This result is the perfect example to showcase the application of high-temperature

NMR measurements for structure elucidation – especially when encountering broad signals in the spectra at room temperature – provided the product is stable at higher temperatures.

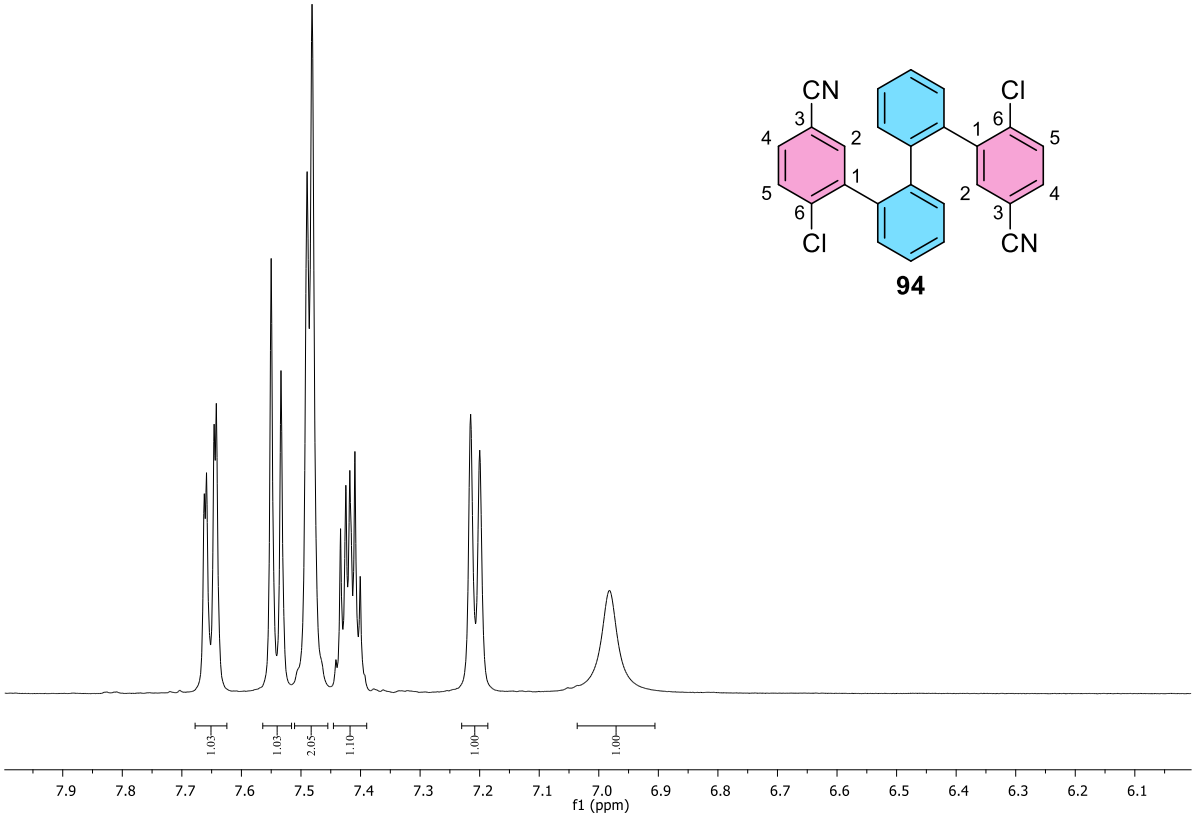

Figure 33: *^{1}H-NMR (400 MHz) spectrum of quaterphenyl **94** in DMSO-d_6 at 125 °C.zoomed into aromatic part of the spectrum (6 – 8 ppm)*

3.2.3 Synthesis of starting material with CN on positions 5 and 4

The Suzuki-Miyaura coupling reaction of the position 5 cyano-substituted starting material **97** using the strategy B with a boron-ester substituted scaffold **109** and the bromine-substituted aromatic ring **110** as well as [Pd(dtbf)Cl_2] as catalyst using the reaction conditions seen in **Scheme 33** gave the expected product **97** with an isolated yield of **58 %**.

For the 4 cyano-substituted starting material **99** strategy A was applied and it was made to react with the brominated scaffold **103** under similar reaction conditions, except for the decision to only use 2.2 equivalents of the substituted aromatic ring **111,** as also shown in **Scheme 33**, to save some of the costly substance as there was just a limited amount available. Nonetheless, the necessary excess of substrate was present and so the desired product **99** was obtained in an isolated yield of **60 %**.

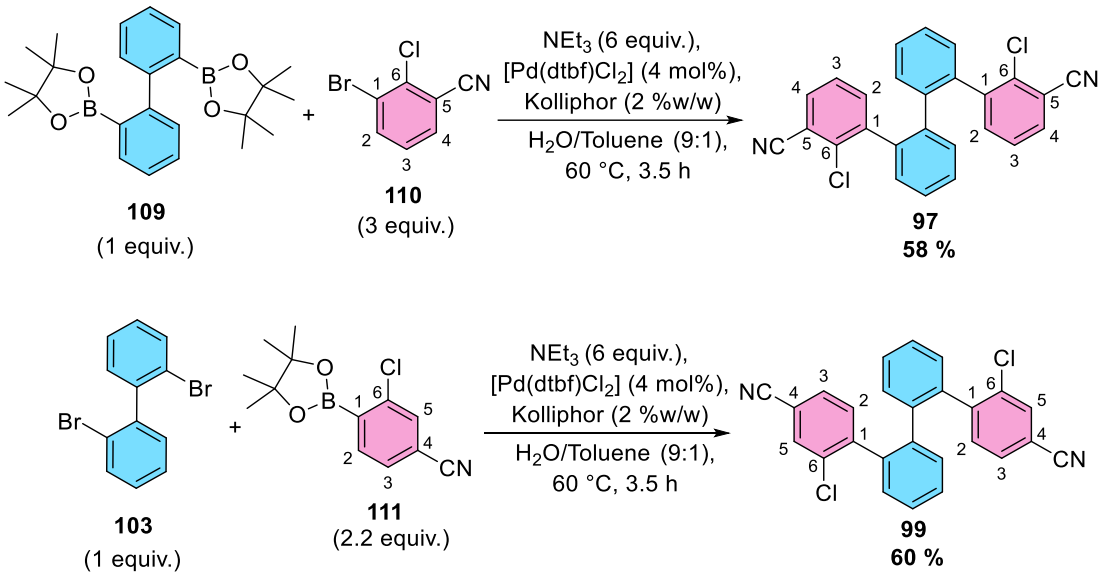

Scheme 33: *Synthesis of quaterphenyls with CN on positions 5 and 4* ***97*** *and* ***99****.*

3.2.4 Synthesis of starting material with CN on position 2

The Suzuki-Miyaura coupling reaction of the position 2 cyano-substituted starting material **101** using the strategy B with a boron-ester substituted scaffold **109** and the bromine-substituted aromatic ring **112** as well as [Pd(dtbf)Cl_2] as a catalyst was performed using the reaction conditions seen in **Scheme 34.** Unfortunately, the reaction was unsuccessful not being able to provide any of the desired quaterphenyl **101** and instead gave the unexpected mono-coupled side product **113** in a yield of **78 %**.

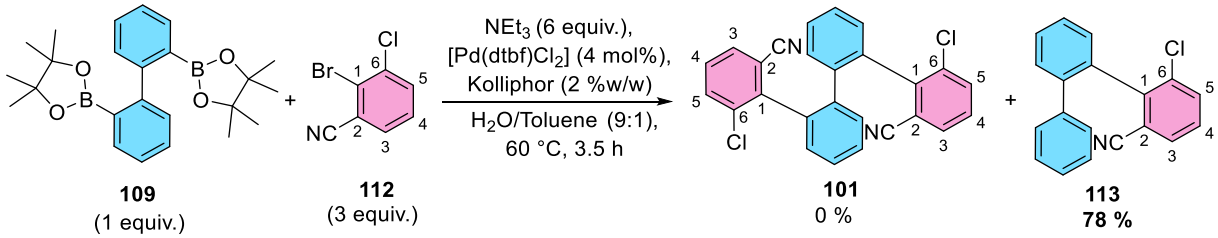

Scheme 34: *Attempted synthesis of quaterphenyl with CN on position 2* ***101****.*

The presence of one of the substituted aromatic rings and the lack of the second boron species on the scaffold suggest that the first Suzuki-Miyaura coupling occurred without issues and that the second step managed to initiate the oxidative addition step leading to debromination. However, it appears that complications arose during the transmetalation or reductive elimination steps of the coupling mechanism. These issues are likely attributable to excessive steric hindrance, resulting from the positioning of both chlorine and cyano groups ortho to the site intended for the formation of the new C-C bond.

3.3 Synthesis of target molecules

3.3.1 General plan for cyclization reactions

The cyclization reactions were planned to be performed using a photoredox catalytic procedure that had already been optimized within the Bonifazi group. It involved a substituted quaterphenyl **107** in a Schlenk tube with DMSO as a solvent, 3 equivalents of DIPEA as base and sacrificial agent and 0.2 equivalents of PXX as a photoredox catalyst. After 3 freeze-pump-thaw cycles to remove air and after backfilling with argon, the mixture would be stirred in a photoreactor for 4 days while being irradiated with blue light at 405 nm as shown in **Scheme 35**.

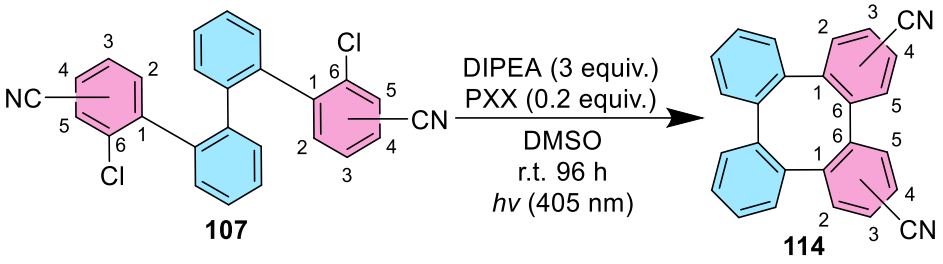

Scheme 35: *General plan for cyclization reactions.*

3.3.2 Synthesis of tetraphenylene with CN on position 3

The first time the reaction was performed it was attempted to be purified by recrystallization but when that failed a separation by two column chromatographies was performed. During the ^{1}H-NMR analysis of the collected fractions, the presence of a second isomer **115a** of the tetraphenylene with CN on position 3 **95** exhibiting the same mass in HRMS measurements was observed (for more information about how the structures were proven see **chapter 3.3.2.1**). After the first attempt, only **1 %** of Structure **95** and **0.3 %** of Structure **115a** could be isolated. A second reaction attempt was performed at a higher scale and gave isolated yields of **18 %** of isomer **95** and **5 %** of isomer **115a**. The amount of isolated products was high enough to set up crystals of highly purified products which later resulted in crystal structures that proved the structures of the two isomers **95** and **115a** (for more information see **chapter 3.3.2.1**). The reaction was repeated once more to determine the yields with an internal standard, which resulted in a **24 %** yield for isomer **95** and a **17 %** yield for isomer **115a**. All the discussed reactions also gave a distinct insoluble precipitate that would be separated during purification but that could never be isolated.

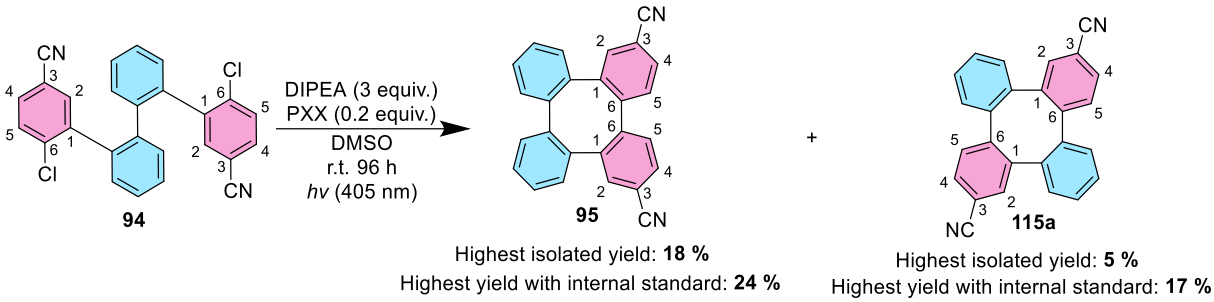

Scheme 36: *Synthesis of tetraphenylene with CN on position 3* ***95****.*

The reaction was repeated two further times with slightly differing reaction conditions. In one attempt the reaction was performed with 3 equivalents of caesium carbonate instead of DIPEA to test whether DIPEA performed a role as a base or as a sacrificial agent in the reaction since caesium carbonate can only function as a base while DIPEA can potentially also fulfil both the roles of a base and a sacrificial agent. After the reaction, an insoluble precipitate that could not be isolated was observed. The outcome of the reaction was a reduced yield of **11 %** for isomer **95** and **6 %** for isomer **115a**, which indicated that PXX was able to catalyse the reaction to a certain degree but needed a sacrificial agent to increase the conversion into the desired product. The second reaction with changed reaction conditions was one where the reaction time was decreased from 96 h to 24 h. After the reaction, an insoluble precipitate was also observed but could not be isolated. The yields with internal standard were **26 %** for isomer **95** and **20 %** for isomer **115a**. This result indicated that the reaction worked slightly better when only performed at 24 h and future syntheses can be shortened to this time saving plenty of time. The decrease in yield over time could be due to the emergence of more side-products over time.

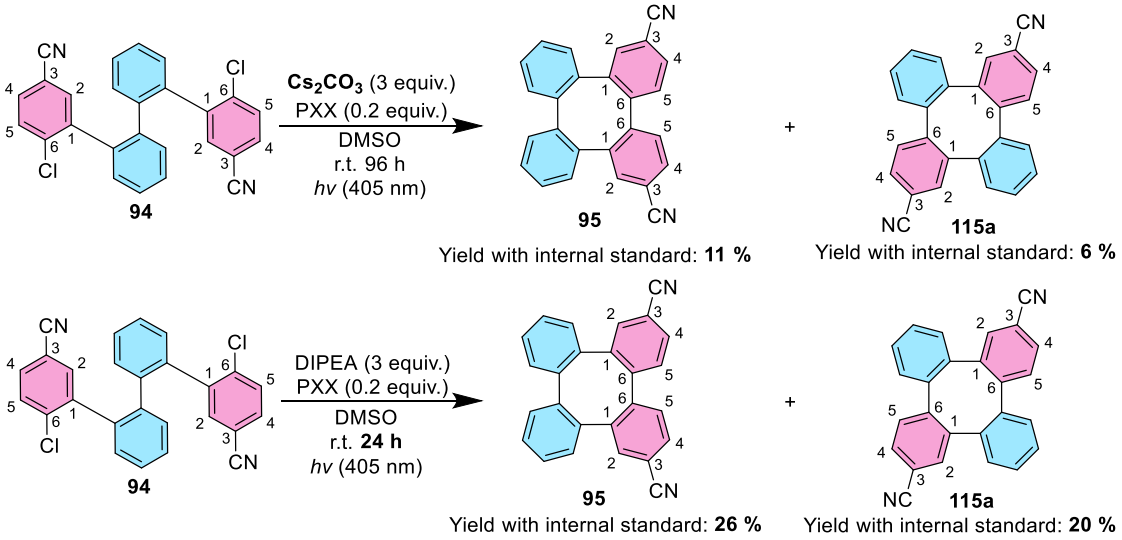

Scheme 37: *Further cyclization reactions with altered reaction conditions.*

In summary, these were all the performed reactions:

Table 1: *Summarized reactions for the synthesis of tetraphenylene with CN on position 3* ***95****.*

Entry	Duration [h]	Base	Yield **95**	Yield **115a**	Conversion
1	96	DIPEA	1%	0.3%	Undetermined
2	96	DIPEA	18%	5%	Undetermined
3	96	DIPEA	24%[a]	17%[a]	100%[a]
4	96	Cs_2CO_3	11%[a]	6%[a]	100%[a]
5	24	DIPEA	26%[a]	20%[a]	100%[a]

[a]*Determined by trimethoxybenzene internal standard.*

3.3.2.1 Structure elucidation of products of synthesis of tetraphenylene with CN on position 3

While working on the purification of the reaction mixture after the first attempt to perform the synthesis of tetraphenylene with CN on position 3 **95**, ^{1}H-NMR analysis of collected fractions resulting from column chromatography could indicate a clear presence of two separate products instead of just the one expected product. The two products had been difficult to separate on column chromatography and would only show as one spot when analysing the initial reaction mixture by thin layer chromatography, indicating a very similar polarity of both products. What was especially surprising was that both products contained similar signals in the aromatic part of the ^{1}H-NMR spectrum from 7.00 ppm to 7.70 ppm with integrals that added up to 7 unique H-atoms as seen in **Figure 34**.

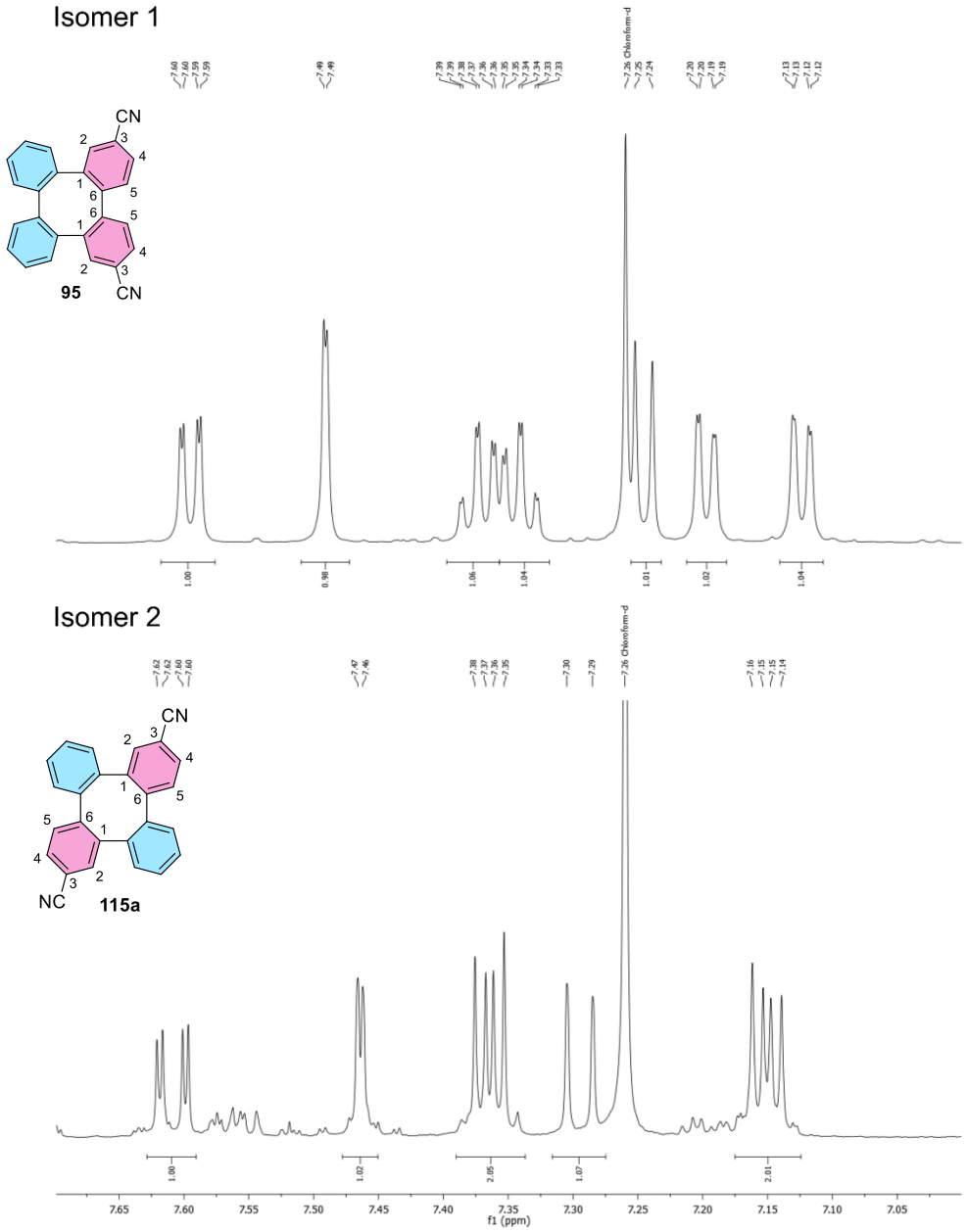

Figure 34: *^{1}H-NMR (400 MHz) Spectra of the two isolated isomers of the first synthesis of tetraphenylene with CN on position 3* ***95*** *and* ***115a*** *zoomed into the aromatic part of the spectrum (7.00 ppm – 7.70 ppm).*

It was initially unclear what the nature of the second product was and after obtaining the masses of 377.1 u from HRMS analysis for both products it seemed likely that the two products were isomers of each other. However, no further conclusions could be made on the exact structure of the second isomer, especially by 2D-NMR. Luckily it was possible to grow crystals of the two products to obtain the crystal structure of both products to prove their exact configuration as depicted in **Figure 35**.

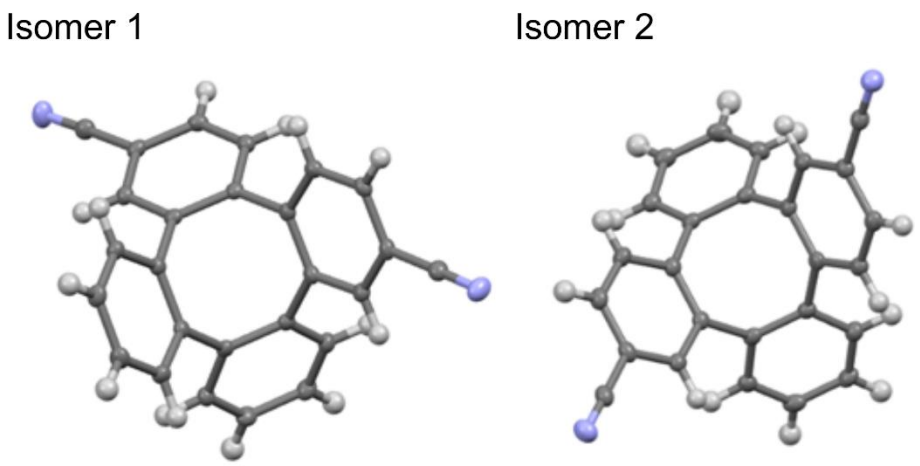

Figure 35: *Crystal Structures of the two products of synthesis of tetraphenylene with CN on position 3* ***95*** *and* ***115a****.*

3.3.2.2 Attempting to trap a radical with TEMPO

2,2,6,6-tetramethylpiperidine-N-oxyl radical (TEMPO) is a prominent member of the class of compounds known as nitroxyl radicals or nitroxides that is often used as a trapping reagent or radical scavenger. TEMPO exhibits a delocalized unpaired electron between the nitrogen and the oxygen atom and it belongs to the class of persistent radicals and no other reagent is needed to generate the radical species.[193] It is known for being fast at trapping carbon-centred radicals with a rate constant ranging from $5 \cdot 10^7$ $M^{-1}s^{-1}$ to $2 \cdot 10^9$ $M^{-1}s^{-1}$ at room temperature.[194]

Since one of the main aims of the project was to get a better understanding of the underlying mechanism of the photoredox-catalysed cyclization reaction of tetraphenylenes, it was attempted to trap a radical intermediate of the reaction assuming that it occurs based on a radical mechanism. For this purpose, the reaction was performed with the same conditions as usual but with a certain amount of added TEMPO as a radical trapping agent as depicted in **Scheme 38**. The goal was to obtain either structure **116** as a trapped biradical form or **117** as a trapped monoradical form. The reaction was performed four times; Twice with 20 equivalents of TEMPO, once with 40 equivalents of TEMPO and once with 80 equivalents of TEMPO. Unfortunately, none of the reactions gave any sign of the presence of neither the product **116** nor **117**. This might indicate that the radical intermediates are too short-lived for TEMPO trapping or that the mechanism might not have a classically understood radical mechanism. Further studies such as EPR studies are however necessary to make more concrete claims.

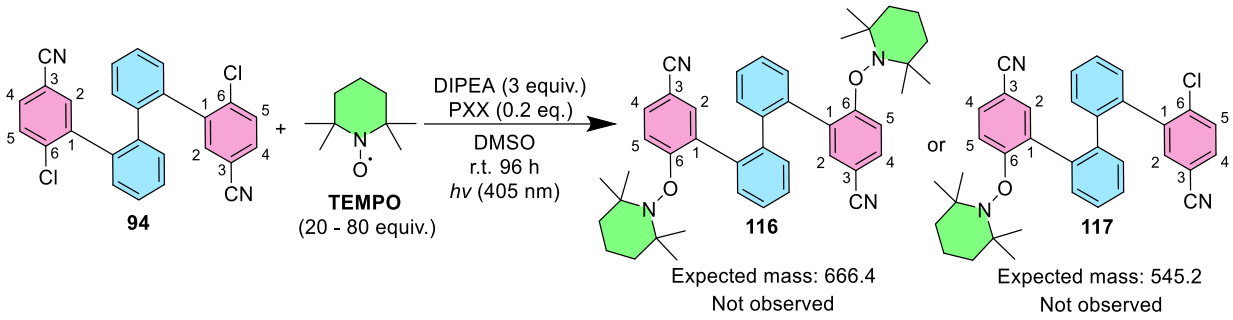

Scheme 38: *Radical trapping reaction with TEMPO. Measured mass spectra can be found in the appendix.*

3.3.3 Synthesis of tetraphenylene with CN on position 4

The synthesis of tetraphenylene with CN on position 4 was performed using the usual procedure, resulting in a mixture of two main products and an insoluble precipitate that could not be isolated. This time, however, the separation of the two tetraphenylenes **100** and **115b** proved difficult, even after column chromatography and recycling GPC. The column chromatography fractions containing only the two products **100** and **115b** together before separation yielded 36 %. However, no fraction could be obtained containing pure tetraphenylene **100**. Fortunately, it was possible to isolate pure tetraphenylene **115b** with a yield of 8 % as seen in **Scheme 39**.

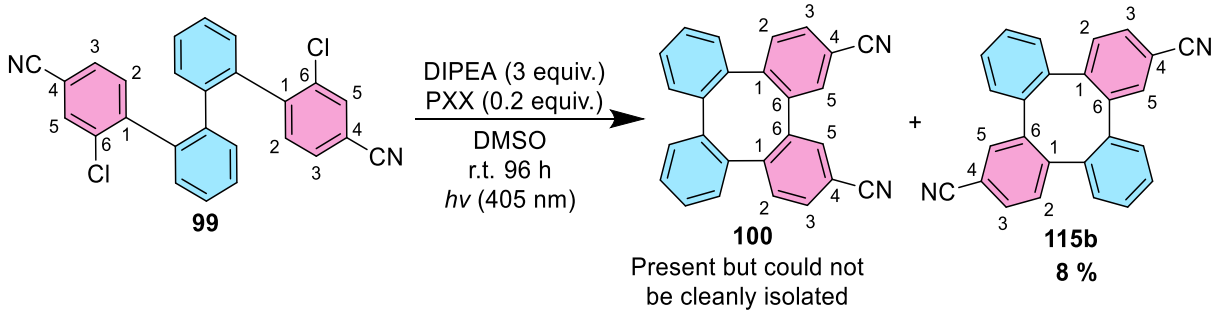

Scheme 39: *Synthesis of tetraphenylene with CN on position 4* ***100****.*

3.3.3.1 Structure elucidation of products of synthesis of tetraphenylene with CN on position 4

The ^{1}H-NMR spectrum for the side product **115b** was identical to the previously isolated side product **115a** from the synthesis of tetraphenylene with CN on position 3 (see **chapter 3.3.2**). The structure could also be proven by the growth of the crystal structure shown in **Figure 36**. This would mean that the same product can be arrived at through the photoredox catalysis of two different starting materials. Unfortunately, no crystal structure of the desired tetraphenylene with CN on position 4 **100** was able to be grown so the structure had to be elucidated based on comparisons to ^{1}H-NMR spectra of previously isolated tetraphenylenes as portrayed in **Figure 37**.

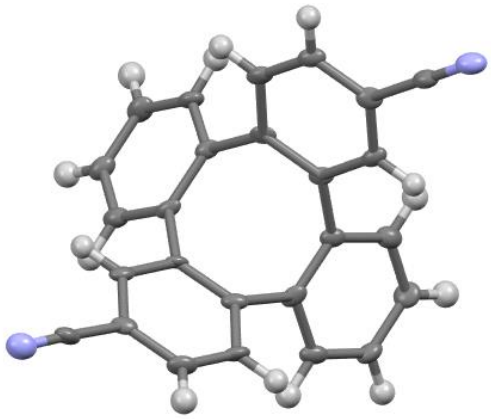

Figure 36: *Crystal structure of side product* ***115b****.*

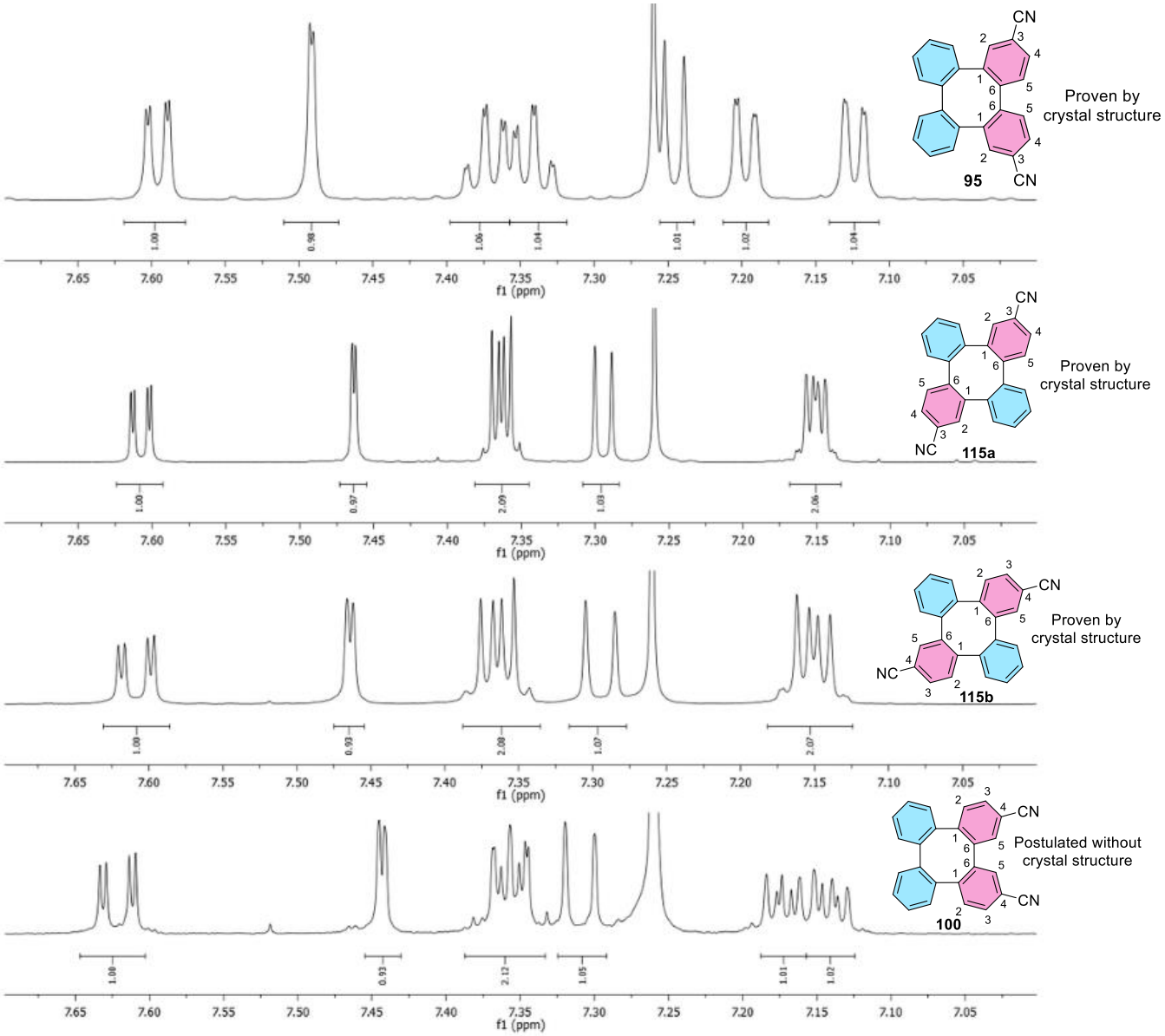

Figure 37: *[1]H-NMR (600 MHz) spectra of various synthesized tetraphenylenes zoomed into the aromatic part of the spectrum (7.00 ppm - 7.70 ppm)*

In future studies of these structures, it would be beneficial to reproduce the synthesis of tetraphenylene with CN on position 4 **100** on a high enough scale to maintain enough of the desired tetraphenylene **100** to grow pure crystals of it to confirm the proposed structure.

3.3.4 Synthesis of tetraphenylene with CN on position 5

When performing the cyclization reaction with the quaterphenyl substituted with cyano-groups on position 5 **97** using the usual photoredox catalytic procedure no tetraphenylene **98** was observed but instead, only the dibenzotetracene **118** could be isolated in a yield of 15 %. The product was highly insoluble in most commonly used solvents like $CHCl_3$, DCM and Acetone.

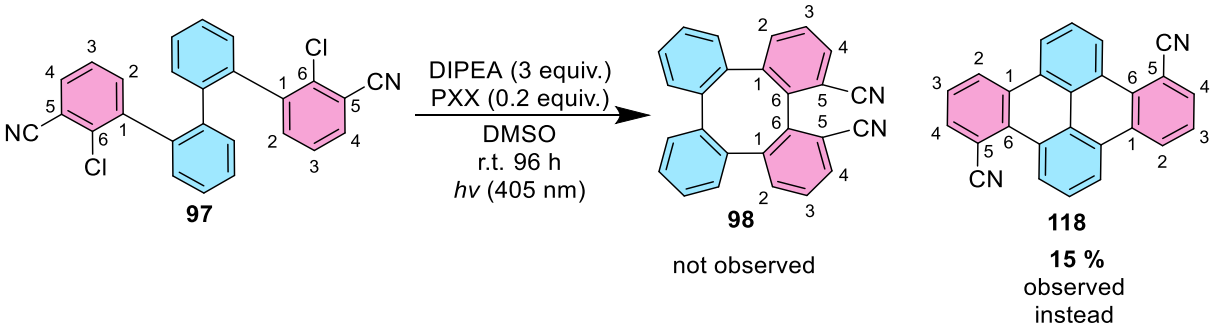

Scheme 40: *Attempted synthesis of tetraphenylene with CN on position 5* ***98****.*

The structure could be easily elucidated by HRMS, 2D-NMR and even a crystal structure was obtained.

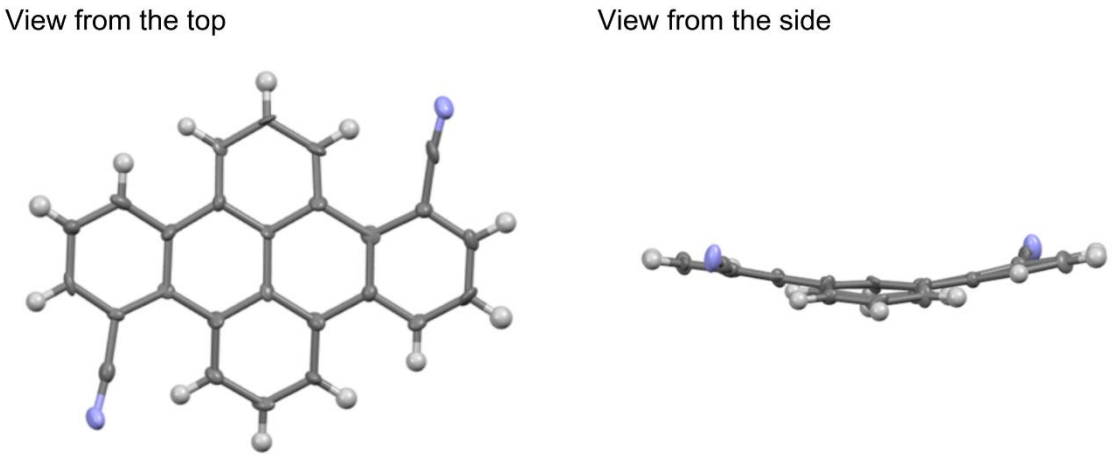

Figure 38: *Crystal structures of product* ***118*** *from the top and the side.*

The crystal structure showed that the whole molecule **118** was almost completely flat, which explained its poor solubility. The ability to form π-π interactions between the

aromatic rings with a large surface while being able to stack very closely on top of each other should make this a molecule that is difficult to solvate with many types of solvent. Based on this result it is assumed that the other syntheses of tetraphenylenes that were performed during this project also lead to a certain yield of flat dibenzotetracene side-product, even though it could not always be isolated. The large issues involving the handling and isolation of these insoluble products made it not worth the effort to determine the exact yields and structures of the emerging precipitates in the other reactions.

The hypothesis for why the expected tetraphenylene **98** was not observed is that the cyano-groups might be too close to the C-C bond forming position 6 during the tetraphenylene formation mechanism leading to steric hindrance. Further experiments with less bulky electron-withdrawing groups on position 5 might be performed to test this hypothesis

3.4 Summary

All previously discussed syntheses are summarized in **Scheme 41** for clarity. Due to the findings during the attempted synthesis of tetratphenylene with CN on position 5 that are described in **chapter 3.3.4**, the presence of insoluble precipitate after the reactions with CN on positions 3 and 4 was deemed to be plausibly interpreted as the formation of the dibenzotetracene side-products **96a** and **96b**. Even though their structures were not clearly determined, their presence would explain why the sum of the yields determined with internal standard of tetraphenylene isomers **95** and **115a** would only be up to 41 %, despite full conversion being observed.

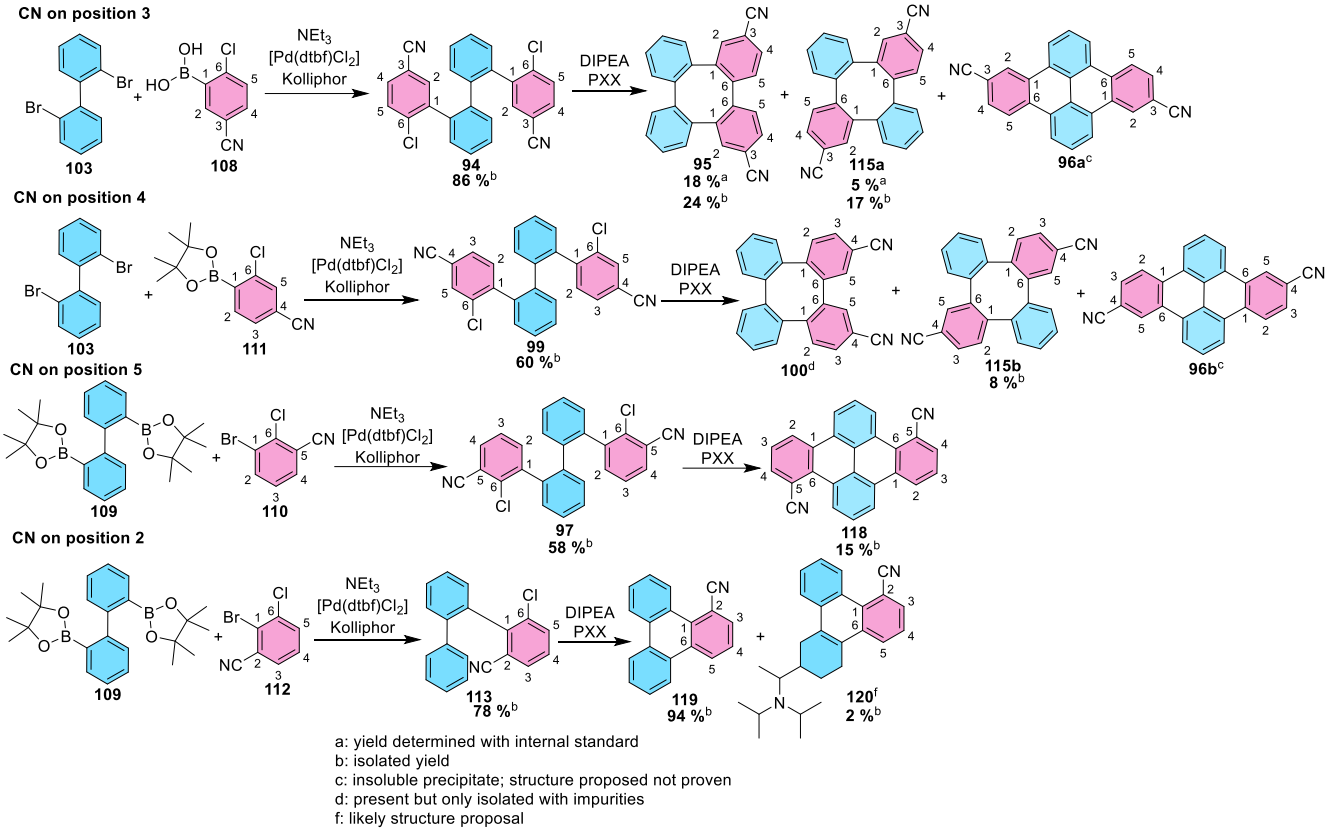

Scheme 41: *Summary of previously discussed reactions.*

To summarize, two of the performed syntheses (CN on position 3 and CN on position 4) lead to the synthesis of the expected tetraphenylenes **935** and **100** as well as the unexpected tetraphenylene isomers **115a** and **115b**, which, in fact, are the same structure. It is also expected that the dibenzotetracenes **96a** and **96b** are further products in the form of an insoluble precipitate. The synthesis for CN on position 5 led to the sole formation of the insoluble dibenzotetracene **118**, likely because of the steric hindrance of the CN groups on the position next to the newly formed bond. The synthesis for CN on position 2 led to the mono-arylated starting material **113**, which was then mistakenly further used to synthesize the products **119** and **120**.

3.5 Discussion of mechanisms

Even though no radical intermediate could be trapped, and the reaction also worked with Cs_2CO_3 as a base instead of DIPEA, the most plausible mechanism for the formation of tetraphenylene **95** from quaterphenyl **94** remains the formation of a biradical species followed by a recombination of the two radicals to form an octagon as visualized in **Scheme 42**. The detailed postulated mechanism likely entails a photoredox catalytic cycle in which PXX is excited to its excited state PXX* which

passes on an electron to single electron transfer (SET) onto the quaterphenyl **94** while transforming into its oxidized state $PXX^{\bullet+}$. DIPEA then acts as a sacrificial agent, giving the photoredox catalyst back the electron to close the catalytic cycle while itself becoming oxidized to a radical carbocation. Meanwhile, the quaterphenyl radical carbanion **121** would probably be formed followed by the loss of a chloride ion leading to the formation of the quaterphenyl radical **122**. Following another photoredox catalytic cycle a second single electron transfer likely occurs following the same cycle as previously described forming the radical carbanion intermediate **123** that is transformed into the biradical species **124a** with radicals at the positions 6 after the loss of a chloride. The aromatic rings of this biradical intermediate then rotate around their Ar-Ar bonds for the two radicals to meet as shown in the intermediate **124b**. Lastly, the two radicals recombine forming the novel Ar-Ar bond between the positions 6 of the teraphenylene **95**.

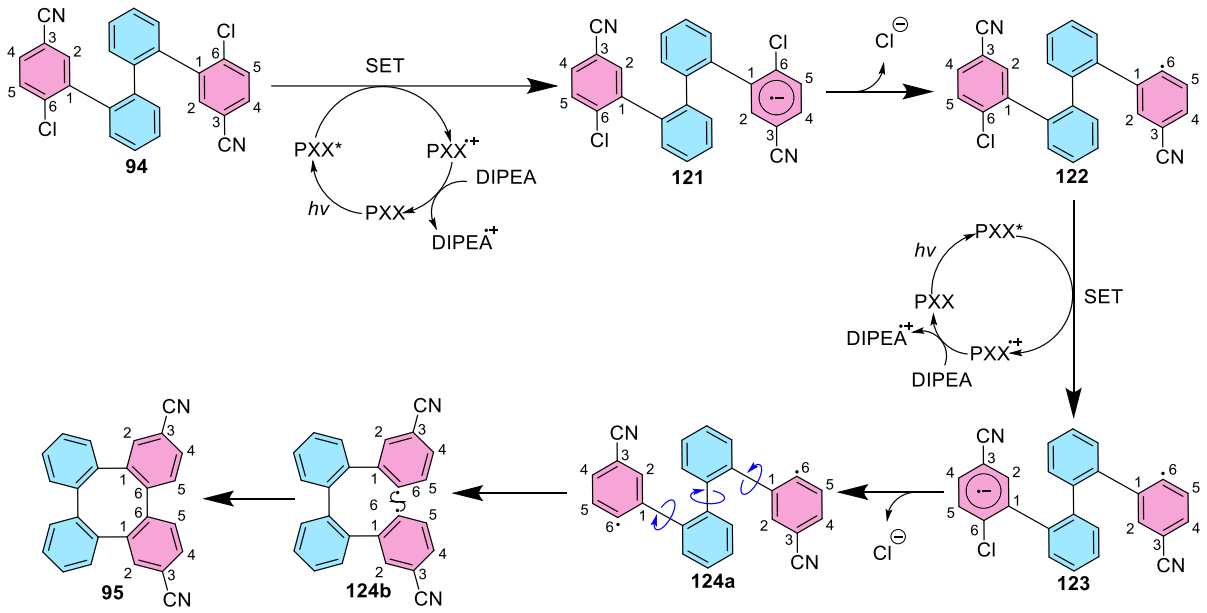

Scheme 42: *Proposed mechanism for the formation of tetraphenylene **95**.*

The reaction mechanism for the formation of the secondary tetraphenylene product **115a** is postulated to involve a novel rearrangement reaction as shown in **Scheme 43**. It likely begins similarly to the previously described mechanism leading to the same biradical intermediate **124a**. However, this time the radicals at position 6 likely form a bond with the *ipso*-bond of the aromatic rings comprising the central “scaffold” leading to the formation of the bifluorene-like biradical species **125a**, which can also be drawn as **125b**. This intermediate is predicted to be highly energetically unfavoured leading to the rapid breaking of the bond between the two blue “scaffold” aromatic rings while re-aromatizing the two rings leading to the formation of the tetraphenylene **115a**.

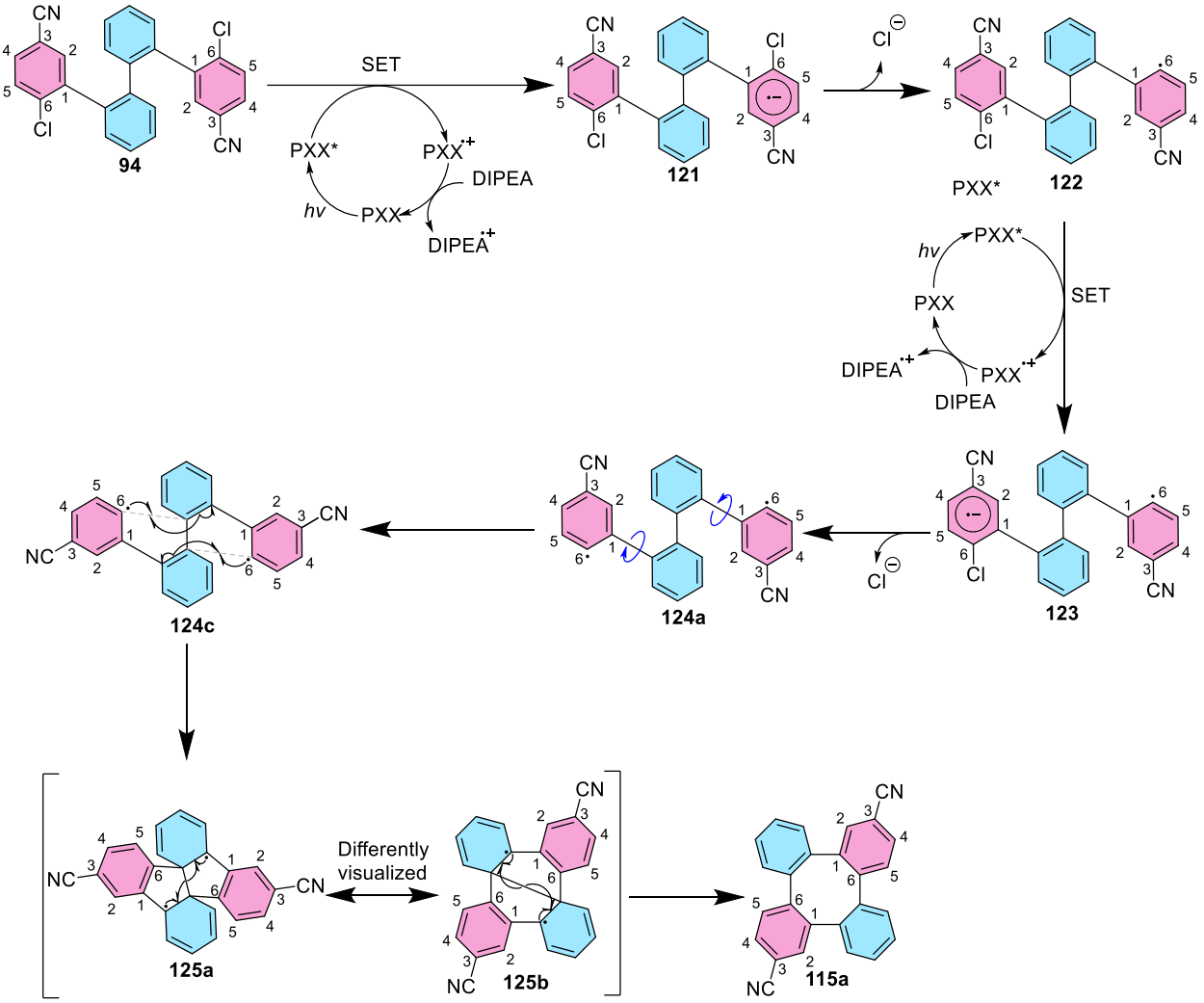

Scheme 43: *Proposed mechanism for the formation of tetraphenylene* ***115a****.*

The photoredox catalytic mechanism of formation of dibenzotetracene **96a** likely occurs through a process already proposed by Zanetti *et al*. in 2023 shown in **Scheme 44**.[190] After excitation of PXX to the excited state PXX* by light, a single electron transfer (SET) to one of the two pink rings occurs and the radical anion **121** is formed. After the loss of a chloride the radical on position 6 of the first pink aromatic ring forms a bond with the *ortho*-position of the blue "scaffold" ring leading to the intermediate radical **122**. This intermediate is then likely capable of transferring an electron to PXX•+ closing the photoredox catalytic cycle without the need for an additional sacrificial agent, leading to the formation of the carbocation intermediate **127**. Here, DIPEA abstracts the proton on the *ortho*-position of the blue "scaffold" ring, rearomatizing the ring and forming the intermediate **128**. At this point, the same mechanism occurs with the second pink ring finally forming the dibenzotetracene **96a**.

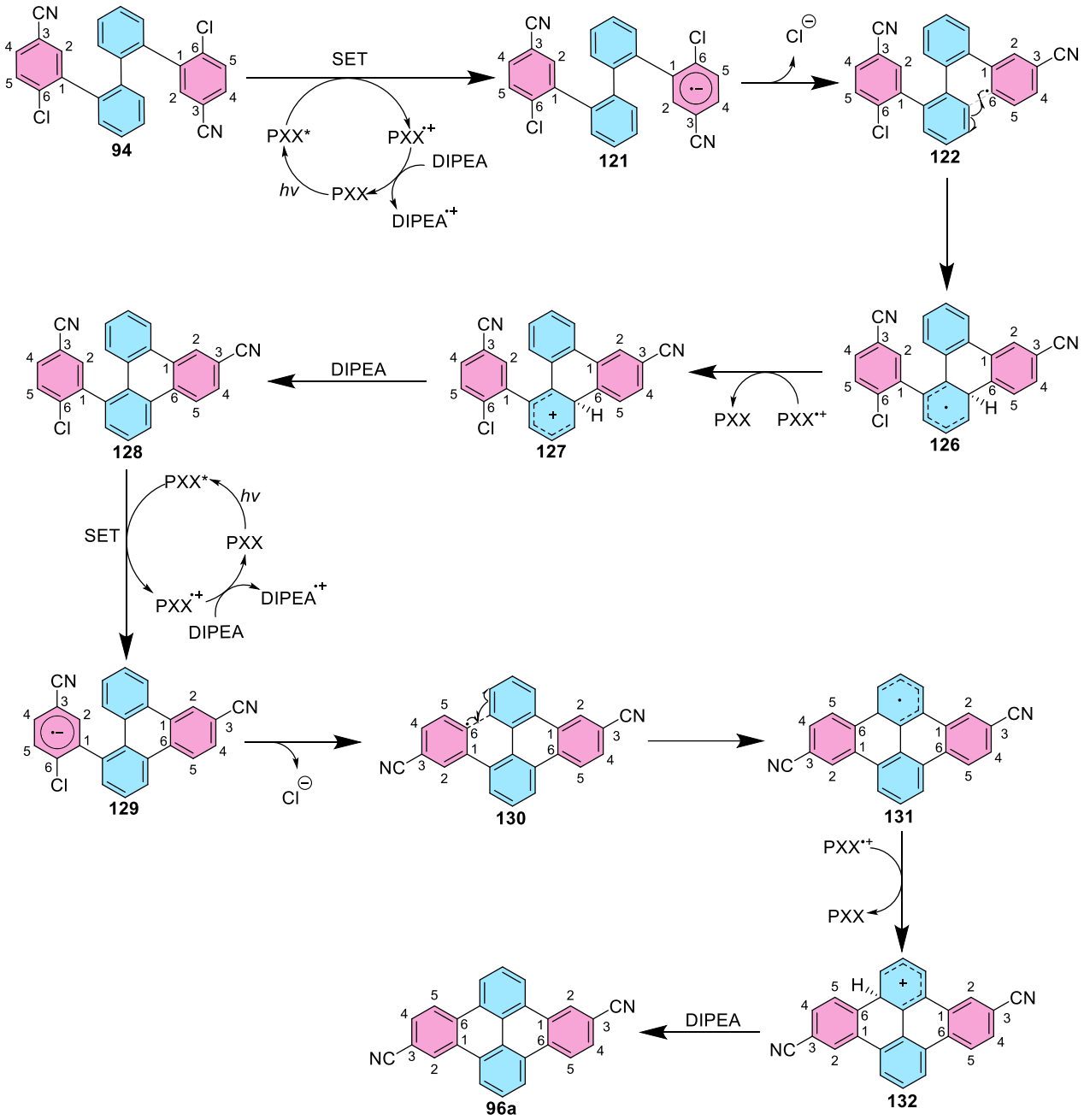

Scheme 44: *Proposed mechanism for the formation of dibenzotetracene* ***96a****.*

3.5.1 Further mechanistic discussions

3.5.1.1 Discussing the issues with the synthesis of tetraphenylene with CN on position 3

Having described the mechanism of the formation of tetraphenylene with CN on position 3 **95** in **chapter 3.5** it can now be discussed why no formation of tetraphenylene with CN on position 5 **98** was observed. The proposed problem is that when the biradical intermediate **133** is formed the CN-groups are too bulky and pointing in the same direction as shown in **Scheme 45**. Since the final product as shown as a 3D model in **Figure 39** has the CN-groups pointing in differing directions in the more

sterically stable structure in the end, the biradical recombination mechanism could be occurring by a more planar configuration in which substituents in position 5 hinder the formation of a bond in position 6. Future reactions could be designed with different less bulky substituents at position 5 to test this effect.

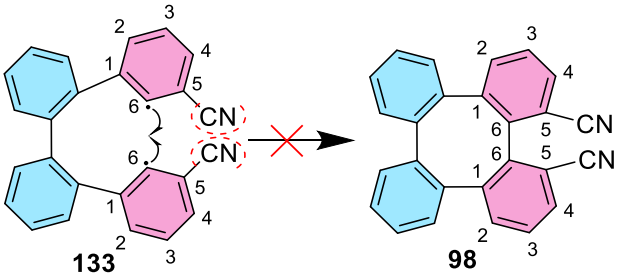

Scheme 45: *Steric hindrance of CN on position 5 hindering the recombination of radicals.*

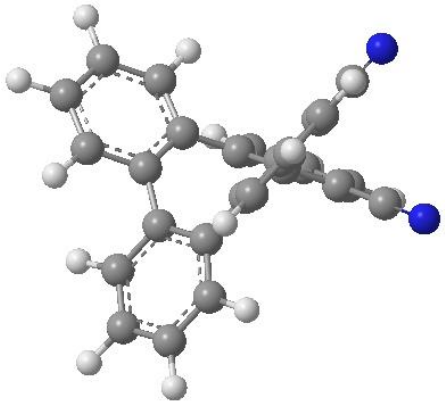

Figure 39: *3D model of tetraphenylene with CN on position 5* ***98.*** *N atoms in blue, C atoms in grey and H atoms in white.*

3.5.1.2 Discussing the results of the synthesis of tetraphenylene with CN on position 3 95 with Cs_2CO_3 instead of DIPEA

Regarding the result of the synthesis of tetraphenylene with CN on position 3 **95** with Cs_2CO_3 instead of DIPEA as the base there is also a possible explanation for the success of the reaction, although with a decreased yield, despite the absence of a sacrificial agent that is illustrated in **Scheme 46**. Since the formation of the insoluble dibenzotetracene **96a** is expected to occur through a photoredox catalytic reaction *in tandem* with the formation of the tetraphenylene **95**, it is plausible that radical intermediates of the dibenzotetracene, like for example **131,** could be acting as electron donors to $PXX^{\bullet+}$ closing the photoredox catalytic cycle back to ground state PXX and allowing for the formation of the two tetraphenylene products **95** and **115a** even in the absence of a sacrificial agent like DIPEA. It is nonetheless surprising that the system shuffles electrons on its own so well that the yield only decreases from 24 % to 11 % for tetraphenylene **95** resulting in just a loss of 54 % of yield and

additionally still allows the rearrangement of 6 % yield of the tetraphenylene **115a** to occur in the absence of a sacrificial agent like DIPEA.

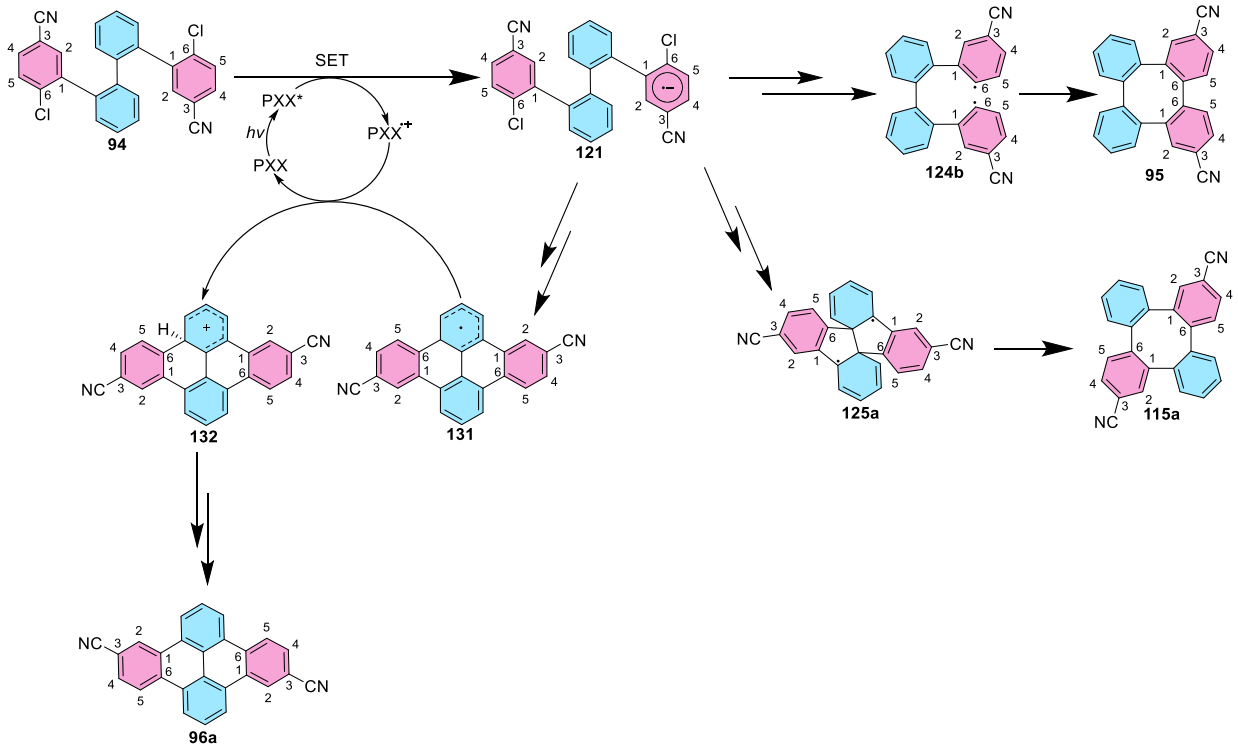

Scheme 46: *Photoredox catalytic reaction in the absence of a sacrificial agent DIPEA.*

3.6 Further exploration of the reactivity of the photoredox catalytic synthesis of tetraphenylenes

The mechanism remains a speculative proposal and further investigation is required to validate the mechanism, particularly regarding the atypical rearrangement to tetraphenylene **115a**. A promising approach to validate whether the mechanism occurs through a biradical mechanism is to perform electron paramagnetic resonance (EPR) studies, which are currently ongoing at the time of writing this thesis. Additionally, a computational approach could be utilized to calculate the enthalpies of the proposed intermediates to build a reaction-enthalpy-diagram to test the plausibility of the proposal. These two methods remain to be utilized since they could not be pursued during the work for the thesis due to time constraints and due to the synthetic focus of the work. Nevertheless, alternative synthetic approaches were explored as described in subsequent chapters.

3.6.1 Enhancing chemoselectivity through substitution of the biphenyl scaffold

An approach that was attempted to be investigated was to control the formation of tetraphenylenes by stopping the formation of dibenzotetracene side-products. This

would not only be predicted to allow the formation of higher yields of tetraphenylenes due to a smaller amount of side-product formation, but it could also be tested what effect further substituents would have on the formation of tetraphenylene – perhaps even allowing to control which of the two tetraphenylene products would be favourably formed. The basis for this approach is depicted in **Scheme 47**. The idea is to block the formation of bonds between the radical on position 6 of the pink outer ring and the unsubstituted carbon in the ortho position of the blue "scaffold" ring in a radical intermediate like **124d** by substituting this ortho position of the blue "scaffold" ring with a rest as in structure **134**. This would likely lead to further reactions favouring either the recombination reaction of the two radicals on position 6 of the pink outer rings or the novel rearrangement following the radical reaction of the radical at position 6 with the *ipso* carbon atom. By substituting the *ortho*-position of the blue "scaffold" ring with an electron donating group (EDG) like a methoxy group as in structure **135**, the carbon in its *ipso*-position would become partially negatively charged making it more appealing for a reaction with a radical. These effects should thus in theory make the rearrangement product **136** the more common product of the reaction rather than **137**. In turn, substituting the *ortho*-position with an electron-withdrawing group (EWG) like a methyl acetate group, as shown in structure **138**, the carbon in the *ipso*-position would oppositely become partially positively charged making it less appealing for a reaction with a radical. The result of this should be the formation of more of the non-rearranged tetraphenylene **140** rather than **139**.

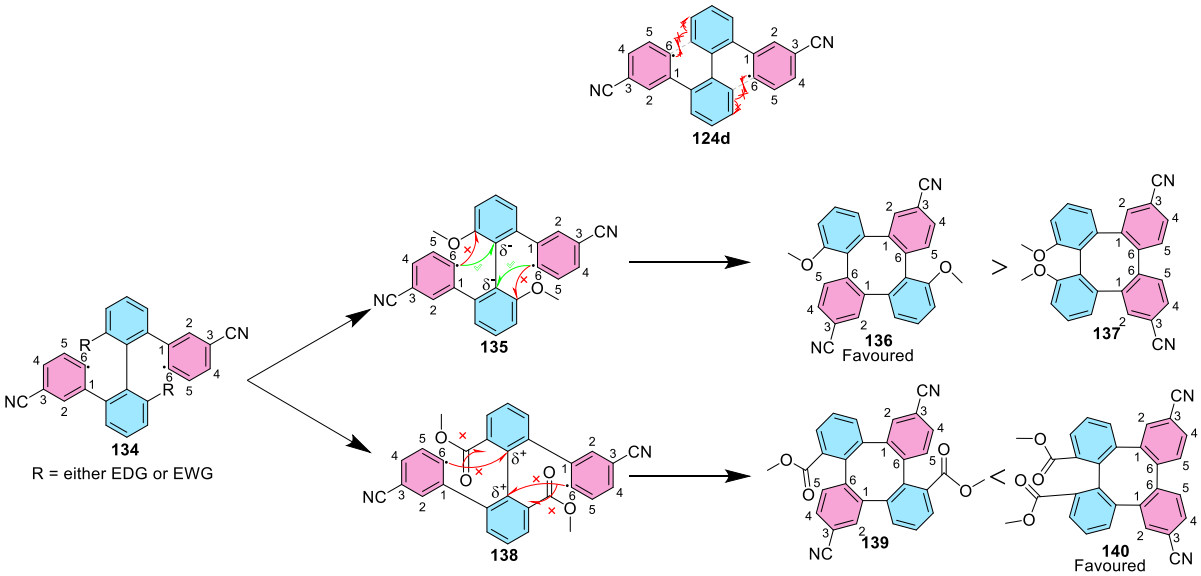

Scheme 47: *Hypothesized effect of EDGs/EWGs in the central "scaffold" rings.*

This approach was seen as synthetically viable, so it was decided to attempt synthesizing such “scaffold” substituted quaterphenyls.

3.7 Synthesis of methoxy and methyl acetate substituted scaffold starting materials

The retrosynthesis for the quaterphenyls substituted with methoxy or methyl acetate moieties shown in **Scheme 48** predicts that they can be formed *via* a Suzuki cross-coupling reaction like the already performed ones from the commercially available boron-substituted aryl species **108** and the dibromine-substituted biaryl species **142**. The biaryl species **142** itself would have to be formed by coupling the iodinated substituted aryl **143** with the boronated substituted aryl **144** *via* another Suzuki cross-coupling reaction. Unfortunately, the boronated species **144** would not be commercially available so it would have to be boronated by coupling the iodinated substituted aryl **143** with B_2pin_2.

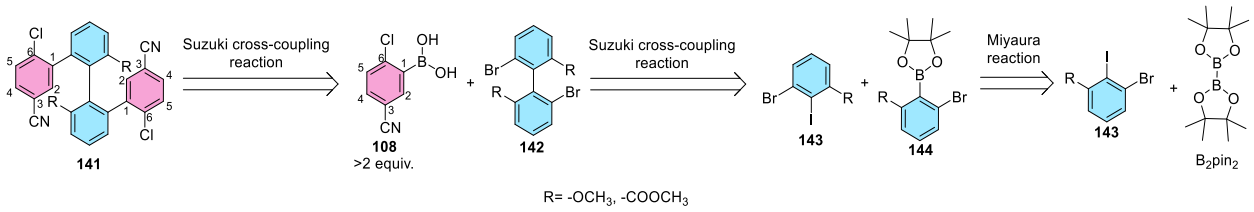

Scheme 48: *Retrosynthesis of substituted quaterphenyls* ***141****.*

The synthesis involving the first Miyaura reaction of the methoxy-substituted substrate **146** was attempted using various approaches based on the one shown in **Scheme 49**. The reaction was performed at varying scales, with dry DMSO or dry 1, 4 Dioxane, trying out approaches using KOAc or Potassium-2-ethylhexanoate as bases *in tandem* with $Pd(dppf)Cl_2$ as a catalyst. Once an approach using CsF/Pyridine without Pd-catalyst was attempted. The results of these reactions are summarized in **Table 2**, but they were all unsuccessful. Once, during the third attempt in dry 1, 4 Dioxane using KOAc and $Pd(dppf)Cl_2$ the desired product could be observed, however, it mainly decomposed during purification *via* a silica column chromatography leading to barely any available product. Since not enough boronated substituted aryl **146** was managed to be synthesized, this project had to be abandoned.

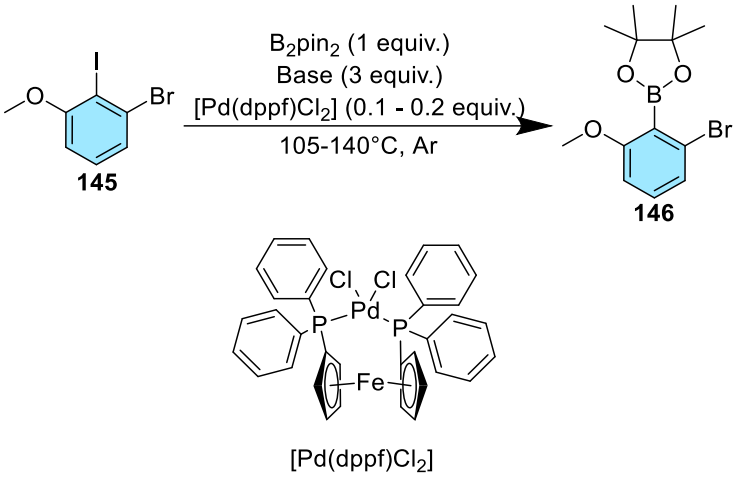

Scheme 49: *Synthesis of boronated methoxy substituted aryl* ***146.***

Table 2: *Synthesis attempts of boronated methoxy substituted aryl* ***146.***

Entry	Scale [mmol]	Solvent	Base	Pd Cat. [eq.]	Time [h]	Result
1	0.15	Dry DMSO	KOAc[a]	0.1	23	Mainly starting material
2	0.15	Dry DMSO	CsF/Pyridine	-	21.5	Only starting material
3	0.15	Dry 1,4 Dioxane	KOAc[b]	0.1	61	Mainly product – lost during purification
4	0.15	Dry 1,4 Dioxane	KOAc[a]	0.1	24	Only starting material
5	0.64	Dry 1,4 Dioxane	KOAc[b]	0.1	12	Only starting material
6	0.15	Dry 1,4 Dioxane	KOAc[b]	0.1	24	Only starting material
7	0.15	Dry 1,4 Dioxane	Potassium-2-ethylhexanoate	0.1	24	Mainly starting material

[a]*Dried in a desiccator.* [b]*Freshly dried in the oven.*

The same reactions were also attempted using the methyl acetate substituted derivative **155** as shown in **Scheme 50** and summarized in **Table 3**. The two performed reactions also proved to be unsuccessful and were therefore abandoned.

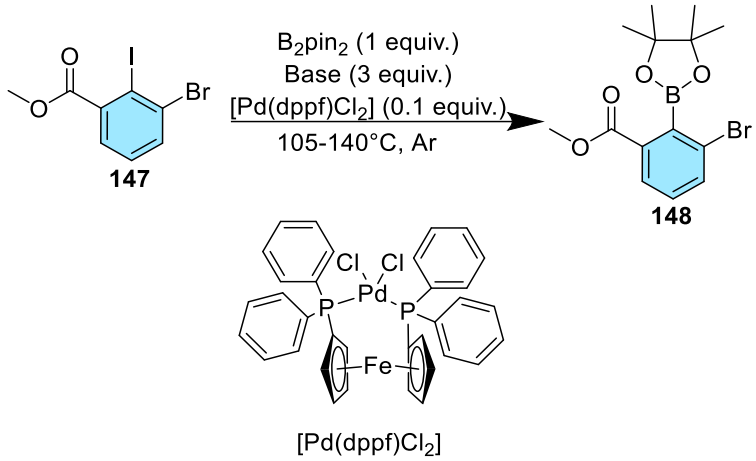

Scheme 50: *Synthesis of boronated methyl acetate substituted aryl* ***148****.*

Table 3: *Synthesis attempts of boronated methyl acetate substituted aryl* ***148****.*

Entry	Scale [mmol]	Solvent	Base	Pd Cat. [eq.]	Time [h]	Result
1	0.15	Dry 1,4 Dioxane	KOAc[a]	0.1	24	Only Starting Material
2	0.587	Dry 1,4 Dioxane	KOAc[b]	0.1	24	Only Starting Material

[a]Dried in a desiccator. [b]Freshly dried in the oven.

IV Conclusion

Various syntheses of CN substituted tetraphenylenes *via* photoredox catalysis with PXX as photocatalyst were performed as well of their quaterphenyl precursours *via* Suzuki-Miyaura coupling. With the aid of various obtained crystal structures, it was discovered that some of the cyclization reactions gave a second tetraphenylene isomer product and that the reaction likely also resulted in the formation of dibenzotetracene side-products.

The quaterphenyl with CN on position 3 **94** could be obtained in an isolated yield of **86 %**, the quaterphenyl with CN on position 4 **99** in an isolated yield of **60 %**, the quaterphenyl with CN on position 5 **97** in an isolated yield of **58 %**. The mono-coupled side-product **113** was obtained in an isolated yield of **78 %** from the Suzuki-Miyaura reaction with CN on position 2.

The tetraphenyls with CN on position 3 **95** and **115a** could be obtained in isolated yields of **18 %** and **5 %** respectively as well as the yields determined by internal standard of **24 %** and **17 %**. The tetraphenyl with CN on position 4 **115b** could be obtained in the isolated yield of **8 %**. The dibenzotetracene with CN on position 5 **118** could be isolated in a yield of **15 %**. The cyclization of **113** afforded the triphenylene **119** in an isolated yield of **94 %** and **120** in **2 %**.

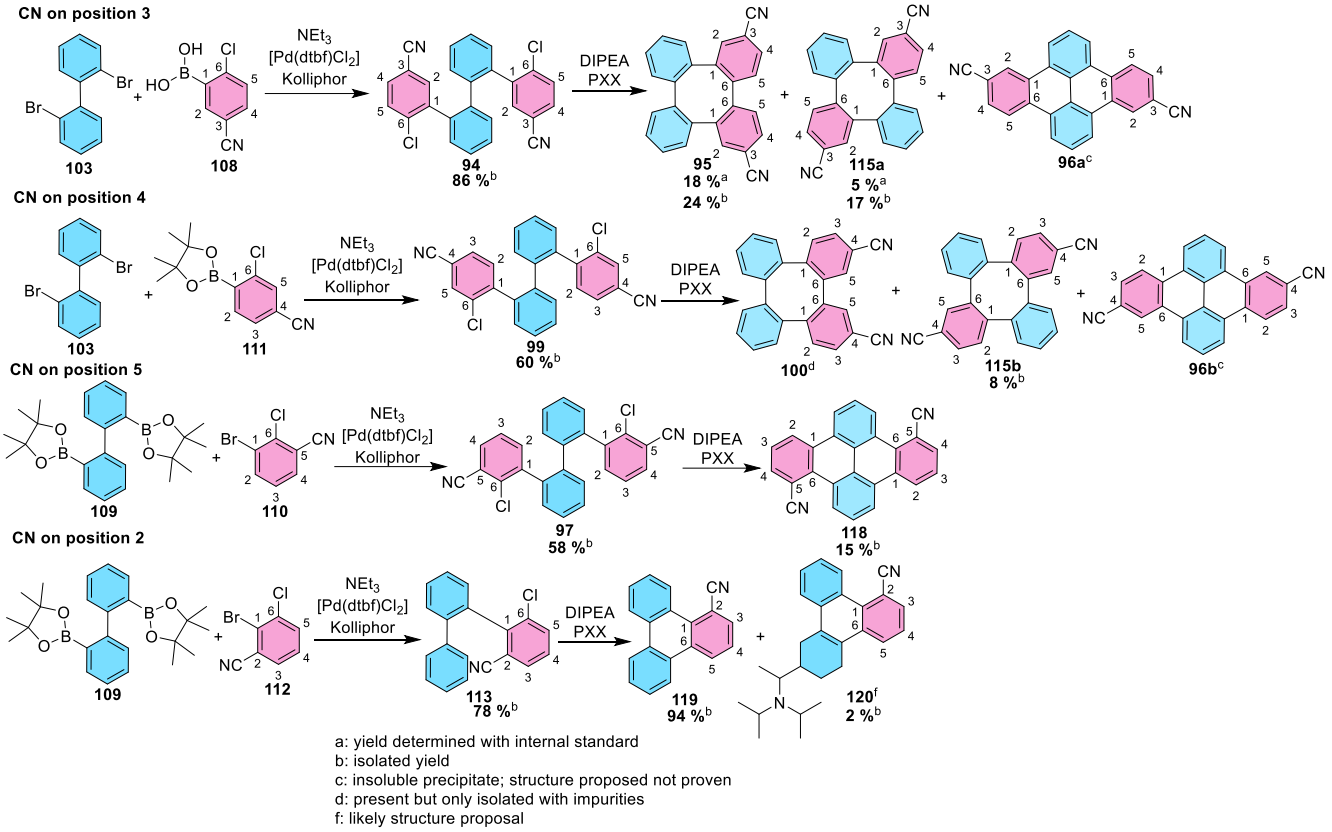

Scheme 51: *Summary of performed cyclizations.*

The structures of products **953**, **115a**, **115b** and **118** were proven by acquiring crystal structures. In addition, the mechanism of the novel photoredox catalysed reaction was analysed and reaction mechanisms involving the radical-radical coupling of aryls were proposed for the expected tetraphenylenes **95** and **100**. Further, a novel photoredox-catalysed recombination mechanism involving a bifluorene-like biradical species was proposed for the unexpected tetraphenylenes **115a** and **115b**. While the synthesis of cubic graphite remains elusory, the performed reactions demonstrate the potential of photoredox catalysis to form novel aryl-aryl bonds through radical-radical coupling under mild and controlled conditions. The formation of the tetraphenylene isomers **115a** and **115b** also shows the potential of novel radical-induced rearrangements to play a part in novel syntheses of cubic graphite.

V Future Perspective

For the future steps, the synthesis of tetraphenylene with CN on position 2 needs to be repeated. Moreover, a photoredox catalysed cyclization of quaterphenyls with EWGs or EDGs on the ortho position of the scaffold aromatic rings could provide valuable insights into the reaction mechanism and methods like ^{13}C-labelling could be investigated. Additional future steps could furthermore include reactions with diversely substituted quaterphenyls or multiple cyclizations.

5.1 Proving the mechanism through ^{13}C-labelling

If it were possible to perform the reaction with the ^{13}C-labelled quaterphenyl **94-^{13}C** depicted in **Scheme 52**, the presence of the ^{13}C-^{13}C bond should be easily visible in ^{13}C-NMR spectra by their coupling patterns. In the case of the tetraphenylene **95-^{13}C** and the dibenzotetracene **96a-^{13}C**, the ^{13}C-^{13}C bond should remain coupling while in the case of the rearranged tetraphenylene **115a-^{13}C**, the bond should be broken and thus the coupling pattern between the ^{13}C atoms greatly altered.

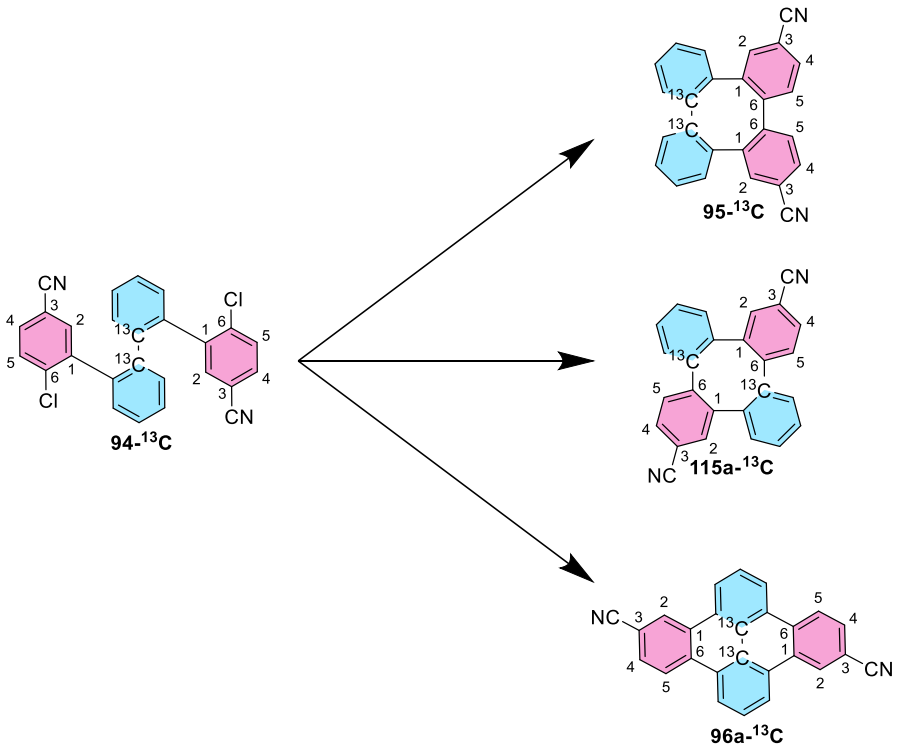

Scheme 52: *Synthesis of various ^{13}C-labelled products.*

The issue, however, is the synthesis of the doubly ^{13}C-labelled quaterphenyl **94-^{13}C**. Utilizing the synthetic approach explored during this thesis for the synthesis of quaterphenyls, the desired quaterphenyl **94-^{13}C** would have to be formed by a Suzuki-Miyaura coupling reaction with a doubly ^{13}C-labelled central “scaffold” that was either di-brominated or di-borylated on the respective ortho position of the aromatic rings.

This approach would involve costly ^{13}C-labelled aromatic starting materials which would have to be substituted with halogen or boron substituents on specific positions of the ring, which could lead to a difficult and expensive synthesis.

5.2 Cyclization of differently substituted quaterphenyls

Repeating the synthesis of tetraphenylene with CN on position 2 **100** would be among additional steps worth investigating and the scope of cyclization products could be expanded to synthesize asymmetrically substituted tetraphenylenes. These could include tetraphenylenes with CN on positions 2 & 3 **150**, 2 & 4 **152**, 2 & 5 **154**, 3 & 4 **156**, 3 & 5 **158** and 4 & 5 **160** as shown in **Scheme 53**. By performing these reactions and analysing their results the proposed mechanisms can be tested and either further proven or disproven. Of particular interest would be the syntheses of tetraphenylenes with one of the CN molecules positioned on position 5 (**154**, **158** and **160**), since the formation of the tetraphenylene with both CN moieties on position 5 had not been possible, which is hypothesized to be occurring because of steric hindrance. If the reactions with only one CN-rest on position 5 were successful, it would be further proof of the steric hindrance hypothesis stated in **chapter 3.5.1.1**. Additionally, if these reactions were to succeed, this would establish a novel method for the controlled synthesis of asymmetrically substituted tetraphenylenes, which has been a hurdle in past reported reactions as discussed in **chapter 1.2.3**.

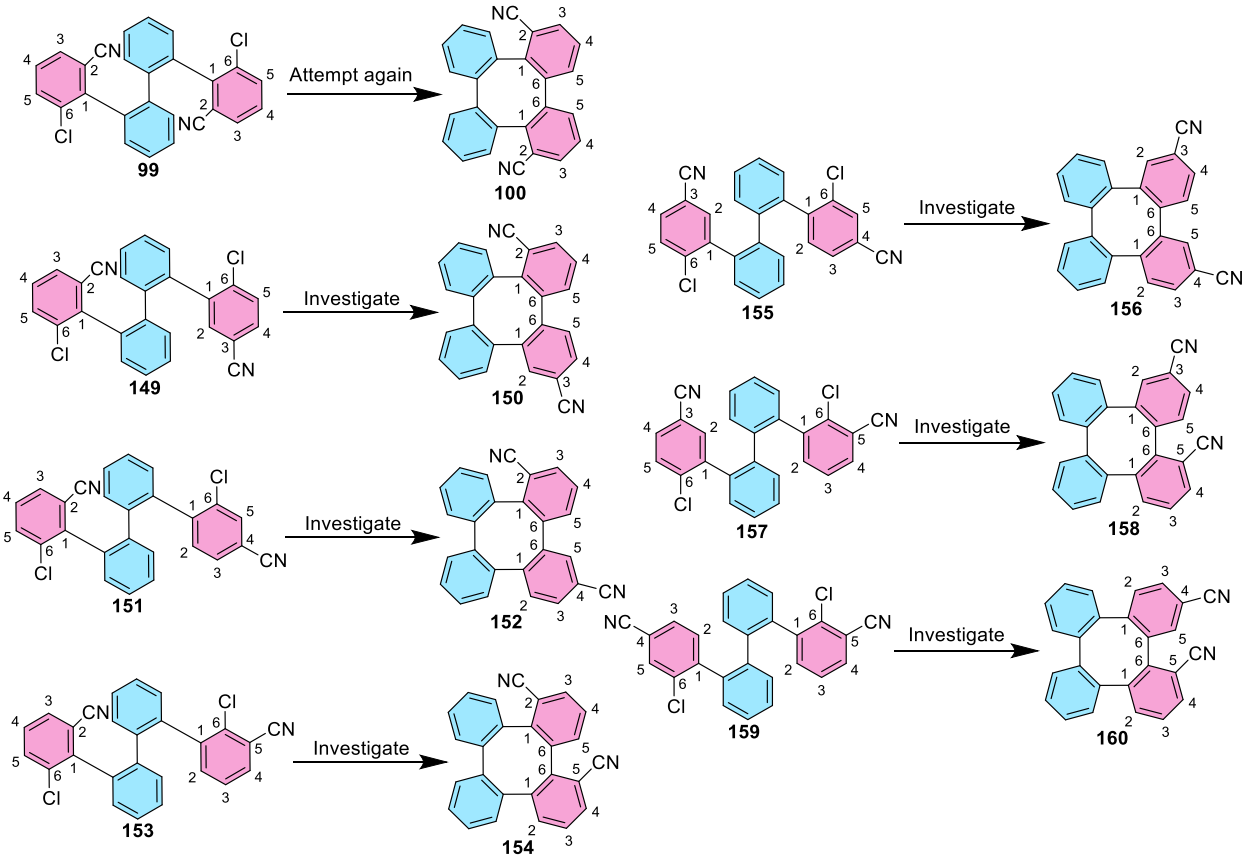

Scheme 53: *Cyclization reactions that could still be investigated.*

An additional strategy of interest would be to add further substituents to the pink outer rings of the quaterphenyls like in **161** as shown in **Scheme 54** with substituents like for example fluoride to test the effect on the reactivity and if there is an influence on the position that forms the aryl-aryl bond.

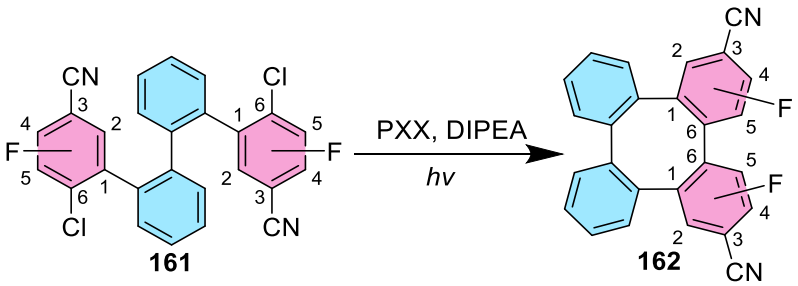

Scheme 54: *Cyclization with additional substituents on outer rings.*

5.3 Double cyclization reactions

A further approach could be attempting to perform a double cyclization reaction with an expanded structure such as **163**. Perhaps a structure like **164** could be made and an analysis of whether a radical-radical coupling mechanism could be observed would be of interest.

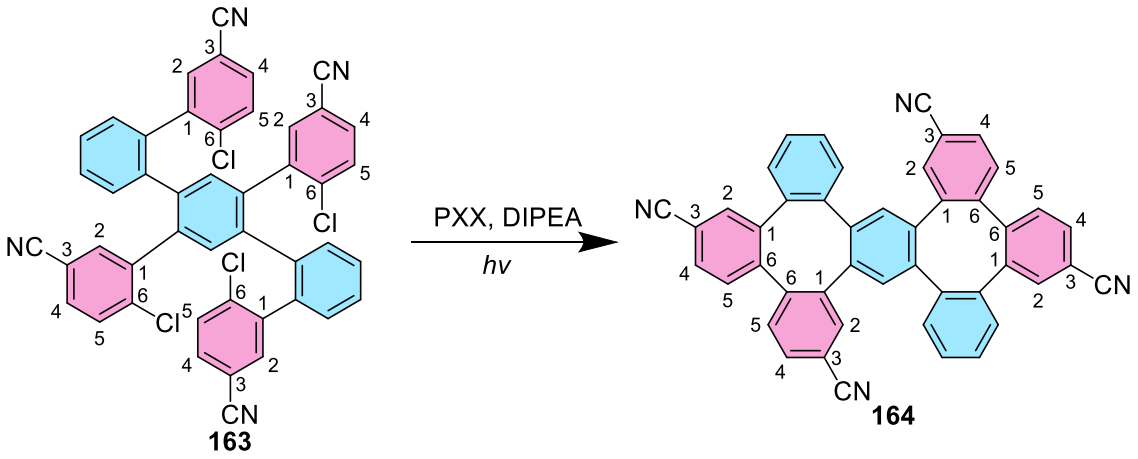

Scheme 55: *Double cyclization with the expanded substrate to be investigated.*

VI Experimental

6.1 General Information

All solvents were distilled from appropriate drying agents prior to use or used as received from the supplier. All reagents were used as received from commercial suppliers unless otherwise stated. Reaction progress was monitored by thin layer chromatography (TLC) performed on aluminium plates coated with silica gel F254 with 0.2 mm thickness. Chromatograms were visualized by fluorescence quenching with UV light at 254 nm or 366 nm. Flash column chromatography was performed using silica gel 60 (230-400 mesh, Merck and co.). Mass spectra were obtained using a Bruker maXis UHR-TOF (Qq-TOF) spectrometer, using electrospray ionization (ESI). All ^{1}H NMR and ^{13}C NMR spectra were recorded using a Bruker AV-400 or AV-600 spectrometer at 300 K. Chemical shifts are given in parts per million (ppm, δ), referenced to the solvent peak of $CDCl_3$, defined at δ = 7.26 ppm (^{1}H NMR) and δ = 77.16 ppm (^{13}C NMR), DCM, defined at δ = 5.30 ppm (^{1}H NMR), or DMSO, defined at δ = 2.50 ppm (^{1}H NMR). Coupling constants are quoted in Hz (*J*). ^{1}H NMR splitting patterns are designated as singlet (*s*), doublet (*d*), triplet (*t*), and quartet (*q*) as they appeared in the spectrum. If the appearance of a signal differs from the expected splitting pattern, the observed pattern is designated as apparent (app). Splitting patterns that could not be interpreted or easily visualized are designated as multiplet (*m*) or broad (*br*). All batch photocatalytic studies were performed in a custom-built photoreactor setups featuring a single high-power LED purchased from Mouser Electronics (405 nm, LZ1-10UB0R00U8; 460 nm, LZ1-10B202-0000; 535 nm, LZ1-10G102-0000) as the light source used for illuminating the reaction vessel from the bottom or the side. The LED was passively cooled by the attached aluminium heatsink, while the reaction temperature was held constant by an external fan or circulating a cooling fluid through the aluminium support connected to a chiller. (**Figure 40**)

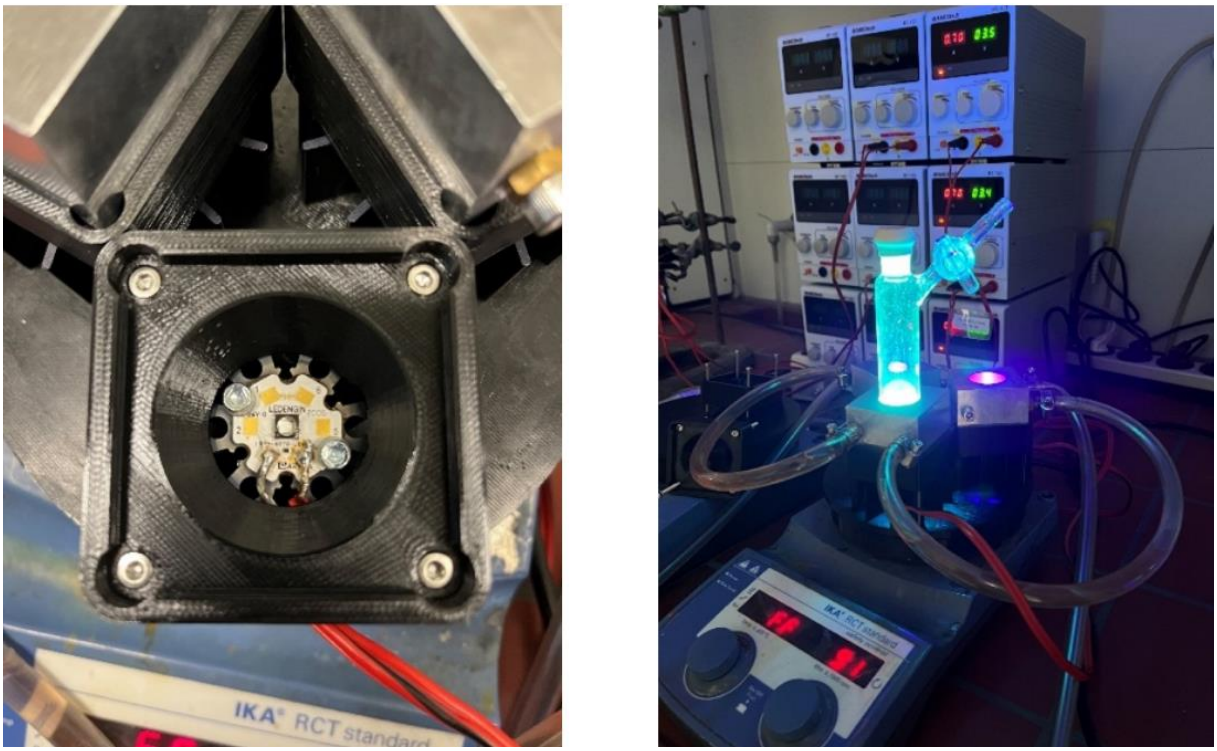

Figure 40: *Reaction setup for photo reactions.*

6.2 Experimental Procedures

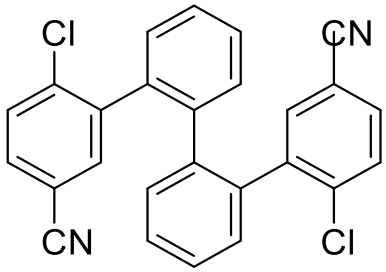

6.2.1 6,6'''-dichloro-[1,1':2',1'':2'',1'''-quaterphenyl]-3,3'''-dicarbonitrile 94

A solution of 2,2'-dibromo-1,1'-biphenyl **108** (627 mg, 2.01 mmol, 1 equiv.), 2-chloro-5-cyanophenyl)boronic acid **103** (1093 mg, 6.03 mmol, 3.01 equiv.), Et_3N (1214 mg, 12 mmol, 6 equiv.) and emulsion of water, toluene and Kolliphor EL (2%w/w) (5 ml) was prepared. Then [Pd(dtbf)Cl_2] (54 mg, 0.08 mmol, 0.04 equiv.) was added. The mixture was stirred for 3.5 h at 60 °C. After cooling to r.t. the mixture was diluted with EtOAc and filtered through a silica plug. The resulting material was concentrated *in vacuo* and triturated with EtOAc. Later, the crude was triturated with EtOH to afford 6,6'''-dichloro-[1,1':2',1'':2'',1'''-quaterphenyl]-3,3'''-dicarbonitrile **94** as a pink-white solid 727 mg (**86 %** yield). m.p. 249.2 – 251.8 °C. **^{1}H NMR (400 MHz, $CDCl_3$)** δ 7.62-

7.32 (*m*, 10H), 7.30-7.20 (*m*, 2H), 7.07-6.91 (*m*, 2H). **^{1}H NMR (500 MHz, DMSO-d$_6$, 125 °C)** δ 7.65 (*dd*, *J* = 8.3, 1.9 Hz, 2H), 7.54 (*d*, *J* = 8.3 Hz, 2H), 7.49 (*d*, *J* = 4.1 Hz, 4H), 7.42 (*dt*, *J* = 8.8, 4.4 Hz, 2H), 7.21 (*d*, *J* = 7.7 Hz, 2H), 6.98 (*br s*, 2H). **^{13}C NMR (151 MHz, CDCl$_3$) δ** 139.79, 138.62, 136.90, 136.18, 134.77, 132.88, 132.41, 132.33, 132.21, 131.47 (3 C Atoms), 130.65, 130.62, 130.29, 129.32, 129.03, 128.74, 128.54, 127.73, 127.46, 118.04, 117.94, 117.64, 110.90, 110.22. **IR (cm^{-1})**: 2230, 2149, 1978, 1591, 1459, 1434, 1385, 1253, 1138, 1123, 1075, 1053, 1044, 1022, 952, 928, 900, 877, 862, 829, 822, 779, 768, 755, 705, 635, 611, 558, 546, 511, 479, 457, 445, 423, 415. Mass spectrum could not be acquired.

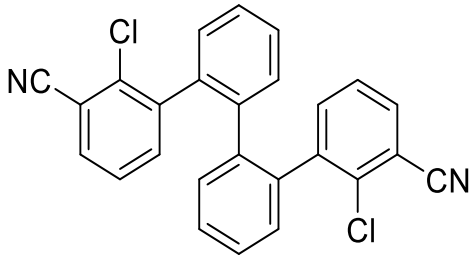

6.2.2 2,2'''-dichloro-[1,1':2',1'':2'',1'''-quaterphenyl]-3,3'''-dicarbonitrile 97

A solution of 3-bromo-2-chlorobenzonitrile **110** (556 mg, 2.57 mmol, 3 equiv.), 2,2'-bis(4,4,5,5-tetramethyl-1,3,2-dioxaborolan-2-yl)-1,1'-biphenyl **109** (348 mg, 0.86 mmol, 1 equiv.), Et_3N (520 mg, 5.14 mmol, 6 equiv.) and emulsion of H_2O, toluene and Kolliphor EL (2%w/w) (2.5 ml) was prepared. Then [Pd(dtbf)Cl_2] (23.9 mg, 0.04 mmol, 0.04 equiv.) was added. The mixture was stirred for 3.5 h at 60 °C. After cooling to r.t. the mixture was diluted with DCM and filtered through a silica plug. The resulting material was concentrated *in vacuo* and recrystallized from Heptane and a purification on silica was performed (1:1 Heptane/Ethyl Acetate) to give 95 mg (26%) of pure product. The crude was triturated with EtOAc, filtered, and combined with the previous product to give 175 mg (48 %). The remaining crude was further triturated with 0 °C EtOH to give additional 32 mg (9 %). In total 213 mg (**58 %** yield) of yellow/white solid product **97** were collected. m.p. 211.1 – 214.5 °C, **^{1}H NMR**

(400 MHz, $CDCl_3$) δ 7.63-7.34 (*m*, 7H), 7.28-7.11 (*m*, 4H), 7.09-6.89 (*m*, 3H). **^{13}C NMR (151 MHz, $CDCl_3$)** δ 140.06, 139.83, 139.61, 137.34, 136.96, 135.80, 135.15, 133.99, 132.93, 132.63, 132.46, 132.32, 131.49, 130.82, 130.63, 128.93, 128.64, 128.16, 127.61, 127.48, 126.96, 126.49, 126.16, 116.35, 116.30, 115.94. **IR (cm^{-1})**: 3061, 2924, 2233, 2171, 2113, 1946, 1725, 1570, 1482, 1457, 1435, 1406, 1274, 1254, 1176, 1125, 1114, 1080, 1051, 1006, 991, 979, 959, 881, 854, 800, 793, 773, 763, 748, 722, 640, 624, 594, 548, 480, 430, 414. **HRMS (LDi-timsTOF):** exact mass calculated for $[M-K]^+$ ($C_{26}H_{14}N_2Cl_2K^+$) requires 463.0166, found *m/z* 463.0163.

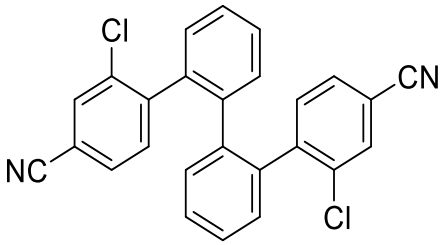

6.2.3 2,2'''-dichloro-[1,1':2',1'':2'',1'''-quaterphenyl]-4,4'''-dicarbonitrile 99

A solution of 2,2'-dibromo-1,1'-biphenyl **103** (62.2 mg, 0.20 mmol, 1 equiv.), 2-Chloro-4-cyanophenylboronic acid pinacol ester **111** (116 mg, 0.44 mmol, 2.2 equiv.), Et_3N (0.167 ml, 1.20 mmol, 6 equiv.) and emulsion of water, toluene and Kolliphor EL (2%w/w) (1.5 ml) was prepared. Then [Pd(dtbf)Cl_2] (5.2 mg, 0.008 mmol, 0.04 equiv.) was added. The mixture was stirred for 3.5 h at 60 °C. After cooling to r.t. the mixture was diluted with DCM and ethyl acetate and filtered through a silica plug. The concentrated reaction mixture was purified on silica (9:1 Heptane/Ethyl Acetate) to give 64 mg (**75 %** yield) of product **99**. m.p. 200.0 -202.0 °C, **^{1}H NMR (400 MHz, $CDCl_3$)** δ 7.71-7.11 (*m*, 12H), 7.02-6.79 (*m*, 2H). **^{13}C NMR (151 MHz, $CDCl_3$)** δ 143.05 (2 C Atoms), 139.55 (2 C Atoms), 135.77 (2 C Atoms), 134.17 (2 C Atoms), 134.00 (2 C Atoms), 132.29 (2 C Atoms), 131.28 (2 C Atoms), 130.57 (2 C Atoms), 129.53 (2 C Atoms), 128.88 (2 C Atoms), 127.48 (2 C Atoms), 117.59 (2 C Atoms), 112.15 (2 C Atoms). **IR (cm^{-1}):** 3063, 2922, 2851, 2230, 2110, 1725, 1596, 1536, 1463, 1438, 1382,

1267, 1196, 1141, 1106, 1076, 1054, 1004, 959, 883, 867, 834, 766, 729, 704, 679, 606, 587, 558, 531, 511, 488, 453, 425, 412. **HRMS (ESI):** exact mass calculated for $[M\text{-}Na]^+$ ($C_{26}H_{14}N_2Cl_2Na^+$) requires 447.0426, found *m/z* 447.0424.

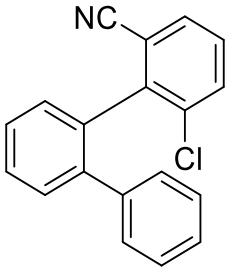

6.2.4 6-chloro-[1,1':2',1''-terphenyl]-2-carbonitrile 113

A solution of 2-Bromo-3-chlorobenzonitrile **112** (649 mg, 3 mmol, 3 equiv.), 2,2'-Bis(4,4,5,5-tetramethyl-1,3,2-dioxaborolan-2-yl)-1,1'-biphenyl **109** (406 mg, 1 mmol, 1 equiv.), Et_3N (0.84 ml, 6 mmol, 6 equiv.) and emulsion of water, toluene and Kolliphor EL (2%w/w) (2.5 ml) was prepared. Then [Pd(dtbf)Cl_2] (26.1 mg, 0.04 mmol, 0.04 equiv.) was added. The mixture was stirred for 3.5 h at 60 °C. After cooling to r.t. the mixture was diluted with EtOAc and filtered through a silica plug with EtOAc. The resulting material was concentrated *in vacuo* and unsuccessfully attempted to be triturated with various solvents. Therefore, a chromatography column using a Heptane/DCM mixture with a gradient from 0 %-30 % DCM as eluent was performed. 170 mg (0.4 mmol, 40 % yield) of the pure product was obtained as white crystals. Further, 117 mg of product contaminated with starting material was obtained. A second purification on silica was performed by copying the previous conditions to obtain additional 56.9 mg (0.13 mmol, 13 % yield) of the pure product **113**. The total obtained yield was 226.9 mg (**78 %** yield) of white crystalline product. m.p. 133.0 – 135.2 °C, **^{1}H NMR (600 MHz, $CDCl_3$)** δ 7.59 – 7.54 (*m*, 2H), 7.52 – 7.48 (*m*, 2H), 7.48 – 7.46 (*m*, 1H), 7.33 – 7.30 (*m*, 1H), 7.26 (*t*, *J* = 8.0 Hz, 1H), 7.20 (*s*, 5H). **^{1}H NMR (700 MHz, Acetone-d_6)** δ 7.73 (*dd*, *J* = 8.2, 1.1 Hz, 1H), 7.67 (*dd*, *J* = 7.8, 1.1 Hz, 1H), 7.61 (*td*, *J* = 7.6, 1.3 Hz, 1H), 7.55 (*td*, *J* = 7.6, 1.3 Hz, 1H), 7.53 – 7.51 (*m*, 1H), 7.48 (*t*,

J = 8.0 Hz, 1H), 7.40 – 7.38 (*m*, 1H), 7.25 – 7.21 (*m*, 3H), 7.21 – 7.19 (*m*, 2H). **^{13}C NMR (151 MHz, $CDCl_3$)** δ 144.32, 141.95, 140.35, 135.44, 134.33, 133.74, 131.11, 130.53, 130.10, 129.66, 129.31 (2 C atoms), 128.88, 127.95 (2 C atoms), 127.60, 127.18, 117.22, 115.84. **IR (cm^{-1}):** 3054, 2920, 2851, 2228, 2180, 2129, 1556, 1483, 1464, 1451, 1437, 1427, 1383, 1270, 1177, 1141, 1113, 1073, 1054, 1010, 911, 881, 846, 834, 789, 780, 764, 751, 739, 724, 701, 650, 617, 606, 581, 563, 527, 512, 466, 452, 428, 408. Mass spectrum could not be acquired.

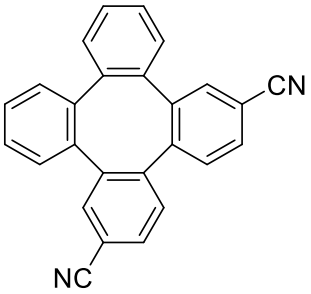

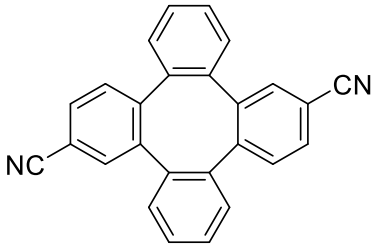

6.2.5 Tetraphenylene-2,7-dicarbonitrile 95 & Tetraphenylene-2,10-dicarbonitrile 115a

Synthesis 1 with isolation:

6,6'''-dichloro-[1,1':2',1'':2'',1'''-quaterphenyl]-3,3'''-dicarbonitrile **94** (213 mg, 0.5 mmol, 1 equiv.) and PXX (28.2 mg, 0.1 mmol, 0.2 equiv.) were placed in a Schlenk tube and set under vacuum for 5 min. They were suspended in DMSO (25 ml). DIPEA (0.261 ml, 1.5 mmol, 3 equiv.) was added and the mixture freeze pump thawed 3 times (frozen with N (l), set under vacuum for 5 min and thawed) and then backfilled with Ar. The reaction mixture was stirred with irradiation from blue LEDs (405 nm). A column chromatography using DCM as eluent was performed to afford the product **95** (32 mg, **18 %** yield) and an impure crude of product **115a** (41.5 mg, 23 % yield). The impure crude of product **115a** was further purified by column chromatography with 1.5/8.5 EtOAc/Heptane as the eluent mixture to afford 9.4 mg (**5 %** yield) of pure product **115a.**

Synthesis 2 with internal standard:

6,6'''-dichloro-[1,1':2',1'':2'',1'''-quaterphenyl]-3,3'''-dicarbonitrile **94** (35.4 mg, 0.0833 mmol, 1 equiv.) and PXX (4.7 mg, 0.0167 mmol, 0.2 equiv.) were placed in a Schlenk tube and set under vacuum for 5 min. They were suspended in DMSO (5 ml). DIPEA (0.0435 ml, 0.25 mmol, 3 equiv.) was added and the mixture freeze pump thawed 3 times (frozen with N (l), set under vacuum for 5 min and thawed) and then backfilled with Ar. The reaction mixture was stirred for 4 days with irradiation from blue LEDs (405 nm). The observed precipitate was filtered off and washed with a bit of DMSO. After drying, 4 mg was weighed. To the filtrate, water and brine were added, and the mixture was extracted with EtOAc. The organic phase was washed with brine, dried with $MgSO_4$, filtered, and concentrated under reduced pressure. By ^{1}H-NMR yield with 1,3,5-Trimethoxybenzene, a **26 %** yield of **95** was obtained and a **20 %** yield of **115a**.

95: m.p. above 260 °C (instrument limit), **^{1}H NMR (600 MHz, $CDCl_3$)** δ 7.60 (*d*, *J* = 7.9 Hz, 2H), 7.49 (*s*, 2H), 7.36 (*dt*, *J* = 19.7, 7.3 Hz, 4H), 7.25 (*d*, *J* = 8.0 Hz, 2H), 7.20 (*d*, *J* = 7.4 Hz, 2H), 7.13 (*d*, *J* = 7.4 Hz, 2H). **^{13}C NMR (151 MHz, $CDCl_3$)** δ 144.60, 142.80, 140.78, 138.59, 132.97, 131.23, 129.58, 129.56, 128.99, 128.79, 128.14, 118.42, 112.49. **IR (cm^{-1}):** 3060, 3026, 2921, 2852, 2325, 2232, 2116, 1932, 1726, 1601, 1486, 1470, 1437, 1395, 1261, 1175, 1160, 1139, 1095, 1026, 1006, 966, 951, 892, 878, 849, 834, 783, 759, 745, 638, 625, 589, 566, 548, 526, 509, 478. **HRMS (LDi-timsTOF):** The mass spectrum gave a mass of 636.1831 which equals the combined mass of **95** (354.1151) and PXX (282.0675) of 636.1832 [M+] ($C_{46}H_{24}N_2O_2^+$). How PXX could be present after purification is unclear and it is not visible in NMR.

115a: m.p. above 260 °C (instrument limit), **^{1}H NMR (700 MHz, $CDCl_3$)** δ 7.61 (*dd*, *J* = 7.9, 1.7 Hz, 2H), 7.46 (*d*, *J* = 1.6 Hz, 2H), 7.38 – 7.35 (*m*, 4H), 7.29 (*d*, *J* = 7.9 Hz, 2H), 7.17 – 7.13 (*m*, 4H). **^{13}C NMR (176 MHz, $CDCl_3$)** δ 145.77, 142.24, 139.80, 139.10, 132.87, 131.39, 130.25, 129.23, 128.95, 128.74, 128.65, 118.58, 111.90. **IR**

(cm^{-1}): 3060, 2921, 2850, 2229, 1937, 1810, 1601, 1487, 1473, 1433, 1388, 1308, 1261, 1170, 1137, 1117, 1034, 1006, 950, 900, 875, 836, 767, 742, 642, 624, 595, 564, 544, 522, 493, 465, 418. **HRMS (LDi-timsTOF):** The mass spectrum gave a mass of 636.1829 which equals the combined mass of **115a** (354.1151) and PXX (282.0675) of 636.1832 [M+] ($C_{46}H_{24}N_2O_2^+$). How PXX could be present after purification is unclear and it is not visible in NMR.

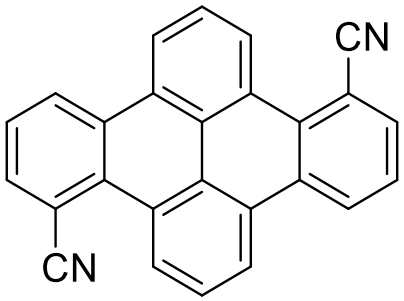

6.2.6 dibenzo[fg,op]tetracene-4,11-dicarbonitrile 118

2,2'''-dichloro-[1,1':2',1'':2'',1'''-quaterphenyl]-3,3'''-dicarbonitrile **97** (101 mg, 0.237 mmol, 1 equiv.) and PXX (13.6 mg, 0.05 mmol, 0.2 equiv.) were placed in a Schlenk tube and set under vacuum for 5 min. They were suspended in DMSO (16 ml). DIPEA (0.125 ml, 0.72 mmol, 3 equiv.) was added and the mixture freeze pump thawed 3 times (frozen with N (l), set under vacuum for 5 min and thawed) and then backfilled with Ar. The reaction mixture was stirred for 4 days with irradiation from blue LEDs (405 nm). Water (20 ml) and brine (4 ml) were added, and the mixture was extracted with EtOAc 3 times. Due to the formation of a suspension in the separation funnel, two further extractions with EtOAc were performed. The organic phase was washed with brine, dried with $MgSO_4$, filtered, and concentrated under reduced pressure. A recrystallization from a minimum of DCM and MeOH was performed.

The product was isolated by silica chromatography using DCM/heptane 9:1 gradient up to DCM/EtOAc 3:1 giving 12.8 mg (**15 %** yield) of product **118** that proved to be insoluble in solvents like $CHCl_3$, DCM and Acetone. m.p. above 260 °C (instrument

limit), **^{1}H NMR (400 MHz, $CDCl_3$)** δ 9.80 (*d*, *J* = 8.1 Hz, 2H), 9.06 (*d*, *J* = 8.4 Hz, 2H), 8.94 (*d*, *J* = 8.0 Hz, 2H), 8.17 (*d*, *J* = 7.4 Hz, 2H), 8.13 (*t*, *J* = 8.0 Hz, 2H), 7.86 – 7.81 (*m*, 2H). **^{13}C NMR (176 MHz, $CDCl_3$)** δ 136.63, 131.71, 130.96, 128.90, 128.33, 127.36, 127.22, 126.97, 125.98, 125.31, 123.64, 121.43. **IR (cm^{-1}):** 2919, 2327, 2211, 2082, 1993, 1939, 1590, 1538, 1422, 1388, 1303, 1236, 1175, 1098, 969, 901, 794, 774, 741, 709, 665, 630, 613, 569, 524, 492, 466, 436, 412. **HRMS (LDi-timsTOF):** exact mass calculated for [M] ($C_{26}H_{12}N_2$) requires 352.0995, found *m/z* 352.0985.

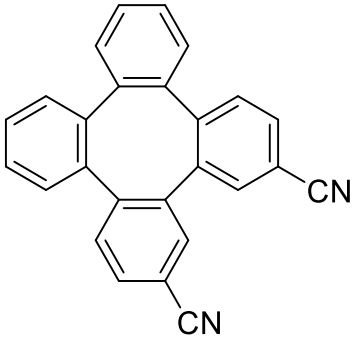

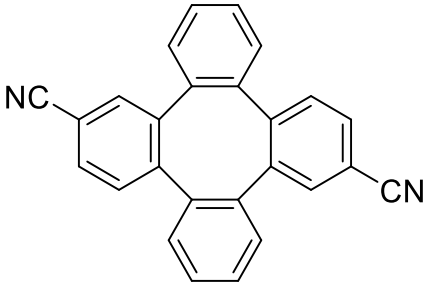

6.2.7 Tetraphenylene-2,15-dicarbonitrile 100 & Tetraphenylene-2,10-dicarbonitrile 115b

2,2'''-dichloro-[1,1':2',1'':2'',1'''-quaterphenyl]-4,4'''-dicarbonitrile **99** (40 mg, 0.094 mmol, 1 equiv.) and PXX (5.3 mg, 0.019 mmol, 0.2 equiv.) were placed in a Schlenk tube and set under vacuum for 5 min. They were suspended in dry DMSO (10 ml). DIPEA (0.049 ml, 0.281 mmol, 2.99 equiv.) was added and the mixture freeze pump thawed 3 times (frozen with N (l), set under vacuum for 5 min and thawed) and then backfilled with Ar. The reaction mixture was stirred for 4 days with irradiation from blue LEDs (405 nm) and probes were taken to track the reaction by TLC. Water and brine were added, and the mixture was extracted with EtOAc 3 times. The organic phase was washed with brine, dried with $MgSO_4$, filtered, and concentrated under reduced pressure. A purification by silica chromatography using Heptane/EtOAc 8:2 as eluent was performed, but the two formed isomers 1 and 2 could not be separated. Therefore, a second purification by silica chromatography was performed using a

60 cm long column and Heptane/Ethyl acetate 9:1 as eluent. After this column, the two isomers could also not be fully separated. As a last measure, a purification by Recycling GPC was performed. 3 mg (**8 %** yield) of a completely pure fraction of isomer 2 **115b** was obtained. The fraction containing isomer 1 was not fully purified and there were issues with growing crystals.

100: m.p. above 260 °C (instrument limit), **^{1}H NMR (400 MHz, $CDCl_3$) δ** 7.62 (*dd*, *J* = 7.9, 1.7 Hz, 2H), 7.44 (*d*, *J* = 1.5 Hz, 2H), 7.37 – 7.34 (*m*, 4H), 7.31 (*d*, *J* = 7.9 Hz, 2H), 7.19 – 7.16 (*m*, 2H), 7.16 – 7.12 (*m*, 2H). **^{13}C NMR (151 MHz, $CDCl_3$)** δ 146.48 (2 C Atoms), 140.70 (2 C Atoms), 140.60 (2 C Atoms), 139.14 (2 C Atoms), 132.36 (2 C Atoms), 131.94 (2 C Atoms), 130.37 (2 C Atoms), 129.60 (2 C Atoms), 128.78 (2 C Atoms), 128.75 (2 C Atoms), 128.14 (2 C Atoms), 118.36 (2 C Atoms), 111.90 (2 C Atoms). **IR (cm^{-1}):** 2920, 2850, 2230, 2211, 2196, 2178, 2130, 2091, 2073, 2058, 2023, 1991, 1977, 1966, 1951, 1942, 1860, 1596, 1472, 1423, 1388, 1305, 1265, 1234, 1096, 1009, 902, 819, 803, 793, 767, 740, 718, 703, 667, 630, 588, 576, 560, 538, 520, 510, 495, 483, 474, 456, 449, 431, 420, 412. Mass spectrum could not be acquired

115b: m.p. above 260 °C (instrument limit), **^{1}H NMR (400 MHz, $CDCl_3$)** δ 7.61 (*dd*, *J* = 7.9, 1.7 Hz, 2H), 7.46 (*d*, *J* = 1.6 Hz, 2H), 7.39 – 7.34 (*m*, 4H), 7.29 (*d*, *J* = 7.9 Hz, 2H), 7.19 – 7.13 (*m*, 4H). **^{13}C NMR (151 MHz, $CDCl_3$)** δ 145.77 (2 C Atoms), 142.23 (2 C Atoms), 139.80 (2 C Atoms), 139.10 (2 C Atoms), 132.86 (2 C Atoms), 131.39 (2 C Atoms), 130.25 (2 C Atoms), 129.23 (2 C Atoms), 128.95 (2 C Atoms), 128.74 (2 C Atoms), 128.65 (2 C Atoms), 118.58 (2 C Atoms), 111.90 (2 C Atoms). **IR (cm^{-1}):** Not enough sample for measurement. Mass spectrum could not be acquired.

Likely Structure Proposal

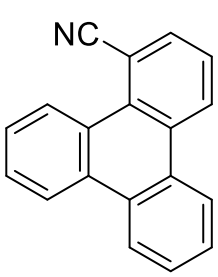

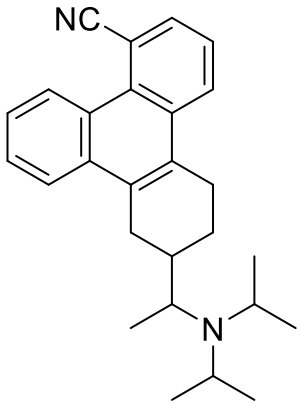

6.2.8 Triphenylene-1-carbonitrile 119 & Likely 7-(1-(diisopropylamino)ethyl)-5,6,7,8-tetrahydrotriphenylene-1-carbonitrile 120

6-chloro-[1,1':2',1''-terphenyl]-2-carbonitrile **113** (106 mg, 0.37 mmol, 1 equiv.) and PXX (14.1 mg, 0.05 mmol, 0.14 equiv.) were placed in a Schlenk tube and set under vacuum for 5 min. They were suspended in DMSO (12 ml). DIPEA (0.13 ml, 0.75 mmol, 2 equiv.) was added and the mixture freeze pump thawed 3 times (frozen with N (l), set under vacuum for 5 min and thawed) and then backfilled with Ar. The reaction mixture was stirred for 4 days with irradiation from blue LEDs (405 nm). Water and brine were added, and the mixture was extracted with EtOAc. The organic phase was washed with brine, dried with $MgSO_4$, filtered, and concentrated under reduced pressure. The crude was purified using column chromatography with Heptane/EtOAc as eluents with a 0 %-50 % EtOAc gradient yielding 87 mg (**94 %** yield) **119** and 2.2 mg (**2 %** yield) **120**.

119: m.p. 122.8 – 127.7 °C, **^{1}H NMR (600 MHz, $CDCl_3$)** δ 9.64 (*dd*, *J* = 8.2, 1.1 Hz, 1H), 8.91 (*dd*, *J* = 8.3, 0.6 Hz, 1H), 8.71 – 8.68 (*m*, 1H), 8.67 – 8.64 (*m*, 1H), 8.60 (*dd*, *J* = 7.9, 0.9 Hz, 1H), 8.07 (*dd*, *J* = 7.4, 1.3 Hz, 1H), 7.79 – 7.67 (*m*, 5H). **^{13}C NMR (151 MHz, $CDCl_3$)** δ 136.33, 131.53, 131.05, 130.91, 130.32, 129.10, 128.80, 128.59, 128.26, 127.94, 127.81, 127.49, 126.53, 126.17, 123.59, 123.56 (2 C Atoms), 121.80, 108.25. **IR (cm^{-1}):** 2958, 2919, 2850, 2214, 1606, 1578, 1500, 1490, 1448, 1433,

1410, 1342, 1293, 1249, 1229, 1168, 1148, 1058, 1043, 966, 949, 851, 809, 771, 746, 719, 669, 626, 620, 544, 512, 475, 448, 429, 407. Mass spectrum could not be acquired.

120: m.p. Not enough sample left for measurement. **^{1}H NMR (700 MHz, $CDCl_3$)** δ 9.74 (*dd*, *J* = 8.2, 1.1 Hz, 1H), 8.35 (*d*, *J* = 8.5 Hz, 1H), 8.12 (*d*, *J* = 7.9 Hz, 1H), 8.03 (*dd*, *J* = 7.2, 0.9 Hz, 1H), 7.73 – 7.70 (*m*, 1H), 7.70 – 7.68 (*m*, 1H), 7.67 – 7.64 (*m*, 1H), 3.34 (*m*, 1H), 3.25 – 3.20 (*m*, 1H), 3.20 – 3.18 (*m*, 1H), 3.06 – 2.98 (*m*, 1H), 2.79 (*td*, *J* = 13.5, 6.8 Hz, 1H), 2.73 (*d*, *J* = 13.5 Hz, 1H), 2.70 – 2.66 (*m*, 1H), 1.76 – 1.70 (*m*, 1H), 1.28 (*d*, *J* = 6.6 Hz, 3H), 1.25-1.24 (*m*, 1H), 1.10 (*d*, *J* = 6.5 Hz, 6H), 1.09 (*d*, *J* = 6.8 Hz, 6H), 1.03 (*d*, *J* = 6.7 Hz, 1H). **^{13}C NMR (176 MHz, $CDCl_3$)** δ 134.98 (CH), 133.38 (C), 133.29 (C), 133.09 (C), 130.20 (C), 129.65 (C), 128.49 (CH), 128.36 (CH), 127.60 (C), 126.10 (CH), 125.71 (CH), 125.27 (CH), 123.68 (CH), 122.25 (C), 107.50 (C), 54.27 (CH), 45.08 (CH), 39.56 (CH), 32.78 (CH_2), 28.34 (CH_2), 27.23 (CH_2), 24.26 (CH & 2*CH_3), 22.27 (2*CH_3), 18.32 (CH_3). **IR (cm^{-1}):** 2956, 2919, 2850, 2358, 2208, 2180, 2136, 2094, 2056, 1449, 1391, 1364, 1211, 1181, 1143, 1111, 1049, 1022.47, 1002, 805, 749, 715, 667, 643, 621, 597, 570, 554, 540, 529, 509, 498, 480, 466, 444, 428, 418. **HRMS (LDi-timsTOF):** exact mass calculated for $[M-H]^+$ ($C_{27}H_{33}N_2^+$) requires 385.2638, found *m/z* 385.2644.

VII References

[1] F. Farjadian, S. Abbaspour, M. A. A. Sadatlu, S. Mirkiani, A. Ghasemi, M. Hoseini-Ghahfarokhi, N. Mozaffari, M. Karimi, M. R. Hamblin, *ChemistrySelect* **2020**, *5*, 10200-10219.

[2] C. Soldano, A. Mahmood, E. Dujardin, *Carbon* **2010**, *48*, 2127-2150.

[3] aC. Lee, X. Wei, J. W. Kysar, J. Hone, *Science* **2008**, *321*, 385-388; bX. Wang, L. Zhi, K. Müllen, *Nano Letters* **2008**, *8*, 323-327; cY. Zhang, Y.-W. Tan, H. L. Stormer, P. Kim, *Nature* **2005**, *438*, 201-204; dP. Blake, P. D. Brimicombe, R. R. Nair, T. J. Booth, D. Jiang, F. Schedin, L. A. Ponomarenko, S. V. Morozov, H. F. Gleeson, E. W. Hill, A. K. Geim, K. S. Novoselov, *Nano Letters* **2008**, *8*, 1704-1708; eY. Yang, C. Han, B. Jiang, J. Iocozzia, C. He, D. Shi, T. Jiang, Z. Lin, *Materials Science and Engineering: R: Reports* **2016**, *102*, 1-72; fA. A. Balandin, S. Ghosh, W. Bao, I. Calizo, D. Teweldebrhan, F. Miao, C. N. Lau, *Nano Letters* **2008**, *8*, 902-907.

[4] aK. Yang, L. Feng, Z. Liu, *Advanced Drug Delivery Reviews* **2016**, *105*, 228-241; bH. Kim, A. A. Abdala, C. W. Macosko, *Macromolecules* **2010**, *43*, 6515-6530.

[5] V. Georgakilas, M. Otyepka, A. B. Bourlinos, V. Chandra, N. Kim, K. C. Kemp, P. Hobza, R. Zboril, K. S. Kim, *Chemical Reviews* **2012**, *112*, 6156-6214.

[6] aB. F. Machado, P. Serp, *Catalysis Science & Technology* **2012**, *2*, 54-75; bS. H. Hu, Y. W. Chen, W. T. Hung, I. W. Chen, S. Y. Chen, *Advanced Materials* **2012**, *24*, 1748-1754; cL. Feng, X. Yang, X. Shi, X. Tan, R. Peng, J. Wang, Z. Liu, *Small* **2013**, *9*, 1989-1997; dC. Berger, Z. Song, T. Li, X. Li, A. Y. Ogbazghi, R. Feng, Z. Dai, A. N. Marchenkov, E. H. Conrad, P. N. First, W. A. de Heer, *The Journal of Physical Chemistry B* **2004**, *108*, 19912-19916; eK. Yang, L. Feng, H. Hong, W. Cai, Z. Liu, *Nature Protocols* **2013**, *8*, 2392-2403; fD. A. C. Brownson, D. K. Kampouris, C. E. Banks, *Journal of Power Sources* **2011**, *196*, 4873-4885.

[7] K. S. Novoselov, A. K. Geim, S. V. Morozov, D. Jiang, Y. Zhang, S. V. Dubonos, I. V. Grigorieva, A. A. Firsov, *Science* **2004**, *306*, 666-669.

[8] aM. S. A. Bhuyan, M. N. Uddin, M. M. Islam, F. A. Bipasha, S. S. Hossain, *International Nano Letters* **2016**, *6*, 65-83; bQ. Zheng, J.-K. Kim, *Graphene for transparent conductors: Synthesis, properties and applications, Vol. 23*, Springer, **2015**.

[9] aN. Camara, G. Rius, J. R. Huntzinger, A. Tiberj, N. Mestres, P. Godignon, J. Camassel, *Applied Physics Letters* **2008**, *93*, 123503; bC. Berger, Z. Song, X. Li, X. Wu, N. Brown, C. Naud, D. Mayou, T. Li, J. Hass, A. N. Marchenkov, E. H. Conrad, P. N. First, W. A. de Heer, *Science* **2006**, *312*, 1191-1196.

[10] aA. A. Green, M. C. Hersam, *Nano Letters* **2009**, *9*, 4031-4036; bZ. Chen, W. Ren, L. Gao, B. Liu, S. Pei, H.-M. Cheng, *Nature Materials* **2011**, *10*, 424-428.

[11] aW. Du, X. Jiang, L. Zhu, *Journal of Materials Chemistry A* **2013**, *1*, 10592-10606; bJ. Zhao, S. Pei, W. Ren, L. Gao, H.-M. Cheng, *ACS Nano* **2010**, *4*, 5245-5252; cZ.-S. Wu, W. Ren, L. Gao, J. Zhao, Z. Chen, B. Liu, D. Tang, B. Yu, C. Jiang, H.-M. Cheng, *ACS Nano* **2009**, *3*, 411-417.

[12] D. D. L. Chung, *Journal of Materials Science* **2002**, *37*, 1475-1489.

[13] aR. W. Powell, F. H. Schofield, *Proceedings of the Physical Society* **1939**, *51*, 153; bR. Sengupta, M. Bhattacharya, S. Bandyopadhyay, A. K. Bhowmick, *Progress in Polymer Science* **2011**, *36*, 638-670; cA. K. Dutta, *Physical Review* **1953**, *90*, 187-192.

[14] aW. Gao, A. Tkatchenko, *Physical Review Letters* **2015**, *114*; bC. A. Mitchell, *The Analyst* **1922**, *47*, 379.

[15] M. S. Dresselhaus, G. Dresselhaus, *Advances in Physics* **2002**, *51*, 1-186.

[16] aH. Zhang, Y. Yang, D. Ren, L. Wang, X. He, *Energy Storage Materials* **2021**, *36*, 147-170; bM. S. Yazici, D. Krassowski, J. Prakash, *Journal of Power Sources* **2005**, *141*, 171-176.
[17] M. Wissler, *Journal of Power Sources* **2006**, *156*, 142-150.
[18] M. S. Nahian, R. Pritom, M. M. Islam, *The Journal of Physical Chemistry C* **2023**, *127*, 20146-20156.
[19] C. Mitchell, **1992**.
[20] H. P. T. S. Hewathilake, N. W. B. Balasooriya, Y. Nakamura, H. M. T. G. A. Pitawala, H. W. M. A. C. Wijayasinghe, M. Satish–Kumar, *Journal of Mineralogical and Petrological Sciences* **2018**, *113*, 96-105.
[21] R. Taylor, D. R. M. Walton, *Nature* **1993**, *363*, 685-693.
[22] P. Bhakta, B. Barthunia, *Journal of Indian Academy of Oral Medicine and Radiology* **2020**, *32*, 159-163.
[23] aY. Pan, X. Liu, W. Zhang, Z. Liu, G. Zeng, B. Shao, Q. Liang, Q. He, X. Yuan, D. Huang, M. Chen, *Applied Catalysis B: Environmental* **2020**, *265*, 118579; bT. Suzuki, Y. Maruyama, T. Akasaka, W. Ando, K. Kobayashi, S. Nagase, *Journal of the American Chemical Society* **1994**, *116*, 1359-1363.
[24] aY. Wang, M. J. Jafari, N. Wang, D. Qian, F. Zhang, T. Ederth, E. Moons, J. Wang, O. Inganäs, W. Huang, F. Gao, *Journal of Materials Chemistry A* **2018**, *6*, 11884-11889; bH. Werner, D. Bublak, U. Göbel, B. Henschke, W. Bensch, R. Schlögl, *Angewandte Chemie International Edition in English* **1992**, *31*, 868-870; cR. Taylor, J. P. Parsons, A. G. Avent, S. P. Rannard, T. J. Dennis, J. P. Hare, H. W. Kroto, D. R. M. Walton, *Nature* **1991**, *351*, 277-277.
[25] H. S. Chen, A. R. Kortan, R. C. Haddon, D. A. Fleming, *The Journal of Physical Chemistry* **1992**, *96*, 1016-1018.
[26] A. D. Darwish, A. G. Avent, P. R. Birkett, H. W. Kroto, R. Taylor, D. R. M. Walton, *Journal of the Chemical Society, Perkin Transactions 2* **2001**, 1038-1044.
[27] A. Hirsch, *Synthesis* **1995**, *1995*, 895-913.
[28] Z. Liu, Z.-C. Yin, W.-Q. Lu, D.-B. Zhou, G.-W. Wang, *Chemical Communications* **2021**, *57*, 13389-13392.
[29] W. A. Kalsbeck, H. H. Thorp, *Journal of Electroanalytical Chemistry and Interfacial Electrochemistry* **1991**, *314*, 363-370.
[30] aT. Suzuki, Q. Li, K. C. Khemani, F. Wudl, O. Almarsson, *Journal of the American Chemical Society* **1992**, *114*, 7300-7301; bP. J. Fagan, J. C. Calabrese, B. Malone, *Science* **1991**, *252*, 1160-1161.
[31] aP. R. Birkett, A. G. Avent, A. D. Darwish, I. Hahn, H. W. Kroto, G. J. Langley, J. O'Loughlin, R. Taylor, D. R. M. Walton, *Journal of the Chemical Society, Perkin Transactions 2* **1997**, 1121-1126; bY. Tajima, K. Takeshi, Y. Shigemitsu, Y. Numata, *Molecules* **2012**, *17*, 6395-6414.
[32] P. J. Krusic, E. Wasserman, B. A. Parkinson, B. Malone, E. R. Holler, Jr., P. N. Keizer, J. R. Morton, K. F. Preston, *Journal of the American Chemical Society* **1991**, *113*, 6274-6275.
[33] S. Yamago, H. Tokuyama, E. Nakamura, K. Kikuchi, S. Kananishi, K. Sueki, H. Nakahara, S. Enomoto, F. Ambe, *Chemistry & Biology* **1995**, *2*, 385-389.
[34] S. Yao, X. Yuan, L. Jiang, T. Xiong, J. Zhang, *Materials* **2020**, *13*, 2924.
[35] aI. Kumar, R. Sharma, R. Kumar, R. Kumar, U. Sharma, *Advanced Synthesis & Catalysis* **2018**, *360*, 2013-2019; bY. Yamakoshi, N. Umezawa, A. Ryu, K. Arakane, N. Miyata, Y.

Goda, T. Masumizu, T. Nagano, *Journal of the American Chemical Society* **2003**, *125*, 12803-12809.
[36] J. Lee, S. Hong, Y. Mackeyev, C. Lee, E. Chung, L. J. Wilson, J.-H. Kim, P. J. J. Alvarez, *Environmental Science & Technology* **2011**, *45*, 10598-10604.
[37] C.-Z. Li, H.-L. Yip, A. K. Y. Jen, *Journal of Materials Chemistry* **2012**, *22*, 4161.
[38] J. Lee, S. Cho, Y. Hwang, H.-J. Cho, C. Lee, Y. Choi, B.-C. Ku, H. Lee, B. Lee, D. Kim, S. H. Kim, *Tribology International* **2009**, *42*, 440-447.
[39] E. Alipour, F. Alimohammady, A. Yumashev, A. Maseleno, *Journal of Molecular Modeling* **2020**, *26*.
[40] T. Mashino, K. Shimotohno, N. Ikegami, D. Nishikawa, K. Okuda, K. Takahashi, S. Nakamura, M. Mochizuki, *Bioorganic & Medicinal Chemistry Letters* **2005**, *15*, 1107-1109.
[41] S. V. Kostyuk, E. V. Proskurnina, E. A. Savinova, E. S. Ershova, O. A. Kraevaya, L. V. Kameneva, P. E. Umryukhin, O. A. Dolgikh, S. I. Kutsev, P. A. Troshin, N. N. Veiko, *Nanomaterials* **2020**, *10*, 1405.
[42] S. Foley, C. Crowley, M. Smaihi, C. Bonfils, B. F. Erlanger, P. Seta, C. Larroque, *Biochemical and Biophysical Research Communications* **2002**, *294*, 116-119.
[43] L. B. Sukhodub, L. F. Sukhodub, M. O. Kumeda, S. V. Prylutska, V. Deineka, Y. I. Prylutskyy, U. Ritter, *Carbohydrate Polymers* **2019**, *223*, 115067.
[44] C. Guo, J. Chen, G. Li, X. Liang, W. Lai, L. Yang, Y. Mai, Z. Li, *Global Challenges* **2019**, *3*, 1800108.
[45] Q. Fu, S. Xiao, X. Tang, Y. Chen, T. Hu, *ACS Applied Materials & Interfaces* **2019**, *11*, 24782-24788.
[46] P. I. Kyesmen, A. Onoja, A. N. Amah, *SpringerPlus* **2016**, *5*.
[47] D.-W. Yan, W. Liu, H.-Z. Wang, C.-R. Wang, *MATERIALS TRANSACTIONS* **2007**, *48*, 700-703.
[48] J. T. McKinnon, W. L. Bell, R. M. Barkley, *Combustion and Flame* **1992**, *88*, 102-112.
[49] M. Mojica, J. A. Alonso, F. Méndez, *Journal of Physical Organic Chemistry* **2013**, *26*, 526-539.
[50] S. Iijima, *Nature* **1991**, *354*, 56-58.
[51] N. Gupta, S. M. Gupta, S. K. Sharma, *Carbon Letters* **2019**, *29*, 419-447.
[52] aJ. Hone, M. C. Llaguno, M. J. Biercuk, A. T. Johnson, B. Batlogg, Z. Benes, J. E. Fischer, *Applied Physics A: Materials Science & Processing* **2002**, *74*, 339-343; bT. W. Ebbesen, H. J. Lezec, H. Hiura, J. W. Bennett, H. F. Ghaemi, T. Thio, *Nature* **1996**, *382*, 54-56; cF. Li, H. M. Cheng, S. Bai, G. Su, M. S. Dresselhaus, *Applied Physics Letters* **2000**, *77*, 3161-3163.
[53] S. T. R. Naqvi, T. Rasheed, D. Hussain, M. Najam ul Haq, S. Majeed, S. shafi, N. Ahmed, R. Nawaz, *Journal of Molecular Liquids* **2020**, *297*, 111919.
[54] A. A. Shvedova, E. R. Kisin, R. Mercer, A. R. Murray, V. J. Johnson, A. I. Potapovich, Y. Y. Tyurina, O. Gorelik, S. Arepalli, D. Schwegler-Berry, A. F. Hubbs, J. Antonini, D. E. Evans, B.-K. Ku, D. Ramsey, A. Maynard, V. E. Kagan, V. Castranova, P. Baron, *American Journal of Physiology-Lung Cellular and Molecular Physiology* **2005**, *289*, L698-L708.
[55] H. Dumortier, S. Lacotte, G. Pastorin, R. Marega, W. Wu, D. Bonifazi, J.-P. Briand, M. Prato, S. Muller, A. Bianco, *Nano Letters* **2006**, *6*, 1522-1528.
[56] K. Besteman, J.-O. Lee, F. G. M. Wiertz, H. A. Heering, C. Dekker, *Nano Letters* **2003**, *3*, 727-730.

[57] A. Bianco, K. Kostarelos, M. Prato, *Current Opinion in Chemical Biology* **2005**, *9*, 674-679.
[58] H. Dai, J. H. Hafner, A. G. Rinzler, D. T. Colbert, R. E. Smalley, *Nature* **1996**, *384*, 147-150.
[59] E. Frackowiak, F. Béguin, *Carbon* **2002**, *40*, 1775-1787.
[60] aJ. Zaumseil, *Semiconductor Science and Technology* **2015**, *30*, 074001; bS. Paul, D.-W. Kim, *Carbon* **2009**, *47*, 2436-2441; cS. Rathinavel, K. Priyadharshini, D. Panda, *Materials Science and Engineering: B* **2021**, *268*, 115095.
[61] K. Kempa, B. Kimball, J. Rybczynski, Z. P. Huang, P. F. Wu, D. Steeves, M. Sennett, M. Giersig, D. V. G. L. N. Rao, D. L. Carnahan, D. Z. Wang, J. Y. Lao, W. Z. Li, Z. F. Ren, *Nano Letters* **2003**, *3*, 13-18.
[62] E. Akbari, Z. Buntat, *International Journal of Energy Research* **2017**, *41*, 92-102.
[63] P. Sehrawat, C. Julien, S. S. Islam, *Materials Science and Engineering: B* **2016**, *213*, 12-40.
[64] S. Arepalli, P. Nikolaev, W. Holmes, B. S. Files, *Applied Physics Letters* **2001**, *78*, 1610-1612.
[65] N. Arora, N. N. Sharma, *Diamond and Related Materials* **2014**, *50*, 135-150.
[66] K. A. Shah, B. A. Tali, *Materials Science in Semiconductor Processing* **2016**, *41*, 67-82.
[67] C. D. Scott, S. Arepalli, P. Nikolaev, R. E. Smalley, *Applied Physics A Materials Science & Processing* **2001**, *72*, 573-580.
[68] R. Purohit, K. Purohit, S. Rana, R. S. Rana, V. Patel, *Procedia Materials Science* **2014**, *6*, 716-728.
[69] Z. Sun, S. Fang, Y. H. Hu, *Chemical Reviews* **2020**, *120*, 10336-10453.
[70] aN. Yousefi, X. Lu, M. Elimelech, N. Tufenkji, *Nature Nanotechnology* **2019**, *14*, 107-119; bY. Zhao, C. Hu, Y. Hu, H. Cheng, G. Shi, L. Qu, *Angewandte Chemie International Edition* **2012**, *51*, 11371-11375; cQ. Zhang, F. Zhang, S. P. Medarametla, H. Li, C. Zhou, D. Lin, *Small* **2016**, *12*, 1702-1708.
[71] Z. Xu, Y. Zhang, P. Li, C. Gao, *ACS Nano* **2012**, *6*, 7103-7113.
[72] R. M. Hensleigh, H. Cui, J. S. Oakdale, J. C. Ye, P. G. Campbell, E. B. Duoss, C. M. Spadaccini, X. Zheng, M. A. Worsley, *Materials Horizons* **2018**, *5*, 1035-1041.
[73] S. Pei, H.-M. Cheng, *Carbon* **2012**, *50*, 3210-3228.
[74] J. Kuang, L. Liu, Y. Gao, D. Zhou, Z. Chen, B. Han, Z. Zhang, *Nanoscale* **2013**, *5*, 12171.
[75] aY. Xie, S. Xu, Z. Xu, H. Wu, C. Deng, X. Wang, *Carbon* **2016**, *98*, 381-390; bW. Zeng, X.-M. Tao, S. Lin, C. Lee, D. Shi, K.-h. Lam, B. Huang, Q. Wang, Y. Zhao, *Nano Energy* **2018**, *54*, 163-174.
[76] J. D. Renteria, S. Ramirez, H. Malekpour, B. Alonso, A. Centeno, A. Zurutuza, A. I. Cocemasov, D. L. Nika, A. A. Balandin, *Advanced Functional Materials* **2015**, *25*, 4664-4672.
[77] Y. Zhang, Y. Huang, T. Zhang, H. Chang, P. Xiao, H. Chen, Z. Huang, Y. Chen, *Advanced materials* **2015**, *27*, 2049-2053.
[78] Y. Zhu, H. Cui, X. Meng, J. Zheng, P. Yang, L. Li, Z. Wang, S. Jia, Z. Zhu, *ACS Applied Materials & Interfaces* **2016**, *8*, 6481-6487.
[79] M.-Q. Zhao, Q. Zhang, J.-Q. Huang, G.-L. Tian, J.-Q. Nie, H.-J. Peng, F. Wei, *Nature Communications* **2014**, *5*.
[80] D. A. C. Brownson, L. C. S. Figueiredo-Filho, X. Ji, M. Gómez-Mingot, J. Iniesta, O. Fatibello-Filho, D. K. Kampouris, C. E. Banks, *Journal of Materials Chemistry A* **2013**, *1*, 5962.

[81] aD. Xia, K. Yi, B. Zheng, M. Li, G. Qi, Z. Cai, M. Cao, D. Liu, L. Peng, D. Wei, Z. Wang, L. Yang, D. Wei, *The Journal of Physical Chemistry C* **2017**, *121*, 3062-3069; bY. Ito, H.-J. Qiu, T. Fujita, Y. Tanabe, K. Tanigaki, M. Chen, *Advanced Materials* **2014**, *26*, 4145-4150.
[82] M. T. Pettes, H. Ji, R. S. Ruoff, L. Shi, *Nano Letters* **2012**, *12*, 2959-2964.
[83] aH. Wang, K. Sun, F. Tao, D. J. Stacchiola, Y. H. Hu, *Angewandte Chemie* **2013**, *125*, 9380-9384; bZ. Xing, B. Wang, W. Gao, C. Pan, J. K. Halsted, E. S. Chong, J. Lu, X. Wang, W. Luo, C.-H. Chang, Y. Wen, S. Ma, K. Amine, X. Ji, *Nano Energy* **2015**, *11*, 600-610.
[84] aW. Wei, K. Sun, Y. H. Hu, *Journal of Materials Chemistry A* **2016**, *4*, 12054-12057; bL. Chang, D. J. Stacchiola, Y. H. Hu, *Industrial & Engineering Chemistry Research* **2018**, *57*, 3610-3616.
[85] W. Wei, K. Sun, Y. H. Hu, *J. Mater. Chem. A* **2014**, *2*, 16842-16846.
[86] Y. Song, A. Osherov, V. Bulović, J. Kong, *Advanced Sustainable Systems* **2018**, *2*, 1700106.
[87] X. Dong, X. Wang, L. Wang, H. Song, H. Zhang, W. Huang, P. Chen, *ACS Applied Materials & Interfaces* **2012**, *4*, 3129-3133.
[88] H. Wang, Y. Li, Y. Li, Y. Liu, D. Lin, C. Zhu, G. Chen, A. Yang, K. Yan, H. Chen, Y. Zhu, J. Li, J. Xie, J. Xu, Z. Zhang, R. Vilá, A. Pei, K. Wang, Y. Cui, *Nano Letters* **2019**, *19*, 1326-1335.
[89] Y. Meng, Y. Zhao, C. Hu, H. Cheng, Y. Hu, Z. Zhang, G. Shi, L. Qu, *Advanced Materials* **2013**, *25*, 2326-2331.
[90] C. Zhu, T. Liu, F. Qian, T. Y.-J. Han, E. B. Duoss, J. D. Kuntz, C. M. Spadaccini, M. A. Worsley, Y. Li, *Nano Letters* **2016**, *16*, 3448-3456.
[91] J. Qin, T. Wang, D. Liu, E. Liu, N. Zhao, C. Shi, F. He, L. Ma, C. He, *Advanced Materials* **2018**, *30*, 1704670.
[92] aE. Yoo, J. Kim, E. Hosono, H.-s. Zhou, T. Kudo, I. Honma, *Nano Letters* **2008**, *8*, 2277-2282; bY. Fang, Y. Lv, R. Che, H. Wu, X. Zhang, D. Gu, G. Zheng, D. Zhao, *Journal of the American Chemical Society* **2013**, *135*, 1524-1530; cZ. Fan, J. Yan, G. Ning, T. Wei, L. Zhi, F. Wei, *Carbon* **2013**, *60*, 558-561.
[93] X. Yu, B. Wang, D. Gong, Z. Xu, B. Lu, *Advanced Materials* **2017**, *29*, 1604118.
[94] aJ. Xiao, D. Mei, X. Li, W. Xu, D. Wang, G. L. Graff, W. D. Bennett, Z. Nie, L. V. Saraf, I. A. Aksay, J. Liu, J.-G. Zhang, *Nano Letters* **2011**, *11*, 5071-5078; bG. Tan, R. Xu, Z. Xing, Y. Yuan, J. Lu, J. Wen, C. Liu, L. Ma, C. Zhan, Q. Liu, T. Wu, Z. Jian, R. Shahbazian-Yassar, Y. Ren, D. J. Miller, L. A. Curtiss, X. Ji, K. Amine, *Nature Energy* **2017**, *2*.
[95] Y. Zhao, J. Liu, Y. Hu, H. Cheng, C. Hu, C. Jiang, L. Jiang, A. Cao, L. Qu, *Advanced Materials* **2013**, *25*, 591-595.
[96] S. Lu, Y. Chen, X. Wu, Z. Wang, Y. Li, *Scientific Reports* **2014**, *4*.
[97] L. Ren, K. N. Hui, K. S. Hui, Y. Liu, X. Qi, J. Zhong, Y. Du, J. Yang, *Scientific Reports* **2015**, *5*, 14229.
[98] Y. Qin, Q. Peng, Y. Ding, Z. Lin, C. Wang, Y. Li, F. Xu, J. Li, Y. Yuan, X. He, Y. Li, *ACS Nano* **2015**, *9*, 8933-8941.
[99] aY. Ito, W. Zhang, J. Li, H. Chang, P. Liu, T. Fujita, Y. Tan, F. Yan, M. Chen, *Advanced Functional Materials* **2016**, *26*, 1271-1277; bF. D'Apuzzo, A. R. Piacenti, F. Giorgianni, M. Autore, M. C. Guidi, A. Marcelli, U. Schade, Y. Ito, M. Chen, S. Lupi, *Nature Communications* **2017**, *8*, 14885.
[100] D. R. Dreyer, S. Park, C. W. Bielawski, R. S. Ruoff, *Chem. Soc. Rev.* **2010**, *39*, 228-240.

[101] R. Muszynski, B. Seger, P. V. Kamat, *The Journal of Physical Chemistry C* **2008**, *112*, 5263-5266.
[102] G. Williams, B. Seger, P. V. Kamat, *ACS Nano* **2008**, *2*, 1487-1491.
[103] V. Abdelsayed, S. Moussa, H. M. Hassan, H. S. Aluri, M. M. Collinson, M. S. El-Shall, *The Journal of Physical Chemistry Letters* **2010**, *1*, 2804-2809.
[104] J. I. Villacampa, C. Royo, E. Romeo, J. A. Montoya, P. Del Angel, A. Monzón, *Applied Catalysis A: General* **2003**, *252*, 363-383.
[105] A. Oberlin, *Carbon* **1984**, *22*, 521-541.
[106] J. A. Rodríguez-Manzo, C. Pham-Huu, F. Banhart, *ACS Nano* **2011**, *5*, 1529-1534.
[107] aJ. Xia, N. Zhang, S. Chong, D. Li, Y. Chen, C. Sun, *Green Chemistry* **2018**, *20*, 694-700; bF. Kapteijn, J. Jurriaans, J. A. Moulijn, *Fuel* **1983**, *62*, 249-251.
[108] H. Marsh, A. P. Warburton, *Journal of Applied Chemistry* **1970**, *20*, 133-142.
[109] H. Cheng, J. G. Shapter, Y. Li, G. Gao, *Journal of Energy Chemistry* **2021**, *57*, 451-468.
[110] C. Jeyaseelan, A. Jain, P. Khurana, D. Kumar, S. Thatai, *Rechargeable Batteries: History, Progress, and Applications* **2020**, 177-194.
[111] J. Asenbauer, T. Eisenmann, M. Kuenzel, A. Kazzazi, Z. Chen, D. Bresser, *Sustainable Energy & Fuels* **2020**, *4*, 5387-5416.
[112] P. U. Nzereogu, A. D. Omah, F. I. Ezema, E. I. Iwuoha, A. C. Nwanya, *Applied Surface Science Advances* **2022**, *9*, 100233.
[113] A. P. Terzyk, S. Furmaniak, P. J. F. Harris, P. A. Gauden, J. Włoch, P. Kowalczyk, G. Rychlicki, *Physical Chemistry Chemical Physics* **2007**, *9*, 5919-5927.
[114] W. Cao, J. Zheng, D. Adams, J. P. Zheng, *ECS Transactions* **2014**, *61*, 37.
[115] Y. Chu, J. Zhang, Y. Zhang, Q. Li, Y. Jia, X. Dong, J. Xiao, Y. Tao, Q. H. Yang, *Advanced Materials* **2023**, *35*, 2212186.
[116] X. Li, X. Sun, X. Hu, F. Fan, S. Cai, C. Zheng, G. D. Stucky, *Nano Energy* **2020**, *77*, 105143.
[117] L. Xie, C. Tang, Z. Bi, M. Song, Y. Fan, C. Yan, X. Li, F. Su, Q. Zhang, C. Chen, *Advanced Energy Materials* **2021**, *11*, 2101650.
[118] J. Gibson, M. Holohan, H. L. Riley, *Journal of the Chemical Society (Resumed)* **1946**, 456.
[119] A. J. Berresheim, M. Müller, K. Müllen, *Chemical Reviews* **1999**, *99*, 1747-1786.
[120] M. O'Keeffe, G. B. Adams, O. F. Sankey, *Physical Review Letters* **1992**, *68*, 2325-2328.
[121] B. Ejlli, P. Nußbaum, F. Rominger, J. Freudenberg, U. H. F. Bunz, K. Müllen, *Angewandte Chemie* **2021**, *133*, 20382-20386.
[122] X. Shen, D. M. Ho, R. A. Pascal, *Organic Letters* **2003**, *5*, 369-371.
[123] X. Shen, D. M. Ho, R. A. Pascal, *Journal of the American Chemical Society* **2004**, *126*, 5798-5805.
[124] R. H. Baughman, C. Cui, *Synthetic Metals* **1993**, *55*, 315-320.
[125] N. W. Ockwig, O. Delgado-Friedrichs, M. O'Keeffe, O. M. Yaghi, *Accounts of Chemical Research* **2005**, *38*, 176-182.
[126] aV. V. Pokropivny, V. L. Bekenev, *Fullerenes, Nanotubes and Carbon Nanostructures* **2005**, *13*, 415-426; bV. V. Pokropivny, A. V. Pokropivny, *Physics of the Solid State* **2004**, *46*, 392-394.
[127] R. B. Aust, H. G. Drickamer, *Science* **1963**, *140*, 817-819.
[128] F. P. Bundy, J. S. Kasper, *The Journal of Chemical Physics* **1967**, *46*, 3437-3446.
[129] D. Fedoseev, B. Deryagin, V. Varnin, *Doklady Akademii Nauk SSSR* **1976**, *228*, 371-374.
[130] V. Slodkevich, *Doklady Akademii Nauk SSSR* **1980**, *253*, 697-700.

[131] A. Smolyar, Y. Sozin, V. Barkholenko, S. Maloshtan, V. Kuts, V. Gurin, A. Arkhipov, A. Gerasimov, N. Razvadovskii, A. Titenko, *JOURNAL OF SUPERHARD MATERIALS C/C OF SVERKHTVERDYE MATERIALY* **2002**, *24*, 74-76.
[132] R. H. Baughman, H. Eckhardt, M. Kertesz, *The Journal of Chemical Physics* **1987**, *87*, 6687-6699.
[133] aJ.-W. Han, X.-S. Peng, H. N. Wong, *National Science Review* **2017**, *4*, 892-916; bJ.-W. Han, J.-X. Chen, X. Li, X.-S. Peng, H. N. Wong, *Synlett* **2013**, *24*, 2188-2198; cH.-R. Ma, X.-S. Peng, J.-F. Cui, H. N. C. Wong, *Tetrahedron Letters* **2023**, *119*, 154429.
[134] W. S. Rapson, R. G. Shuttleworth, J. N. Van Niekerk, *Journal of the Chemical Society (Resumed)* **1943**, 326.
[135] I. L. Karle, L. O. Brockway, *Journal of the American Chemical Society* **1944**, *66*, 1974-1979.
[136] H. Irngartinger, W. R. K. Reibel, *Acta Crystallographica Section B Structural Crystallography and Crystal Chemistry* **1981**, *37*, 1724-1728.
[137] N. Z. Huang, T. C. W. Mak, *Journal of the Chemical Society, Chemical Communications* **1982**, 543.
[138] aD. F. Lindow, L. Friedman, *Journal of the American Chemical Society* **1967**, *89*, 1271-1272; bD. V. Avila, A. G. Davies, M. L. Girbal, K. M. Ng, *J. Chem. Soc., Perkin Trans. 2* **1990**, 1693-1699.
[139] aH. Schwager, S. Spyroudis, K. P. C. Vollhardt, *Journal of Organometallic Chemistry* **1990**, *382*, 191-200; bB. L. Edelbach, R. J. Lachicotte, W. D. Jones, *Journal of the American Chemical Society* **1998**, *120*, 2843-2853.
[140] Y. D. Xing, N. Z. Huang, *The Journal of Organic Chemistry* **1982**, *47*, 140-142.
[141] J.-F. Wen, W. Hong, K. Yuan, T. C. W. Mak, H. N. C. Wong, *The Journal of Organic Chemistry* **2003**, *68*, 8918-8931.
[142] G. Wittig, G. Klar, *Justus Liebigs Annalen der Chemie* **1967**, *704*, 91-108.
[143] A. Rajca, A. Safronov, S. Rajca, R. Shoemaker, *Angewandte Chemie International Edition in English* **1997**, *36*, 488-491.
[144] X. Li, J.-W. Han, H. N. C. Wong, *Asian Journal of Organic Chemistry* **2016**, *5*, 74-81.
[145] aB. Wan, Y. Zhang, *Synthesis* **2021**, *53*, 3299-3306; bG. González Miera, S. Matsubara, H. Kono, K. Murakami, K. Itami, *Chemical Science* **2022**, *13*, 1848-1868.
[146] aT. Shibata, T. Chiba, H. Hirashima, Y. Ueno, K. Endo, *Angewandte Chemie International Edition* **2009**, *48*, 8066-8069; bT. Shibata, T. Uchiyama, H. Hirashima, K. Endo, *Pure and Applied Chemistry* **2011**, *83*, 597-605; cT. Shibata, M. Fujimoto, H. Hirashima, T. Chiba, K. Endo, *Synthesis* **2012**, *44*, 3269-3284.
[147] Y. Sakamoto, T. Suzuki, *Journal of the American Chemical Society* **2013**, *135*, 14074-14077.
[148] aJ. Eskildsen, T. Reenberg, Jørn, *European Journal of Organic Chemistry* **2000**, *2000*, 1637-1640; bF. Wang, X.-C. Li, W.-Y. Lai, Y. Chen, W. Huang, F. Wudl, *Organic Letters* **2014**, *16*, 2942-2945.
[149] L. Yang, H. Matsuyama, S. Zhang, M. Terada, T. Jin, *Organic Letters* **2020**, *22*, 5121-5125.
[150] M. H. Shaw, J. Twilton, D. W. C. MacMillan, *The Journal of Organic Chemistry* **2016**, *81*, 6898-6926.
[151] N. A. Romero, D. A. Nicewicz, *Chemical Reviews* **2016**, *116*, 10075-10166.
[152] D. M. Hedstrand, W. H. Kruizinga, R. M. Kellogg, *Tetrahedron Letters* **1978**, *19*, 1255-1258.

[153] aJ. W. Tucker, C. R. J. Stephenson, *The Journal of Organic Chemistry* **2012**, *77*, 1617-1622; bJ. D. Bell, J. A. Murphy, *Chemical Society Reviews* **2021**, *50*, 9540-9685; cL. Marzo, S. K. Pagire, O. Reiser, B. König, *Angewandte Chemie International Edition* **2018**, *57*, 10034-10072.
[154] aJ. J. Douglas, M. J. Sevrin, C. R. J. Stephenson, *Organic Process Research & Development* **2016**, *20*, 1134-1147; bS. P. Pitre, L. E. Overman, *Chemical Reviews* **2022**, *122*, 1717-1751.
[155] M. Moir, J. J. Danon, T. A. Reekie, M. Kassiou, *Expert Opinion on Drug Discovery* **2019**, *14*, 1137-1149.
[156] aX. Shu, D. Zhong, Q. Huang, L. Huan, H. Huo, *Nature Communications* **2023**, *14*, 125; bH. Huang, C. Yu, Y. Zhang, Y. Zhang, P. S. Mariano, W. Wang, *Journal of the American Chemical Society* **2017**, *139*, 9799-9802.
[157] C.-S. Wang, P. H. Dixneuf, J.-F. Soulé, *Chemical Reviews* **2018**, *118*, 7532-7585.
[158] M. S. Ahmad, P.-H. Lin, Q. Zhang, B. Zeng, Q. Wang, K. Meguellati, *Reactions* **2023**, *4*, 189-230.
[159] A. G. Condie, J. C. González-Gómez, C. R. J. Stephenson, *Journal of the American Chemical Society* **2010**, *132*, 1464-1465.
[160] T. Zhang, Y. Zhang, S. Das, *ChemCatChem* **2020**, *12*, 6173-6185.
[161] aA. Sciutto, A. Fermi, A. Folli, T. Battisti, J. M. Beames, D. M. Murphy, D. Bonifazi, *Chemistry – A European Journal* **2018**, *24*, 4382-4389; bI. Ghosh, B. König, *Angewandte Chemie International Edition* **2016**, *55*, 7676-7679.
[162] aC. Pezzetta, A. Folli, O. Matuszewska, D. Murphy, R. W. Davidson, D. Bonifazi, *Advanced Synthesis & Catalysis* **2021**, *363*, 4740-4753; bM. Majek, A. Jacobi von Wangelin, *Accounts of Chemical Research* **2016**, *49*, 2316-2327.
[163] aN. Kobayashi, M. Sasaki, K. Nomoto, *Chemistry of Materials* **2009**, *21*, 552-556; bT. Miletić, A. Fermi, I. Orfanos, A. Avramopoulos, F. De Leo, N. Demitri, G. Bergamini, P. Ceroni, M. G. Papadopoulos, S. Couris, D. Bonifazi, *Chemistry – A European Journal* **2017**, *23*, 2363-2378; cC. Song, T. M. Swager, *Macromolecules* **2009**, *42*, 1472-1475; dL. Wang, G. Duan, Y. Ji, H. Zhang, *The Journal of Physical Chemistry C* **2012**, *116*, 22679-22686.
[164] H. Zipse, in *Radicals in Synthesis I* (Ed.: A. Gansäuer), Springer Berlin Heidelberg, Berlin, Heidelberg, **2006**, pp. 163-189.
[165] Y.-R. Luo, **2002**.
[166] M. Heinrich, A. Gansäuer, *Radicals in synthesis III, Vol. 320*, Springer Science & Business Media, **2012**.
[167] F. De Vleeschouwer, P. Geerlings, F. D. Proft, in *Theoretical Chemistry in Belgium: A Topical Collection from Theoretical Chemistry Accounts* (Eds.: B. Champagne, M. S. Deleuze, F. De Proft, T. Leyssens), Springer Berlin Heidelberg, Berlin, Heidelberg, **2014**, pp. 111-123.
[168] N. Kvasovs, V. Gevorgyan, *Chemical Society Reviews* **2021**, *50*, 2244-2259.
[169] H. Meerwein, E. Büchner, K. van Emster, *Journal für Praktische Chemie* **1939**, *152*, 237-266.
[170] C. P. Andrieux, J. Pinson, *Journal of the American Chemical Society* **2003**, *125*, 14801-14806.
[171] F. Weick, N. Hagmeyer, M. Giraud, B. Dietzek-Ivanšić, H.-A. Wagenknecht, *Chemistry – A European Journal* **2023**, *29*, e202302347.
[172] I. Ghosh, T. Ghosh, J. I. Bardagi, B. König, *Science* **2014**, *346*, 725-728.

[173] K. Grudzień, A. Zlobin, J. Zadworny, K. Rybicka-Jasińska, B. Sadowski, *Organic Chemistry Frontiers* **2024**.
[174] H. Kim, H. Kim, T. H. Lambert, S. Lin, *Journal of the American Chemical Society* **2020**, *142*, 2087-2092.
[175] L. Candish, M. Freitag, T. Gensch, F. Glorius, *Chemical Science* **2017**, *8*, 3618-3622.
[176] D. Ravelli, S. Protti, M. Fagnoni, *Chemical Reviews* **2016**, *116*, 9850-9913.
[177] A. Studer, D. P. Curran, *Angewandte Chemie International Edition* **2016**, *55*, 58-102.
[178] M. Zhou, T. Qin, *Science of Synthesis: Free Radicals: Fundamentals and Applications in Organic Synthesis, Vol. 2*, Thieme Chemistry, **2020**.
[179] H. Fischer, *Chemical Reviews* **2001**, *101*, 3581-3610.
[180] D. Griller, K. U. Ingold, *Accounts of Chemical Research* **1976**, *9*, 13-19.
[181] R. Spaccini, N. Pastori, A. Clerici, C. Punta, O. Porta, *Journal of the American Chemical Society* **2008**, *130*, 18018-18024.
[182] L. Zhang, L. Jiao, *Journal of the American Chemical Society* **2019**, *141*, 9124-9128.
[183] D. Lehnherr, Y.-h. Lam, M. C. Nicastri, J. Liu, J. A. Newman, E. L. Regalado, D. A. DiRocco, T. Rovis, *Journal of the American Chemical Society* **2020**, *142*, 468-478.
[184] H. Xu, C. Zhao, Q. Qian, W. Deng, H. Gong, *Chemical Science* **2013**, *4*, 4022-4029.
[185] M. T. Pirnot, D. A. Rankic, D. B. C. Martin, D. W. C. MacMillan, *Science* **2013**, *339*, 1593-1596.
[186] N. C. Yang, D.-D. H. Yang, *Journal of the American Chemical Society* **1958**, *80*, 2913-2914.
[187] P. Wessig, O. Mühling, *Angewandte Chemie International Edition* **2001**, *40*, 1064-1065.
[188] U. C. Yoon, S. W. Oh, J. H. Lee, J. H. Park, K. T. Kang, P. S. Mariano, *The Journal of Organic Chemistry* **2001**, *66*, 939-943.
[189] T. Magauer, H. J. Martin, J. Mulzer, *Angewandte Chemie International Edition* **2009**, *48*, 6032-6036.
[190] D. Zanetti, O. Matuszewska, G. Giorgianni, C. Pezzetta, N. Demitri, D. Bonifazi, *JACS Au* **2023**, *3*, 3045-3054.
[191] S. Mattiello, M. Rooney, A. Sanzone, P. Brazzo, M. Sassi, L. Beverina, *Organic Letters* **2017**, *19*, 654-657.
[192] W. S. MacGregor, *Annals of the New York Academy of Sciences* **1967**, *141*, 3-12.
[193] A. Studer, T. Vogler, *Synthesis* **2008**, *2008*, 1979-1993.
[194] J. Sobek, R. Martschke, H. Fischer, *Journal of the American Chemical Society* **2001**, *123*, 2849-2857.

VIII Appendix

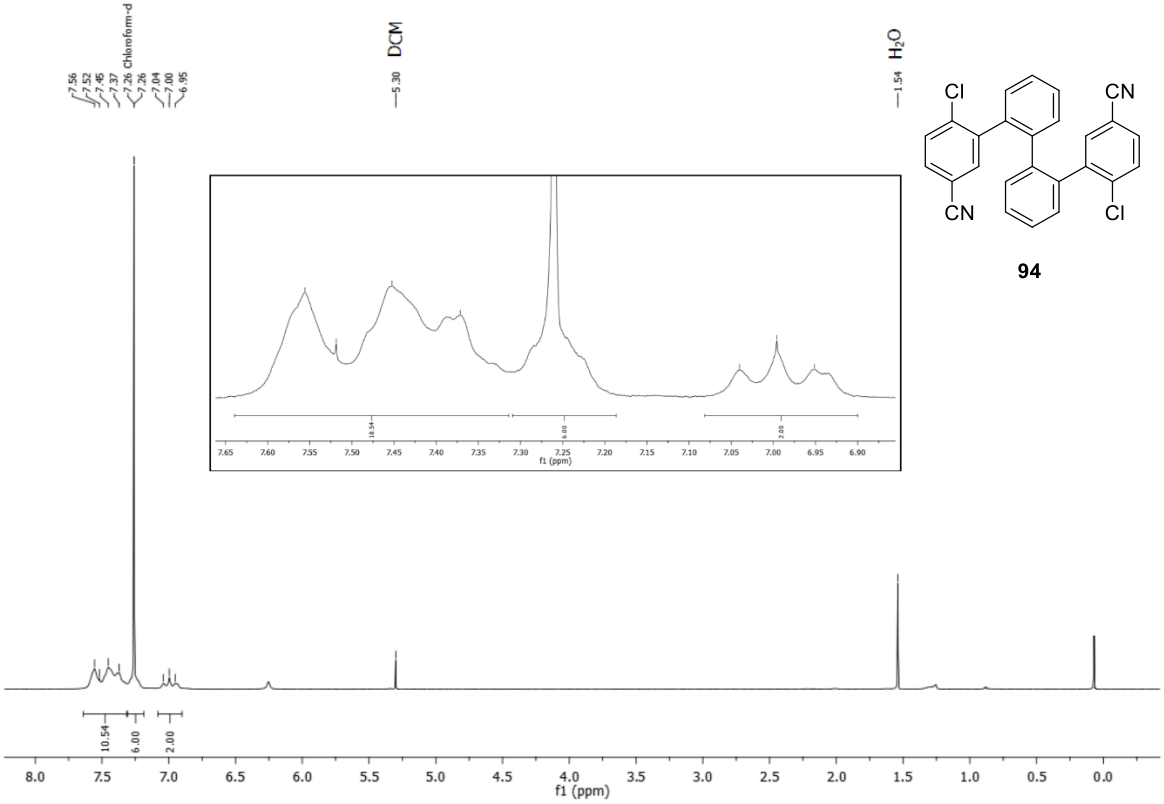

Figure 41: *^{1}H-NMR (400 MHz) spectrum of **94** at r.t. in $CDCl_3$.*

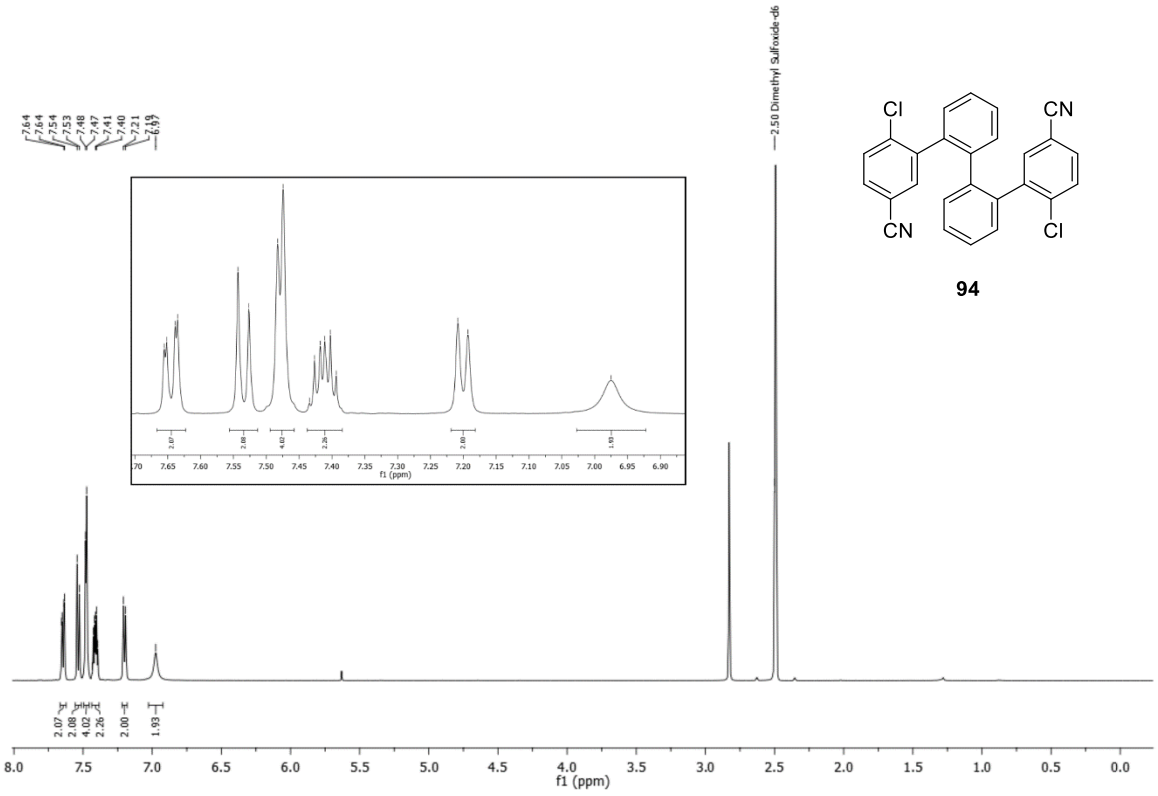

Figure 42: *^{1}H-NMR (500 MHz) spectrum of **94** at 125 °C in DMSO-d_6.*

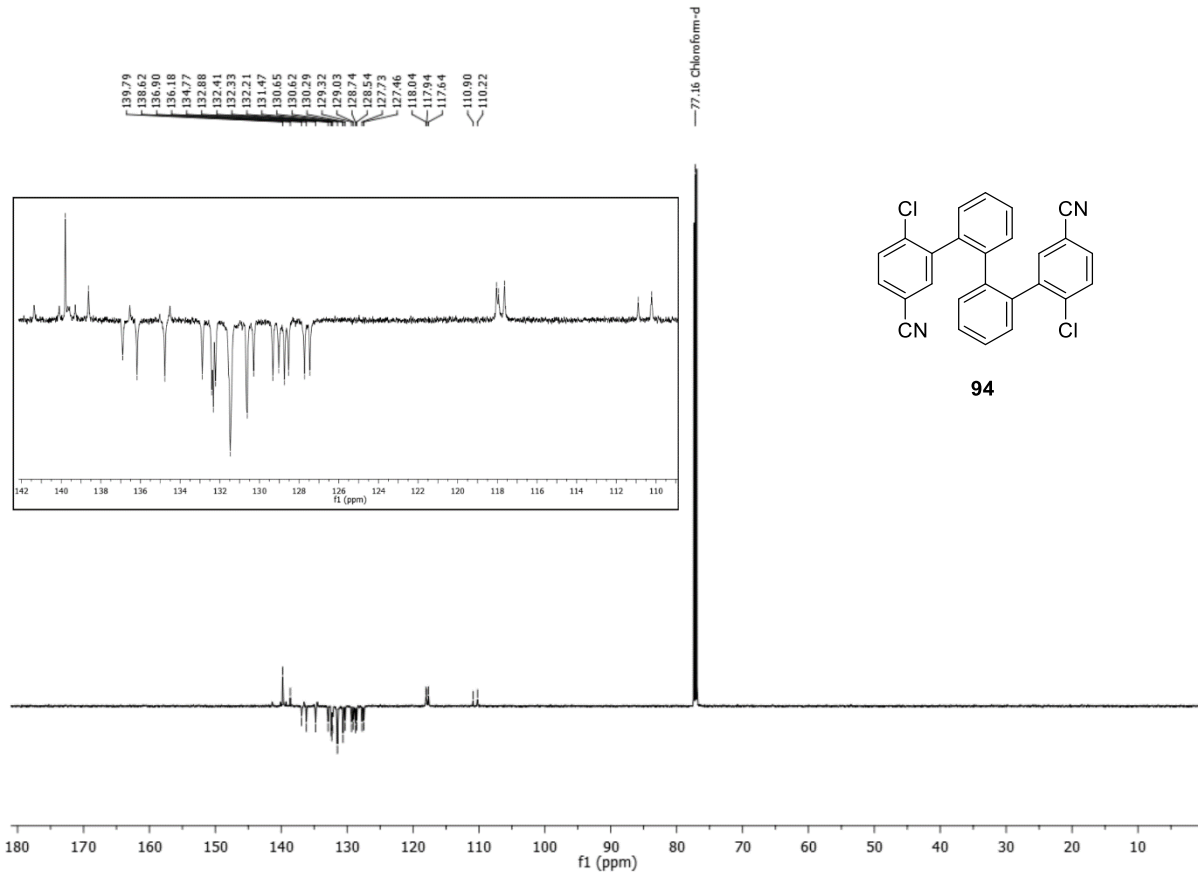

94

Figure 43: *^{13}C-NMR (151 MHz) spectrum of **94** in $CDCl_3$.*

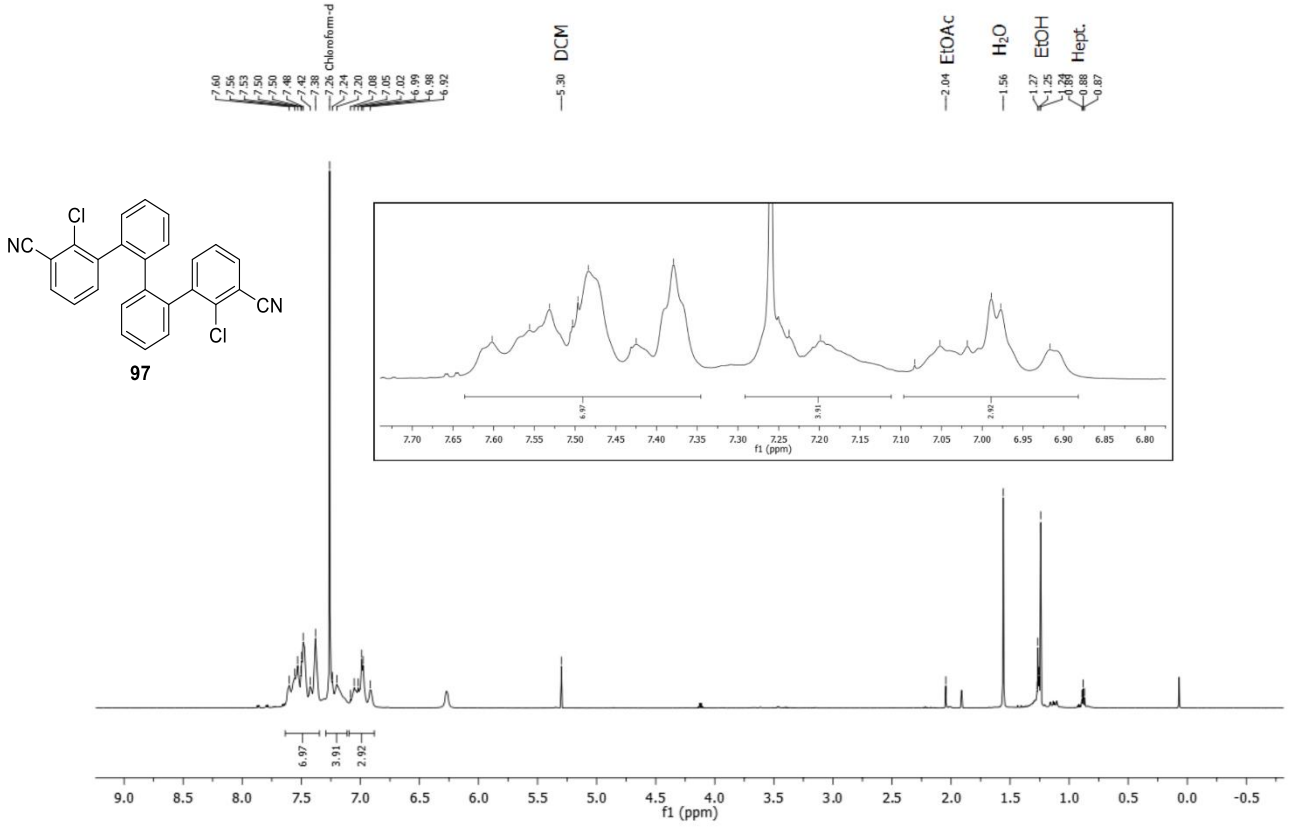

97

Figure 44: *^{1}H-NMR (400 MHz) spectrum of **97** in $CDCl_3$.*

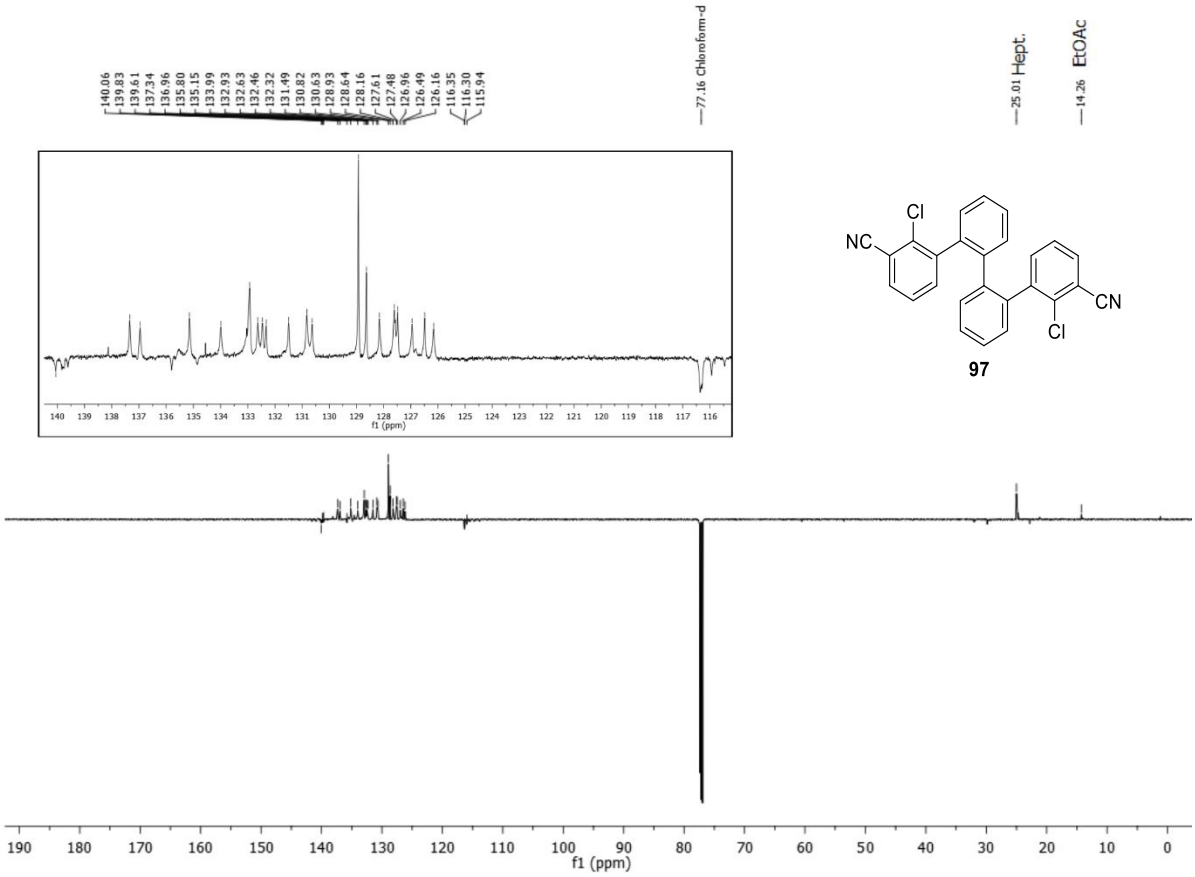

Figure 45: *^{13}C-NMR (151 MHz) spectrum of spectrum of **97** in $CDCl_3$.*

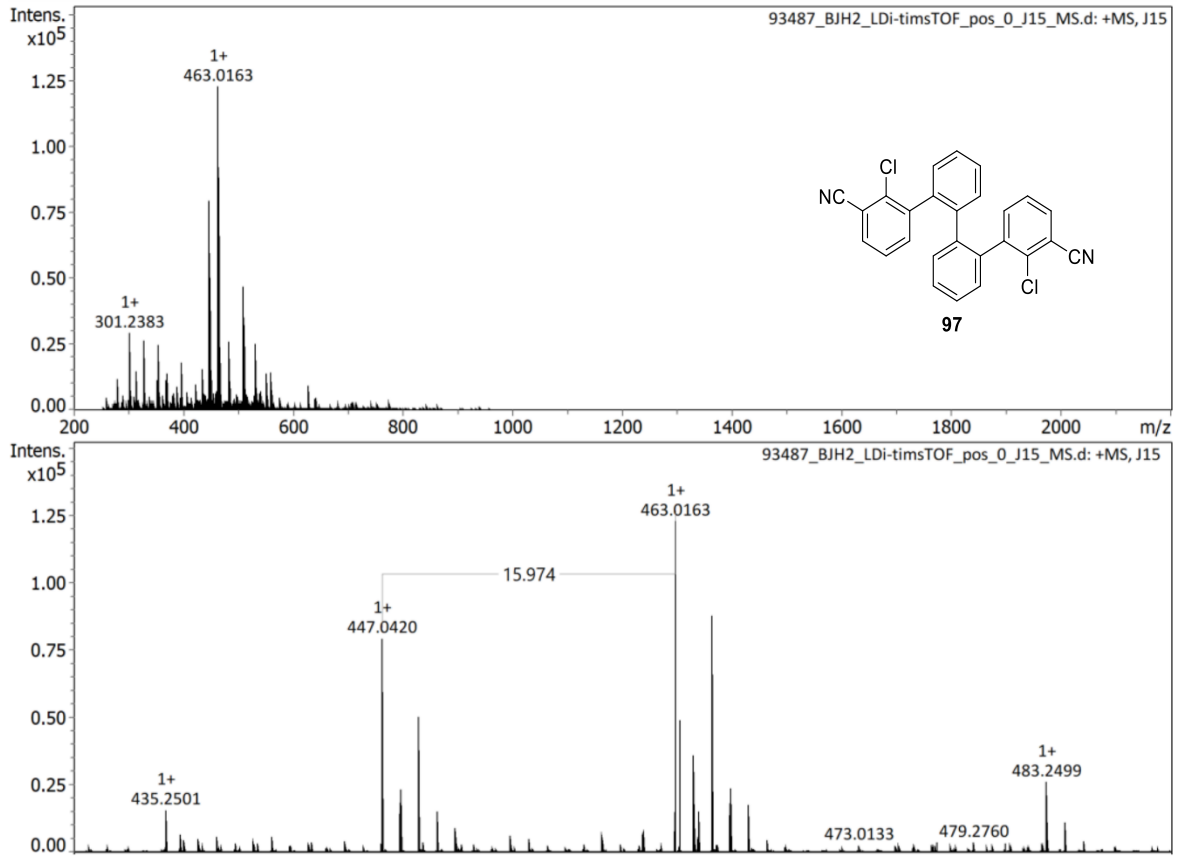

Figure 46: *LDi-timsTOF-MS spectrum of **97**.*

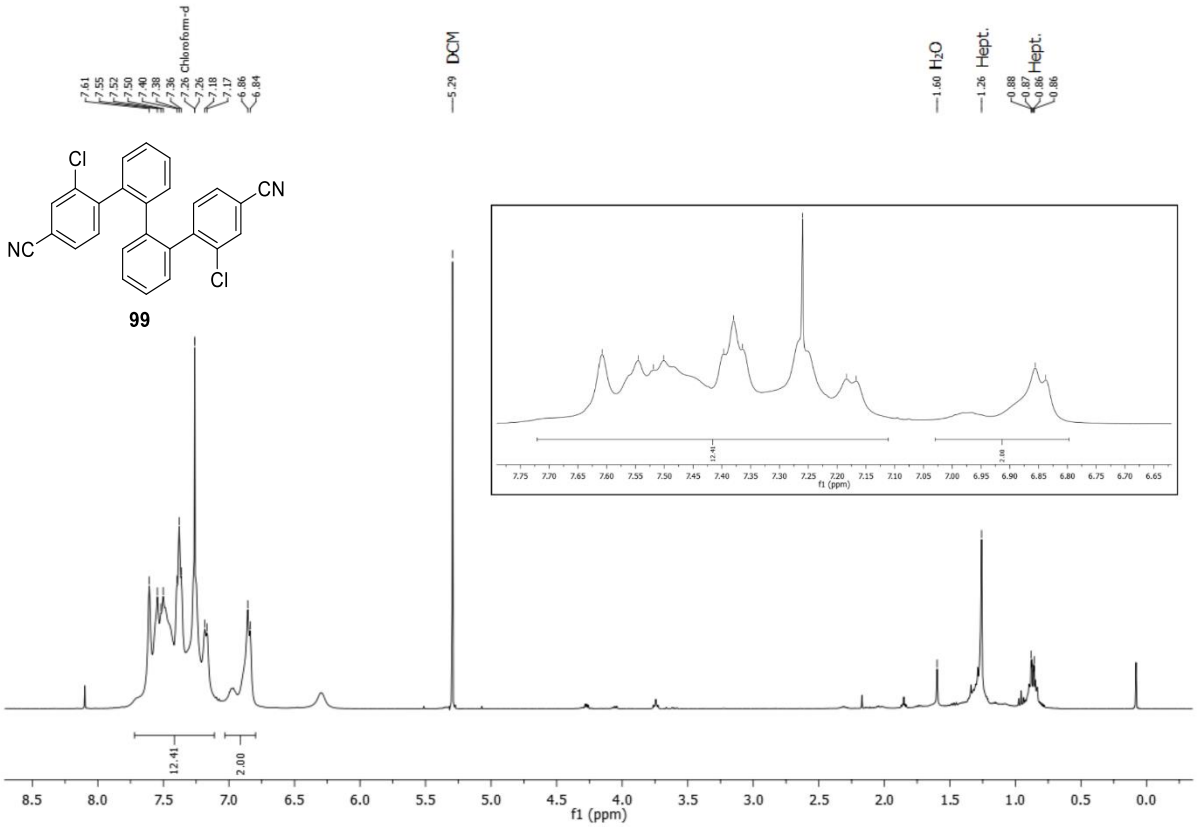

Figure 47: *^{1}H-NMR (400 MHz) spectrum of **99** in $CDCl_3$.*

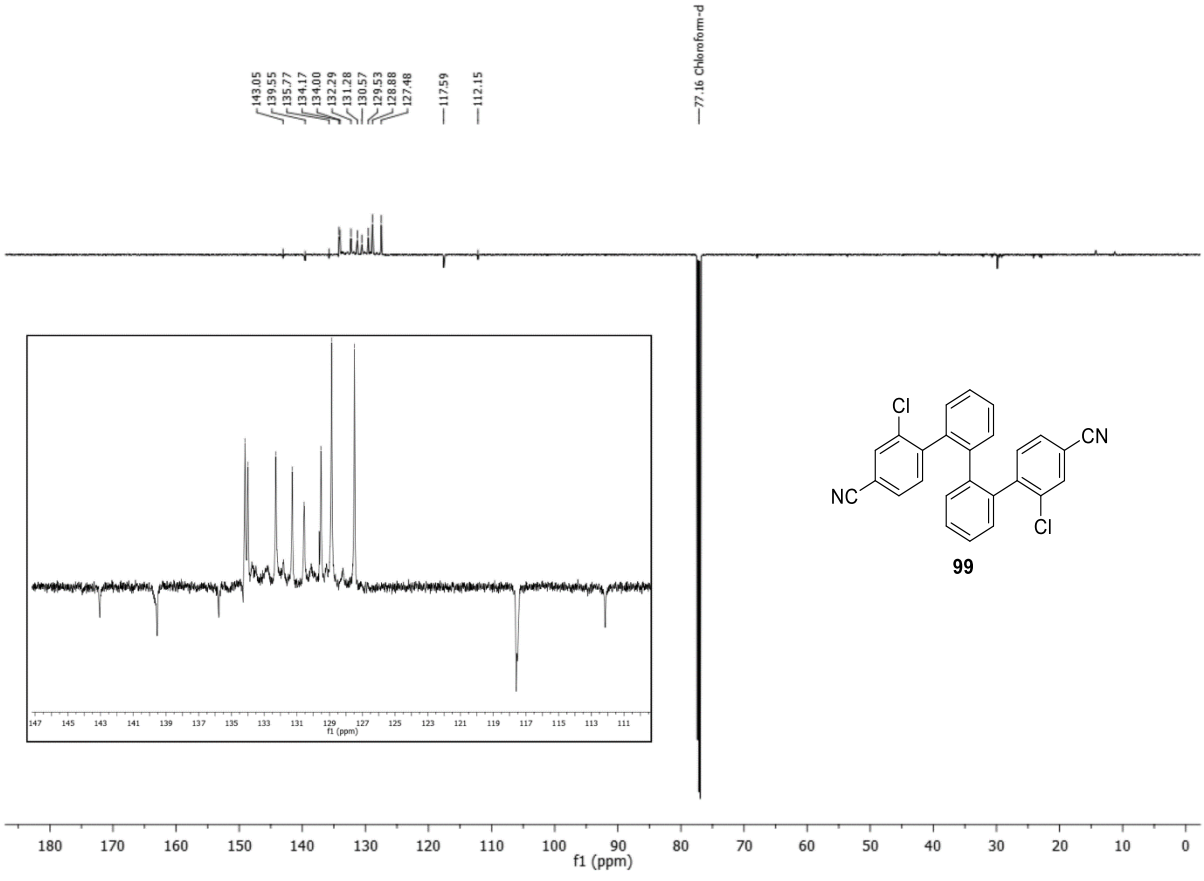

Figure 48: *^{13}C-NMR (151 MHz) spectrum of spectrum of **99** in $CDCl_3$.*

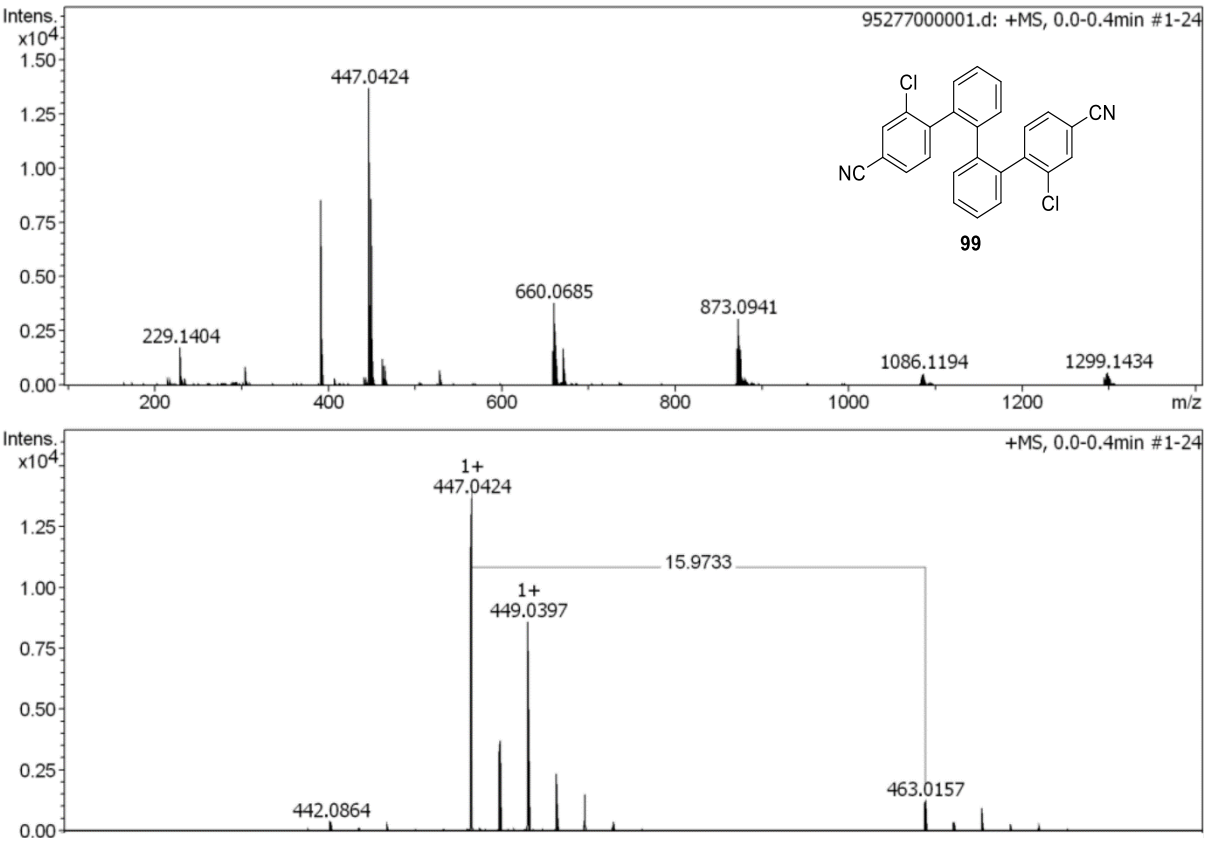

Figure 49: *ESI-MS spectrum of* ***99****.*

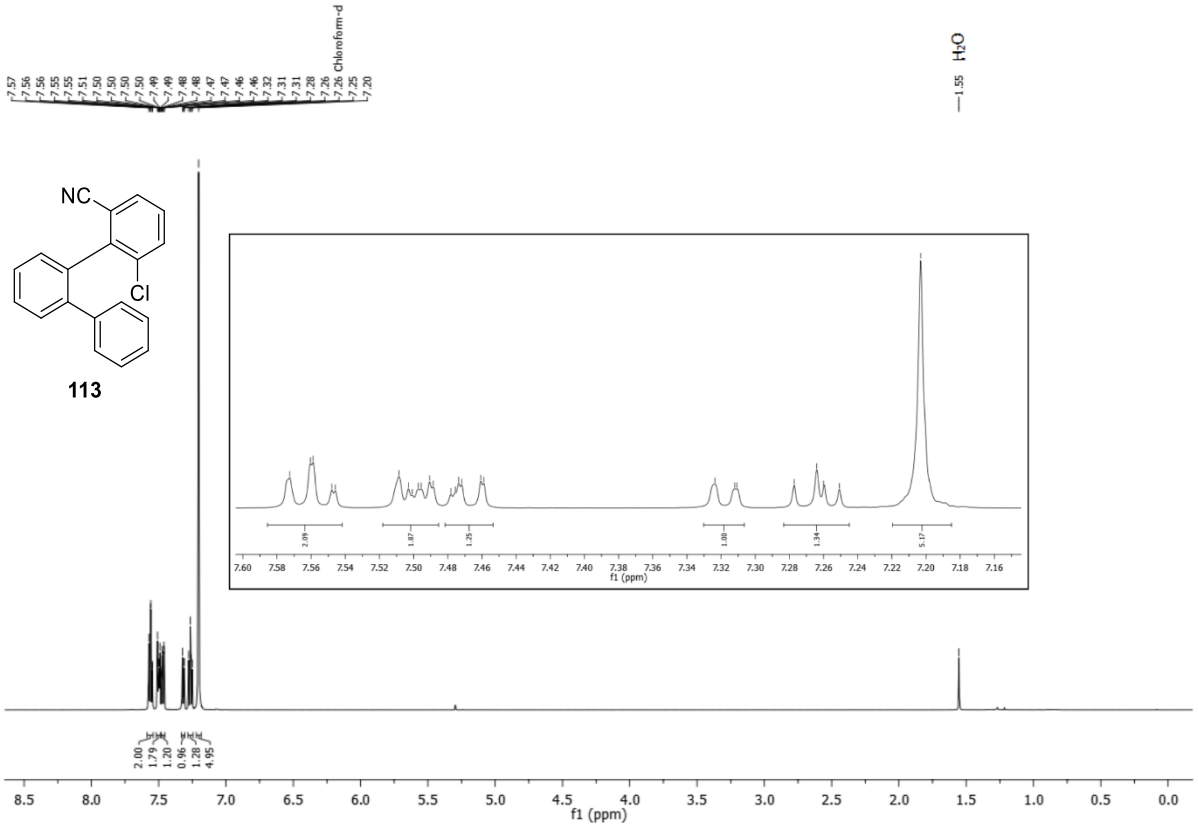

Figure 50: *^{1}H-NMR (600 MHz) spectrum of* ***113*** *in $CDCl_3$.*

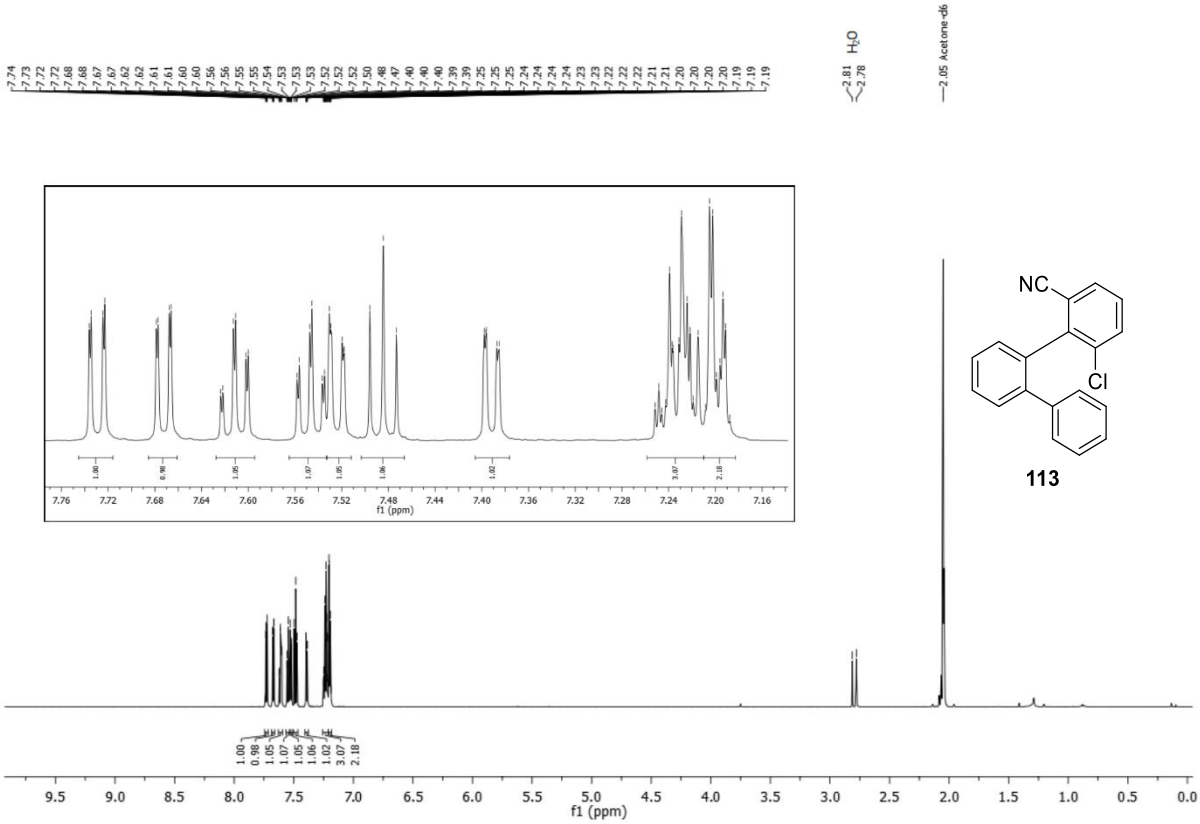

Figure 51: *^{1}H-NMR (700 MHz) spectrum of **113** in Acetone-d_6.*

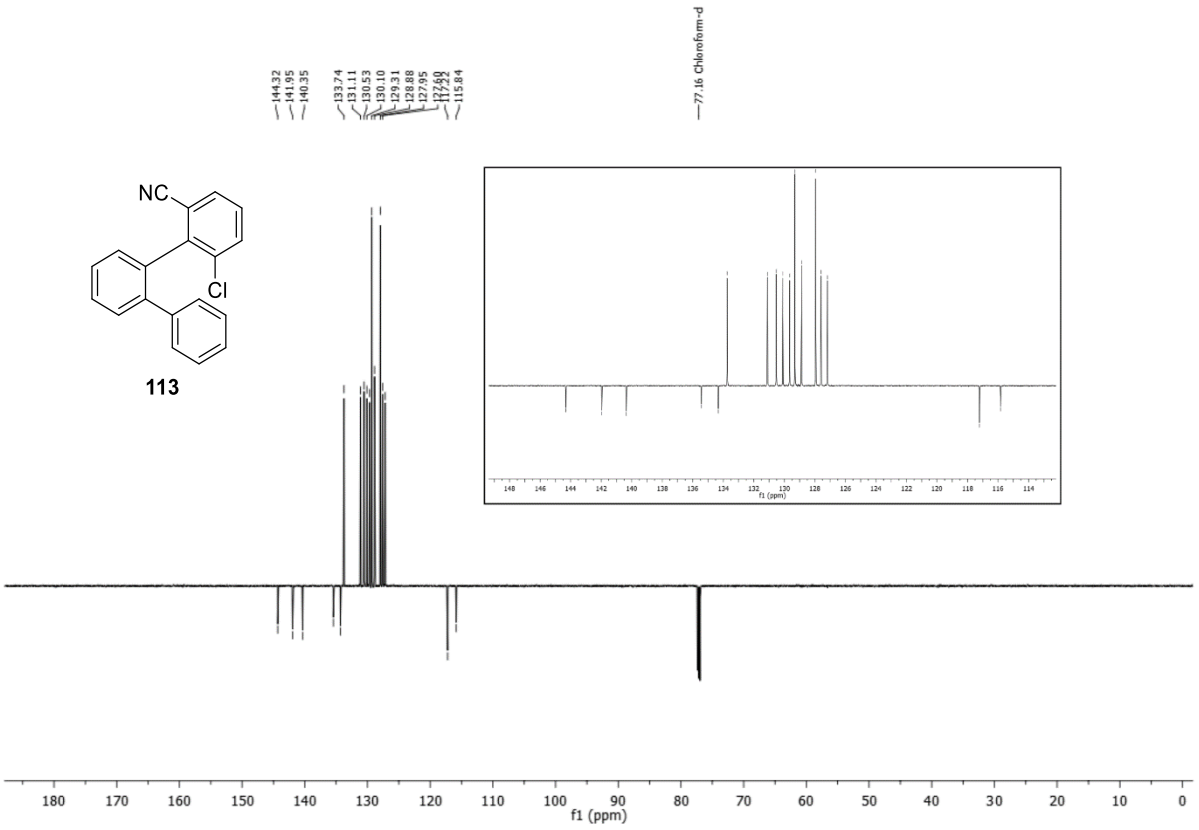

Figure 52: *^{13}C-NMR (151 MHz) spectrum of **113** in $CDCl_3$.*

The HRMS spectra measured for the isolated product of the reaction gave the following spectra which could not be assigned to any of the shown structures:

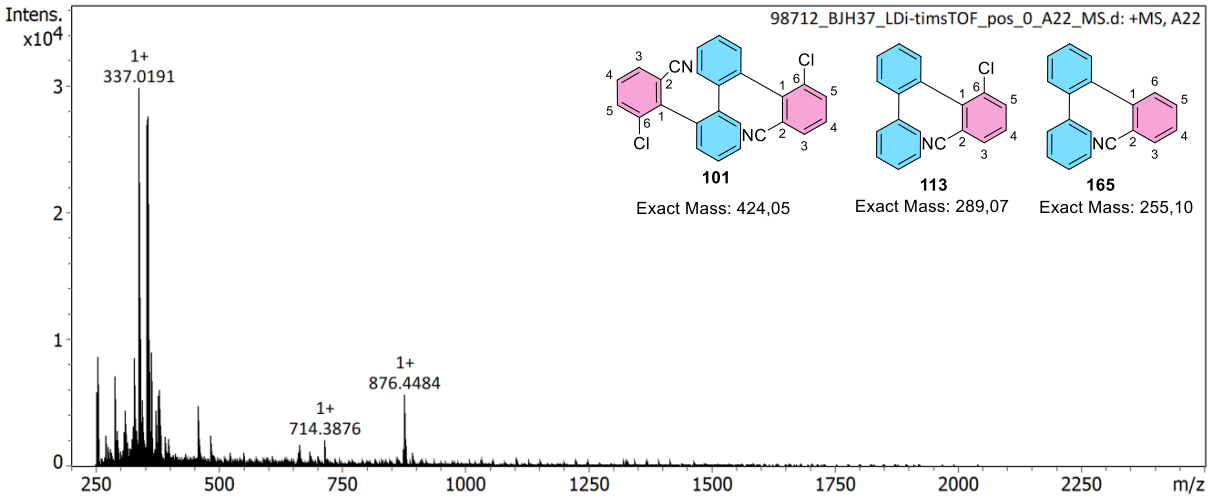

Figure 53: *HRMS spectrum 1 of reaction targeting the quaterphenyl with CN on position 2* ***101.***

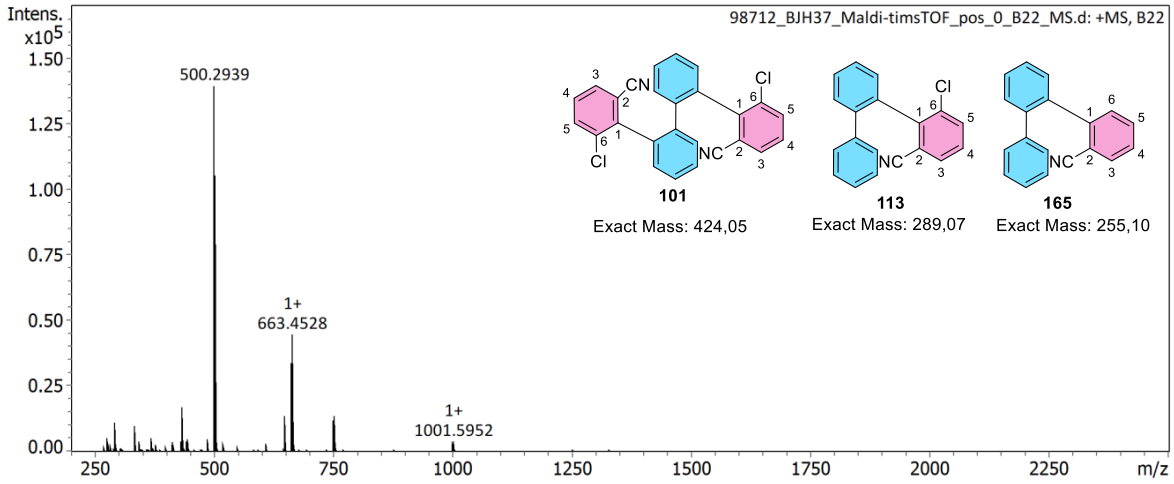

Figure 54: *HRMS spectrum 2 of reaction targeting the quaterphenyl with CN on position 2* ***101****.*

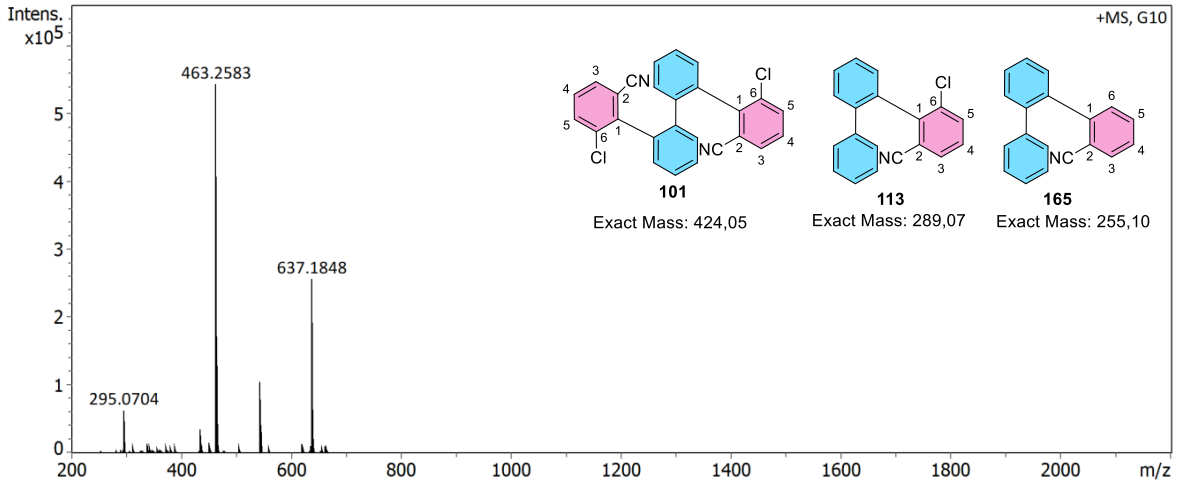

Figure 55: *HRMS spectrum 3 of reaction targeting the quaterphenyl with CN on position 2* ***101****.*

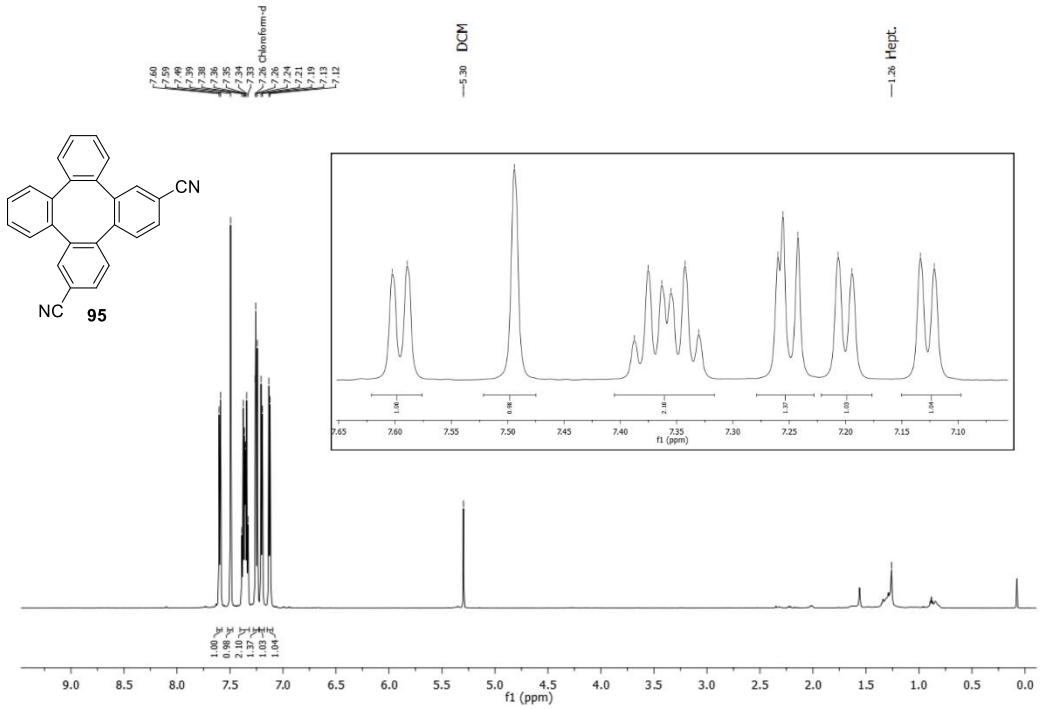

Figure 56: *^{1}H-NMR (600 MHz) spectrum of **95** in $CDCl_3$.*

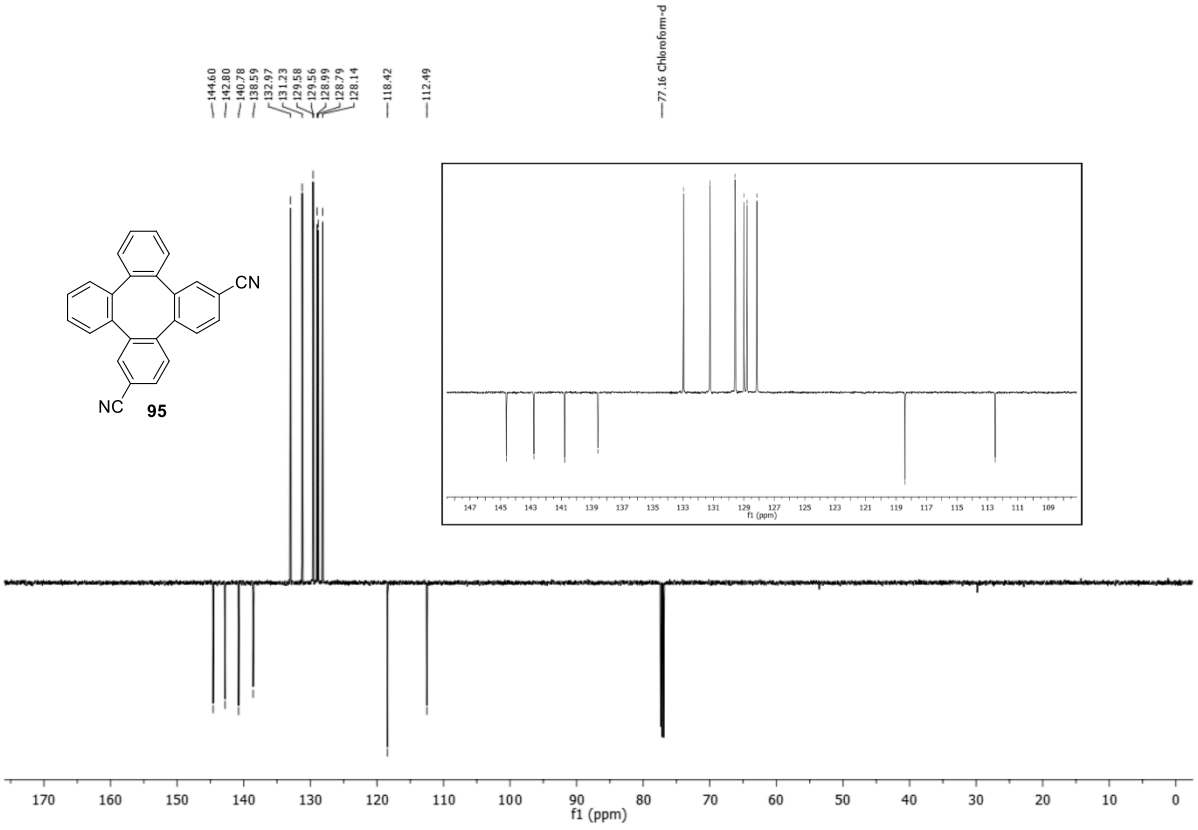

Figure 57: *^{13}C-NMR (151 MHz) spectrum of spectrum of **95** in $CDCl_3$.*

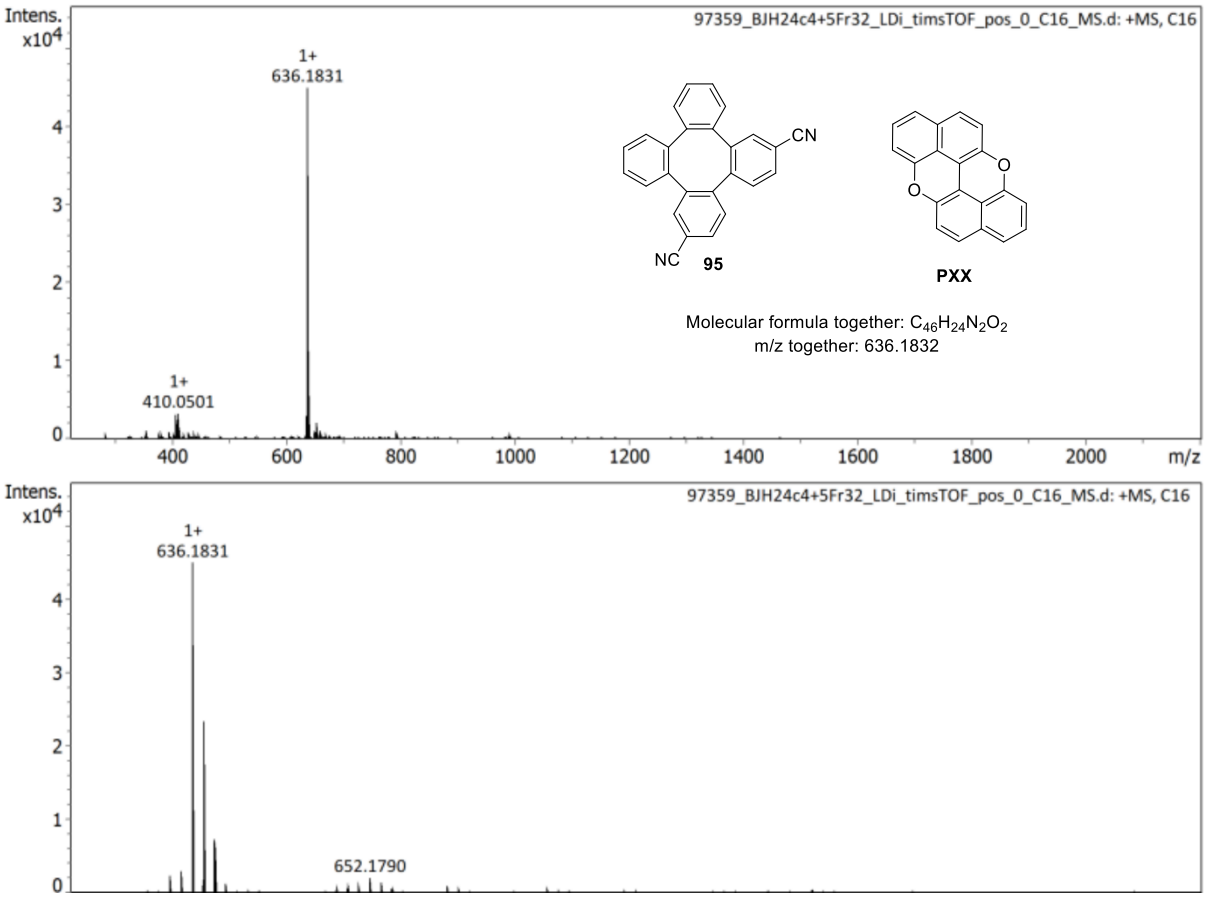

Figure 58: *LDi-timsTOF-MS spectrum of* ***95****.*

Datablock: BJH24Sp2_5-3_a

Bond precision: C-C = 0.0017 A Wavelength=1.54186

Cell: a=10.4985(4) b=10.4985(4) c=32.7441(18)
alpha=90 beta=90 gamma=90
Temperature: 100 K

	Calculated	Reported
Volume	3609.0(3)	3609.0(3)
Space group	I 41/a	I 41/a
Hall group	-I 4ad	-I 4ad
Moiety formula	C26 H14 N2	?
Sum formula	C26 H14 N2	C26 H14 N2
Mr	354.39	354.40
Dx,g cm-3	1.304	1.304
Z	8	8
Mu (mm-1)	0.597	0.597
F000	1472.0	1472.0
F000'	1476.01	
h,k,lmax	12,12,40	12,12,40
Nref	1763	1733
Tmin,Tmax	0.972,0.976	0.705,0.977
Tmin'	0.836	

Correction method= # Reported T Limits: Tmin=0.705 Tmax=0.977
AbsCorr = MULTI-SCAN

Data completeness= 0.983 Theta(max)= 71.456

R(reflections)= 0.0347(1364) wR2(reflections)= 0.0950(1733)

S = 1.035 Npar= 127

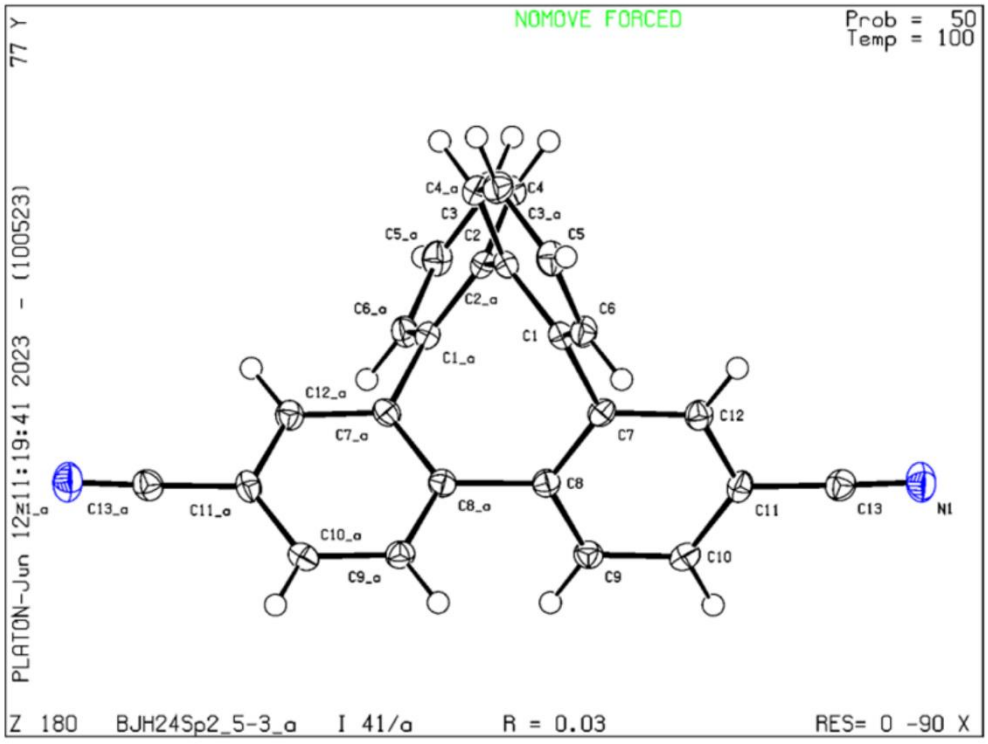

Figure 59: *Crystal data and structure refinement for* ***95.***

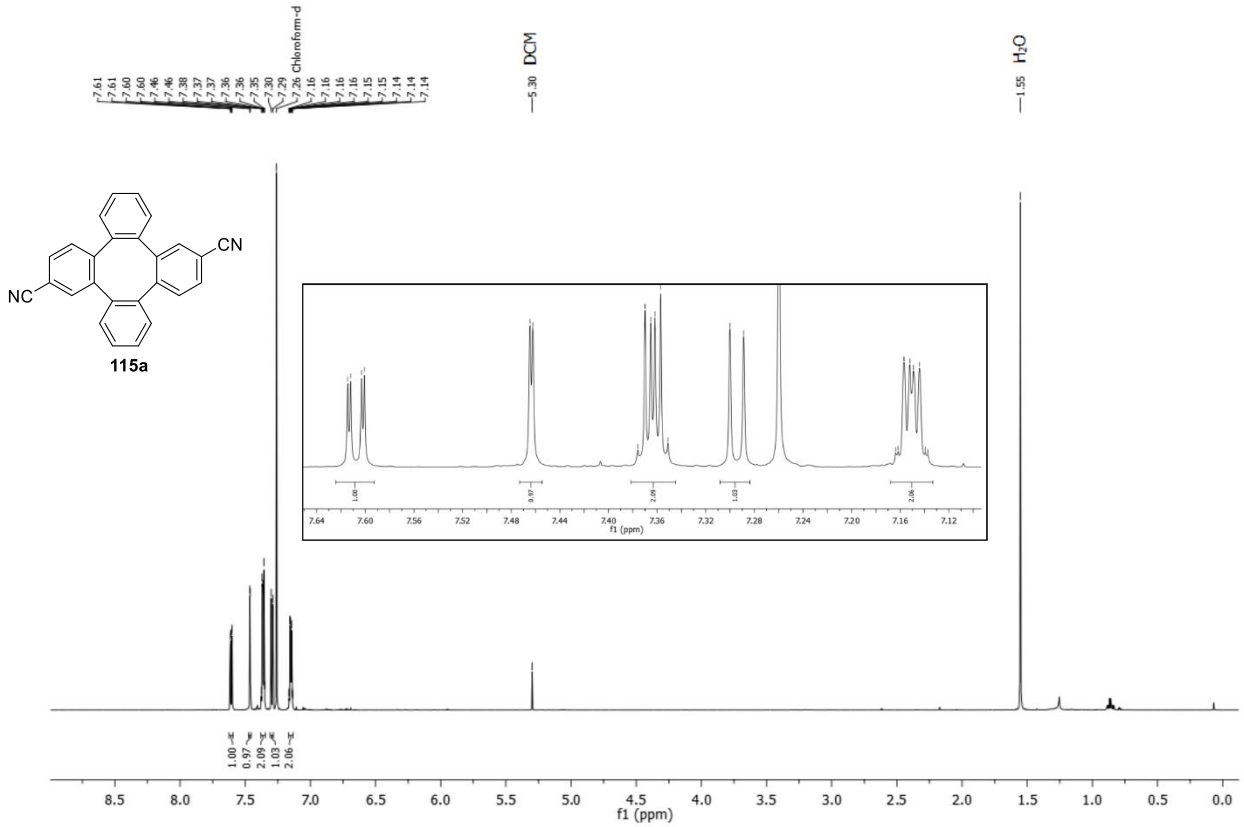

Figure 60: *^{1}H-NMR (700 MHZ) spectrum of **115a** in $CDCl_3$.*

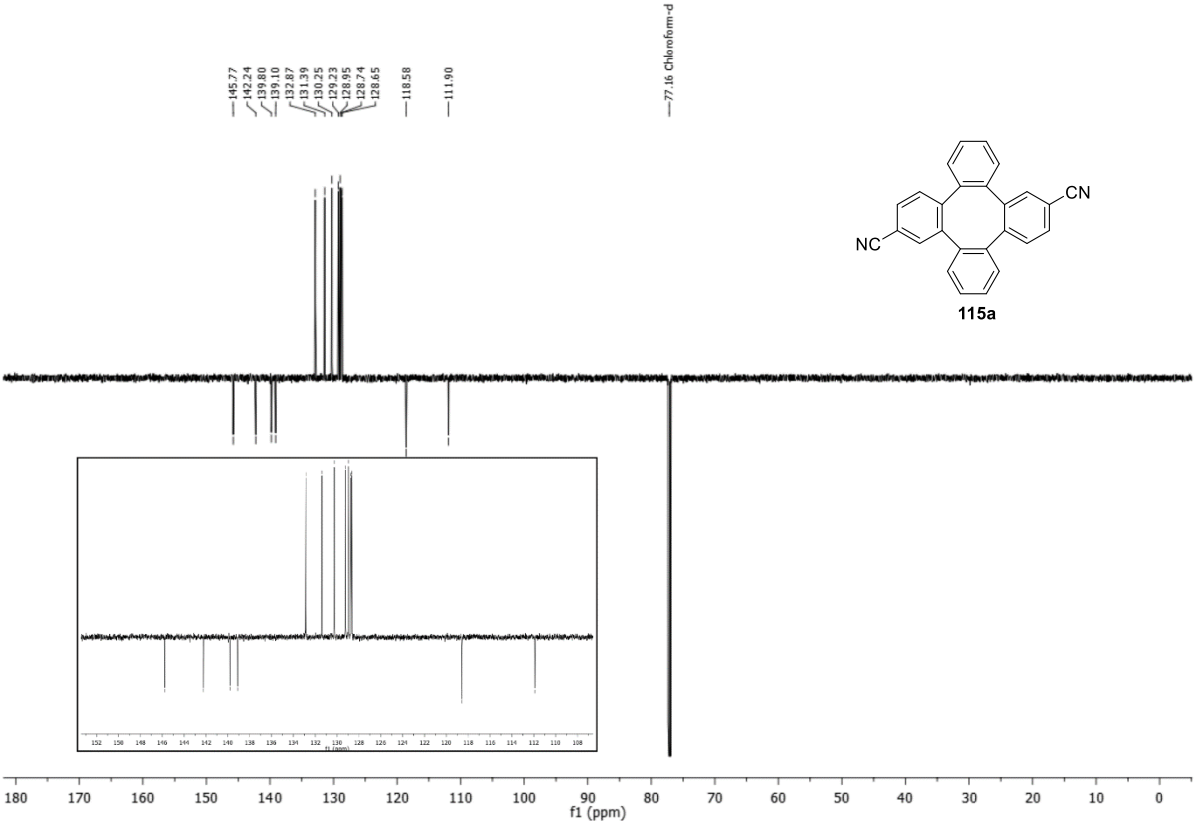

Figure 61: *^{13}C-NMR (176 MHz) spectrum of spectrum of **115a** in $CDCl_3$.*

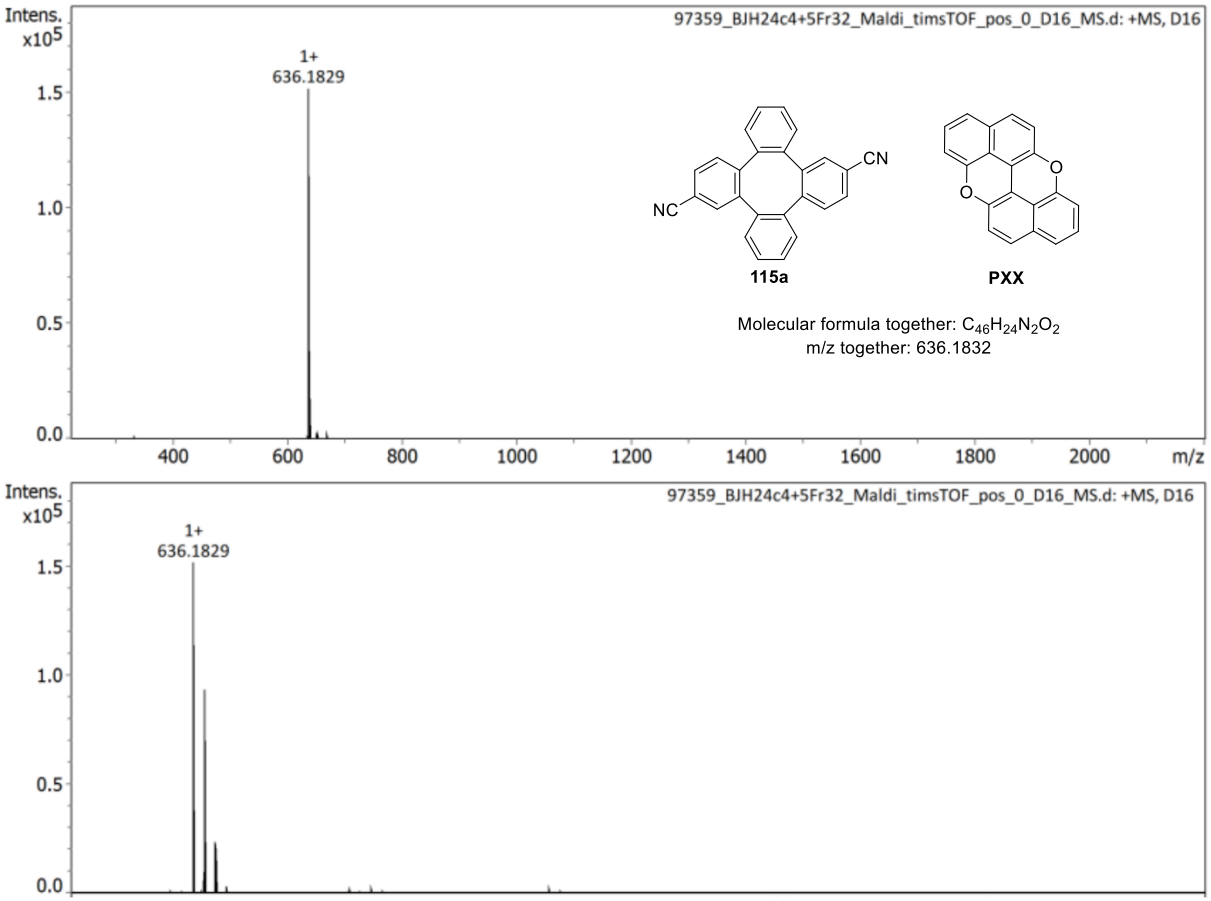

Figure 62: *Maldi-timsTOF-MS spectrum of* ***115a****.*

Datablock: BJH24c45Fr32_a

```
Bond precision:   C-C = 0.0026 A          Wavelength=1.54186

Cell:             a=9.6919(2)      b=12.9510(3)      c=14.3605(4)
                  alpha=90         beta=90           gamma=90
Temperature:      100 K

                  Calculated                  Reported
Volume            1802.53(8)                  1802.54(8)
Space group       P 21 21 21                  P 21 21 21
Hall group        P 2ac 2ab                   P 2ac 2ab
Moiety formula    C26 H14 N2                  ?
Sum formula       C26 H14 N2                  C26 H14 N2
Mr                354.39                      354.40
Dx,g cm-3         1.306                       1.306
Z                 4                           4
Mu (mm-1)         0.598                       0.598
F000              736.0                       736.0
F000'             738.00
h,k,lmax          11,15,17                    11,15,17
Nref              3419[ 1960]                 3097
Tmin,Tmax         0.948,0.959                 0.987,0.990
Tmin'             0.948

Correction method= # Reported T Limits: Tmin=0.987 Tmax=0.990
AbsCorr = MULTI-SCAN

Data completeness= 1.58/0.91        Theta(max)= 69.833

R(reflections)= 0.0284( 2847)                wR2(reflections)=
                                             0.0712( 3097)
S = 1.066                  Npar= 253
```

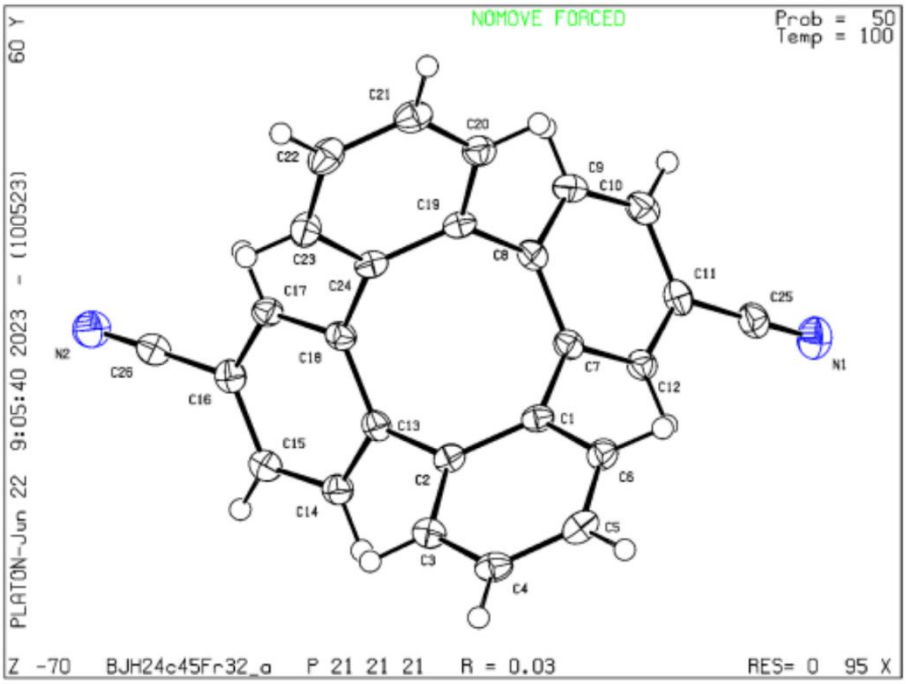

Figure 63: *Crystal data and structure refinement for* ***115a.***

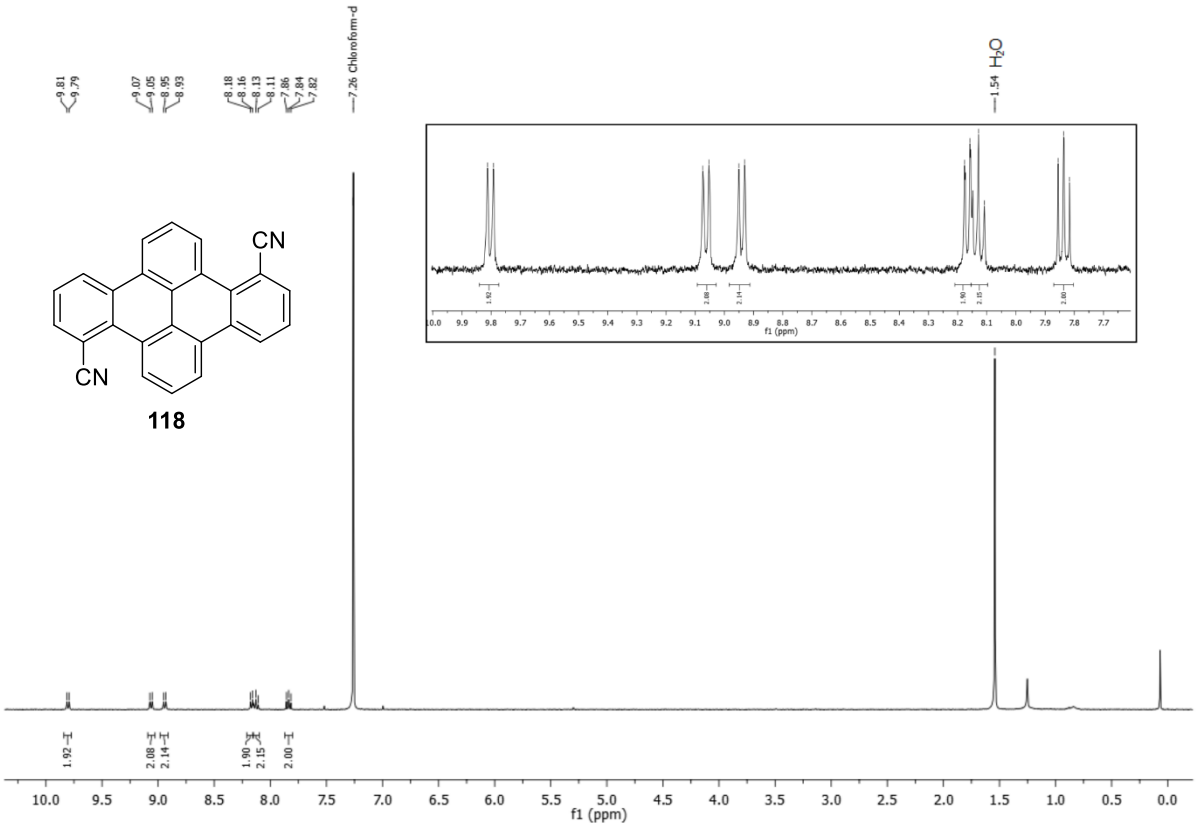

Figure 64: *^{1}H-NMR (400 MHz) spectrum of **118** in $CDCl_3$.*

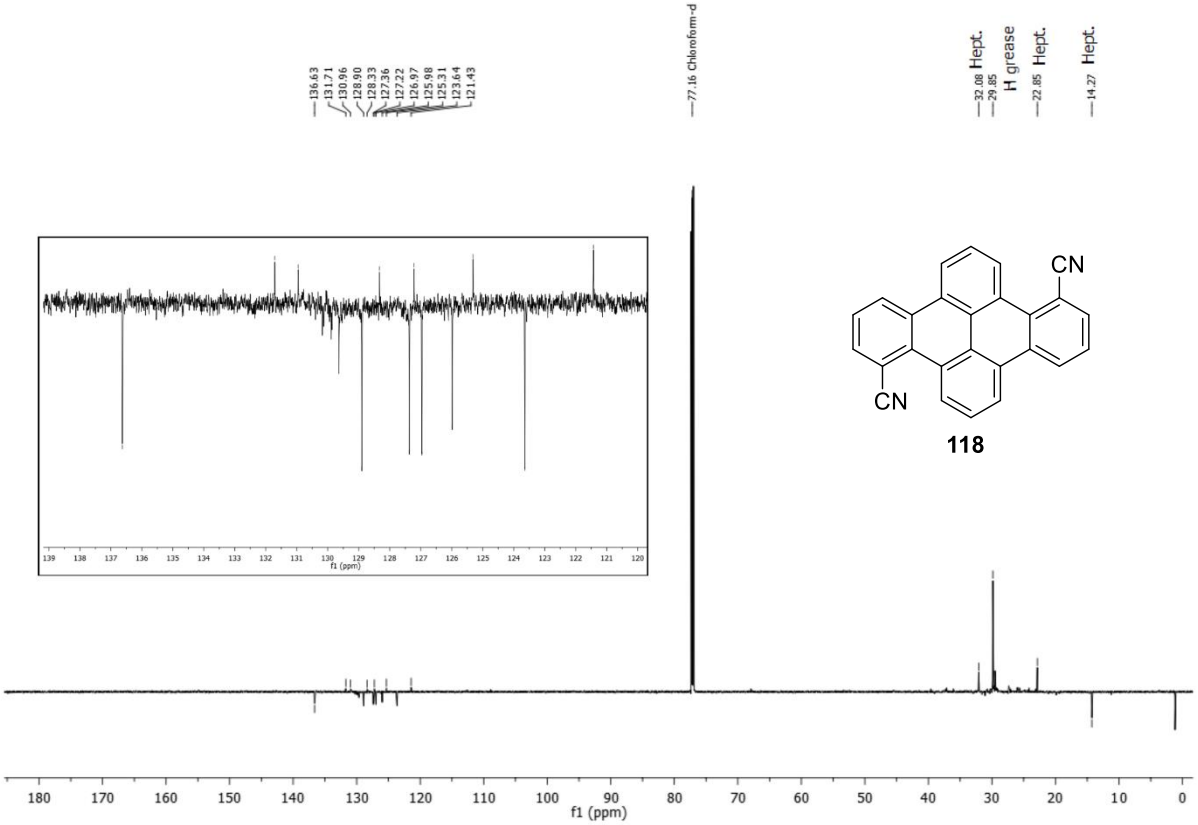

Figure 65: *^{13}C-NMR (176 MHz) spectrum of spectrum of **118** in $CDCl_3$.*

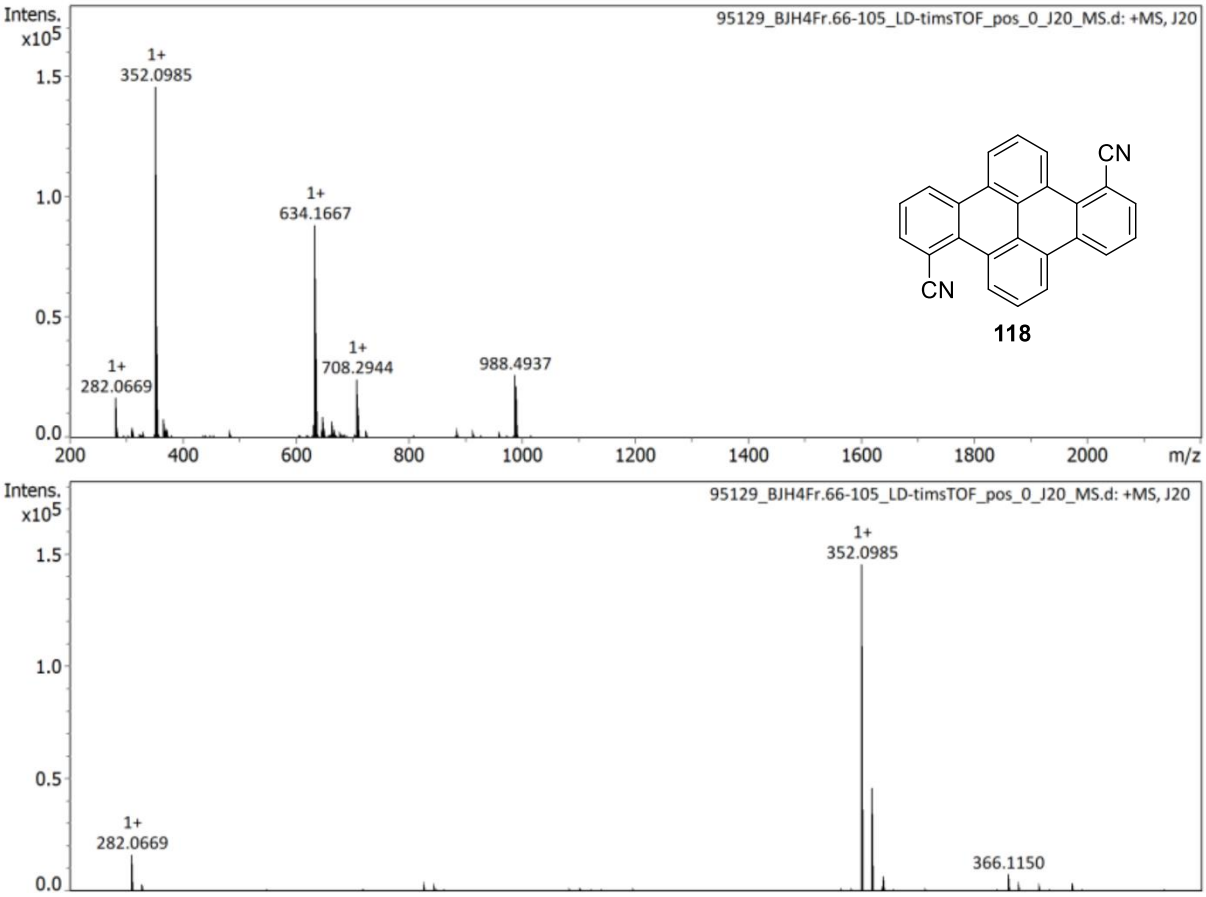

Figure 66: *LD-timsTOF-MS spectrum of* ***118****.*

Datablock: BJH4Fr66-105_flat-ring_a

Bond precision: C-C = 0.0100 A Wavelength=0.71073

Cell: a=12.752(2) b=3.7722(7) c=16.760(3)
alpha=90 beta=103.036(13) gamma=90
Temperature: 100 K

	Calculated	Reported
Volume	785.4(2)	785.4(2)
Space group	P 21	P 21
Hall group	P 2yb	P 2yb
Moiety formula	C26 H12 N2	?
Sum formula	C26 H12 N2	C26 H12 N2
Mr	352.38	352.39
Dx,g cm-3	1.490	1.490
Z	2	2
Mu (mm-1)	0.088	0.088
F000	364.0	364.0
F000'	364.13	
h,k,lmax	14,4,18	15,4,21
Nref	2252[1328]	2026
Tmin,Tmax	0.998,0.998	0.084,0.999
Tmin'	0.947	

Correction method= # Reported T Limits: Tmin=0.084 Tmax=0.999
AbsCorr = MULTI-SCAN

Data completeness= 1.53/0.90 Theta(max)= 23.256

R(reflections)= 0.0533(950) wR2(reflections)= 0.1101(2026)

S = 0.848 Npar= 253

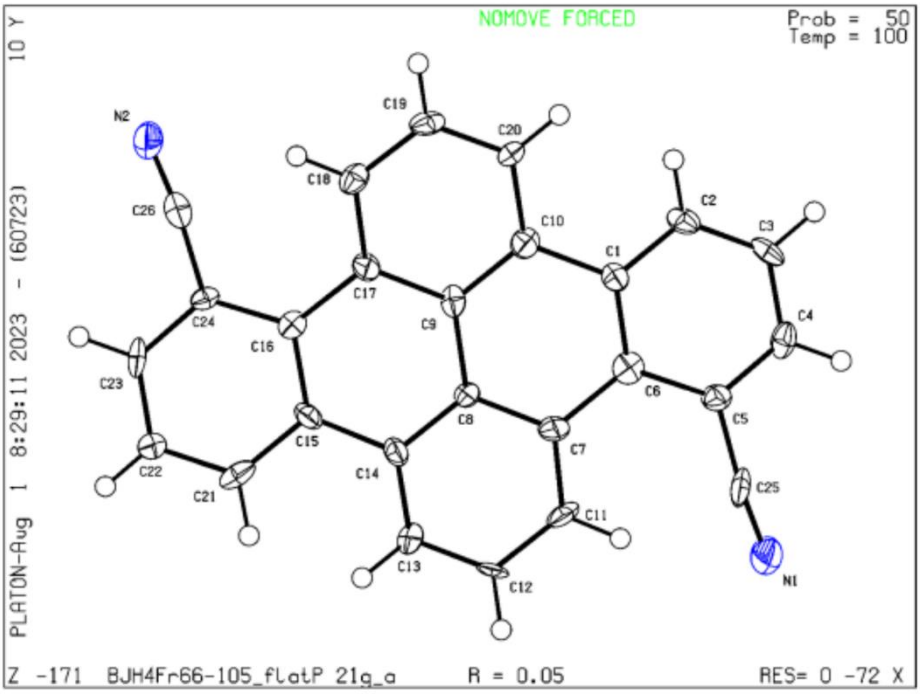

Figure 67: *Crystal data and structure refinement for* ***118.***

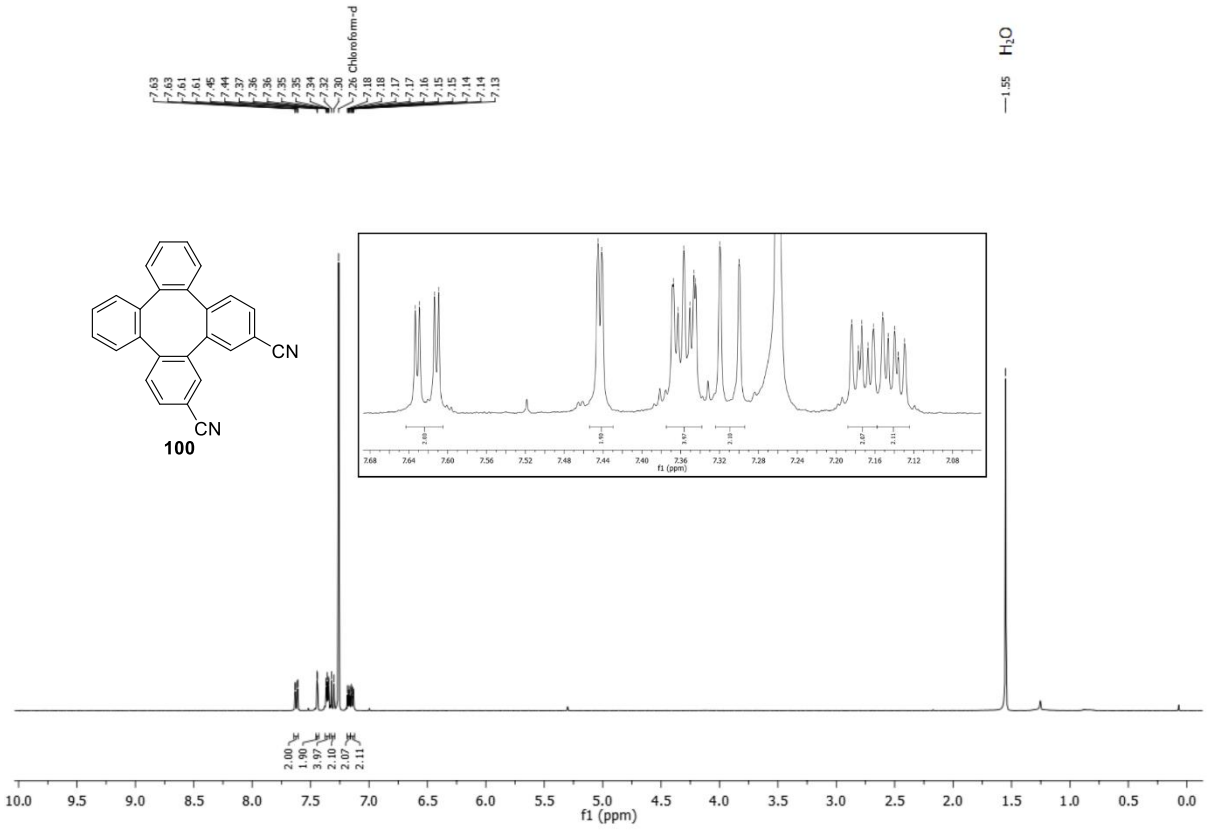

Figure 68: *[1]H-NMR (400 MHz) spectrum of* ***100*** *in $CDCl_3$.*

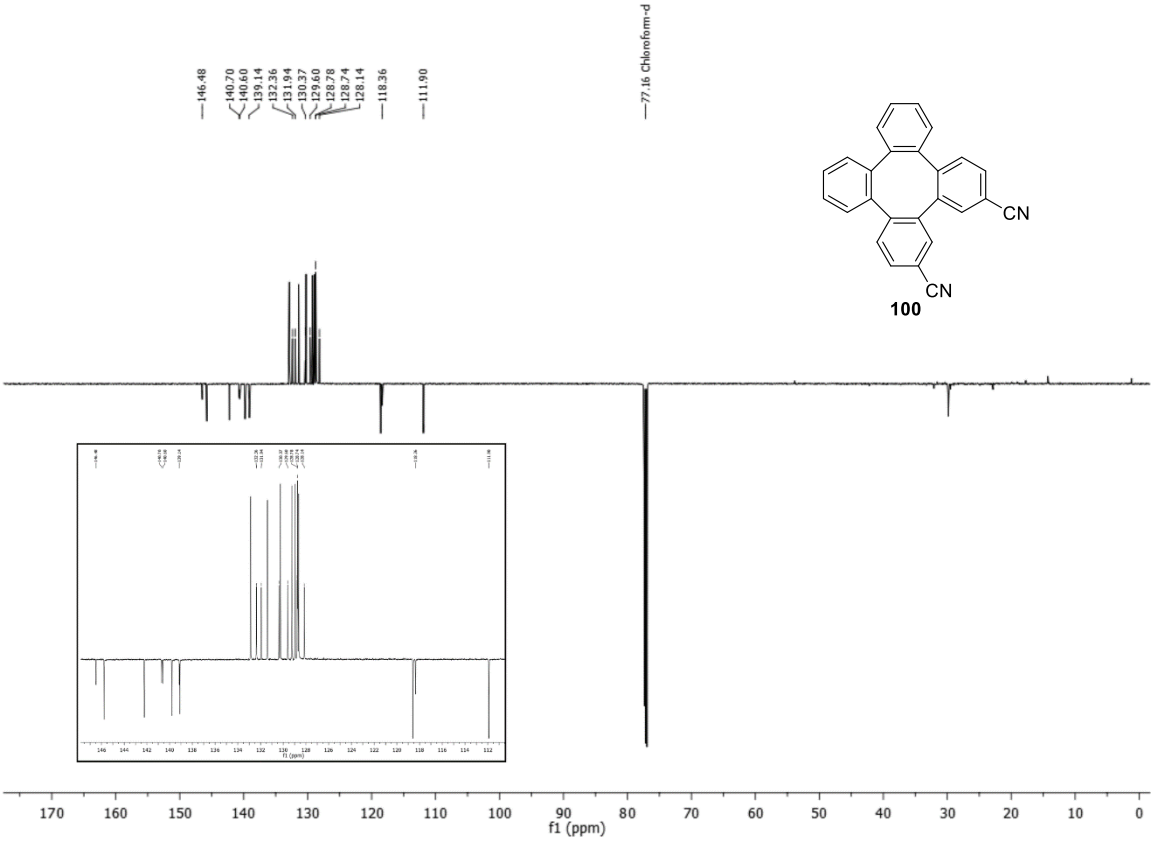

Figure 69: *[13]C-NMR (151 MHz) spectrum of spectrum of* ***100*** *in $CDCl_3$.*
Spectrum was taken from a mixture of ***100*** *and* ***115b****. The signals shown belong to* ***100*** *as determined by 2D-NMR.*

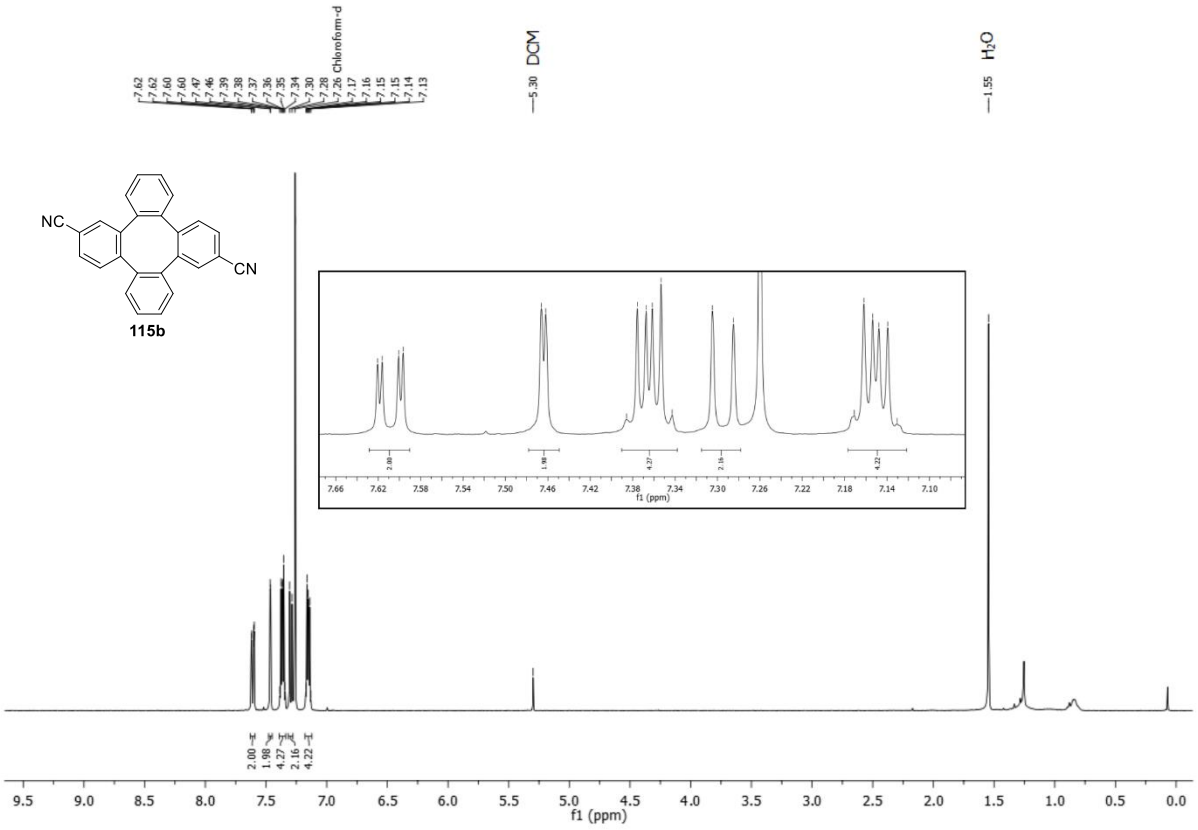

Figure 70: *^{1}H-NMR (400 MHz) spectrum of **115b** in $CDCl_3$.*

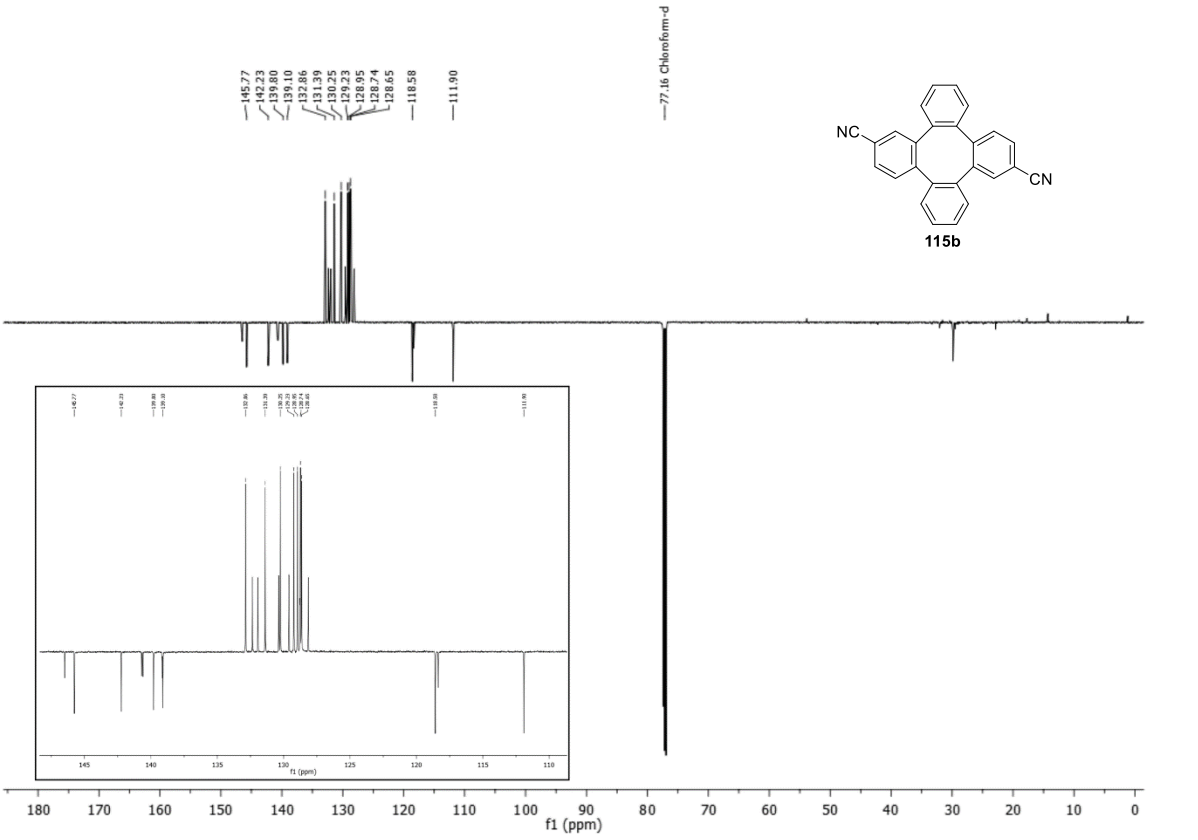

Figure 71: *^{13}C-NMR (151 MHz) spectrum of spectrum of **115b** in $CDCl_3$.*
*Spectrum was taken from a mixture of **100** and **115b**. The signals shown belong to **1135** as determined by 2D-NMR.*

Datablock: bjh25gpc34p1_a

Bond precision: C-C = 0.0069 A Wavelength=0.71073

Cell: a=9.6972(8) b=12.9562(7) c=14.3755(8)
alpha=90 beta=90 gamma=90
Temperature: 100 K

	Calculated	Reported
Volume	1806.1(2)	1806.1(2)
Space group	P 21 21 21	P 21 21 21
Hall group	P 2ac 2ab	P 2ac 2ab
Moiety formula	C26 H14 N2	?
Sum formula	C26 H14 N2	C26 H14 N2
Mr	354.39	354.39
Dx,g cm-3	1.303	1.303
Z	4	4
Mu (mm-1)	0.077	0.077
F000	736.0	736.0
F000'	736.26	
h,k,lmax	12,16,18	12,16,18
Nref	4151[2363]	4134
Tmin,Tmax	0.989,0.991	0.997,0.998
Tmin'	0.989	

Correction method= # Reported T Limits: Tmin=0.997 Tmax=0.998
AbsCorr = MULTI-SCAN

Data completeness= 1.75/1.00 Theta(max)= 27.498

R(reflections)= 0.0642(1843) wR2(reflections)= 0.1400(4134)

S = 0.792 Npar= 254

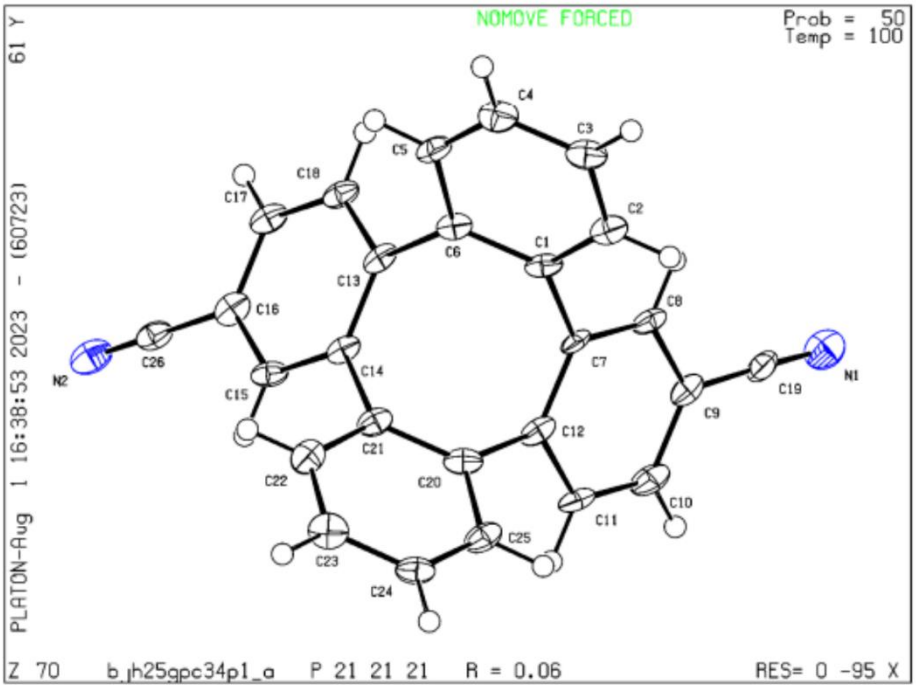

Figure 72: *Crystal data and structure refinement for* ***115b.***

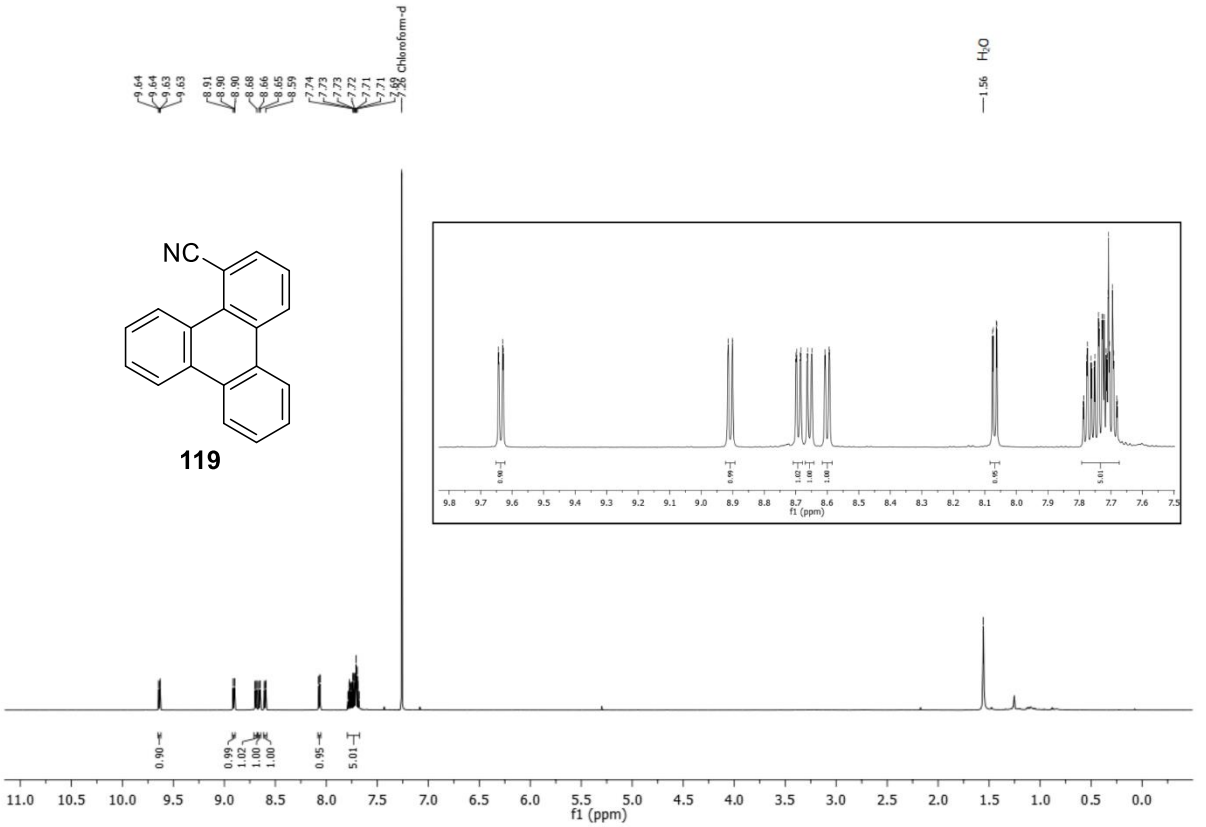

Figure 73: *^{1}H-NMR (600 MHz) spectrum of **119** in $CDCl_3$.*

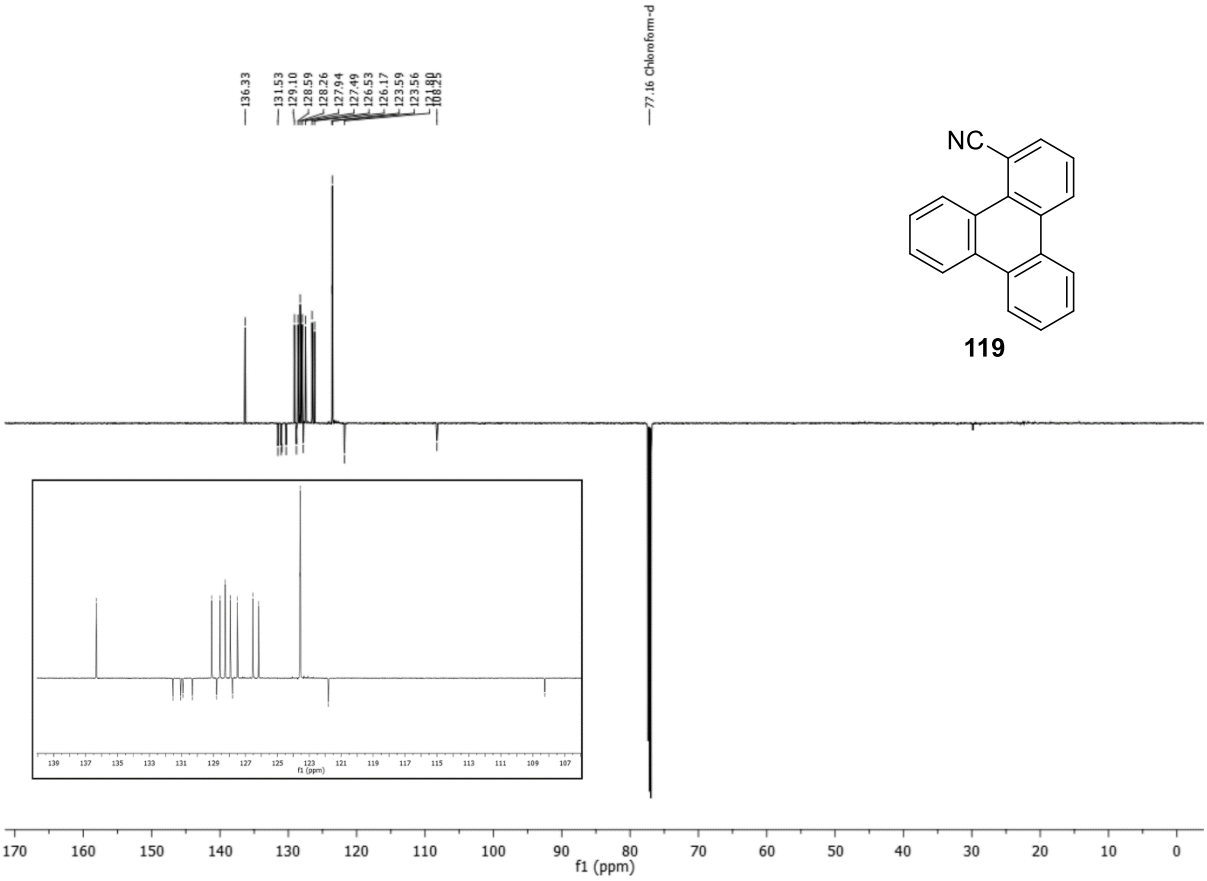

Figure 74: *^{13}C-NMR (151 MHz) spectrum of spectrum of **119** in $CDCl_3$.*

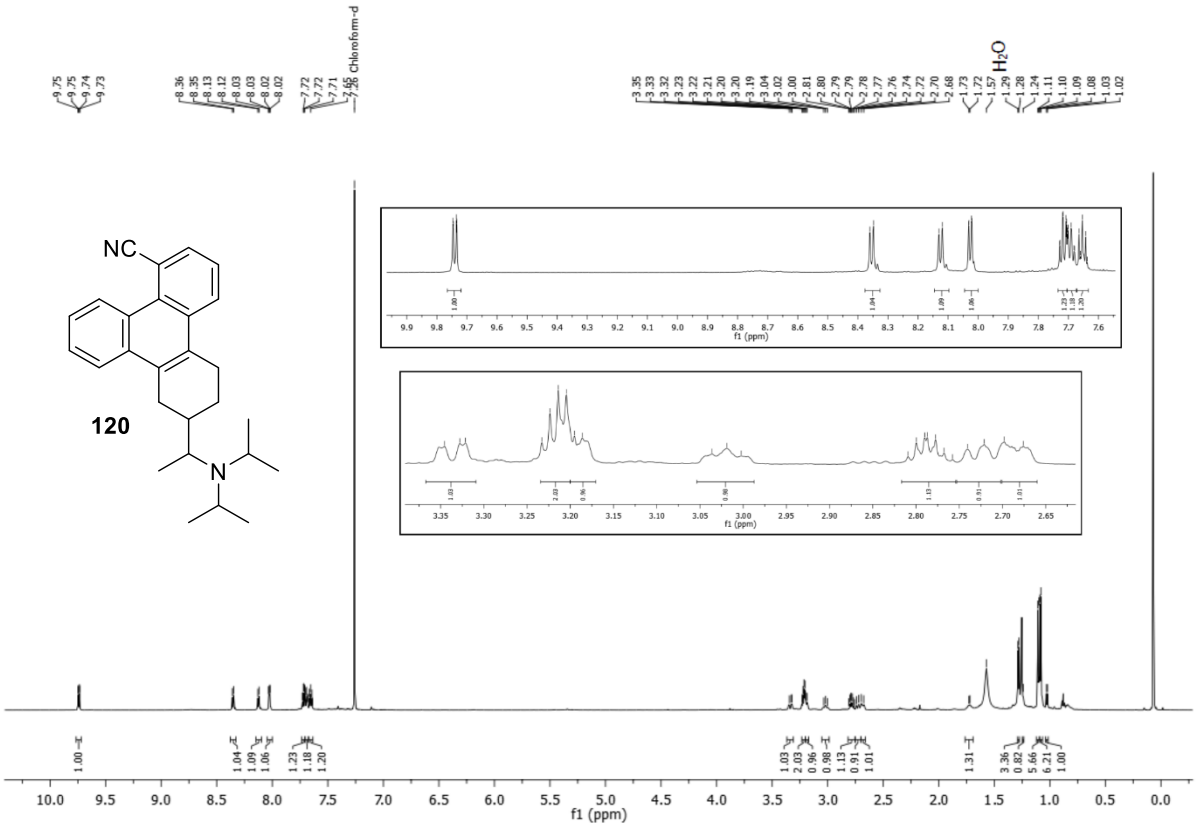

Figure 75: *^{1}H-NMR (700 MHz) spectrum of **120** in $CDCl_3$.*

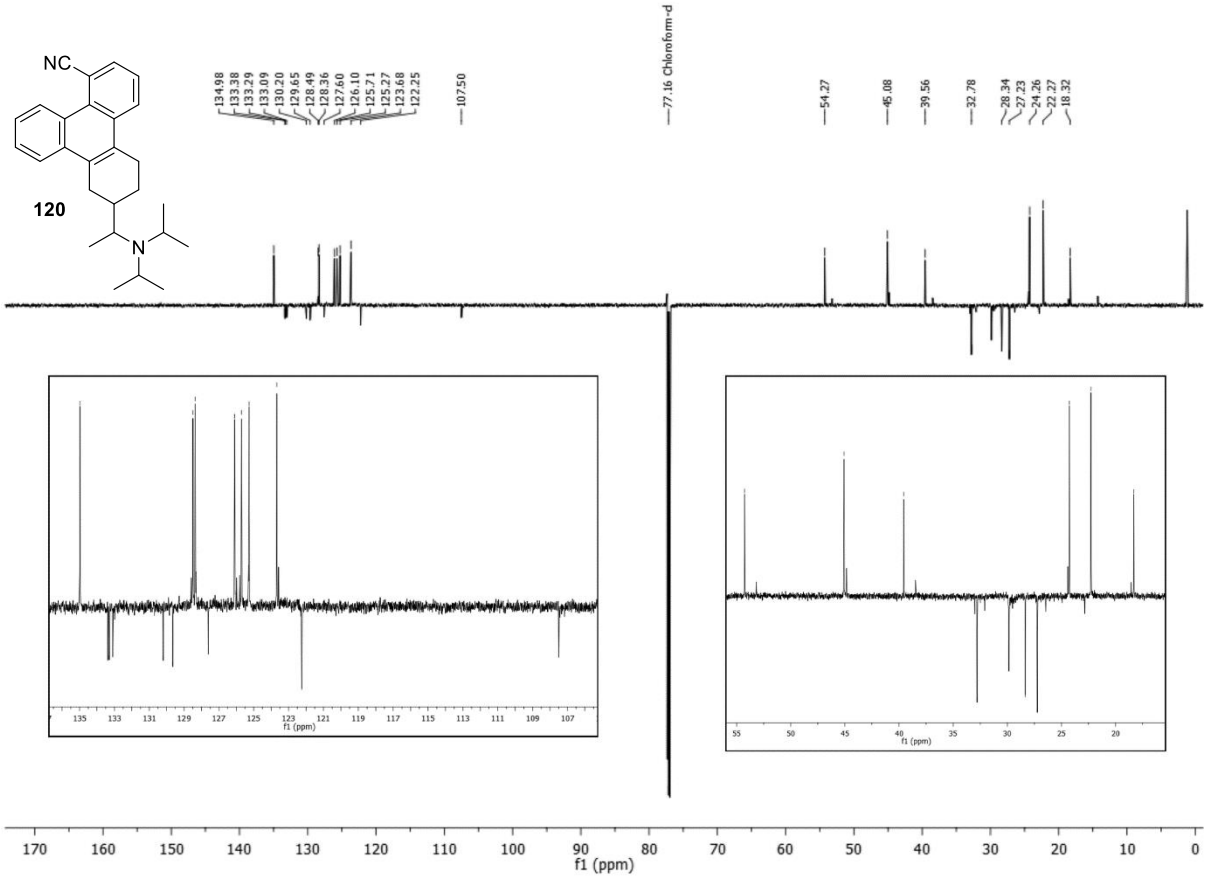

Figure 76: *^{13}C-NMR (176 MHz) spectrum of spectrum of **120** in $CDCl_3$.*

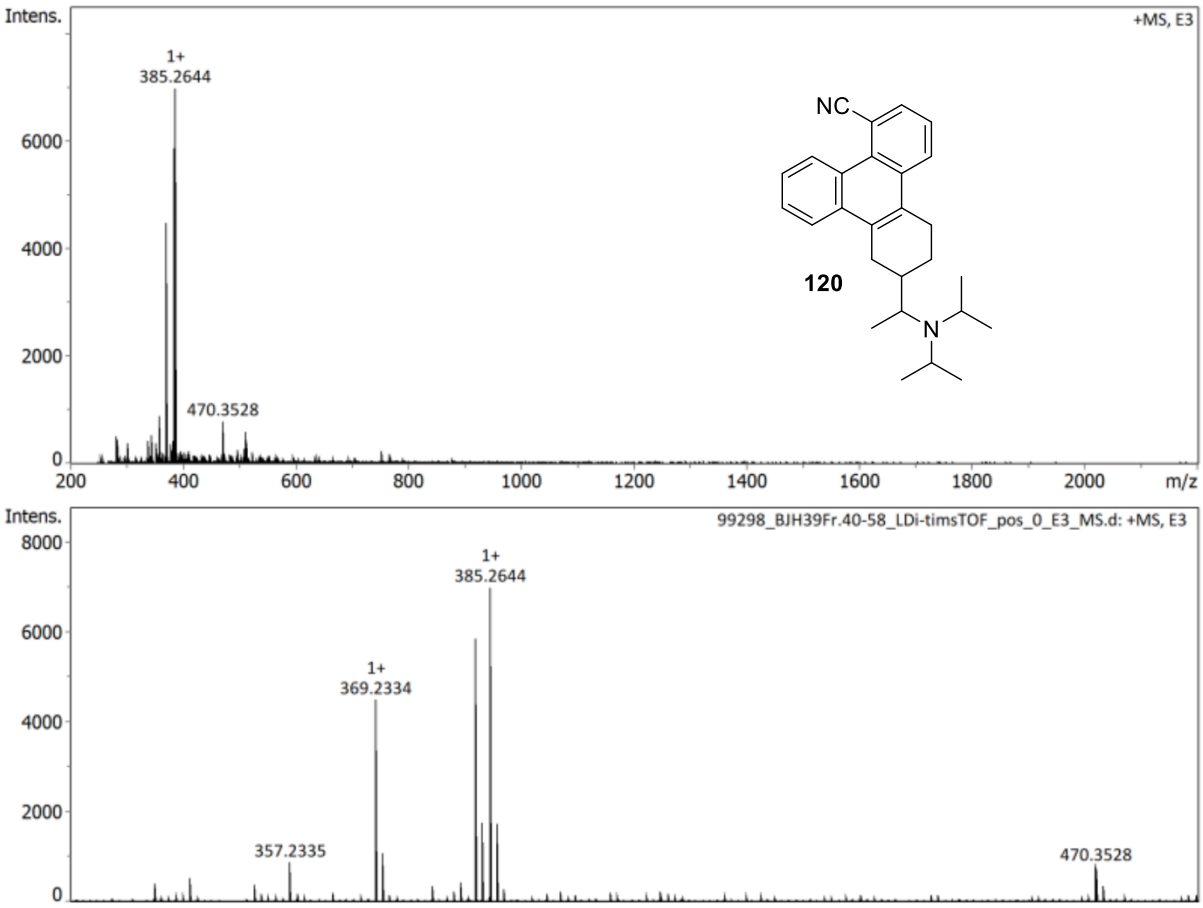

Figure 77: *Maldi-timsTOF-MS spectrum of* ***120****.*